Deploying single-cell transcriptomics for assessing CAR T cell generation: alleviating antiviral restriction factors enhances gene transfer

At the Faculty of Biology of the Technical University of Darmstadt
submitted in fulfilment of the requirements for the degree of
Doctor rerum naturalium
(Dr. rer. nat.)

Doctoral thesis by
Filippos Theofilos Charitidis, M. Sc.
from Kavala, Greece

Assessors:
Prof. Dr. Ulrike A. Nuber
Prof. Dr. Christian J. Buchholz

Paul-Ehrlich-Institut

TECHNISCHE
UNIVERSITÄT
DARMSTADT

Darmstadt 2023

ACKNOWLEDGEMENTS

As this doctoral thesis has approached to the finishing line, it brings together all these memories of efforts, struggles and success, that gently sketched an eternal mark on me. It gives me my immense pleasure to express my deep gratitude to my supervisor, Prof. Dr. Christian Buchholz, who honored me with this prestigious thesis project. This lifetime experience would not have been achieved without his trust and continuous support. His valuable help and constructive guidance led to the smooth completion of this project, which nourished my scientific and intellectual skills, and further cultivated my self-esteem and confidence. My sincere acknowledgements to my mentor and coordinator of STACCATO Consortium, Dr. Colin Clarke. Without him, this project would not have been carried out. I also want to express my sincere appreciations to Dr. Csaba Miskey, Dr. Liam Childs, Dr. Vadir Lopez-Salmeron, Dr. Siobhan Cashman, Edyta Kowalczyk, Dr. Jonathan Bones, Dr. Ciara Tierney, Dr. Lisa Strasser, Björn Becker, Dr. Christel Kamp, Kay-Martin Hanschmann, Dr. Stefan Günther, Prof. Dr. Michael Rieger and WeiJia Yu for their significant help with my project.

I will also grasp the opportunity at this point to thank my internal supervisor Prof. Dr. Ulrike Nuber, and the examination committee, Prof. Dr. Cristina Cardoso and Prof. Dr. Alexander Löwer, for their time evaluating this dissertation.

I feel honored that I have collaborated with such a dedicated and skillful team of scientific and technical staff. This joyful team building spirit and priceless assistance makes my departure full of heartwarming emotions. So many fantastic experiences with such lovely people that cannot fit in a piece of paper…Thus, Gundi, Angi, Elham, Frederic, Naphang, Sami, Mar, Luca, Doro, Alex, , Annika, Shiwani, Vanessa, Arezoo, Burak, Merle, Svenja, Lea S., Lea K., Josefine, Johanna, Fabian, Nora, Laura, Tati, Mehryad, Jessica, Iris, Manu, Julia, Marina, Ludmilla, Nicole, Barbara, Antonia and all STACCATO ESRs team, I thank you all from the bottom of my heart.

My heartfelt thanks to my family, Alla, Panayiotis and Christos, and all my friends for their unconditional love and support for every step and challenge in my life.

Filippos Theofilos Charitidis

TABLE OF CONTENTS

SUMMARY

T lymphocytes comprise one of the two major classes of cells in the adaptive immunity. Bearing a T cell receptor (TCR), T cells undergo somatic recombination to specialize against antigenic epitopes, during the invasion of a pathogen. Separated into two distinct types, the CD4 helper and CD8 cytotoxic, T cells differentiate into certain subsets depending on the origin of the pathogen, capable of orchestrating a particular immune response in order to eradicate it from the system. Long-lasting antigen-specific memory T cells are responsible for protection against subsequent infections with the same pathogen. Able to be *ex vivo* manipulated, T cells constitute an attractive source for adaptive immunotherapy, as they sustain a long-lasting effector function against specific targets. Genetically modified chimeric antigen receptor (CAR) T cells have emerged in clinical application with outstanding beneficial outcomes, particularly in B cell malignancies. However, this individualized therapy relies on complex genetically modified cellular products that have shown evidences of correlating factors with unresponsiveness, cancer progression and potentially with adverse events. In addition, the complicated and multifactorial manufacturing process involving gene delivery often by lentiviral vectors (LVs) could potentially contribute to these outcomes. The vesicular stomatitis virus G glycoprotein pseudotyped LV (VSV-LV) comprises a common tool in gene therapy capable of transducing a wide range of cells expressing the low-density lipoprotein receptor (LDLR). In order to selectively manipulate specific T cell types, CD8- and CD4-targeted LVs have been developed and characterized. Engineered with Nipah or measles paramyxoviral envelope proteins, the tropism has been redirected through a conjugated single-chain variable fragment (scFv) of an antibody or a designed ankyrin repeat protein (DARPin). Nevertheless, more contemporary monitoring methods are required to precisely investigate the molecular insights of CAR T cell products generated by different types of LVs, in order to better understand and optimize manufacturing processes. Ideally, the downstream optimization includes effective and efficient transduction of T cells by LVs, while preserving a beneficial T cell profile. The T cell specific CD8-LV and CD4-LV have been developed to bypass complicated manufacturing processes and potentially to be used for direct *in vivo* gene transfer applications. However, their on-target selectivity needs to be further evaluated and the phenotypic alterations compared to the conventional VSV-LV should be investigated.

For this purpose, single-cell RNA sequencing (scRNA-seq) was established for thorough investigation of CAR T cell products. While other studies have been conducted with at least 10-day expanded CAR T cell pre-infusion products investigating phenotypic profiles and correlating them with disease progression, this thesis focused on early events during CAR T generation. This

approach allowed a better correlation of distinct transcriptomic profiles driven by the different LVs, rather than later acquired phenotypes. Initially, a targeted gene analysis (TGA) approach for scRNA-seq was carried out to guarantee the detection and, subsequently, the identification of *CAR* expressing T cells, but also to provide high resolution in differential gene expression analysis. Thus, implementation of a *CAR* mRNA detection tool was necessary. For that reason, primers were designed to be compatible with the premade panel of primers targeting immune response related genes. The exact polyadenylation (poly-A) starting site on the CAR transgene expression cassette was defined, in order to confirm that the customized primers bind within the limited region, designated for the TGA approach, of 800 base pairs at the 3'-end. Thus, 6-day expanded human T cells inoculated with CD8-LV or VSV-LV were assessed by scRNA-seq. A trimodal distribution of *CAR* and *CD8A* expression became obvious, thus a computational subsetting strategy was set up. This allowed to distinguish transduced from non-transduced cells in scRNA-seq, which was confirmed to match with the frequency of CAR T cells detected by protein expression in flow cytometry. Furthermore, clustering analysis revealed different immune cell populations present in the CAR T cell products, such as CD4 and CD8 T cells, γδ T cells and natural killer T cells (NKT). Some leftover B cells were detected only in the untransduced control cells, which were not inoculated with any LV. These cells were totally absent in LV-inoculated samples, implying a cytotoxic activity of CAR T cells leading to their eradication. Focusing on differentially expressed genes in CD8 cell populations, overall greater differences were observed between untransduced and LV-inoculated cells, disregarding the LV type used. However, some distinct gene expression profiles were detected for each particular vector sample and also between transduced and non-transduced cells. The latter revealed the expression of antiviral restriction factors, which could have prevented proper LV-mediated gene transfer, but also genes related to naïve-like phenotype. Furthermore, CAR T cells sustained a more activated and proliferating status, skewing towards T helper 1 phenotype. Exhaustion markers were slightly increased in the transduced cells, possibly induced by CAR tonic signaling. Apoptosis-related genes were downregulated in CAR T cells and, vice versa, upregulated in non-transduced cells, in LV-inoculated samples.

To validate these findings and explore all the genes and pathways that might be dysregulated upon LV inoculation, whole transcriptome analysis was next conducted. Peripheral blood mononuclear cells (PBMC) from three donors were inoculated with VSV-LV, CD8-LV or CD4-LV, and cultured for shorter time. The 3-day expansion allowed both, CAR mRNA and protein detection, and thus investigation at earlier time points of LV exposure and cell transduction. The inclusion of CD4-LV provided the opportunity to confirm that the observed differences were not CD8 T cell type specific.

Summary

Focusing on differentially expressed genes, an overview of average gene expression between different groups of control, transduced and non-transduced cells revealed that overall many more genes were induced in CAR T cells generated with VSV-LV than the other LVs. By investigating differences between *CAR-* and *CAR+* cells from LV-inoculated samples, smaller changes were identified in CD8-LV sample than in VSV-LV or CD4-LV, indicating a more intensive induction of transcriptomic alteration by the latter two vectors. Nevertheless, overall, similar pathways were found to be associated with the differentially expressed genes between *CAR-* and *CAR+* cells for each LV sample. Namely, in *CAR-* cells the genes were associated with immune response against viral infections and inflammation, while in *CAR+* cells pathways related with metabolic processes, signaling and proliferation were upregulated. Looking closer at the biologically relevant genes, antiviral restriction factors induced by type I interferons (IFN) were found to be upregulated in *CAR-* cells, potentially inhibiting their proper transduction by the LVs. Quiescence and apoptosis related genes were also upregulated in *CAR-* cells, indicating that other factors and cellular profile might be implicated in unsuccessful gene transfer. On the other hand, *CAR+* cells showed increased gene expression of proteins related to LV trafficking and nuclear transport, but also increased genes of antioxidant enzymes. The latter could be associated with the active metabolic state of CAR T cells, triggered by CAR tonic signaling.

Taking into account that antiviral restriction might be implicated with the inhibition of LV-mediated gene transfer into T cells, various potential enhancers interfering with the IFN-induced pathways were screened during spin-inoculation of T cells with the LVs. Among them, the homonymous inhibitor of the mammalian target of rapamycin (mTOR) was found to impressively enhance CD8-LV and CD4-LV mediated transduction up to 7-fold, but did not improve VSV-LV. This effect was linked with the downregulation of the cell membrane residing IFN-induced transmembrane protein 1 (IFITM1), rather than the endosomal IFITM2 and IFITM3, which are known to restrict late stage of pH-dependent VSV-LV entry. While IFITMs inhibit the membrane fusion mediated by enveloped viruses, their downregulation alleviates this innate viral restricting mechanism.

Testing whether rapamycin could also enhance the direct *in vivo* gene transfer, PBMC-humanized non-obese diabetic severe combined immunodeficiency gamma (NSG) mice were pre-treated with rapamycin prior green fluorescent protein (GFP) gene transfer with CD8-LV. This resulted in obvious and more consistent gene transfer enhancement in mice treated with the highest dose of rapamycin (8 mg/kg) compared to vehicle. In addition, the treatment did neither influence the composition of the human T cell engraftment nor the frequency of target CD8 T cells. By analyzing the whole proteome of T cells treated with rapamycin, several other antiviral factors were observed to be downregulated. These antiviral proteins are controlled and stimulated by IFN

type I during viral infections, but they can also be constitutively expressed under normal circumstances. Among IFITMs, only IFITM1 was found to be downregulated, while the rest were not detected in mass-spectrometry. However, they were identified by western-blot, which further validated the findings and thresholds used in differential protein analysis. In order to assess this concept in a more clinically relevant manner, first, *in vitro* assessments were performed, proving that rapamycin does not impact CAR T cell performance and cytotoxicity against tumor cells. Following that, CD19-CAR T cells were generated *in vivo* with CD8-LV, in humanized mice engrafted with CD19 positive tumor cells. Once again, the pre-treatment with rapamycin showed a 2-fold higher generation of CAR T cells, correlated also with the faster tumor regression, particularly in mice receiving the lower rapamycin dose (3 mg/kg). *Ex vivo* re-stimulation of mouse splenocytes with tumor cells, re-boosted the expansion of CAR T cells as well in rapamycin groups, indicating potentially no impact of rapamycin on *in vivo* reconstitution of T cell memory phenotypes, as observed in the *in vitro* assessments.

Taken together, this thesis highlights the distinct transcriptomic alterations of T cells following LV-inoculation and successful transduction. Antiviral restriction mechanisms were identified as the most relevant indications of improper LV-mediated transduction of human T cells. Among these, IFITM1 was implicated in inhibition of CD8-LV and CD4-LV mediated transduction. Downmodulation of IFITM1 by rapamycin led to enhanced and highly selective *in vitro* and *in vivo* gene transfer by receptor-targeted LVs, and, consequentially, to faster tumor killing. Hence, introducing state-of-the-art single-cell transcriptomic in CAR T cell therapy can provide insights and key factors for product optimization in both, conventional and targeted gene therapy.

1 INTRODUCTION

1.1 GENETIC ENGINEERING OF T CELLS

Genetically modified T cells comprise one of the most successful immunotherapeutic treatments for hematological malignancies, autoimmune and infectious diseases, conferring remarkable outcomes currently in clinics (Ellis et al., 2021). The T cells are engineered to express a chimeric antigen receptor (CAR) or an alternative T cell receptor (transgenic TCR T cells) on their surface, which target the pathogenic cells via a certain extracellular marker presented on them or via an epitope presented on major histocompatibility complex (MHC). Upon recognition and binding to the ligand, the CAR molecule orchestrates a series of intracellular signaling events, resulting in re-directed cytotoxicity. Targeting the CD19 molecule on B cell malignancies comprises the most common CAR T cell therapeutic products. The transfer of the coding sequence for the CAR into T cell is frequently achieved by lentiviral (LV) or γ-retroviral vectors (RV) (Hartmann et al., 2017). Nevertheless, genetic engineering of T cells has broad applications in medicine with various gene editing approaches apart from LV or RV (Ellis et al., 2021). The choice of engineering T cells, the current practices and challenges are introduced in this section.

1.1.1 T lymphocytes

T lymphocytes or T cells constitute a major cell type of the adaptive immunity in jawed vertebrates, which undergo a series of TCR rearrangements, known as V(D)J recombination (Cooper & Alder, 2006). This results in a T cell clone specific for recognizing a certain exogenous peptide presented on major histocompatibility complex (MHC) molecules, also known as human leukocyte antigens (HLA), from antigen presenting cells (APCs) (Alberts et al., 2002).

Diverse T cell clones are capable to either eliminate diseased cells bearing these exogenous stimuli or prime other adaptive immune cells, the B lymphocytes or B cells, to produce antibodies against pathogens, which have bypassed the innate immune defense. Thus, the two major T cell types are divided into cytotoxic T cells (T_C), expressing the cluster of differentiation receptor 8 (CD8) and also known as CD8 T cells, and the helper T cells (T_H), expressing the CD4 receptor. The former cells, upon recognition of a peptide on MHC class I molecules, release cytotoxic granules constituted by perforin and granzymes, that permeabilize and activate apoptotic pathways in target cells (Alberts et al., 2002). Other apoptotic pathways can be also triggered by Fas-FasL engagement or with a family of tumor necrosis factor (TNF) cytokines, such as the TNF-related apoptosis-inducing ligand (TRAIL) (S. Wang & El-Deiry, 2003; Alberts et al., 2002).

Whereas, CD4 T cells interact with B cells through MHC class II, helping them to undergo genetic recombination and antibody class switching to mature into antibody-secreting cells, and secrete cytokines that regulate a wide network of innate and adaptive immune cells, but also neurons, epithelial cells and other (Jacobson et al., 2021; Alberts et al., 2002).

Depending on which cytokines are predominantly secreted from the helper T cells, they are divided into subtypes, taking part in a certain immune response. Hence, interferon gamma (IFNγ) and interleukin-12 (IL-12) producing T cells are accounted to be T_H1 cells, fighting intracellular pathogens, T_H17 cells release IL-17 and IL-21 in response to extracellular pathogens, and T_H2 cells secrete IL-4, IL-5 and IL-13 in response to multicellular parasites (Raphael et al., 2015). In addition, other subtypes also exist and named after the major cytokines they produce, such as T_H9 producing IL-9 and T_H22 secreting IL-22 cells (Raphael et al., 2015). T lymphocytes serving inhibitory functions against other immune cells via secretion of IL-10 and TGF-β belong to a specialized subset of T lymphocytes, the regulatory T cells (T_{REG}) (Raphael et al., 2015). The destiny of a naïve T cell to obtain a certain profile is regulated by autocrine or paracrine signals present in the extracellular milieu during T cell activation and the downstream expression of transcriptional factors. Hence, IFNγ, IL-12 and IL-2 promote the activation of T-bet and STAT4, leading to T_H1 phenotype, IL-23, IL-1β and TGF-β differentiate T cells to T_H17 through RORγt and STAT3 activation, IL-4 to T_H2 via GATA3 and STAT6, and TGF-β to T_{REG} via FoxP3 and STAT5 activation (Raphael et al., 2015). In addition, the extracellular milieu regulates the fate cytotoxic CD8 cells as well, which can also acquire a relative phenotype to that of a respective T helper cell (T_C1, T_C17, T_C2 etc.) (Mittrücker et al., 2014).

Each of the pre-mentioned T cell subtype predominates in a certain immune response to infectious agents, but particular subtypes have been also implicated in immunological disorders, such as allergies, autoimmune and inflammatory diseases. A hyperactive immune response can lead to a serious condition known as cytokine release syndrome (CRS). This acute syndrome is characterized by dysregulated massive release of cytokines, such as IL-6, TNF-α, IFNγ and IL-10, causing life-threatening adverse events (Shimabukuro-Vornhagen et al., 2018). Current treatments majorly rely on immunosuppressant molecules and biologics, such as cyclophosphamide, corticosteroids, IL-1 receptor antagonist (anakinra) and anti-IL-6 therapy (Tvedt et al., 2021; Shimabukuro-Vornhagen et al., 2018).

Depending on their maturation status, proliferative capacity, tissue homing and effector functions T cells, they are further divided into naïve, memory and effector cells (Mousset et al., 2019). Thus, naïve T (T_N) cells that have not yet recognized any exogenous peptide presented on MHC molecules express CD45RA, CD62L, CCR7 and CD127 (IL-7Rα) (Mousset et al., 2019; Golubovskaya & Wu, 2016). Upon activation, T cells differentiate into memory cells, a phenotype

that enables their proliferation and clonal expansion. Stem cell-like memory T cells (T_{SCM}) are defined by the expression of CD62L, CCR7, CD45RA and CD95 (Fas), and they have been shown to persist better in tumors than other phenotypes (Gattinoni et al., 2011). Central memory (T_{CM}), expressing CD62L, CD45RO and CCR7, reside in secondary lymphoid organs (lymph nodes, spleen, Peyer's patches) and effector memory T cells (T_{EM}), expressing CD45RO, reside in tissues. Both of these phenotypes quickly expand upon subsequent encounter with the specific antigen, resulting in a faster and more effective secondary immune response (Mousset et al., 2019; Golubovskaya & Wu, 2016). Finally, the effector T cells (T_{EFF}) are short-lived antigen-specialized cells, expressing CD45RA (+/-), CD45RO (+/-), CD25 and other effector molecules, such as CD95, KLRG1, IFNγ or other cytokines and cytolytic enzymes (perforin and granzymes) (Mousset et al., 2019; Golubovskaya & Wu, 2016; Henson & Akbar, 2009). T_{REG} cells display similar phenotypes, while they are also recognized by the expression of CD25 and immune checkpoint inhibitors, such as CTLA-4 and PD-1 (Golubovskaya & Wu, 2016).

When T cells encounter the antigen persistently, they tend to deteriorate and lose their functional ability to eliminate the pathogen. That is especially observed in chronic infections, cancer and inflammatory diseases (Schietinger & Greenberg, 2014; Wherry, 2011). Hence, molecules expressed on dysfunctional T cells have been associated with the regulation of their activation, proclaiming their exhaustion phenotype. Such markers include LAG3, TIM3, PD-1, CTLA-4, 2B4, CD160 and BTLA (Schietinger & Greenberg, 2014; Wherry, 2011).

Overall, T cells comprise an attractive resource for adoptive immunotherapy, as they are able to be easily *ex vivo* expanded, manipulated and re-infused into the patients. They display potent effector capacity, remain highly specific against their targets and have long lasting lifespan.

1.1.2 Chimeric antigen receptor T cell therapy

Since it has been firstly described by Gross et al. (1989), CAR T cell immunotherapy has been sharply developed, bringing next-generation receptors in clinical applications, with profound outcomes, especially in acute lymphoblastic leukemia (ALL) and B cell malignancies (Maude et al., 2018; Schuster et al., 2017; Maher et al., 2002). Tumor remission is achieved by re-directing the natural target of the T cells and subsequently the effector functions against a tumor extracellular marker, which in case of B cell leukemias most frequently is the CD19 molecule (Maude et al., 2018; Schuster et al., 2017; Maher et al., 2002).

The structure of the CAR molecule has been optimized from the first simplified version to second, third and fourth generations, which are currently in use (Hartmann et al., 2017; Chmielewski & Abken, 2015). In more details, CAR molecules comprise the extracellular targeting domain, bearing a single-chain variable fragment (scFv) antibody, which recognizes the tumor

antigen (i.e. CD19), followed by a flexible hinge region linked to a transmembrane domain (Figure 1). The intracellular signaling domain is typically composed of either CD28 or 4-1BB co-stimulatory domain, while the final activation step is mediated by a CD3ζ (Figure 1). The combination of two co-stimulatory domains or the co-expression of a cytokine or ligand classifies the CAR into 3rd or 4th generation, respectively (Figure 1).
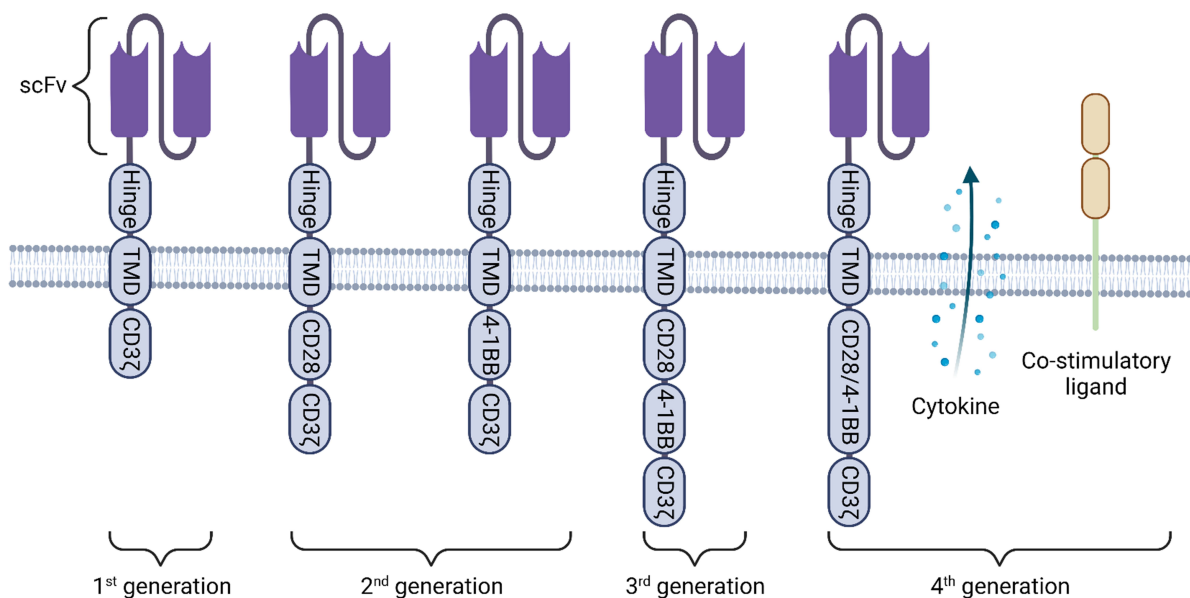
Figure 1: Molecular structure of CAR and next-generation therapies.
Structural characteristics of a CAR molecule, composed of single-chain variable fragment (scFv) antibody region targeting the tumor antigen (i.e. CD19), a flexible hinge region and a transmembrane domain (TMD), followed by the intracellular signaling domain. Different generations of CAR T cell therapeutic products are depicted here. Created with BioRender.

1.1.3   Current practices and challenges for manufacturing CAR T cells

The manufacturing of a CAR T cell infusion product is a multistep complex procedure. T cells are isolated from the peripheral blood of a donor (allogeneic) or the patient (autologous) in a procedure called leukapheresis. In order to genetically engineer and expand the T cells, a 1- to 3-day pre-activation step with anti-CD3, anti-CD28 antibodies and cytokines, IL-2 or IL-7 and IL-15, is required (Hartmann et al., 2017; Mock et al., 2016). Then, the gene of interest (CD19-CAR) is transferred via a lentiviral or γ-retroviral vector, which stably integrates the transgene into the genomic DNA. The cellular transduction is followed by 8-10 days expansion and the adoptive transfer into the patient (Mock et al., 2016). The implementation of a fully automated system, such as the CliniMACS® Prodigy from Miltenyi Biotech, carrying out all the pre-mentioned steps till CAR T cell expansion is a way to automate the manufacturing, limiting human errors and minimizing cell loss and contaminations (Mock et al., 2016).

Several factors can affect the outcomes in CAR T cell therapy, but foremost the cellular composition and diversity of the *ex vivo* generated CAR T cell product. Thus, the persistence of CAR T cells into patients has been associated with the frequency of CD4 and central memory cells present in the pre-infusion product (Louis et al., 2011). In addition, conditioning of patients with lymphodepleting regimen prior CAR T cell infusion has shown a faster *in vivo* expansion, greater persistence and longer disease-free survival (Turtle et al., 2016; Dai et al., 2015). The stimulation and cultivation of T cells in presence of IL-7 and IL-15, rather than IL-2, promotes the development of the beneficial T_{SCM} phenotype in the pre-infusion product, associated with better antitumor activity (T. Zhang et al., 2015; Xu et al., 2014).

The compromised fitness of harvested T cells, especially from elderly patients undergoing series of chemotherapies, is correlated with lower antitumor response rates, thus allogeneic cell therapy might be more preferable (P. H. Mehta et al., 2021). Even though the use of off-the-self CAR T cell products has many benefits regarding standardization, quality and quick availability, the risk of graft-versus-host disease (GvHD) remains critical. However, various approaches have been developed to ablate GvHD, such as generation of CAR T cells from umbilical cord blood stem cells, deletion or interruption of the TCR locus and use of non-T cell sources, such as natural killer (NK) cells (Depil et al., 2020; R. S. Mehta & Rezvani, 2018; Brudno et al., 2016; Poirot et al., 2015). In addition, encoding the 4-1BB instead of CD28 co-stimulatory domain can minimize the exhaustion of CAR T cells driven by the CAR tonic signaling itself (Long et al., 2015).

CAR T cell therapy is not limited to hematological malignancies, but it has been also used for solid tumors. However, the outcomes are so far not as impressive as for leukemias (K. Chen et al., 2022; Safarzadeh Kozani et al., 2022; Marofi et al., 2021). Major challenges need to be overcome when CAR T cell therapy is intended for solid tumors. The infiltration of CAR T cells into tumor sites is evidently among the most important prerequisites for tumor eradication, but also the lowest possible on-target off-tumor toxicity, achieved by discriminating tumor cells from healthy tissue (Marofi et al., 2021; Ma et al., 2019; H. Zhang et al., 2016). In addition, the immunosuppressive tumor microenvironment considerably impacts the killing efficiency of CAR T cells, thus more innovative strategies should be considered in regard to CAR T cell therapy in solid tumors (Marofi et al., 2021; Ma et al., 2019; H. Zhang et al., 2016).

The current gene editing tools have been mainly applied *ex vivo,* but several efforts have brought promising *in vivo* gene delivery applications in clinical trials. Lipid nanoparticles and adeno-associated vectors (AAVs), coupled with CRISPR-Cas9 or other gene targeting nucleases, have been utilized for stable transgene insertion into target cells *in vivo*, for treating mainly hepatocytes due to their scavenging functionality or isolated compartments, such as retinal cells in the eye (Maeder et al., 2019; Lokugamage et al., 2018; Finn et al., 2018). *In vivo* CAR T cell

5

generation though has been achieved so far in mouse models, utilizing T cell specific lentiviral vectors or lipid nanoparticles coupled with targeting molecules, such as scFv or designed ankyrin repeat proteins (DARPins), which selectively transduce T cells (Michels et al., 2022). Bypassing the complex *ex vivo* manufacturing process would minimize the risks and the high costs, but would also provide a more straightforward and universal standard operating procedure (Xin et al., 2022).

Overall, the complicated nature of the CAR T cell product remains a challenge to control in individualized medicine, as different cellular compositions and fitness can influence the outcomes. By optimizing the therapeutic product and identifying more insights, life-threatening adverse events, such as CRS, immune effector cell-associated neurotoxicity syndrome (ICANS) and on-target off-tumor toxicity, could be hampered and tumor-free survival could be improved.

1.2   LENTIVIRAL VECTOR

Lentiviral vectors (LV) have been widely utilized in gene therapy as a versatile and efficient gene delivery tool in eukaryotic cells, since the discovery of the human immunodeficiency virus type 1 (HIV-1). The vector is produced by co-transfecting producer cells with a plasmid cassette transcribing the main components of a functional, but replication-deficient, vector, including its transferred RNA genome. Upon cell entry and reverse transcription, the gene of interest integrates into the genomic DNA, and the incorporated gene is transcribed, leading to the expression of a functional protein. In order to alter the tropism of LVs, the envelope proteins can be engineered with different targeting molecules, such as a scFv or a DARPin. Hence, transforming LVs into a more selective tool, *in vivo* gene transfer to T cells has become feasible. Studying the life-cycle of the HIV-1 and other viruses has revealed innate cellular antiviral restriction factors, which can influence the efficiency of LVs as well.

1.2.1   History and technical aspects of the 2nd generation lentiviral vector

While the concept of gene therapy was introduced in early 1970s, the development of a gene transfer has been burst since the discovery and first isolation of the HIV-1 from a patient with acquired immunodeficiency syndrome (AIDS) by Luc Montagnier and his colleagues in 1983 (Friedmann, 1992; Barré-Sinoussi et al., 1983). Although the Moloney murine leukemia virus (MLV) based replication deficient γ-retroviral vector was the first to be generated and used for gene transfer and integration into cells, it can only transduce dividing cells (Miller et al., 1990; Mann et al., 1983). On the other hand, HIV-derived LVs have been proven to be an effective and flexible tool for gene transfer and integration into non-diving cells (Marcucci et al., 2018; Naldini et al., 1996; Richardson et al., 1995).

By fragmentizing the HIV-1 genome into separate plasmids expressing the structural components of the packaging (*gag, pol*), the envelope (*env*) and the transfer gene (gene of interest – GOI) under the influence of a human cytomegalovirus promoter (CMV), it has become possible to *in vitro* generate lentiviral vectors (Figure 2). To deprive the vectors from other virulent factors of the HIV-1, nef, vpr, vpu and vif accessory proteins have been removed from the packaging plasmid, while necessary elements have been retained (Luban & Goff, 1994; H. J. Kim et al., 1994; Aldovini & Young, 1990; Lever et al., 1989). Two other regulatory factors are present in the packaging plasmid of a 2nd generation LV system, *tat* and *rev* expressing genes, whereas in the 3rd generation LV, the *tat* has been deprecated and *rev* has been separated from the packaging plasmid (Johnson et al., 2021; Dull et al., 1998). The latter is responsible for post-transcriptional nuclear export of the viral gRNA via binding to the rev-responsive element (RRE), while the Ψ element drives the encapsidation of the two single-stranded genomic RNA (ssRNA) molecules into the LV (Johnson et al., 2021). Another element, the central polypurine tract (cPPT), might be implicated in integration of viral genome into host, however it is not yet fully understood (Johnson et al., 2021). The LV transfer genome, surrounded by two long terminal repeats (LTRs), integrates into the genomic DNA of the target cell. The LTRs comprise three regions, the U3, which serves as a promoter and enhancer promoting the transcription of viral gRNA from the R region until the polyadenylation signal situating in ΔU3/R, in 3'-LTR (Pereira et al., 2000; Richardson et al., 1995; Guntaka, 1993). Deletion in the U3 region of the 3'-LTR causes the inactivation of the U3 promoter in 5'-LTR, in the integrated construct, letting only the gene of interest to be transcribed from its promoter, frequently either the CMV or the spleen focus-forming virus (SFFV) promoter. Following the gene of interest, the woodchuck hepatitis virus posttranscriptional regulatory element (WPRE) serves as an enhancer for the transgene mRNA integrity, improving the expression of the gene (Zufferey et al., 1999).

In order to alter the natural tropism of the HIV-1, the envelope gene has been replaced by the vesicular stomatitis virus glycoprotein (VSV-G), which binds to low-density lipoprotein receptor (LDLR), in fact expressed on the surface of every cell (Finkelshtein et al., 2013; Naldini et al., 1996; Lusso et al., 1990).
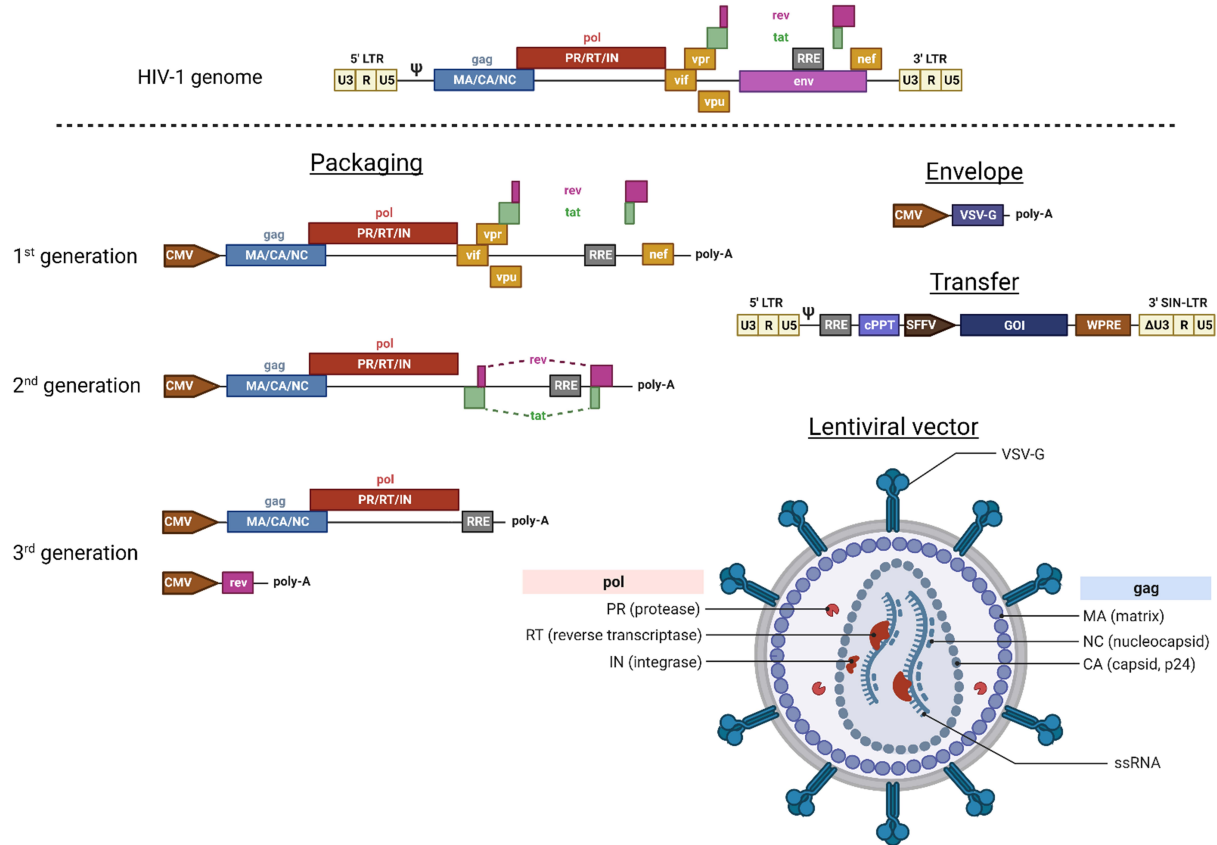
Figure 2: Plasmid cassette and molecular structure of a lentiviral vector.
Origin of lentiviral vector plasmid cassette, transcribing the key components for a functional vector in transfected HEK293 cells. *RRE:* rev-responsive element, *GOI:* gene of interest, *CMV:* human cytomegalovirus promoter, *LTR:* long terminal repeat, *SIN:* self-inactivating, *WPRE:* woodchuck hepatitis virus posttranscriptional regulatory element, *SFFV:* spleen focus-forming virus promoter, *cPPT:* central polypurine tract. Adapted from BioRender template of "HIV Genome and Structure".

Typically, the plasmids are chemically co-transfected into producer human embryonic kidney 293 (HEK293) cells, LVs are harvested from the supernatant and concentrated through sucrose cushion centrifugation (Backliwal et al., 2008).

1.2.2 CD8 and CD4 receptor-targeted lentiviral vectors

The VSV-G glycoprotein mediates both, binding to LDLR and membrane fusion activity, while it also renders VSV-LV capable of transducing almost any human cell (Figure 3) (Finkelshtein et al., 2013). Although LDLR is expressed by the majority of cells, its expression in T cells is induced only upon stimulation (Amirache et al., 2014). Hence, T cells need to be activated with a regimen comprising anti-CD3, anti-CD28 and either IL-2 or IL-7 and IL-15 cytokines, to enable their transduction by VSV-LV (Mock et al., 2016; Amirache et al., 2014).

Introducing two separate mechanisms for LV attachment and cell penetration have broadened the spectrum of engineering LVs for retargeting purposes. Especially, paramyxoviral envelope

proteins have served for such engineering repurposing. Nipah glycoprotein (G) or measles hemagglutinin (H) have been successfully modified by mutationally destructing their natural tropism, while simultaneously fusing to a scFv or a DARPin, selective for a molecule constitutively and uniquely expressed on cells of interest (Figure 3) (Frank & Buchholz, 2019). Upon recognition and attachment to the target cells, a truncated version of the respective viral fusion protein (F) mediates the cell entry (Figure 3).
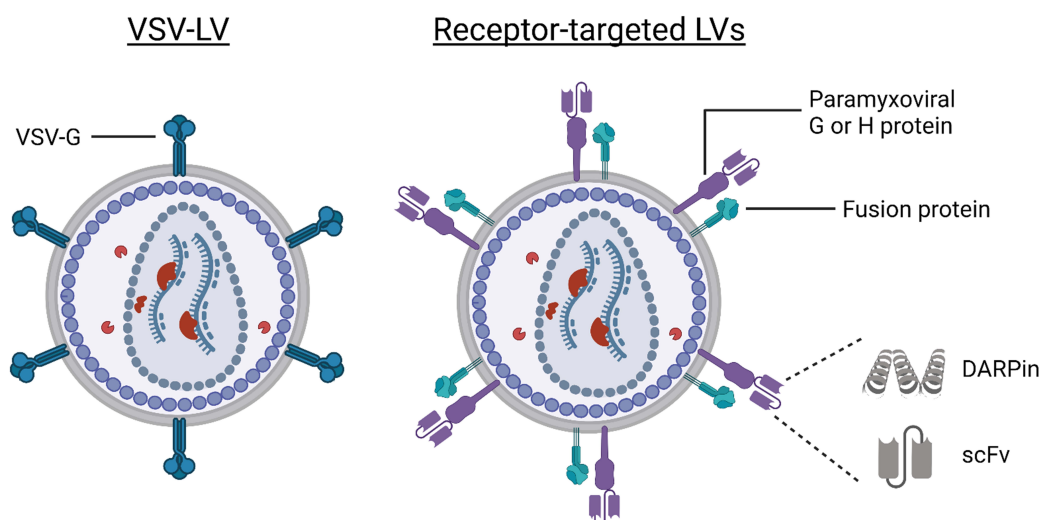
Figure 3: Molecular structure of VSV-LV and receptor-targeted LVs.
VSV-G glycoprotein expressed on a vector conferring both targeting and fusion activity (left), while receptor-targeted LVs utilize a targeting domain, composed of either DARPin or scFv, conjugated to a paramyxoviral G or H protein. Fusion is mediated by a truncated fusion protein.

The development of CD8 Nipah- and CD4 measles-pseudotyped receptor-targeted LVs has recently become a powerful tool in targeted gene therapy. Capable of transducing resting or minimally activated T cells, both CD8-LV and CD4-LV have displayed high T cell receptor-specific selectivity (Pfeiffer et al., 2018; Bender et al., 2016; Zhou et al., 2015). Apart from the potent *ex vivo* transduction efficacy, CD8-LV and CD4-LV can modify target T cells *in vivo*, in NSG mouse models humanized with either CD34 stem cells or PBMC (Agarwal et al., 2019, 2020; Pfeiffer et al., 2018; Zhou et al., 2015). Even though it has not been proven yet for CD4-LV and CD8-LV, indirect evidences of measles pseudotyped HER2/*neu* targeted LV (D9.29-LV) can resemble the minimal to abrogated off-target gene transfer, especially escaping the uptake by hepatocytes (Münch et al., 2011).

In a clinically applicable aspect, CD8-LV and CD4-LV have enabled the *in vivo* generation of CAR T cells in humanized NSG mice. The direct *in vivo* transduction of target T cells with CD8-LV and CD4-LV encoding CD19-CAR has shown prominent tumor eradication and increased survival of the xenograft mouse model, but also good tolerability (Agarwal et al., 2019, 2020; Pfeiffer et al., 2018).

In general, apart from T cells, other immune cells expressing the CD8 or CD4 receptors can be targeted and potentially modified by CD8-LV or CD4-LV. These are some subsets of dendritic cells (DCs), natural killer (NK), NK T cells (NKT) and γδ T cells for CD8α (Agarwal et al., 2019), as well as DCs, monocytes, macrophages and γδ T cells for CD4 (Ziegler et al., 2014; Jardine et al., 2013).

Transduction enhancers, facilitating the attachment of LVs to cells by neutralizing the repulsive negative charges of the membranes, have been widely utilized *ex vivo* to increase the potency of the LV-mediated gene transfer. Among them, the cationic polymer polybrene increases the transduction efficiency of the conventional VSV-LV on human T cells (Rajabzadeh et al., 2021). In the concept of T-cell targeted vectors, the histidine-rich amphipathic peptide vectofusin-1 has been shown to substantially improve the *ex vivo* gene transfer mediated by CD8-LV and CD4-LV (Jamali et al., 2019).

1.2.3 Cellular transduction and innate antiviral restriction factors

The structural differences of VSV-LV and receptor-targeted LVs confer unique cell entry pathways to these vectors. VSV-LV enters the cell via clathrin-mediated endocytosis and trafficking into endosomes (Figure 4) (Duvergé & Negroni, 2020; Frank & Buchholz, 2019). There, the low pH alters the conformation of VSV-G, which leads to membrane fusion and exit of the pre-integration complex (PIC) into the cytoplasm (Florkiewicz & Rose, 1984; Riedel et al., 1984). Receptor-targeted LVs enter in a more direct way, mediating fusion at the cell membrane (Figure 4), according to evidences of cell entry pathway of wild-type measles virus and Nipah pseudotyped LV or wild-type virus (Frank et al., 2020; Aguilar & Iorio, 2012; Navaratnarajah et al., 2009).

The different steps of the LV-mediated transduction can be affected by innate antiviral restriction factors, regulated especially by the type I IFN pathway (Colomer-Lluch et al., 2018; Schoggins, 2014). Thus, viral entry can be inhibited by the interferon-induced transmembrane proteins (IFITMs), particularly IFITM1 expressed on the cell membrane can prevent enveloped viruses from fusing directly to the target cell (S. E. Smith et al., 2019; Weston et al., 2014). On the other hand, IFITM2 and IFITM3, residing in endosomal compartments, can inhibit viruses entering pH-dependently (X. Zhao et al., 2019; Weston et al., 2014; Lu et al., 2011). Another potent inhibitor, SAMHD1, hydrolyzes and reduces dNTPs, impairing the viral reverse transcriptase enzymatic activity (Colomer-Lluch et al., 2018; Schoggins, 2014). In addition, other interferon-stimulated gene (ISG) products can sense and degrade non-self RNA (PARPs, ISGs, OAS, ADA2) and inhibit nuclear entry, transgene expression or other pathways during cell transduction (IFITs, IFIs, MX, TRIMs, GBPs, EIF2AK2) (Figure 4). Most of the type I IFN inducible genes are under the influence of IFN related factors (IRFs), maintaining the intrinsic pool of antiviral restriction

factors in any cell (Panda et al., 2019; Jefferies, 2019). On the other hand, cyclophilin A (PPIA) and proteins from the nuclear pore complex (NPC) associate with the pre-integration complex of the LVs and facilitate the trafficking and translocation into the nucleus (Figure 4) (Di Nunzio et al., 2012; Braaten & Luban, 2001).
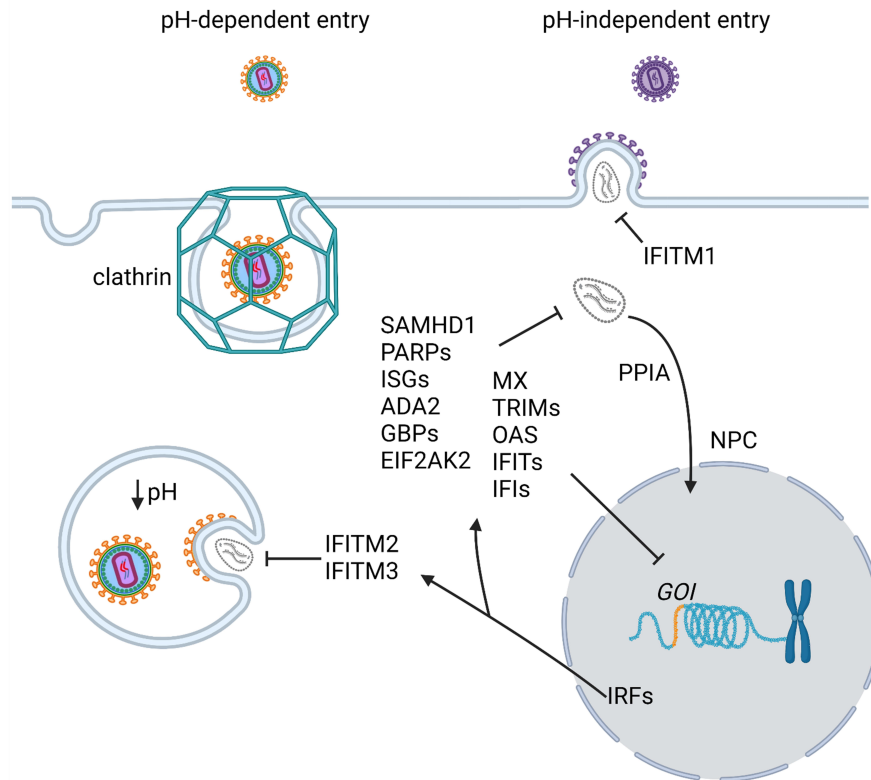
Figure 4: Entry pathways and innate inhibitory mechanisms of pH-dependent and pH-independent LVs.
A pH-dependent LV (i.e. VSV-LV) enters via clathrin-mediated endocytosis and the glycoprotein orchestrates the membrane fusion in endosomes at lower pH. A pH-independent LV enters via direct fusion to the cell membrane. All the steps from the LV entry to transgene expression are influenced by antiviral restriction mechanisms, some of them are listed here. *NPC:* nuclear pore complex, *GOI:* gene of interest. *IFI(T):* interferon-induced. *ISG:* IFN-stimulated genes. *PPIA*: cyclophilin A. Created with BioRender.

By alleviating intrinsic antiviral restriction mechanisms, it is possible to enhance the infectivity of viruses, subsequently the LV-mediated gene transfer and integration. Such an example is the inhibition of the mammalian target of rapamycin by the homonymous small molecule. The pre-treatment of hematopoietic stem and progenitor cells (HSPC) with rapamycin has shown to enhance their genetic modification by VSV-LV, through downmodulation of IFITM2 and IFITM3 (G. Shi et al., 2018; Petrillo et al., 2015; L. Li et al., 2014; C. X. Wang et al., 2014). This ameliorates the pH-dependent entry of the VSV-LV via envelope fusion to endosomal membrane and subsequent release of the viral capsid into the cytoplasm.

Next cellular defense is the SAMHD1 protein, which inhibits the reverse transcription of the two viral genomic copies of ssRNA (Colomer-Lluch et al., 2018; Schoggins, 2014). Both IL-7 and IL-15 cytokines have shown to phosphorylate SAMHD1 in CD4 T cells, leading to increased HIV-1 infectivity (Manganaro et al., 2018; Coiras et al., 2016). In addition, lentiviruses, including HIV-2 and simian immunodeficiency virus (SIV), express the Vpx accessory protein, which directly inhibits SAMHD1, facilitating the life-cycle and replication of them (Hofmann et al., 2012). While HIV-1 does not express any homologous to Vpx, by incorporating the SIV Vpx molecule into LVs has been shown to improve their transduction efficiency (Tada et al., 2022; Baldauf et al., 2012).

Regarding capsid trafficking, cyclophilin A (CypA) is known to coat, stabilize and protect the viral capsid from inhibitory mechanisms, and it regulates its nuclear translocation (C. Liu et al., 2016; Braaten & Luban, 2001). The protection is mediated through preventing the restriction factor TRIM5α to interact with the viral capsid (K. Kim et al., 2019; Hatziioannou et al., 2004; Towers et al., 2003). However, cyclosporin A (CsA), which competes for the CypA capsid binding site, has been shown to enhance the *ex vivo* infectivity of HIV-1 up to 50- and 100-fold in human and non-human primates cells, respectively (Towers et al., 2003). The use of CsA can also improve VSV-LV-mediated transduction of HSPC (Petrillo et al., 2015). This enhancement has been also associated with the alteration of capsid binding to nucleoporins and nuclear import pathway (Schaller et al., 2011).

1.3 NEXT-GENERATION SEQUENCING

Next-generation sequencing (NGS) is a state-of-the-art technological application for conducting in-depth characterization of cellular transcriptomes and genomes. Both DNA and RNA sequencing have provided insights for differential gene expression and splicing, DNA mutations or chromatin condensation states. Different methodological approaches in NGS, such as DNA-sequencing (DNA-seq), ATAC-seq, RNA-seq as well as SMART-seq, have been developed and utilized as monitoring tools in clinical applications to diagnose a disease, predict the progression and even modify treatments in a prospective manner. Both, bulk and single-cell high-throughput sequencing can be achieved and the vast majority of library preparation methods are compatible with the Illumina sequencing platform. For single cell isolation and DNA or RNA processing, droplet- and nanowell-based systems are used. Focusing on single-cell RNA sequencing (scRNA-seq), while whole transcriptome analysis provides an unbiased readout of the total differentially expressed genes, the targeted gene analysis facilitates a more focused investigation of the most relevant genes in higher sensitivity and better resolution (Pokhilko et al., 2021; Mair et al., 2020).

1.3.1 DNA sequencing

Developed in 1977 by Sanger et al., the homonymous DNA 1st generation sequencing method revolutionized the field of genomic research, bringing scientists one step closer to understand the living matter. The technological advancements of automation and replacement of radiolabeling with a fluorescence detection approach in Sanger sequencing led to initiation of ambitious genome sequencing projects, such as the Human Genome Project (Collins & Fink, 1995; L. M. Smith et al., 1986). However, the low throughput of sequencing one DNA molecule at a time and the high cost makes this method unsuitable for analyzing enormous genomes (Petersen et al., 2017).

Overcoming these challenges, the NGS techniques have enabled the simultaneous massive parallel sequencing of thousands or even million molecules (Hall, 2007). Various NGS platforms have emerged, among them the most popular is the Illumina sequencing platform (Garrido-Cardenas et al., 2017). DNA libraries are sequenced on a chip, where the technology allows the detection of fluorescently-labelled nucleotide bases incorporated into the newly synthetized complementary strand during a polymerase chain reaction (PCR) (Morozova et al., 2009). The principle is similar to Sanger sequencing and relies on the blockade of PCR amplification by the labeled analogs, but this termination is reversible and the amplification continuous in contrast to Sanger's (Garrido-Cardenas et al., 2017; Morozova et al., 2009). The molecules are captured in the Illumina cartridge by primers complementary to the adapter sequences ligated to the two extremities of the DNA molecule, priming also the amplification, particularly called bridge amplification, for each cycle (Garrido-Cardenas et al., 2017).

The output provides the coordinates of the raw reads in the chip, their sequence and the quality of each base pair detected by the device. Raw reads can be used for different aims, either to build a whole or partial genome of an organism, identify single nucleotide polymorphisms (SNPs), mutations, deletions, translocations or duplications. Various approaches have allowed delicate genetic investigations, such as assessing chromatin accessibility with the ATAC-seq, sequencing of immunoprecipitated chromatin regions with ChIP-seq, other epigenomic assessments, and even sequencing on a single-cell level (Buenrostro et al., 2015; P. J. Park, 2009).

1.3.2 Single-cell RNA sequencing

For transcriptomic analyses, sequencing libraries are prepared from cellular RNA source, for either bulk quantification measurements or single-cell resolution. The principle relies on reverse transcription of cellular messenger RNA (mRNA) to complementary DNA (cDNA), in a random or targeted amplification way and, eventually, sequencing the library of DNA molecules. Bulk RNA-seq can provide the average expression of a gene from a sample containing multiple cells from a tissue or a cell line, whereas scRNA-seq deciphers the profile of each individual cell. Such

information can display distinct cell populations residing in a tissue, cell subtypes from a formerly considered homogeneous tissue, and reveal novel cellular networks (G. Chen et al., 2019).

The isolation of single cells and processing can nowadays be carried out by microfluidics or nanowell cartridges (Prakadan et al., 2017). Chromium from 10X Genomics comprises the most common microfluidic system, conducting droplet-based single-cell isolation and processing of the genomic or transcriptomic content (Zheng et al., 2017). In addition, the nanowell-based single-cell capturing BD Rhapsody system has sped up the isolation and library preparation compared to Chromium (Gao et al., 2020; Shum et al., 2019).

Both systems have established various single-cell protocols, ameliorating thorough investigations, with the droplet-based approach to be more flexible in both DNA and RNA techniques than the BD Rhapsody (Gao et al., 2020). Hence, 3'-end sequencing for transcriptome analysis, 5'-end sequencing for TCR clonotyping of T cells (VDJ recombination), and extracellular protein analysis with oligo-conjugated antibodies (AbSeq) are possible to be performed with the BD Rhapsody pipeline (Gao et al., 2020). Whereas with 10X Chromium, in addition to the pre-mentioned, sequencing libraries can be prepared for full-length cDNA analysis, genomic DNA sequencing, scATAC-seq, scChIP-seq and so on (Gao et al., 2020; Tsoucas & Yuan, 2017). However, while the full-length cDNA analysis can reveal differential splicing events, SNPs and other information apart from the gene expression levels, it is relatively expensive compared to 3'-end or 5'-end sequencing (Sholder et al., 2020; Wilkening et al., 2013). Thus, the two latter provide a cost-effective solution for an efficient transcriptome analysis (Sholder et al., 2020; Wilkening et al., 2013).

Two different approaches have been developed for 3'-end scRNA-seq transcriptomic analysis, the whole transcriptome (WTA) and targeted gene analyses (TGA). WTA covers all mRNA transcribed genes in each cell, allowing an unbiased analysis and thorough exploration of genes and pathways. On the other hand, the TGA approach results in a higher resolution by selectively amplifying those genes relevant for the particular analysis, in a cost-efficient way (Mair et al., 2020). This approach allows sensitive detection of low-expressing genes at a low sequencing depth (Mair et al., 2020). Hence, while a typical WTA requires 50,000 reads per cell for a deep sequencing analysis, TGA can outperform between 2,000 to 4,000 reads per cell, ameliorating the analysis of 10-fold bigger sample size (Mair et al., 2020). In general, premade panels for amplifying and detecting genes associated with immune response, T cells and other are available by BD Biosciences and compatible with the BD Rhapsody pipeline (Mair et al., 2020). The addition of customized primers in order to expand the analyzed panel of genes and detect other targets is generally feasible (Mair et al., 2020).

1.4 OBJECTIVES

This thesis project primarily aimed at establishing a scRNA-seq pipeline with the BD Rhapsody system at Paul-Ehrlich-Institut in order to develop a protocol for monitoring the generation of CAR T cells by a receptor-targeted LV. An initial TGA approach was decided as the most suitable for high-resolution analysis, increasing the chance of distinguishing CAR expressing from nonexpressing cells. For that reason, it was necessary to implement customized primers for *CAR* mRNA detection and confirm whether they bind within the designated region at the 3'-end. Thus, the exact poly-A tail starting position had to be defined.

Furthermore, a subsetting method for distinguishing CAR T cells from non-transduced cells in scRNA-seq had to be optimized, especially when a multimodal gene expression was noticed. This allowed to evaluate whether the frequency of CAR T cells identified by protein expression matched with the scRNA-seq data. The use of CD8-LV validated the subsetting strategy as well for the VSV-LV incubated sample and allowed for the first time to interrogate the selectivity of a receptortargeted LV by scRNA-seq. Differences in transcriptomic profiles of cell subsets inoculated by CD8-LV and VSV-LV were investigated, with a special focus on successful LV-mediated transduction.

Although the TGA approach allowed a sensitive differential gene expression analysis, the WTA approach aimed to decipher more genes and pathways associated with the successful transduction of T cells or inhibition of LV-mediated gene transfer, and further validated the initial findings. In addition, the use of the CD4-LV allowed to evaluate whether the observations were also relevant for CD4 T cells.

By identifying any restriction factors inhibiting proper T cell transduction, their alleviation was a further goal in order to enhance LV transduction efficiency. Thus, potential enhancers downregulating or interfering with some of these pathways were screened. Selecting one good candidate, its ability to enhance *in vivo* gene transfer had to be tested in a proof-of-concept study with humanized NSG mice injected with CD8-LV delivering GFP expressing gene. A whole proteome analysis deciphered other possible targets of the transduction enhancer and provided clues regarding other alterations in protein expression of T cells. Furthermore, the impact of the transduction enhancer on CAR T cell performance and the transduction efficiency for *in vivo* gene transfer had to be examined with a CD19-CAR transferring CD8-LV in humanized NSG mice, engrafted with tumor cells. Induction of *in vivo* CAR T cell generation as well as the tumor response were monitored.

2 RESULTS

2.1 TARGETED GENE ANALYSIS

Commencing with the first in-house scRNA-seq at Paul-Ehrlich-Institut (PEI), the technology needed to be established in our lab in a way to be compatible with our research tools. Firstly, targeted gene analysis (TGA) of CAR T cells generated with CD8-LV or VSV-LV was decided to be performed, analyzing 399 genes related with immune response. By carrying out TGA scRNA-seq, a high resolution and sensitive detection of the analyzed genes and CAR T cells was aimed. Customized primers amplifying and, thus, detecting *CAR* mRNA expressing T cells were also implemented. The high selectivity of CD8-LV on target cells was confirmed for the first time by scRNA-seq and differentially expressed genes were identified in the examined cell subsets. In addition, the use of the CD8-LV validated the subsetting strategy for distinguishing transduced from non-transduced cells. Finally, the consequences of the vector exposure to the cells and transcriptomic differences between transduced and non-transduced cells were explored. The following section presents the published data of Charitidis et al. (2021), but also adjacent to these. Practical help during sample preparations was kindly offered by Elham Adabi (PEI), while validation of data analysis was done by Dr. Colin Clarke (National Institute for Bioprocessing, Research and Training (NIBRT, Ireland). Technical and customer support for primer customization were provided by Dr. Vadir Lopez-Salmeron, Edyta Kowalczyk, Dr. Siobhan Cashman (all BD Biosciences, Europe).

2.1.1 Identifying the polyadenylation starting site in gRNA and CAR gene cassette for primer design in targeted gene panel

For the detection of CAR T cells by targeted gene amplification scRNA-seq it was necessary to customize two primers binding at the 3' end of the *CAR* gene within 800 bp close to the polyadenylation (poly-A) tail. The limitations regarding primer design include the distance from the poly-A tail where the primers can target and the avoidance of primer-dimer formation with the rest of pre-defined primers from the targeted panel in use. While the latter is assessed by the manufacturer's *in silico* pipeline, for the former the region that primers bind is within the 800 bp close to the poly-A starting site needed to be validated.

Initially, the poly-A signal hexamer (5'-AATAAA-3') was *in silico* predicted to be located in the 3' self-inactivating (SIN) long terminal repeat (LTR), which also aligns with the already known findings in HIV virology (Valsamakis et al., 1991). Based on that prediction and the expectation

that poly-A starting point should be located 10-30 nucleotides after that hexamer (J. Zhao et al., 1999), primers were designed by BD Biosciences and tested (N1_BD, N2_BD shown in 0).

For the exact identification of the poly-A starting point of the CD19-CAR, MOLT4.8 cells were inoculated with VSV-LV transferring the CAR transgene at MOI of 4, after 1 day cells were washed twice to remove any remnant LV and transduced cells were expanded for 6 more days, reaching a transduction of 98% (Figure 5A). To confirm that both CAR mRNA and viral gRNA share the same poly-A signal and starting site, total RNA was extracted from both transduced cells and LVs. Plasmid contaminants were observed to be present in LV stocks, thus both cellular mRNA and viral gRNA were purified with DNase I before the cDNA synthesis (Figure 5B).
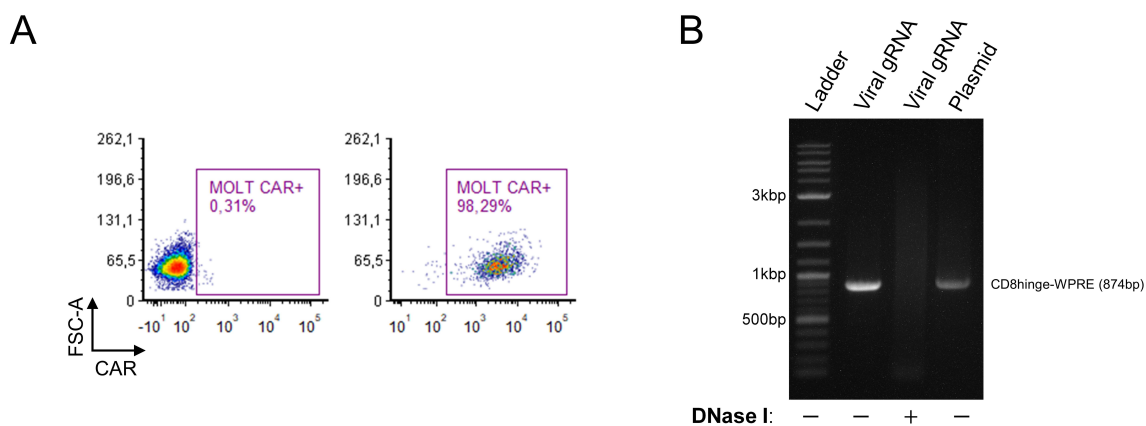
Figure 5: CAR mRNA and viral gRNA extraction.
(**A**) MOLT4.8 cells inoculated with VSV-LV (MOI=4) and expanded for 7 days. (**B**) PCR amplification of CAR transgene region between CD8 hinge and WPRE (874 bp). Viral gRNA was used as template, purified or not with DNase I.

Reverse transcription was performed with the 3' RACE kit as described in 4.2.1.13, incorporating an adapter at the 3' end of the gene after the poly-A tail. The cDNA was PCR amplified and the DNA amplicons were extracted from the agarose electrophoresis gel and sequenced (Figure 6A). Plasmid DNA was included as a control. The sequencing results were aligned to the reference plasmid, where both viral gRNA and CAR mRNA were confirmed to harbor the same poly-A tail starting point located in the 3' self-inactivating (SIN) long terminal repeat (LTR), 20 nucleotides after the poly-A signal site (Figure 6B).
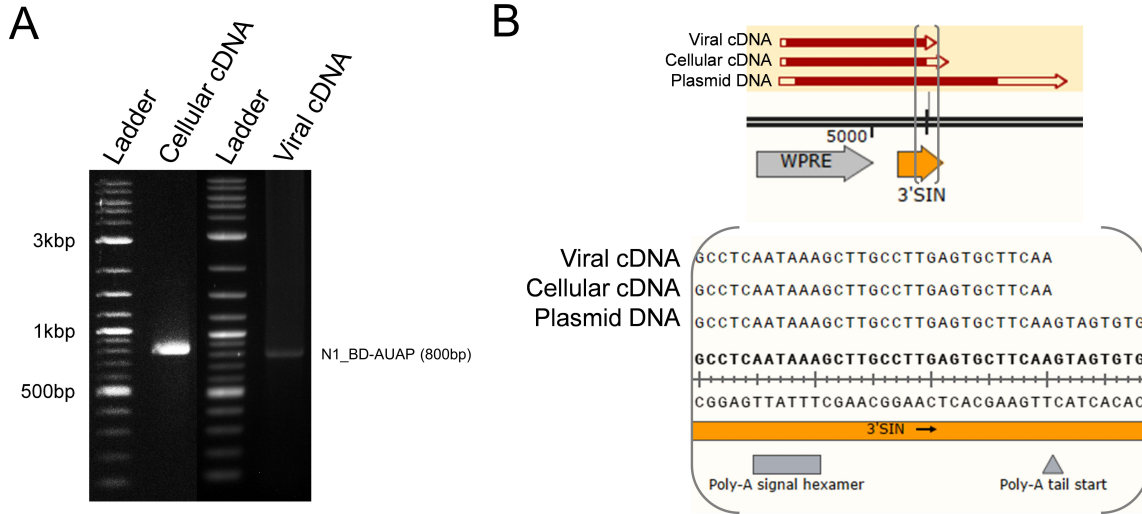
Figure 6: Cellular and viral cDNA 3' end gene amplification.
(**A**) Synthesized cellular and viral cDNA from DNase I digested RNA was PCR amplified with the N1_BD and AUAP primers (0), according to the 3' RACE kit's instructions (4.2.1.13), resulting in an amplicon of 800 bp. (**B**) Sequenced amplicons and plasmid DNA aligned to the reference transgene sequence. Poly-A starting site was found to be located 20 bp downstream of the signal site. SIN: self-inactivating. (Source: SnapGene).

Hence, the TGA scRNA-seq primers designed for the detection of the CD19-CAR mRNA transcribed in the transduced cells were confirmed to bind within the ideal distance from the poly-A tail (Figure 7).
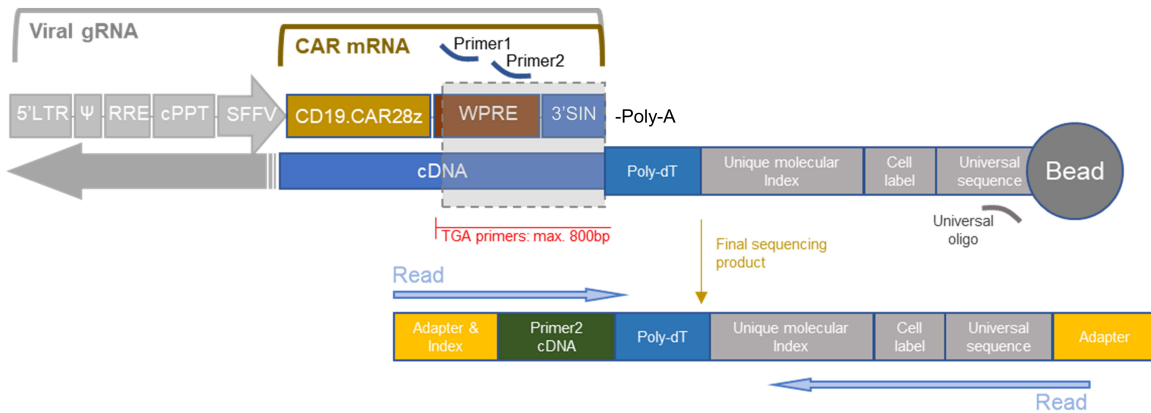
Figure 7: Detection of CAR mRNA.
Detection of CAR mRNA expression in transduced cells and/or viral gRNA in TGA with the customized primers (primer 1 ~N1_BD, primer 2 ~N2_BD). Barcode elements identifying cell and mRNA molecules are coupled with magnetic beads. Details for sequencing are described in 4.2.6.8. Adapted from Charitidis et al., 2021.

2.1.2   Experimental layout of TGA

The first in-house scRNA-seq analysis was performed on 6-day expanded CAR T cells generated from PBMC of one donor with CD8-LV or VSV-LV. More specifically, cryopreserved human PBMC were thawed and pre-activated with anti-CD3 and anti-CD28 in a T cell medium supplemented with IL-7 and IL-15 cytokines. After 3 days, cells were spinoculated with a certain LV and cultured for 6 more days (4.2.2.6). Untransduced sample served as a control (Figure 8). This study aimed primarily to set-up the scRNA-seq pipeline, to compare mRNA and protein detection methods, to evaluate the selectivity of CD8-LV, to get an overview of differential expression along 400 genes related with the immune response and promptly to investigate transcriptomic profiles related with LV-mediated transduction, such as the differences between CAR+ and CAR- cells and the two vector types.
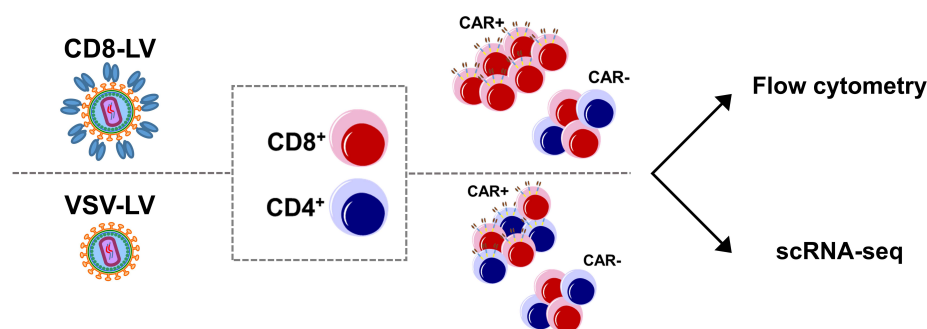
Figure 8: Experimental layout of the TGA study.
CAR T cells generated with VSV-LV or CD8-LV expanded for 6 days and processed for flow cytometry or scRNA-seq analysis. Adapted from Charitidis et al., 2021.

2.1.3   Downstream plotting and clustering analysis

Following the single cell RNA isolation, reverse transcription, PCR amplification and sequencing, the samples were then visualized to identify the composition of immune clusters, present in the bulk CAR T cell products.

After filtering out the low-quality cells (4.2.6.12), principal component analysis (PCA) was performed and the first 40 principal components were chosen for constructing the uniform manifold approximation and projection (UMAP) plots (Figure 9) (4.2.6.14, 4.2.6.15). Evaluating any technical variation driven from the three different cartridges that the samples were processed with, no distinct batch effect was observed in UMAP plot (Figure 9A). In order to characterize different immune cells present in the samples, unsupervised clustering analysis was initially performed, which identified 14 distinct clusters (Figure 9B).
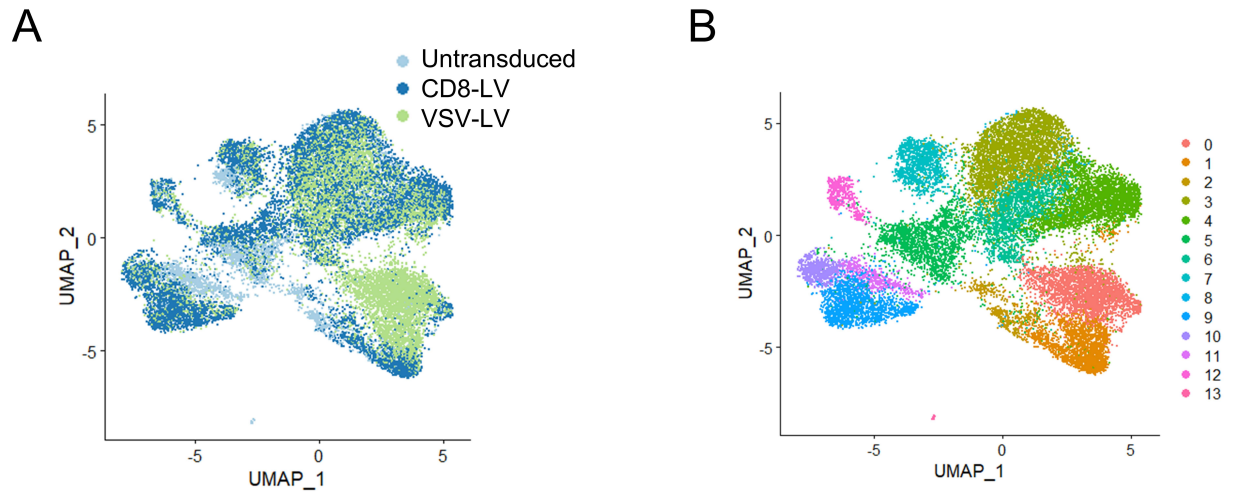
Figure 9: Targeted gene scRNA-seq analysis UMAP plots.
(**A**) UMAP plot of sample distribution and overlapping, evaluating cartridge-mediated technical variation. (**B**) Unsupervised clustering analysis. Adapted from Charitidis et al., 2021.

By examining the expression of marker genes certain for specific immune cells (*CD8A, CD4, TRDC, FCGR3A, MS4A1*), the major immune cell types were identified (Figure 10A). For better visualization purposes and easier representation of the data, clusters of the same cell type were subsequently merged (Figure 10B).
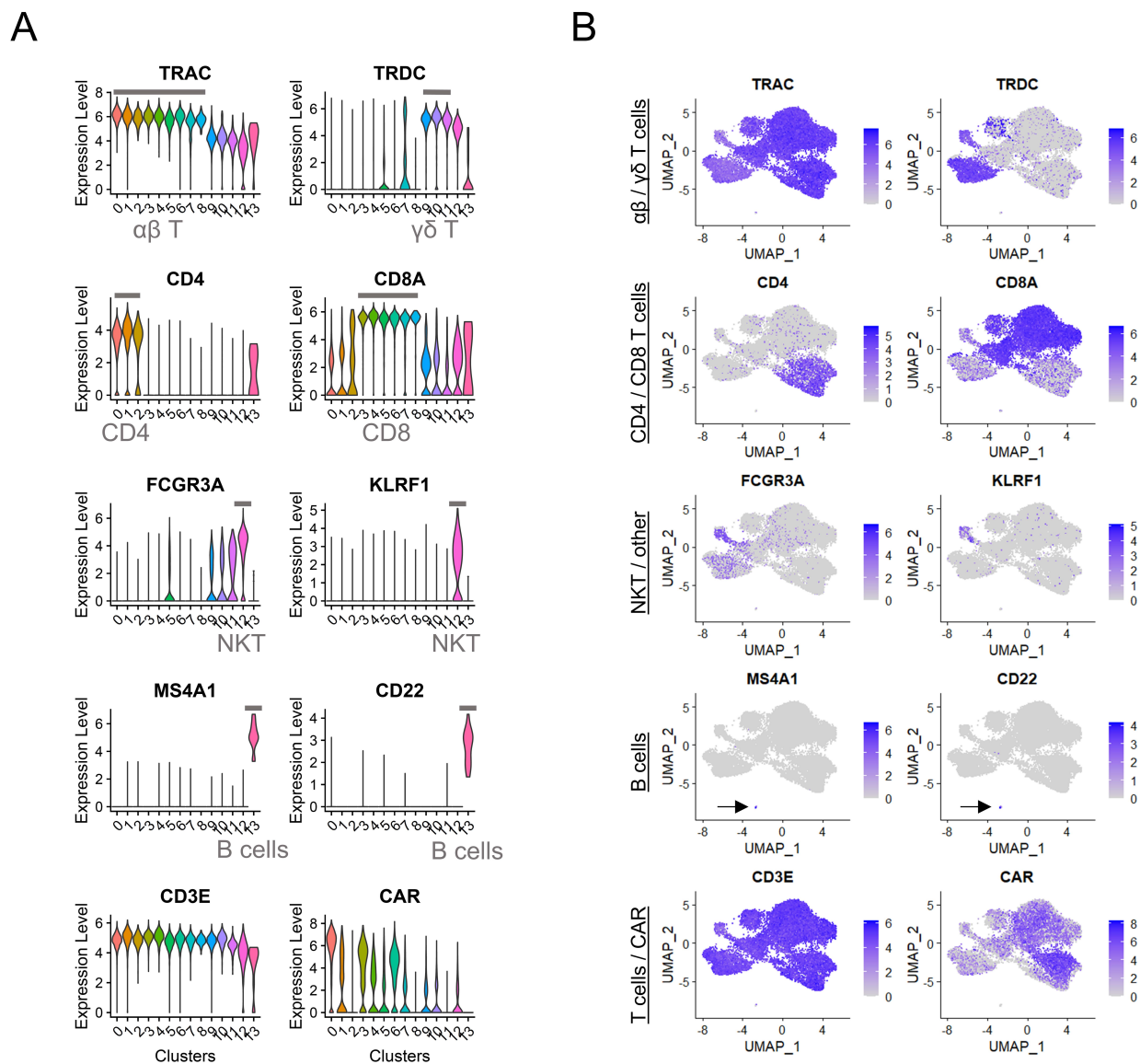
Figure 10: Unsupervised clustering analysis.
(**A**) Grouping of clusters according to major immune cell type markers as observed in violin plots of gene expression. (**B**) Localization of the major immune cell types in UMAP plot as seen based on gene expression. Arrows indicate the B cell cluster. Adapted from Charitidis et al., 2021.

Hence, CD4, CD8, γδ T cell and natural killer T cells (NKT) were identified and showed similar composition across the samples, both in LV-inoculated and untransduced cells (Figure 11). Even though the culturing medium was not optimal for B cell survival and proliferation, some B cells seemed to have survived in the control sample (Figure 11). However, no B cell were detected in the CAR T cell products (CD8-LV and VSV-LV), indicating their eradication by the generated CD19-CAR T cells (Figure 11).
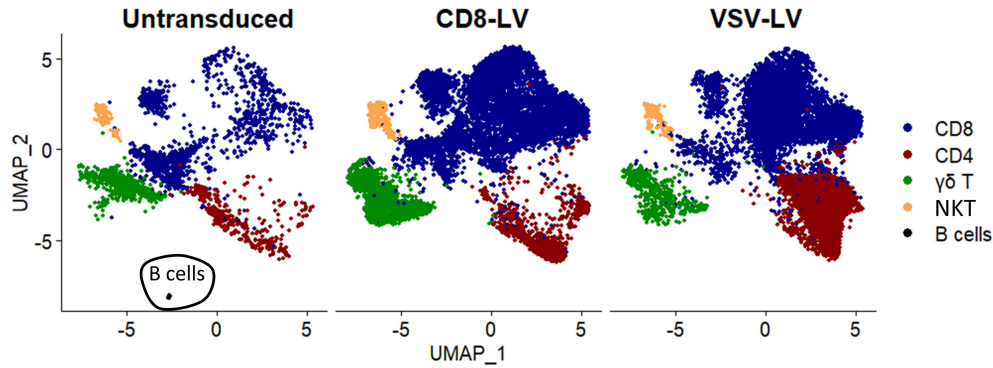
Figure 11: Cluster annotated UMAP plots split by samples.
UMAP plots of the three samples with annotated clusters of the major immune cell subtypes. Total post-filtered cell number of untransduced N=2654, CD8-LV N=9713, VSV-LV N=8975. Adapted from Charitidis et al., 2021.

2.1.4 Identifying CAR T cells in scRNA-seq by multimodal analysis

Focusing on the CD8 cell populations, as both of the LVs transduce, a subsetting strategy based on expression of *CD8A* and *CAR* needed to be settled.

Both genes showed a trimodal expression of negative, low and high expressing cells (Figure 12). Thus, a computational multimodal analysis was performed, where the antimodes (pits) of the distributed cells were chosen as thresholds (Figure 12).
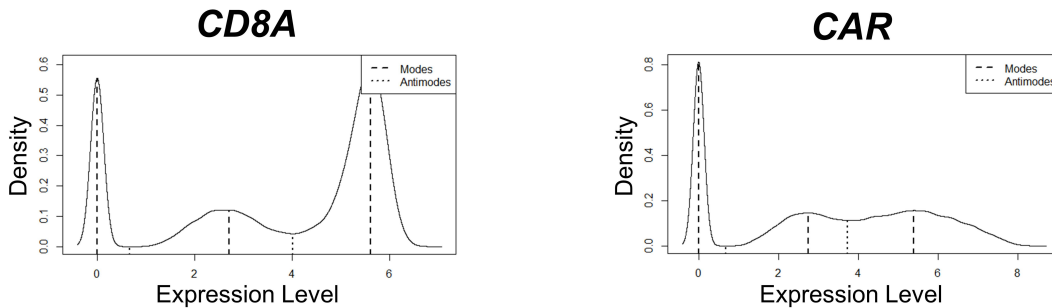
Figure 12: Multimodal analysis of *CD8A* and *CAR* expression.
Computational multimodal analysis on normalized expression level of *CD8A* or *CAR* genes, performed with the *multimode* package. *Dashed lines: modes, dotted lines: antimodes.* Adapted from Charitidis et al., 2021.

Consequently, each resulted population was evaluated by observing its localization in UMAP plots, where previously main T cell populations were identified and labelled (Figure 11). In this way, *CD8A^{neg}* and *CD8A^{low}* cells were found to overlap mainly with the non-CD8 cells in the UMAP plots, while the vast majority of *CD8A^{high}* cells was located in the previously identified CD8 T cell population (Figure 13). Likewise, *CAR^{neg}* and *CAR^{low}* comprised all the immune cell populations, while *CAR^{high}* were observed to overlap with the target cell populations of each vector, the CD8

cells for CD8-LV and both CD4 and CD8 for VSV-LV (Figure 13). Hence, *CD8A^high* expressing cells were defined as CD8 cells and CAR+ transduced T cells were the *CAR^high* expressing cells.
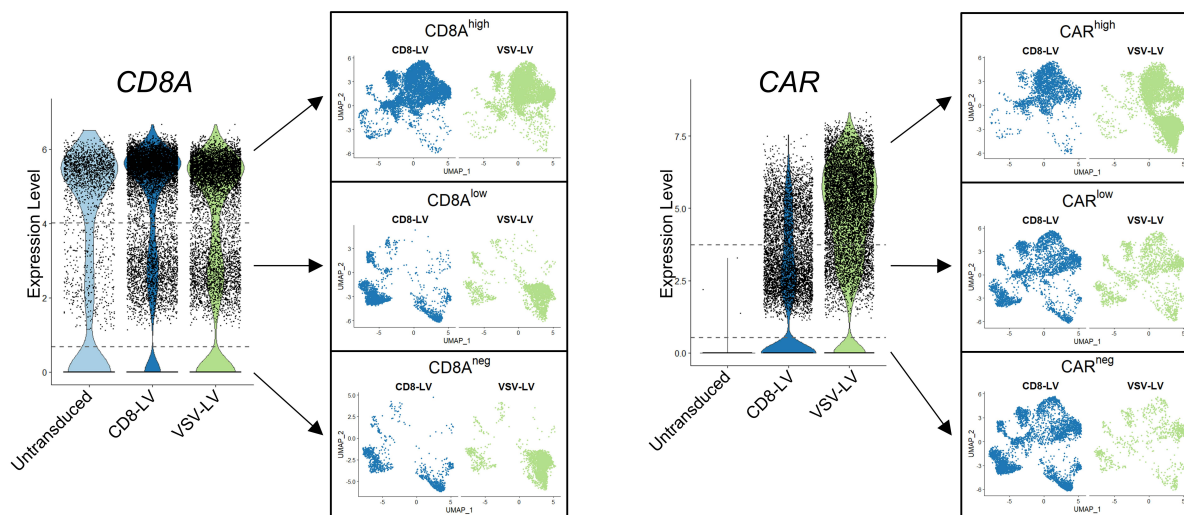
Figure 13: Identification of CD8 transduced and non-transduced cells.
Violin plots of *CD8A* (left) and *CAR* (right) expression across the three processed samples. Dashed lines indicate the antimodes (pits) identified by the multimodal analyses, separating negative, low and high expressing cells. Each subset (neg, low, high) was overlaid on UMAP plots, where previously the location of major immune types was identified, and the cell type match was evaluated. Adapted from Charitidis et al., 2021.

In addition, the higher *CAR* expression level in VSV-LV sample was correlated with of higher vector copy number (VCN) integrations in the particular product as assessed by qPCR analysis (Table 1, Figure 13).

Table 1: Vector dose and VCN in TGA CAR T cell products.

Sample	MOI	Particles / cell	VCN[⚹]
Untransduced	-	-	nd
CD8-LV	0.045	12×10^3	0.91 ± 0.71[☾]
VSV-LV	33.3	5.8×10^3	3.94 ± 1.76

[⚹] VCN was measured in replicates from different samples generated using different batches of LVs on three donors, including the batch and donor used in the scRNA-seq experiment (untransduced N=3, CD8-LV N=7, VSV-LV N=14) (mean ± SD).
[☾] VCN quantified from whole samples was extrapolated on CD8 cells based on their frequency determined by flow cytometry.
nd: non-detectable.
Adapted from Charitidis et al., 2021.

Questioning the low-expressing cells, their true identity was assessed by the degree of their transcriptomic difference with the negative populations. Thus, differential gene expression analysis was performed, where no major variations were observed between *CD8A^neg* and *CD8A^low*

as well as between *CAR^neg* and *CAR^low* cells (Figure 14). Hence, at least the merged population of *CAR^neg* and *CAR^low* (*CAR^neg//low*) cells was considered to be the non-transduced cells, as at least observed in flow cytometry. On the other hand, even though the *CD8A^high* cells were classified as factual CD8 cells, the low expression of *CD8A*, while regulated by an intrinsic non-constitutively active promotor, opposite to *CAR*, could be biologically possible.
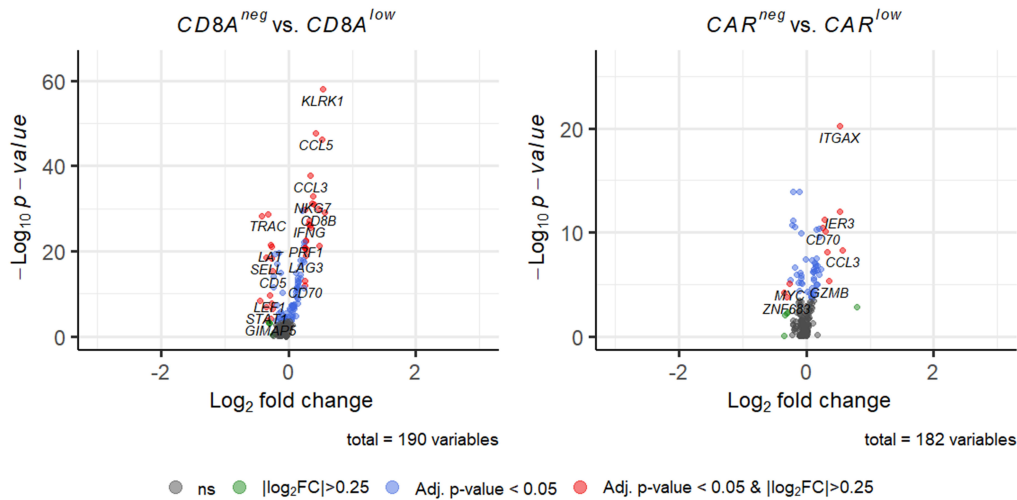
Figure 14: Volcano plots of negative versus low expressing *CD8A* or *CAR* cells.
Transcriptional differences between *CD8A^neg* versus *CD8A^low* (left) and *CAR^neg* versus *CAR^low* (right). Differential expressed genes are accounted genes that differ between the groups with $|\log_2 FC| > 0.25$ and adjusted p-value < 0.05. Fold changes of *CD8A* and *CAR* are not plotted due to $\log_2 FC > 3$. ns: non-significant.

Adapting this subsetting strategy, the detection of CAR T cells via protein expression was compared to that of mRNA-based detection in scRNA-seq, in the identical samples. Thus, frequencies of CAR+ cells in LV-inoculated samples was calculated out of the total CD3 compartment within each approach.

Notably, the frequencies of CAR T cells identified in flow cytometry were in perfect agreement with those determined by scRNA-seq analysis. Particularly, by subsetting *CD8A^high CAR^high*, the transduced CD8 cells in CD8-LV sample were 23.2%, while in flow cytometry the identical sample had 22.6% CAR+ cells out of total CD3 cells (Figure 15). The high selectivity of the CD8-LV for CD8 cells was also confirmed at this point by flow cytometry (Figure 15). Similarly, CD8+CAR+ T cells in VSV-LV reached to 32.2% in flow cytometry, closely matching that of 34.4% detection in scRNA-seq. Even though CD4 cells were not analyzed in this study, by checking the frequency of CD4+ CAR T cells in VSV-LV, the scRNA-seq reproduced the results seen in flow cytometry (Figure 15).
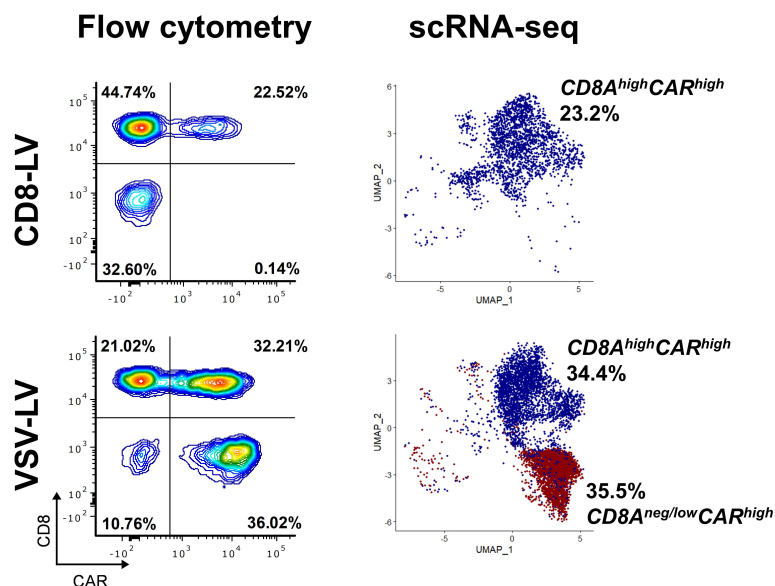
Figure 15: Side-by-side comparison of flow cytometry and scRNA-seq CAR T cell frequency.
Flow cytometry staining of CD8 and CAR expression (left) and frequency of CAR T cells detected by scRNA-seq based on the multimodal subsetting strategy. Adapted from Charitidis et al., 2021.

Overall, the multimodal-based subsetting strategy for disintegrating transduced from non-transduced T cells, highly matched with the results found in flow cytometry. In addition, the use of the CD8-LV further validated the identification of transduced and non-transduced CD8 cells in both CD8-LV and VSV-LV samples.

2.1.5   High selectivity of CD8-LV confirmed by scRNA-seq

This is the first time of evaluating the on-target specificity of a receptor-targeted LV via scRNA-seq. Thus, all the CAR^{high} expressing cells in CD8-LV were interrogated.

Remarkably, this multimodal-based subsetting strategy showed that 97.5% (N=2317 cells) of total CAR^{high} cells in CD8-LV sample were particularly $CD8A^{high}$ cells, thus definite CD8 cells (Figure 16A). However, 59 cells, accounted for 2.5% of CAR^{high} cells in CD8-LV, were either $CD8A^{neg}$ or $CD8A^{low}$ (Figure 16A). Investigating the identity of these potential off-target cells, their positivity in other major immune cell marker genes, such as *CD8B, CD4, TRDC* (γδ T) and *FCGR3A* (NKT), was assessed (Figure 16A, B).

A

B
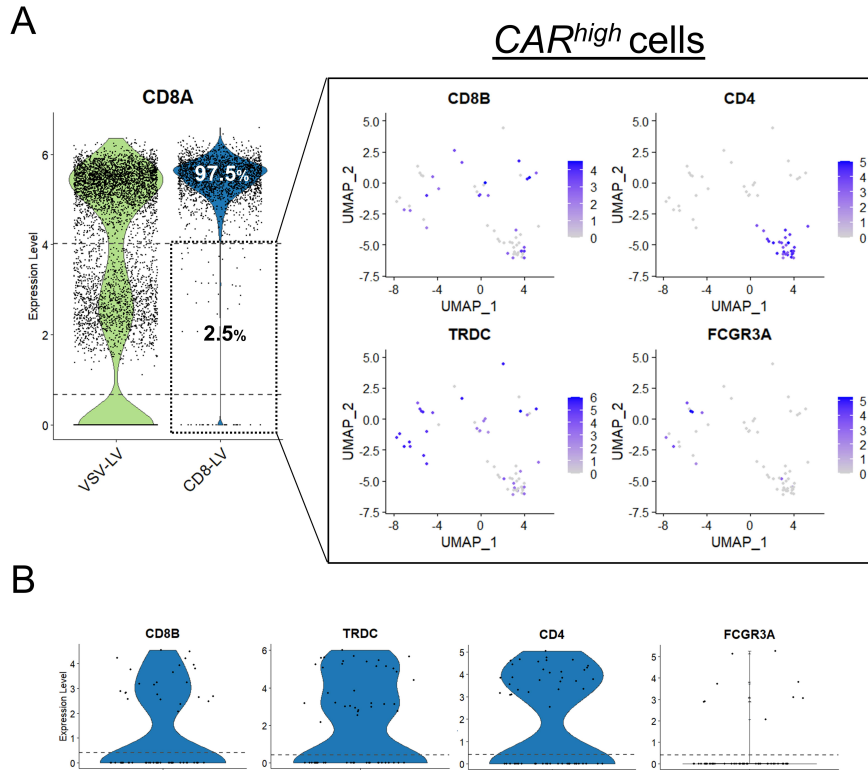
Figure 16: Interrogating potential off-target cells in CD8-LV.
(**A**) Plotting *CAR^high* expressing cells in violin (left) and UMAP plots (right). The 97.5% accounts for 2317 putative cells. (**B**) Violin plots of marker gene expression of the 2.5% *CAR^high CD8A^neg/low* cells of CD8-LV sample (N=59). Adapted from Charitidis et al., 2021.

Out of the remaining 59 cells (2.5%) being *CAR^high* but *CD8A^neg/low* in the CD8-LV sample, 9 were *CD8B* positive, low-expressing or negative for *CD8A*, thus accounted as CD8 or CD4/CD8 double positive cells (Table 2). The majority of cells (N=32) were identified as γδ T cells, while only 9 of them did not express *CD8A* neither *CD8B.* In addition, of the possible 15 CD4 cells, 7 were in fact *CD8A^low*, and 8 were *CD8A* and *CD8B* negative. The few NKT and remaining cells expressed either *CD8B* or *CD8A^low*. Overall, this brought only 17 out of 59, or in total out of 2317 *CAR^high*, cells to be classified as possible off-target cells (*CD8B^neg CD8A^neg*). Thus, this confirmed the high selectivity of the CD8-LV, reaching at 99.27% for CD8 positive cells (Table 2).

Table 2: Evaluation of *CAR^high^CD8A^neg/low^* cells in CD8-LV sample.

Cell type	Marker genes[1]	Cell number[2]
CD4 T cells	$CD4^{pos}CD8B^{neg}$	**15**
	$CD8A^{low}$	7
	$CD8A^{neg}$	8[†]
CD8 T cells	$CD8B^{pos}$	**5**
	$CD8A^{low}$	5
CD4/CD8 T cells	$CD4^{pos}CD8B^{pos}$	**4**
	$CD8A^{low}$	2
	$CD8A^{neg}$	2
NKT	$FCGR3A^{pos}$	**2**
	$CD8B^{pos}CD8A^{low}$	1
	$CD8B^{neg}CD8A^{low}$	1
γδ T	$TRDC^{pos}$	**32**
	$CD8B^{pos}CD8A^{low}$	7
	$CD8B^{pos}CD8A^{neg}$	7
	$CD8B^{neg}CD8A^{low}$	9
	$CD8B^{neg}CD8A^{neg}$	9[†]
Remaining cells	$CD8B^{neg}CD4^{neg}TRDC^{neg}FCGR3A^{neg}$	**1**
	$CD8A^{low}$	1

[1]Letters in bold indicate of the gene, -s expressed in all of the subfractions listed below.
[2]Numbers in bold indicate total counts of the subfractions listed below.
[†]Potential off-targets.
Adapted from Charitidis et al., 2021.

2.1.6 Differential gene expression analysis in CD8 populations

Transcriptomic differences across control and LV-inoculated cell populations were next investigated. Thus, the CD8 cells were divided into control cells and groups expressing or not the *CAR* transgene, and differential gene expression analysis was conducted.

Gene expression profiles were found to be altered across all populations as shown in Figure 17A. Overall, bigger differences on average gene expression across the subsets were observed between untransduced cells and every other subset of cells, exposed to a LV (Figure 17A). More specifically, untransduced cells had higher number of differentially expressed (DE) genes with higher fold-change differences when compared to either transduced *CAR^high^* or non-transduced *CAR^neg/low^* cells (Figure 17B, left). Accordingly, untransduced CD8 cells had similarly higher

number of DE genes with higher fold-change differences, when compared to CD8 cells inoculated with any LV, disregarding their *CAR* expression status (Figure 17B, right). However, the fold-change differences and number of DE genes were clearly less pronounced when comparing *CAR^neg/low* with *CAR^high* or CD8-LV versus VSV-LV (Figure 17B).

The Venn diagrams confirmed these findings and showed the overlaps of DE genes between the comparisons (Figure 17C). Particularly, the majority of genes (130 out of 155) were found to be differentially expressed when comparing untransduced with *CAR^high* cells (Figure 17C, left). From these genes, 71 were uniquely identified between control and LV-inoculated cells, while 33 were particularly in common between all three comparisons (Figure 17C, left), showed in the volcano plots above (Figure 17B, left). Accordingly, the majority of 127 out of 149 DE genes were found when comparing control cells with VSV-LV inoculated CD8 cells (Figure 17C, right). Whereas, 71 genes were uniquely shared between the comparisons of each vector with the control cells and 29 were in common with all three comparisons (Figure 17C, right), presented above in the plots above (Figure 17B, right).
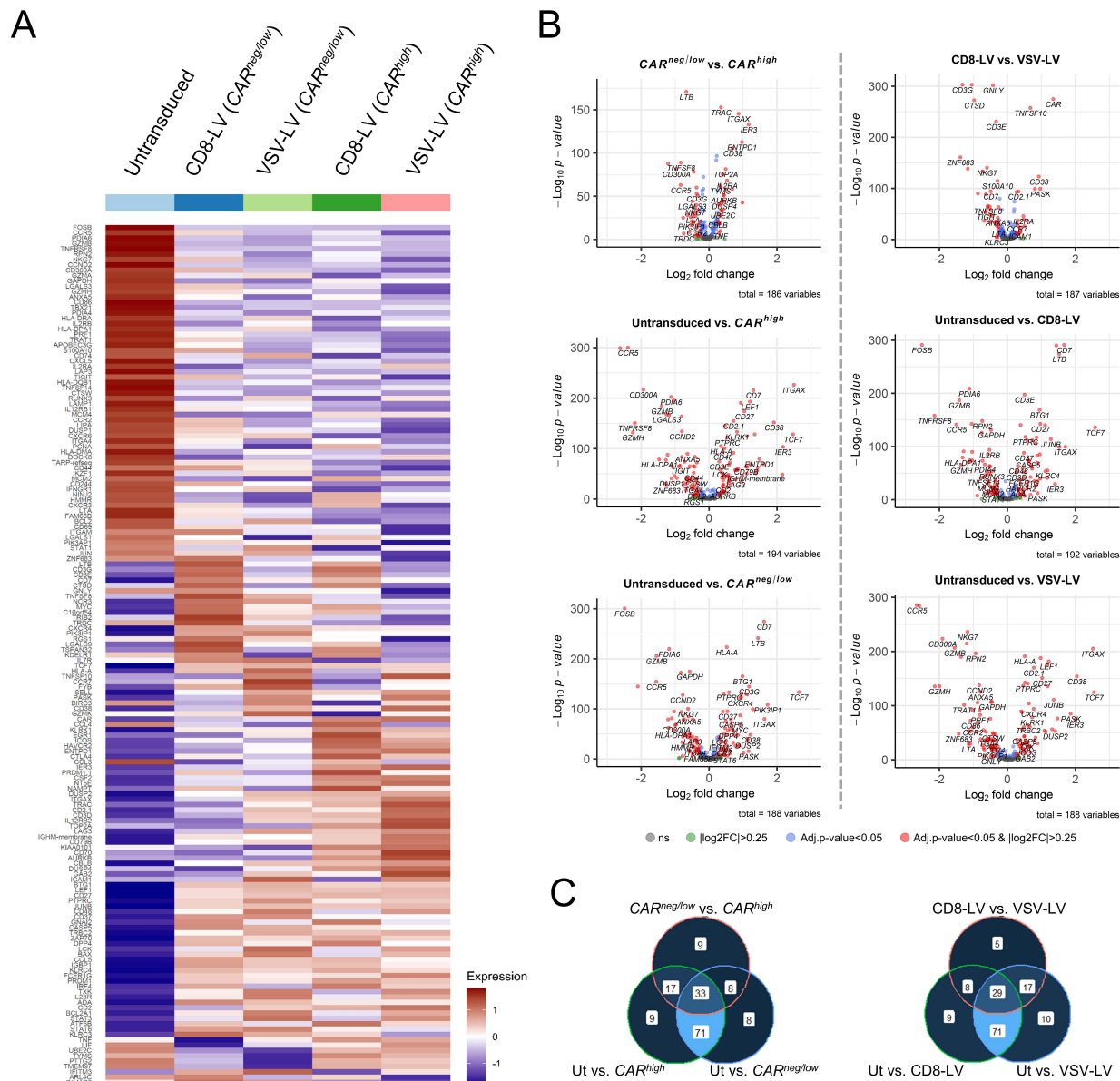
Figure 17: Differential gene expression analysis of TGA study.
(**A**) Heatmap plots of 161 DE genes among all the CD8 subsets (cell numbers: untransduced N=1444; CD8-LV (*CAR^neg/low*) N=4216; VSV-LV (*CAR^neg/low*) N=1739; CD8-LV (*CAR^high*) N=2257; VSV-LV (*CAR^high*) N=3084) identified by FindAllMarkers function in *Seurat* ($|\log_2 FC| > 0.25$, adjusted p-value < 0.05). (**B**) Volcano plots comparing *CAR^neg/low*, *CAR^high* and untransduced (Ut) cells, disregarding the LV used (left) or the CD8 cells among the CD8-LV, VSV-LV and Ut samples (right). For centering the graphs, $|\log_2 FC|$ of 3 was set as limit, where only *CAR* was above that in few comparisons. ns: non-significant. (**C**) Overlaps of DE genes identified based on subsets (left) and samples (right), corresponding to the volcano plots above. Adapted from Charitidis et al., 2021.

To identify which pathways are affected between the different groups of cells and samples, gene set enrichment analyses were performed. The DE genes from the major comparisons were analyzed across gene sets of the Gene Ontology - Biological Process (GO-BP), which revealed

enrichment of genes especially related with cytokine-mediated signaling, T cell activation, immune response, and cell proliferation or apoptosis (Figure 18).
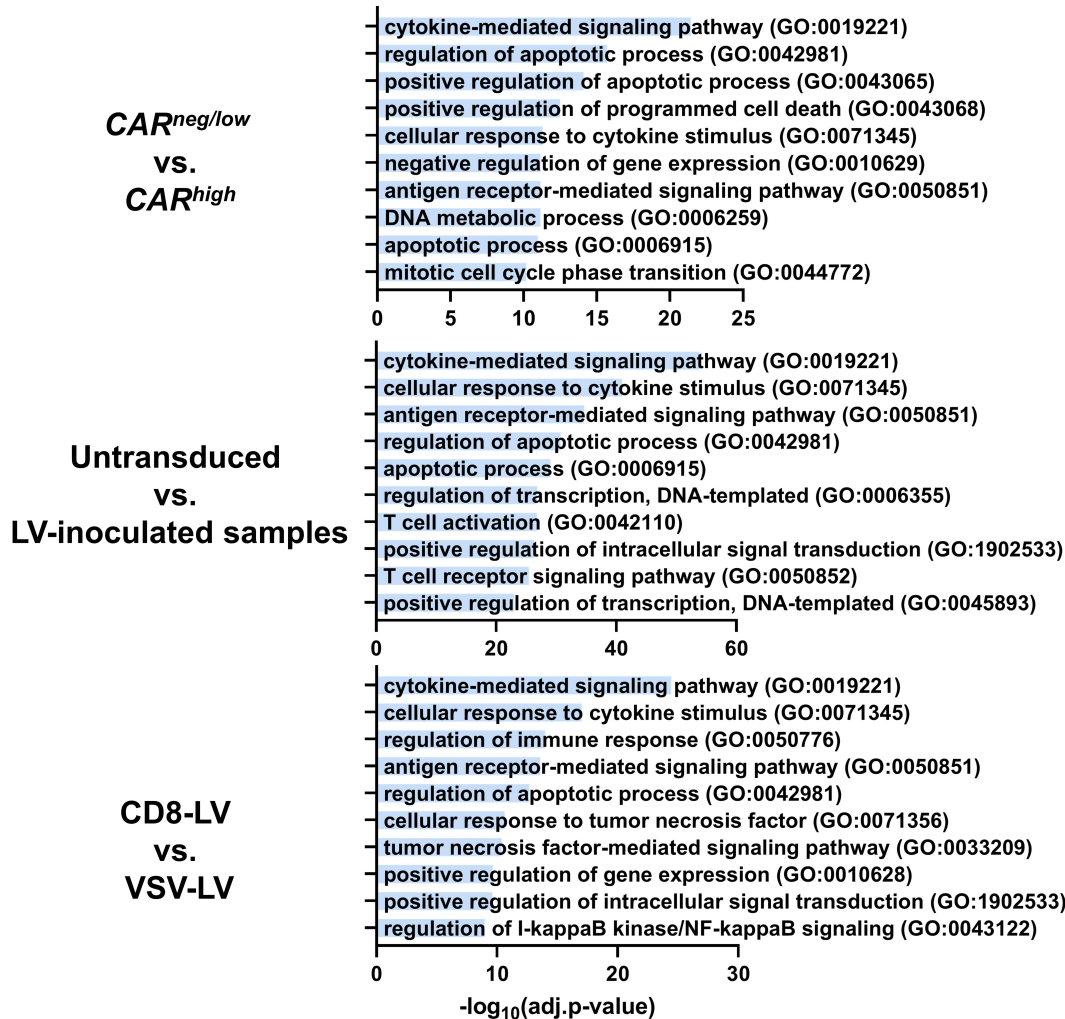
Figure 18: Gene set enrichment analysis in TGA study.
Gene set enrichment analysis of DE genes identified in the indicated comparisons of from the TGA study across gene sets of Gene Ontology - Biological Process (GO-BP) pathways using the independent enrichment analysis tool (Appyters). Top 10 significant results are plotted. $CAR^{neg/low}$: merged CAR^{neg} and CAR^{low} cells. LV-inoculated samples: concatenated CD8-LV and VSV-LV samples. Adapted from Charitidis et al., 2021.

Nevertheless, a closer look at the differences between CD8 populations showed up- or down-modulation of genes related to CAR expression and/or vector-host interactions (Figure 19). Specifically, genes related to T cell activation and co-stimulation (*CD70, ICOS*), exhaustion and immune check point (*ENTPD1, LAG3, HAVCR2, LAT2*) were upregulated in CAR^{high} expressing cells, which could be partially a result of CAR-driven tonic signaling (Figure 19) (Long et al., 2015). In addition, CAR^{high} cells favored a T_H1 phenotype, also known for CD8 cells as T_C1, by expressing genes for IL-12 receptor, IFNγ, GM-CSF and other related genes (*IL12RB2, IFNG, STAT4, DUSP4, CSF2*) (Figure 19) (Haddock et al., 2019; Al-Mutairi et al., 2010).

However, cellular intrinsic factors could have contributed to prevention from a proper transduction by the LVs in *CAR^neg/low* cells (Figure 19). For instance, *IL2RA* was downregulated in the latter cells not only compared to *CAR^high*, but also to untransduced CD8 cells, indicating a possible low activation level that could have impeded their transduction. In agreement with this, *PIK3IP1* and *CD37*, which inhibit T cell activation and proliferation, respectively, were found to be upregulated in non-transduced *CAR^neg/low* cells (Figure 19) (Uche et al., 2018; van Spriel et al., 2004). Furthermore, genes expressing two interferon-induced transmembrane proteins (*IFITM2, IFITM3*), which inhibit viral fusion and subsequently viral entry, were slightly, but still significantly, higher in *CAR^neg/low* cells (Figure 19) (X. Zhao et al., 2019; Hornick et al., 2016; Li et al., 2013;).

The exposure to LV seemed also to affect the gene expression profile, while differences between untransduced control cells with LV-exposed cells (both *CAR^neg/low* and *CAR^high*) were observed (Figure 19). Among these, T cell activation and proliferation inhibitors (*PIK3IP1, BTG1*), memory markers (*CD7, CD62L - SELL, TCF7*), apoptosis (*CASP5*), exhaustion (*HAVCR2, LIF, C10orf54*), antiviral-related expressing genes (*IRF4, IFITM2, IFITM3, ITGAX*), as well as the immune surveillance receptor *KLRK1*, were found to be elevated upon LV inoculation, disregarding the transduction status of the cells (Figure 19). On the other hand, genes expressing cytotoxic molecules, granzymes (*GZMA, GZMB*) and perforin (*PRF1*), and the lysosomal enzyme lipase A (*LIPA*) were down-modulated upon viral exposure (Figure 19).

Apart from the common differences between *CAR^neg/low* and *CAR^high* cells independently of the LV used, the choice of the LV also resulted in measurable differences in gene expression profiles between the two CAR T cell products (Figure 19). Among these were the *LIPA*, which was less expressed in CD8 cells of VSV-LV sample, opposite though to *CCR7, SELL* and to the cytotoxic cytokine TRAIL gene (*TNFSF10*) (Figure 19). In addition, the cathepsin D (*CTSD*), the chemokines *CCL3* and *CCL4* and granulysin (*GNLY*) were particularly expressed in CD8 cells of CD8-LV product (Figure 19).
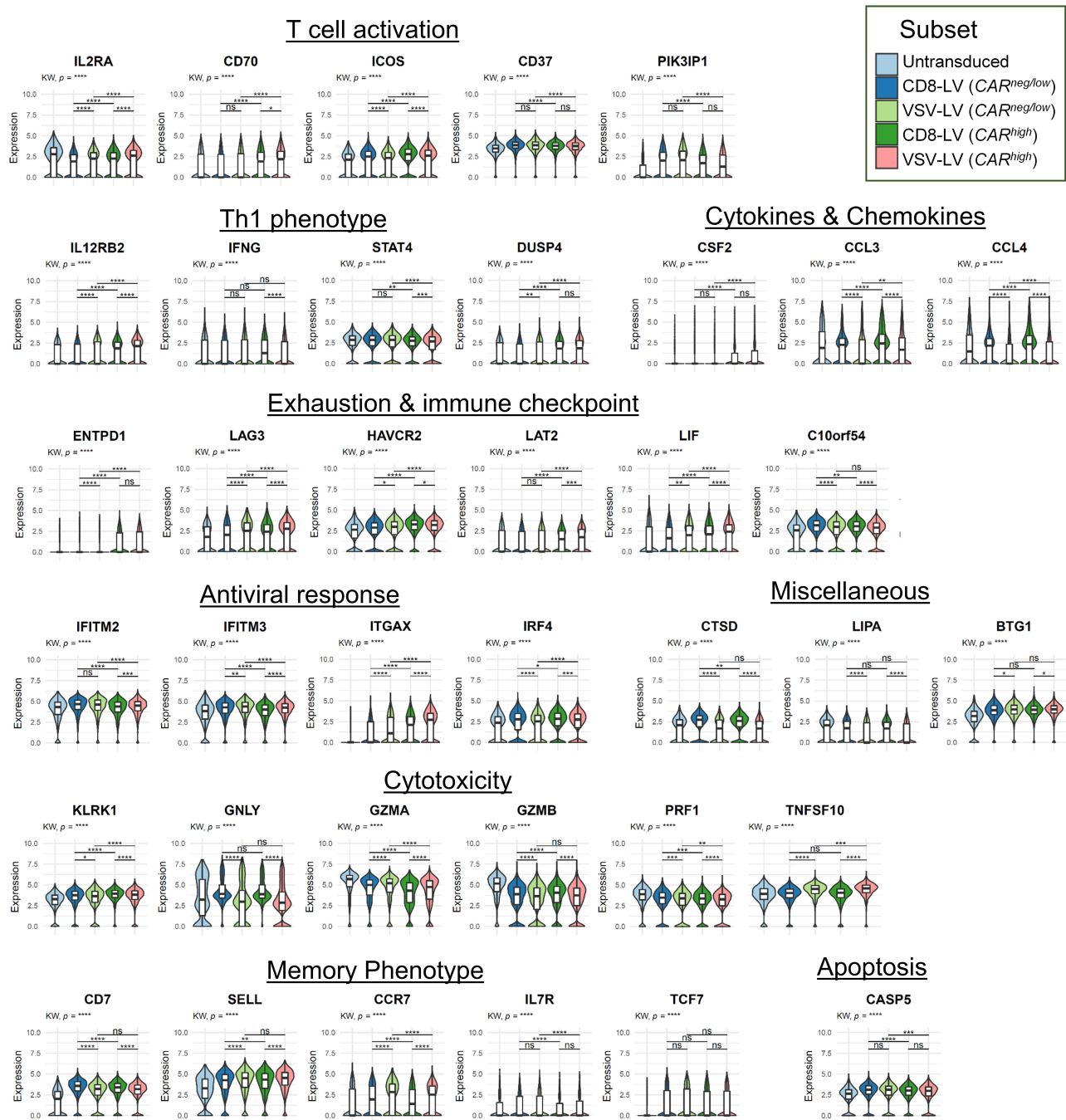
Figure 19: Violin plots of genes of interest in TGA.
Violin plots of gene expression across CD8 cell subsets. Selected genes are presented into thematic groups representing pathways, functions and cellular phenotypes and states. Kruskal-Wallis (KW) with Wilcoxon multiple comparison test was performed (Bonferroni p-value adjustment). ns: non-significant, *p<0.05, **p<0.01, ***p<0.001, ****p<0.0001. Adapted from Charitidis et al., 2021.

Overall, the first scRNA-seq study revealed transcriptional differences upon LV inoculation, where the choice of VSV-LV or CD8-LV for the gene transfer also resulted in unique gene expression traits in the CAR T cells, which could potentially positively or negatively influence the outcome of the CAR T cell products. The genetically engineered products originated from PBMC

comprised mainly CD4, CD8, γδ T, NKT cells. Moreover, the differences between non-transduced and transduced cells revealed gene profiles that were likely prone for transduction or inhibitory factors that prevent the LV-mediated gene transfer. Nonetheless, further investigations including more donors at earlier time points of CAR T cell generation, while also covering the whole transcriptome could possibly confirm these observations and, even more, enlighten the factors contributing to LV-mediated gene transfer.

2.2 WHOLE TRANSCRIPTOME ANALYSIS OF EARLY GENERATED CAR T CELLS

The first scRNA-seq on 400 genes of the immune response panel provided some valuable insights not only for the detection of CAR T cells in scRNA-seq analysis and the differentially expressed genes across the analyzed cell populations, but also regarding technical aspects of establishing the whole pipeline of BD Rhapsody™ system, from single cell capturing, library preparation and sequencing to raw data pre-processing and downstream bioinformatics analyses. Next, a more comprehensive whole transcriptome analysis (WTA) was conducted in order to comprehensively investigate blocking mechanisms of LV-mediated transduction in T cell types. For that reason, PBMC from 3 donors were inoculated with VSV-LV, CD8-LV or CD4-LV. The cells were cultivated for 3 days, sorted and processed for whole transcriptome scRNA-seq analysis, bringing the analysis closer to LV-related events at earlier time point compared to TGA. Eventually, distinct transcriptomic alterations were observed between transduced and non-transduced cells. The inclusion of the CD4-LV allowed the evaluation of CD4 cells as well, thus eliminating T cell type specific bias. Practical help was kindly offered by Elham Adabi (PEI) and validation of scRNA-seq analysis was done by Dr. Liam Childs (PEI) and Dr. Colin Clark (NIBRT). Sequencing was performed by experienced scientific staff, Dr. Csaba Miskey (PEI) and Dr. Stefan Günther (Max-Planck-Institute for Heart- and Lung Research, Germany). Technical support was provided by Dr. Vadir Lopez-Salmeron, Edyta Kowalczyk, Dr. Siobhan Cashman (all BD Biosciences) and Michael Rieger and WeiJia Yu (Goethe University Hospital Frankfurt, Germany). For the following experiment, up to this moment of thesis writing, a manuscript has been drafted.

2.2.1 Experimental layout of the WTA study

For the whole transcriptome (WTA) approach on single-cell level, pre-activated PBMC from 3 donors were incubated with CD8-LV, CD4-LV or VSV-LV having the CD19-CAR-28z packaged (Figure 20). Untransduced cells that were not exposed to any LV were used as a control, accounting in total to 4 samples per donor. While the target selectivity in scRNA-seq had been

determined before to be over 99% for CD8-LV (Figure 16, Table 2), the main focus here was to identify any potential blocks preventing successful CAR delivery in particular T cells. Thus, the cells were magnetically sorted 3 days after vector exposure into live CD8 cells (CD8-LV), CD4 cells (CD4-LV) and CD3 cells (VSV-LV, untransduced), and then processed for scRNA-seq (Figure 20).
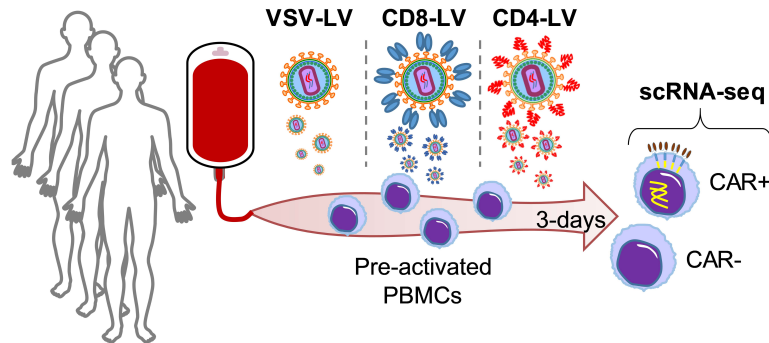
Figure 20: Experimental layout of the WTA study.
PBMC isolated from 3 donors, pre-activated and transduced with VSV-LV, CD8-LV or CD4-LV. T cells were expanded for 3 days and then processed for scRNA-seq analyzing the whole transcriptome.

2.2.2   Subsetting populations and plotting

To separate populations of interest, mainly CAR- and CAR+ cells from each setting, thresholds on normalized gene expressions of *CAR* and *CD8A* were selected via multimodal analyses (Figure 21A, B), similarly as described above (2.1.4). To simplify the nomenclature of cell populations, the symbols for positive (+) and negative (-) were used to indicate the expression (previously "high") or not (previously "neg/low") of a particular gene. Although a trimodal distribution was not observed for *CD8A* expression, there was a tendency in *CAR* expression (Figure 21A, B). Thus, once again, CAR^{low} cells were considered as non-transduced cells and were subsequently merged with CAR^{neg}.

A

B
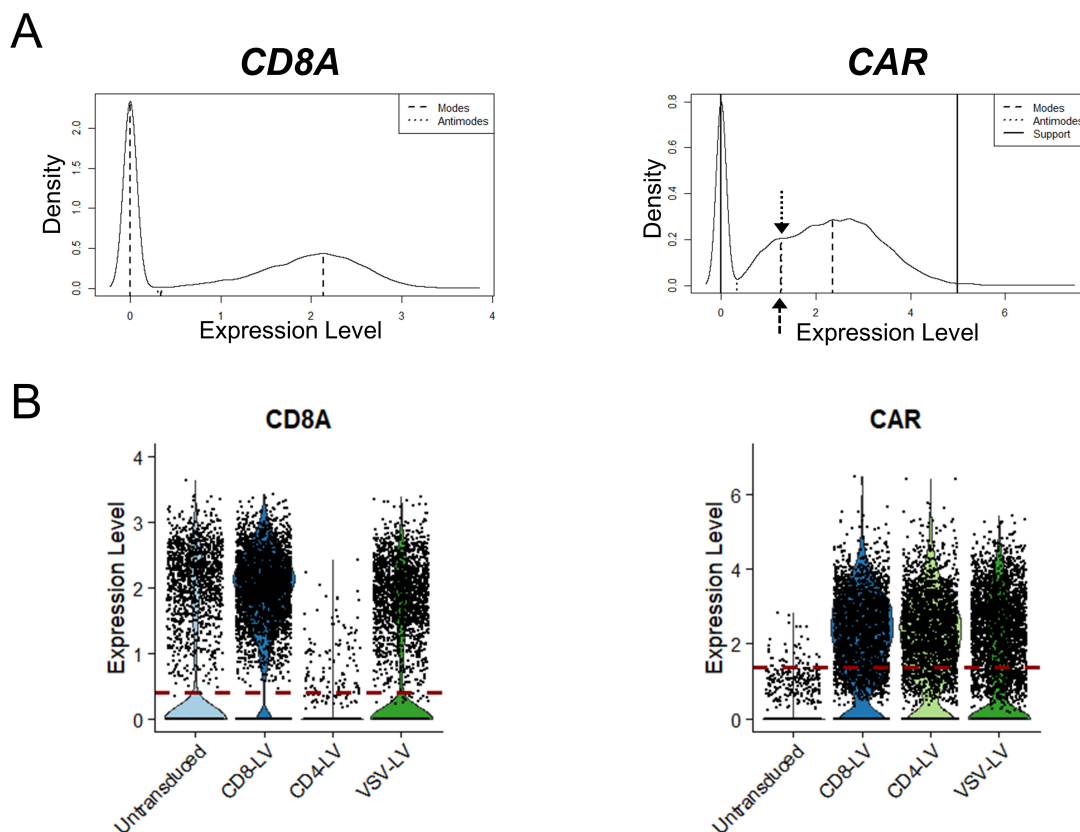
Figure 21: Multimodal analysis and *CD8A* and *CAR* expression across samples.
(**A**) Multimodal analysis of *CD8A* and *CAR* expression to define the cutoffs for CD8± or CAR± cells. *Arrows* indicate the close proximity of a mode and antimode. The support line defines the limits for performing the analysis. (**B**) Violin plots of *CD8A* and *CAR* expression across samples. *Dashed lines* indicate the cutoffs for subsetting and separating negative from positive cells. CD4 cells were defined as *CD8A*- expressing cells.

Subsetting the CD8 and CD4 cells, due to the enrichment of target cells by magnetic sorting, the CD8 and CD4 cells could be nicely separated via *CD8A* expression, reaching to 95.3% and 96.4% of pure cell population, respectively. On the other hand, the *CD4* expression seemed not to be the appropriate one for subsetting, as there were more cells detected as CD4 negative in the CD4-LV sample and although the overall purity of the CD8 cells in CD8-LV was as high as 95.4%, CD4 cells were less detectable presenting a frequency of 84.4% (Figure 22).
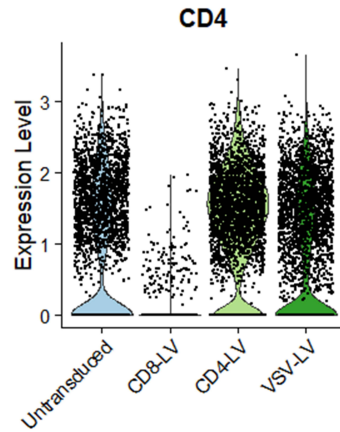
Figure 22: *CD4* gene expression across samples.
Violin plot of *CD4* mRNA expression in WTA processed samples.

By looking at the flow cytometry results of the sorted samples, the high purity of the corresponding target cells in CD8-LV and CD4-LV products post-sorting was verified, reaching to 97% and 98%, respectively (Figure 23). Thus, the choice of subsetting based on the expression of *CD8A* gene for both CD8 (*CD8A+*) and CD4 (*CD8A-*) cells was identified as the most suitable.
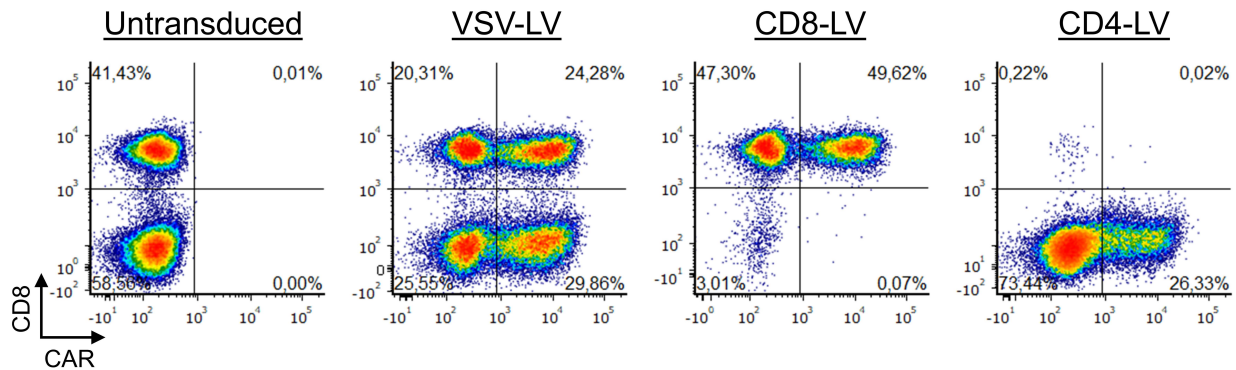
Figure 23: CAR protein expression and purity evaluation of sorted cells in WTA samples.
Flow cytometry analysis of magnetically sorted samples for live CD3 (untransduced, VSV-LV), CD8 (CD8-LV) and CD4 (CD4-LV) cells, prior processing for scRNA-seq. Samples were merged for all 3 donors.

Furthermore, the average VCN of the analyzed samples was ranged between 1.2 to 2, while the frequency of CAR T cells out of target cells for the certain LV were as low as 6.6%, reaching up to 64.4% (Table 3). While initially aiming for approximate 50% transduction, the efficient dose to reach this frequency was 272 particles/cells for VSV-LV, while both CD8-LV and CD4-LV needed at least 10-fold higher dose (Table 3). However, donor to donor variability in T cell transduction rates was noticeable for every LV (Table 3). Intriguingly, the frequencies of *CAR* mRNA expressing cells were higher than expected, compared to flow cytometry analysis inoculated with any receptor-targeted LV (Table 3), indicating a possible latency of CAR protein

expression in transduced cells on day 3 post-inoculation. That was particularly more pronounced in T cells inoculated with any receptor-targeted LV.

Table 3: Vector dose, VCN and CAR expression in WTA CAR T cell products.

Sample	MOI*	Particles / cell	VCN[+]	CAR % (FACS)[◊]	*CAR* % (scRNA-seq) [‡]
Untransduced	-	-	nd[¤]	-	-
CD8-LV	0.0275	3163	1.2 ± 0.8	D1: 62.8% D2: 13.1% D3: 24.8%	D1: 78.0% D2: 62.7% D3: 71.5%
CD4-LV	0.195	4419	1.8 ± 1.3	D1: 50.4% D2: 6.6% D3: 14.2%	D1: 80.7% D2: 69.7% D3: 64.5%
VSV-LV	1.3	272	2.0 ± 0.2	D1: 64.4% D2: 22.6% D3: 54.4%	D1: 55.6% D2: 40.3% D3: 53.9%

[+] VCN was measured in at least 2 technical replicates from the original post-sorted samples of each donor. Due to low sample size of one donor after sorting, DNA from its CD8-LV generated sample was not recovered (untransduced N=6, CD8-LV N=4, CD4-LV N=6, VSV-LV N=6) (mean ± SD).
[¤] Non-detectable.
[◊] Frequency of CAR T cells detected in flow cytometry (FACS) out of target cells.
[‡] Frequency of *CAR* mRNA expressing T cells detected in scRNA-seq out of target cells.
D1=donor 1, D2=donor 2, D3=donor 3.

For plotting the scRNA-seq data, principal component analysis, cell cycle and batch effect due to donor variability corrections were performed as described in *Materials & Methods* (4.2.6.14, 4.2.6.16). The first 22 principal components were chosen for projecting the single cells in the UMAP plots (Figure 24A). For in-depth and more sensitive analysis, CD8 and CD4 cells were separated and cell populations were divided based on *CAR* expression into *CAR-* and *CAR+* expressing cells (Figure 24A). Different immune cells were identified based on the expression of marker genes. Among them, CD4 and CD8 cells, γδ T cells, but also some B cells (Figure 24B). Even though the culturing conditions were not favorable for B cell expansion and samples were enriched for the target cells that each LV can transduce, some B cells seemed to have survived and passed the sorting process. However, for downstream differential gene expression analyses, B cells were removed according to the expression of marker genes (*MS4A1*, *CD22 and CD19*).
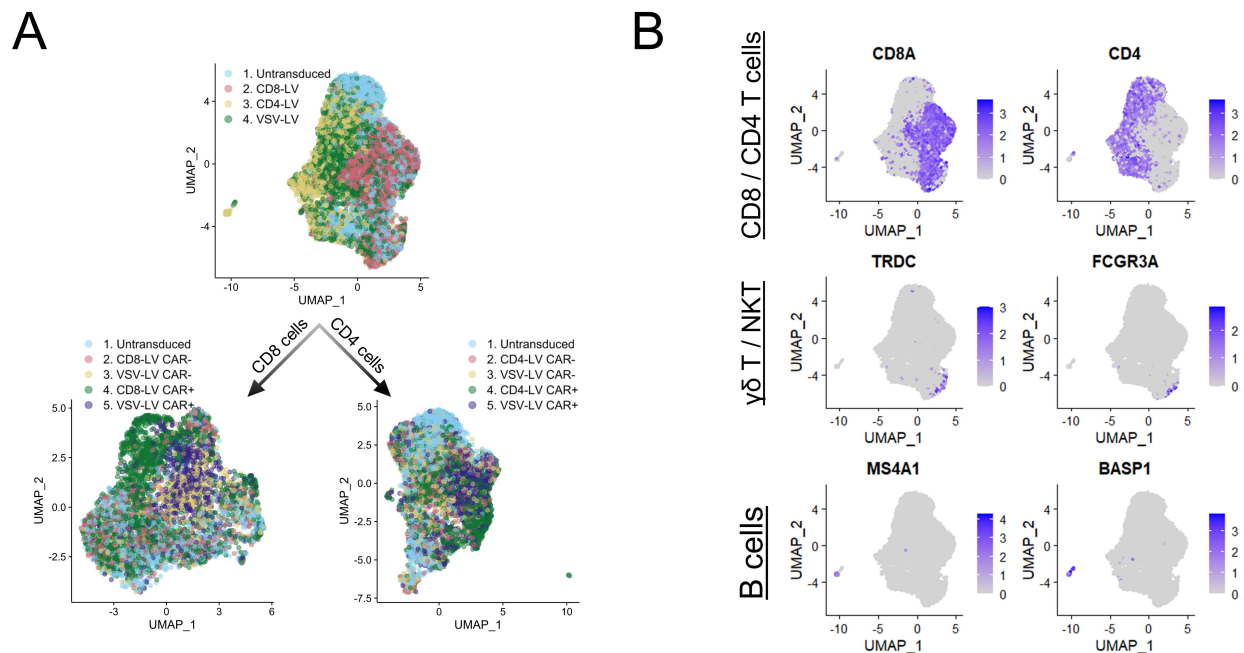
Figure 24: UMAP plots of WTA processed and subset samples.
(**A**) UMAP plot of the processed samples in WTA, corrected for cell-cycle and donor variability effects (Total cell numbers: untransduced N=3419, CD8-LV N=2978, CD4-LV N=2881, VSV-LV N=3900) (top). Initial samples were divided into CD8 and CD4 populations and further subset based on *CAR* expression (cell numbers for CD8 populations: untransduced N=1218, CD8-LV CAR- N=748, VSV-LV CAR- N=837, CD8-LV CAR+ N=2075, VSV-LV CAR+ N=899; cell numbers for CD4 populations: untransduced N=2146, CD4-LV CAR- N=745, VSV-LV CAR- N=992, CD4-LV CAR+ N=1867, VSV-LV CAR+ N=1098) (bottom). (**B**) Localization of major immune cell populations in UMAP plot of whole samples (depicted in A, top), based on the expression of marker genes. B cells were excluded from downstream analyses based on *MS4A1* (CD20), *CD22* and *CD19* and expression.

2.2.3 Distinct gene expression profiles in CAR T cell caused by different vector types

Investigating differences between the isolated subsets of cells, differential gene expression analysis was performed, in CD8 and CD4 cell populations. Transcriptomic alterations were observed between control cells and cells that came across with LVs as well as between *CAR*+ and *CAR*- cells, both in CD8 and CD4 T cell types (Figure 25). Furthermore, each particular type of LV caused distinct transcriptomic patterns either in *CAR*+ or *CAR*- cells. *CAR*+ cells generated by VSV-LV showed an induction of a greater number of genes, when comparing to the average expression of all the rest analyzed subsets (Figure 25).
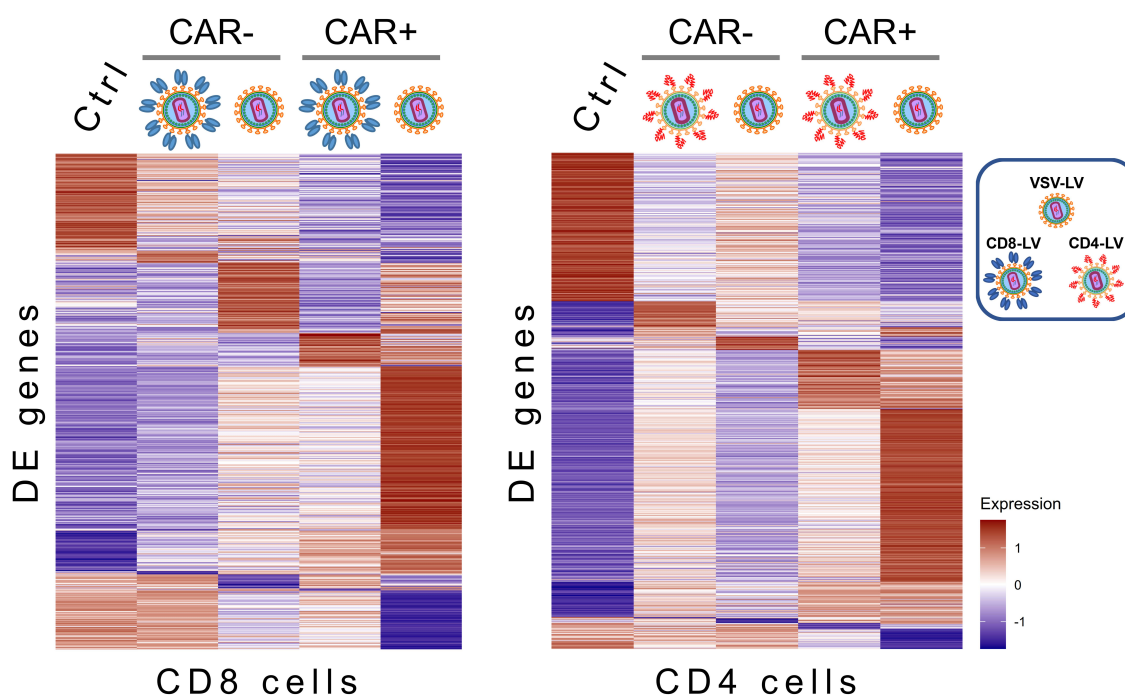
Figure 25: Differential gene expression analysis across subsets in WTA.
Heatmap plots of all differentially expressed genes per subset of CD8 cells (left) and CD4 cells (right), as identified by the function of FindAllMarkers in *Seurat* ($|\log_2 FC| > 0.2$, FDR < 0.05).

However, when exploring which vector induced greater transcriptomic alterations compared to the untransduced bystander cells, it appeared that both VSV-LV and CD4-LV had a bigger impact on the inoculated cells, disregarding their transduction status (*CAR-* and *CAR+*) (Figure 26). Whereas CD8-LV induced the least changes in the CD8 cells (Figure 26). Specifically, CD8-LV altered 211 genes, while CD4-LV affected 624, and VSV-LV 527 and 564, in CD8 and CD4 cells, respectively (Figure 26). A large number of DE genes was in common across CD4-LV and VSV-LV, while 82 DE genes found to be affected by all LVs, in both CD8 and CD4 cell types (Figure 26).
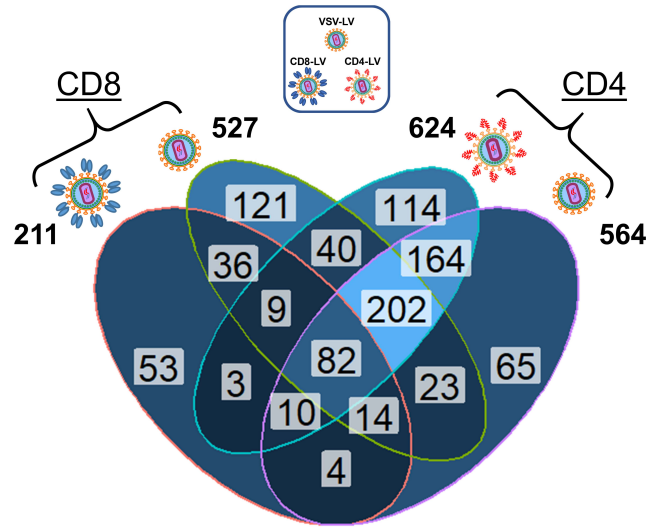
Figure 26: Venn diagram of differentially expressed genes between untransduced and LV-inoculated cells.
Venn plots showing the overlaps of DE genes ($|\log_2 FC| > 0.2$, FDR<0.05) identified by comparing the respective untransduced control cells with each individual LV-inoculated sample, disregarding the CAR expression status of the cells. Numbers outside the plot indicate the total DE genes identified for each vector and cell type.

Examining the common 82 DE genes altered upon LV inoculation, they were associated with metabolic pathways, cell proliferation, and also viral infections (Figure 27).
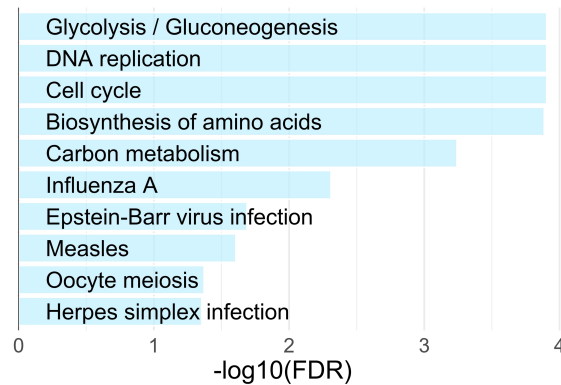
Figure 27: Over-representation analysis of common DE genes between control and all LV inoculated samples.
Enrichment analysis of the 82 common DE genes identified across the comparisons of LV-inoculated cells with the respective control cells.

Focusing on the gene expression profiles regulating the susceptibility of T cells for LV-mediated transduction, differential gene expression analyses were performed between *CAR+* and *CAR-* cells from each particular LV product and T cell type (Figure 28). Similarly to what was observed in heatmap plots (Figure 25), VSV-LV induced greater transcriptional changes compared to the two targeted LVs, when comparing *CAR-* versus *CAR+* cells (Figure 28).

40
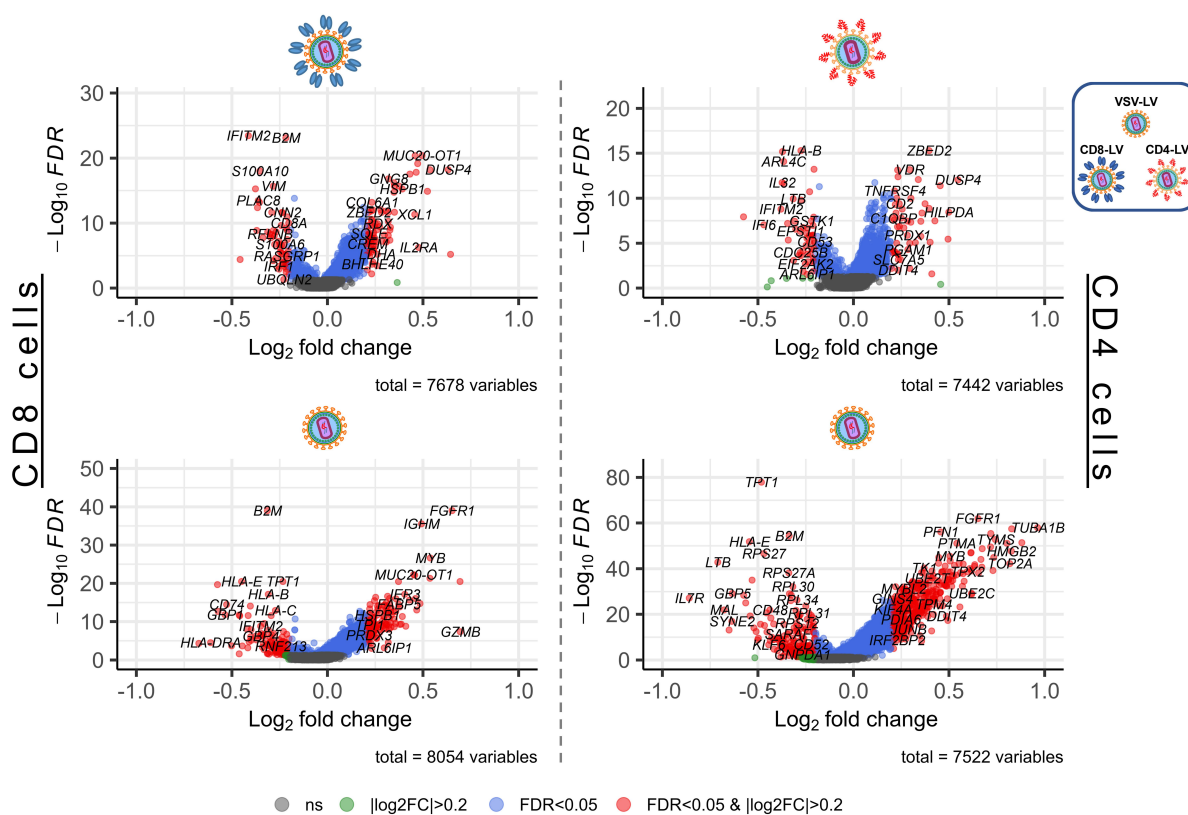
Figure 28: Volcano plots of *CAR+* versus *CAR-* cells of each vector and cell type.
Differential gene expression analysis performed between *CAR+* versus *CAR-* cells for CD8 cells in case of CD8-LV and VSV-LV (left) and CD4 cells of CD4-LV and VSV-LV (right). Genes with negative $\log_2$FC were upregulated in *CAR-* cells and *vice versa.* Significant DE genes were defined as $|\log_2$FC$|$>0.2 and FDR<0.05. ns: non-significant.

To simplify the comparisons an overview of DE genes was brought up by comparing the concatenated *CAR-* and *CAR+* cells from all LV-inoculated samples, regardless their cell and LV type (Figure 29A). Examining the overlap of DE genes a Venn diagram was created with the DE genes from each individual comparison of *CAR-* versus *CAR+* cells (Figure 29B).

Unique up- or down-regulated genes were detected when comparing *CAR-* with *CAR+* cells in each vector type or comparison, while only 24 DE genes were in common between all comparisons (Figure 29B). Interestingly, 382 unique DE genes were detected in CD4 *CAR-* versus *CAR+* cells in VSV-LV sample (Figure 29B). In addition, many DE genes were overlapping between CD8 and CD4 cells from VSV-LV sample (Figure 29B). More specifically, the total number of DE genes detected from each analysis between *CAR-* and *CAR+* cells were: 135 in CD8-LV, 277 in VSV-LV (CD8 cells), 98 in CD4-LV, 619 in VSV-LV (CD4 cells) and 161 in total *CAR-* and *CAR+* cells.
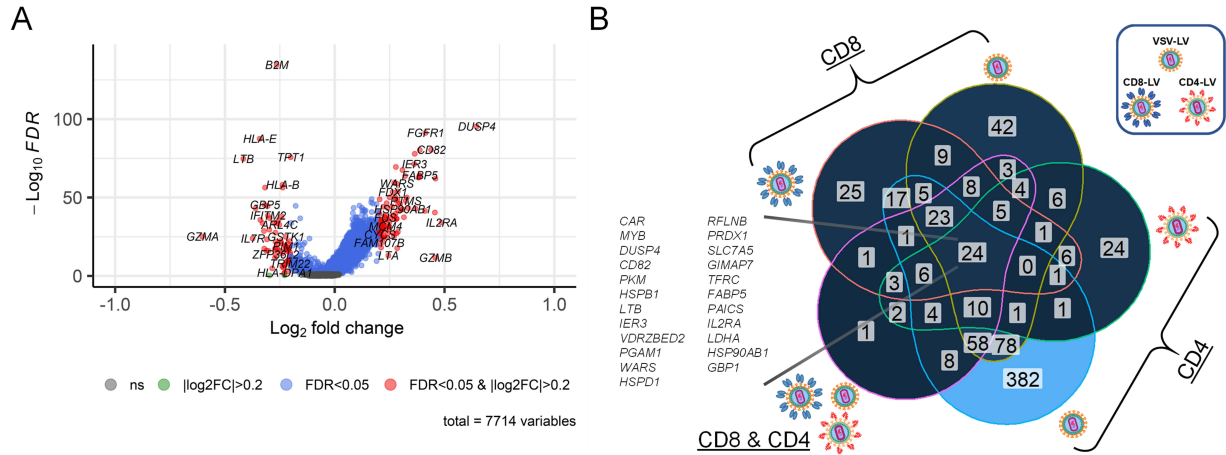
Figure 29: DE genes in total *CAR+* versus *CAR-* cells and overlaps of DE genes.
(**A**) Volcano plot of differential gene expression analysis between total *CAR+* and *CAR-* cells regardless cell and vector type. Significant DE genes were defined as $|\log_2 FC|>0.2$ and FDR<0.05. ns: non-significant. (**B**) Venn diagram showing overlaps of significant DE genes across the comparisons. Most common 24 DE genes are displayed next to the plot.

Gene set enrichment analysis was performed with the DE genes from comparing the total *CAR+* and *CAR-* cells, disregarding the T cell subtypes and the LVs used (Figure 29A), investigating the relevance of gene sets from Kyoto Encyclopedia of Genes and Genomes (KEGG) pathway (Figure 30). Genes upregulated in *CAR+* cells matched with pathways related to metabolism, cell cycle progression, amino acids biosynthesis and signaling, being in agreement with an activated cellular state and proliferation, which was expected from CAR mediated activities (Figure 30). On the other hand, DE genes in *CAR-* cells related to viral infections, antigen presentation and interferon signaling, indicating a prominent antiviral defense status present in cells that did not become successfully transduced by the LVs (Figure 30).
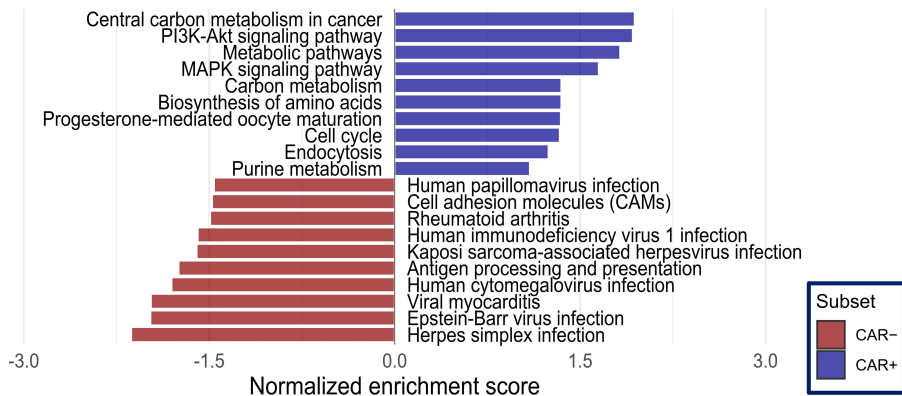
Figure 30: Gene set enrichment analysis in WTA.
Gene set enrichment analysis on Kyoto Encyclopedia of Genes and Genomes (KEGG) pathways using the DE genes identified from the *CAR+* versus *CAR-* comparison of concatenated cells and LV samples ($|\log_2$FC|>0.2, FDR<0.05). *Red bars* indicate pathways enriched in *CAR-* cells, while *blue bars* show the pathways associated with *CAR+* cells.

42

Enrichment analyses with the DE genes from each individual comparison shown in Figure 28 resembled to comparable KEGG pathways as in the former analysis (Figure 30, Figure 31). This indicated that common genes and pathways are regulated leading to successful transduction of PBMC or inhibition of gene transfer, disregarding the vector type used and cell type targeted (Figure 30, Figure 31).
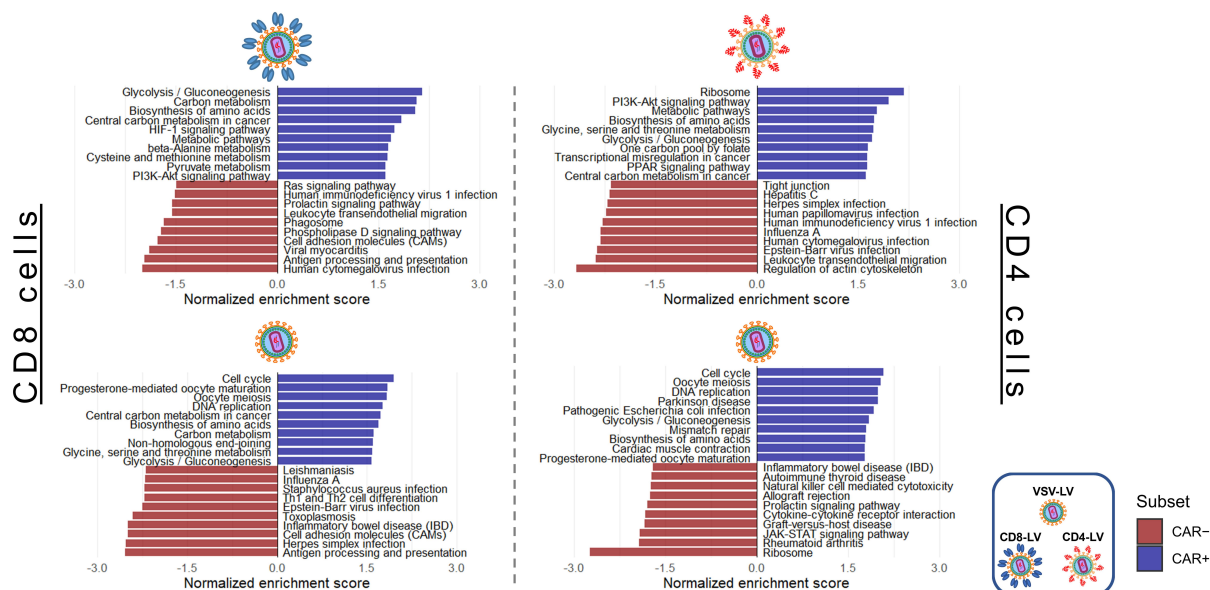
Figure 31: Gene set enrichment analyses of individual subset comparisons.
Gene set enrichment on KEGG pathways with DE genes found in individual comparisons of *CAR+* versus *CAR-* cells, from the subsets of CD8 or CD4 cells, VSV-LV or receptor-targeted LVs ($|\log_2FC|>0.2$, FDR<0.05). *Red bars* indicate pathways enriched in *CAR-* cells, while *blue bars* show the pathways associated with *CAR+* cells.

These analyses revealed that the possible reasons behind unsuccessful LV-mediated gene transfer could primarily be the immunological reaction against the vectors, while the lower metabolic activity and proliferation rate could be also driven by CAR tonic signaling.

Navigating through the list of DE genes from each pre-mentioned analysis, biologically relevant genes were selected to be plotted here. Even though 24 genes found to be shared between all the possible comparisons of *CAR+* versus *CAR-* cells (Figure 29B), significant DE genes exhibiting antiviral activity or even promoting viral infectivity were identified, but also genes that pertain to cellular stress and state (Figure 32).

A big class of interferon-stimulated genes (ISGs) was found to be upregulated in *CAR-* cells, exhibiting antiviral activity against various RNA and DNA viruses with a special focus on human immunodeficiency virus type 1 (HIV-1), severe acute respiratory syndrome coronavirus 2 (SARS-CoV-2), measles (MV), influenza A, hepatitis C (HCV) and poxviruses (Figure 32). Notably, the interferon-induced transmembrane proteins (*IFITM1, IFITM2, IFITM3*) and *LY6E,* which can prevent viral entry, were significantly increased in *CAR-* cells (Figure 32) (Pfaender et al., 2020;

Hornick et al., 2016; Lu et al., 2011). In addition, genes restricting reverse transcription (*SAMHD1*), discriminating and digesting non-self RNA or DNA (*PARP9, ISG20, ADA2*) were up in *CAR-* cells (Figure 32) (Xing et al., 2021; Wu et al., 2019; Goldstone et al., 2011; Khodadadi et al., 2011). In addition, *CAR-* cells had increased expression of genes suppressing the transcription of viral elements (*MX1, TRIM22*) as well as increased IFN type I related transcription factors (*STAT1, IRF1*), regulating the expression of other prominent antiviral restriction factors (*GBP1, IFI6, IFI44L, SAMD9L*) (Figure 32) (Sajid et al., 2021; Y. Li et al., 2021; Meng et al., 2018; Turrini et al., 2015; Verhelst et al., 2012; Haller & Kochs, 2011; Anderson et al., 1999).

On the other hand, cyclophilin A (*PPIA*) and karyopherin subunit alpha 2 (*KPNA2*), which fulfill a crucial role in capsid trafficking and nuclear entry of the HIV-1 pre-integration complex (PIC), were found to be slightly upregulated in *CAR+* cells (Figure 32) (Song et al., 2022; Braaten & Luban, 2001).

Regarding the antioxidant status, we observed that the thioredoxin interacting protein gene (*TXNIP*), which promotes the formation of oxidative radicals by suppressing the activity of thioredoxin, was increased in *CAR-* cells (Figure 32) (Nishiyama et al., 1999). Vice versa, genes of antioxidant enzymes protecting against free radicals were increased in *CAR+* cells, possibly a result of the proliferative and metabolic activities induced by CAR expression (Figure 32). Among them were peroxiredoxin-1 and -2 (*PRDX1, PRDX2*), superoxide dismutase 1 (*SOD1*) and glutathione S-transferases (*GSTP1, GSTO1*) (Figure 32) (Hayes et al., 2020).

With respect to the cell phenotype, *CAR-* cells seemed to sustain a quiescent state by expressing genes related to the naïve or resting phenotype (*IL7R, RIPOR2*), as well as genes inhibiting NF-κB and T cell activation (*AES, PIK3IP1, BTN3A2*) (Figure 32) (Froehlich et al., 2016; Ammann et al., 2013; Defrances et al., 2012; Tetsuka et al., 2000; Schluns et al., 2000). In addition, the expression of pro-apoptotic genes was increased in these cells (*CASP4, STK17B, SHISA5, CYFIP2*) (Figure 32) (Mao et al., 2008; Jackson et al., 2007; Bourdon et al., 2002; Zhivotovsky et al., 1999).
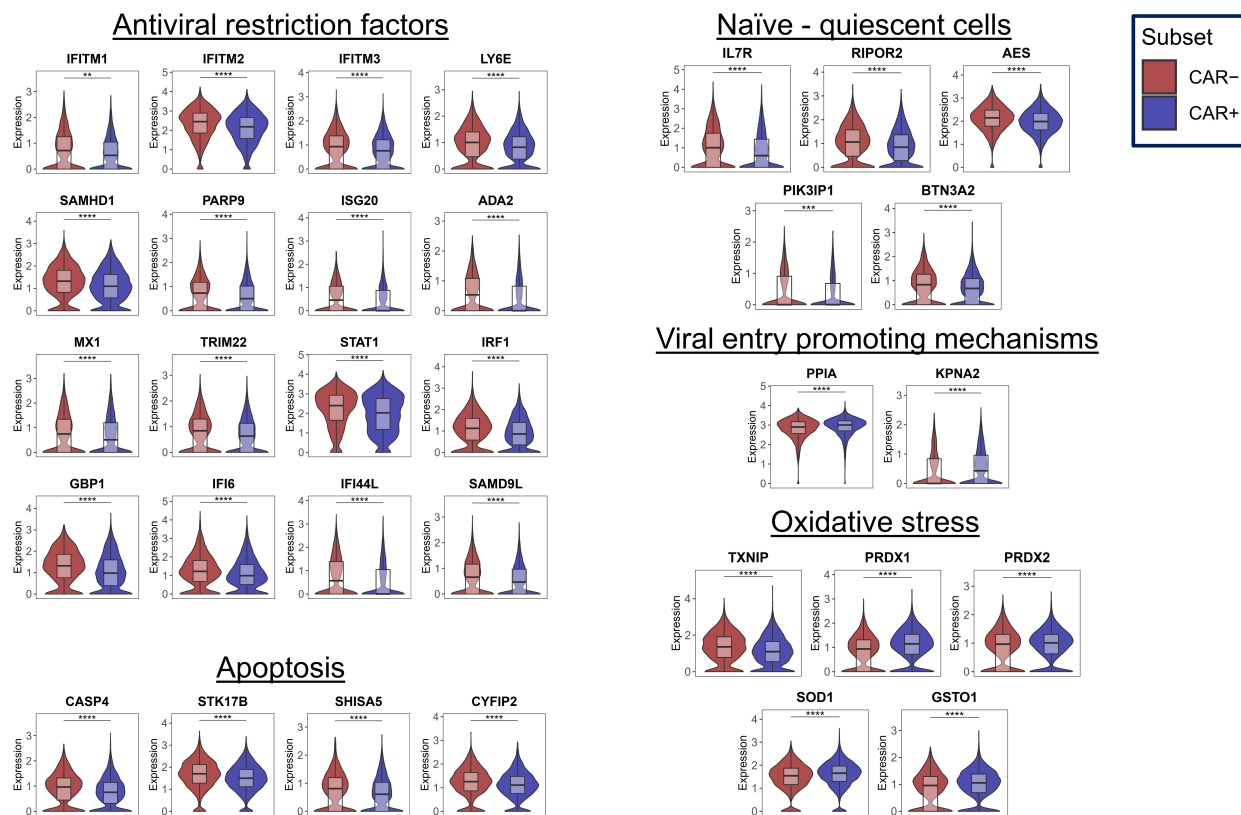
Figure 32: Genes of interest in WTA between *CAR*- and *CAR*+ cells.
Violin plots of differentially expressed genes selected from any individual analysis of cell subset (|log$_2$FC|>0.2, FDR<0.05) and plotted for the concatenated populations of *CAR*- and *CAR*+ cells. Wilcoxon test was performed and FDR was calculated based on multiple gene number. **p<0.01, ***p<0.001, ****p<0.0001.

Overall, these results suggested that antiviral restriction or viral promoting factors implicating in infectivity of enveloped viruses could potentially affect the LV-mediated transduction of human T cells. In addition, the naïve-like, quiescent and/or apoptotic phenotype could negatively impact the successful transduction.

2.3 ENHANCING LV-MEDIATED GENE TRANSFER BY INHIBITION OF ANTIVIRAL RESTRICTION FACTORS

The scRNA-seq data analysis revealed restriction factors that could inhibit the proper transduction of T cells. By screening potential enhancers interfering with antiviral pathways, the mTOR inhibitor rapamycin was found in this study to vastly enhance the CD8-LV and CD4-LV mediated gene transfer. An *in vitro* protocol for preventing drug-induced cytotoxicity, while keeping transduction level at the optimal level, was set up. Although rapamycin was confirmed to downregulate all three IFITMs in human PBMC, the decreased IFITM1, rather than IFITM2 and

IFITM3, was mostly possible to alleviate the restriction of cell membrane fusion entry mediated by the receptor-targeted LVs. To explore which other pathways and proteins related with innate defense are affected by rapamycin, collaboration partners, Dr. Ciara Tierney, Dr. Lisa Strasser and Dr. Jonathan Bones (NIBRT), performed tandem liquid chromatography – mass spectrometry analysis using the Orbitrap Eclipse™ Tribid™. The partners carried out the technical procedures, evaluated the quality and provided the differential protein expression data. Investigation of the data was performed at PEI Mouse studies collaboratively designed by Naphang Ho, Angela Braun and Dr. Frederic Thalheimer (all from PEI) were carried out to examine whether rapamycin can enhance *in vivo* gene delivery with CD8-LV, resulting also in a better tumor control by generated CAR T cells. Validation of statistical analyses was done by experienced biostatisticians, Dr. Christel Kamp and Kay-Martin Hanschmann (both from PEI). For the following experiments, up to this moment of thesis writing, a manuscript has been drafted.

2.3.1 Screening of possible transduction enhancers

According to scRNA-seq data, antiviral restriction factors are upregulated in *CAR-* cells, possibly interfering with the LV-mediated gene transfer and successful transduction of these cells. By hijacking these genes and pathways, the enhancement of LV transduction efficiency was aimed. Thus, small molecules interfering with IFN-induced pathways and LV trafficking were screened during spinfection. These included rapamycin (rapa), cyclosporine A (CsA) as well as their combination (Figure 33). Anti-IFNα was also tested, in order to minimize possible type I IFN secretion due to detection of pathogen-associated molecular patterns (PAMPs) from the viral vectors.

Compared to isotype control, anti-IFNα did not result in any increase of PBMC transduction for both VSV-LV and CD8-LV (Figure 33). In fact, cyclosporine A seemed to suppress the transduction mediated by the two vectors (Figure 33). On the other hand, the addition of rapamycin during spinfection resulted in improved CD8-LV mediated transduction of target cells, reaching to as high transduction efficiency as the VSV-LV (Figure 33). However, rapamycin did not improve the gene transfer with VSV-LV (Figure 33). Furthermore, the combination of rapamycin and cyclosporine A negatively impacted the transduction efficiency for both vectors, as seen in cyclosporin A alone (Figure 33). It was also noticed that the viability of PBMC incubated with 10 µM of cyclosporine A was affected.
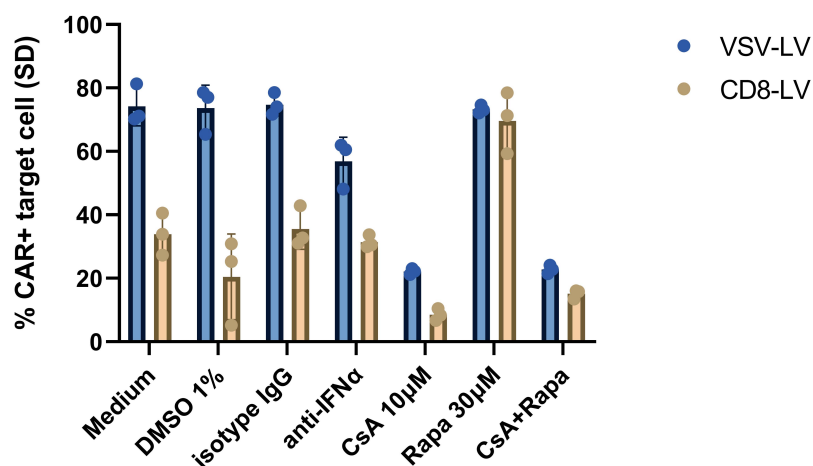
Figure 33: Screening possible LV transduction enhancers.
Pre-activated T cells inoculated with same dose of VSV-LV or CD8-LV transferring CD19-CAR in presence of anti-IFNα (clone LT27:295, 1 µg/mL), cyclosporine A (CsA, 10 µM), rapamycin (rapa, 30 µM) or combination of the last two. Maximum DMSO concentration (1% v/v) and isotype IgG were used as control. Medium was renewed after 1.5 hours of spinfection. Transduction of target cell populations was assessed by flow cytometry 3 days later (N=3). *SD: standard deviation.*

2.3.2   Rapamycin enhances *in vitro* transduction of CD8-LV and CD4-LV

The observation that rapamycin could possibly enhance CD8-LV gene transfer in human PBMC was thoroughly investigated. Hence, more transduction assessments were performed with PBMC from multiple donors, titrating CD8-LV, CD4-LV and VSV-LV.

A vast increase in gene delivery was observed, and thus conversion of T cells into CAR T cells, with both CD8-LV and CD4-LV (Figure 34A, B). The increase accounted to up to 7.3-fold for CD8-LV and 3.5-fold for CD4-LV and was more pronounced for lower particle doses, reaching transduction rates of more than 90% of the CD8 target cells or more than 50% of CD4 target cells, respectively (Figure 34A, B). Notably, rapamycin did not increase transduction mediated by VSV-LV (Figure 34A, B).
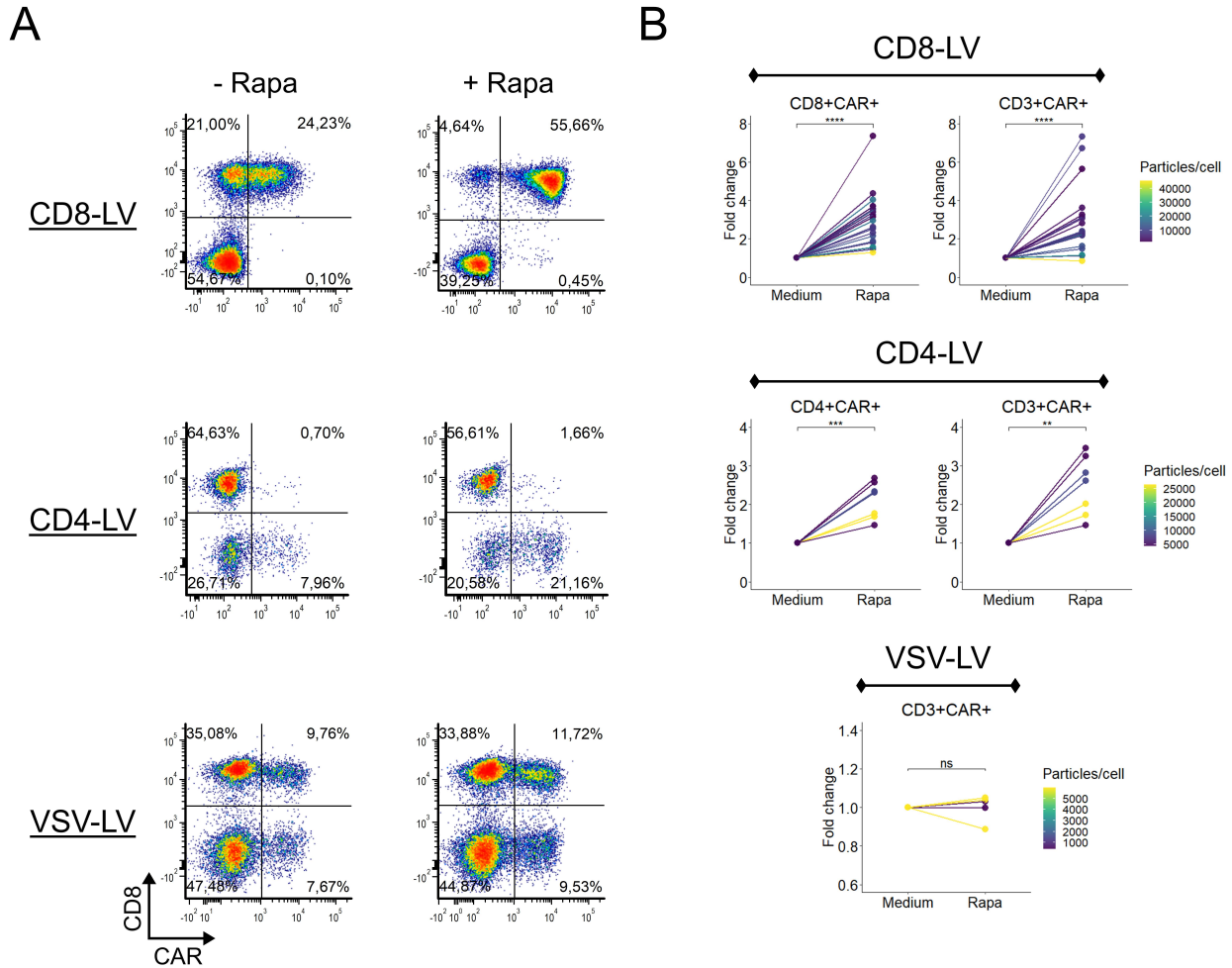
Figure 34: Enhancement of CAR T cell generation via receptor targeted LVs in presence of rapamycin.
(**A**) Representative flow cytometry results of CAR T cells generated with CD8-LV, CD4-LV or VSV-LV in presence or absence of 30 µM rapamycin. (**B**) Fold change difference in the percentage of CAR+ cells upon transduction of targeted T cell subtypes (left) or total CD3 cells (right) with CD8-LV, CD4-LV or VSV-LV (only on CD3 cells) in presence or absence of 30 µM rapamycin (CD8-LV: N=16-18, donors=4, particles/cell=1.79×10^3-4.97×10^4; CD4-LV: N=7, donors=2, particles/cell=4.42×10^3-2.65×10^4; VSV-LV: N=5, donors=2, particles/cell=435 or 6×10^3). Paired t-test was performed. ns: non-significant, **$p < 0.01$, ***$p < 0.001$, ****$p < 0.0001$.

Focusing more on the effects of rapamycin on CD8-LV, as it resulted in most pronounced differences, we observed a significantly higher mean fluorescence intensity (MFI) of extracellular CAR, showing that the rapamycin treatment improved the expression of CAR on the cell surface (Figure 35).
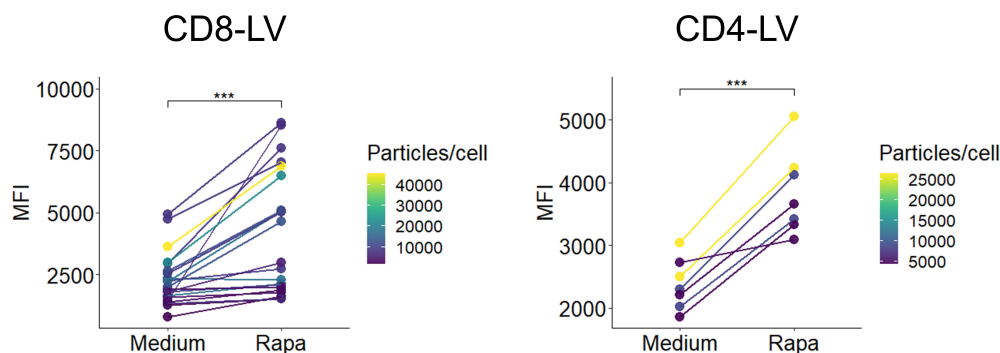
Figure 35: Enhanced MFI of CAR T cells pre-treated with rapamycin.
Fold change difference of mean fluorescence intensity (MFI) of CAR expression on target cells pre-treated with rapamycin compared to untreated. Paired t-test was performed. ***p<0.001.

2.3.3 Medium change post-spinfection rescues T cell viability

Arguing about rapamycin's cytotoxic and immunosuppressive potency against T cells, the optimal concentration and way of usage were examined. Thus, PBMC were spinoculated with the same dose of CD8-LV vector, in an increasing concentration of rapamycin. After spinfection, medium was either renewed or cells were further incubated in presence of the drug for 3 days, until flow cytometry analysis.

It seemed that 30 µM was indeed the most suitable concentration, resulting in the highest transduction of target cells by the CD8-LV (Figure 36A). In addition, when the medium was renewed directly after spinfection, the viability of the cells treated with 30 µM was not compromised (Figure 36A). The effect of lower concentrations even without renewing the medium did not result in any greater enhancement (Figure 36A). On the other hand, higher concentrations of rapamycin, above than the optimal 30 µM one, following medium change, impacted the T cell viability (Figure 36B).
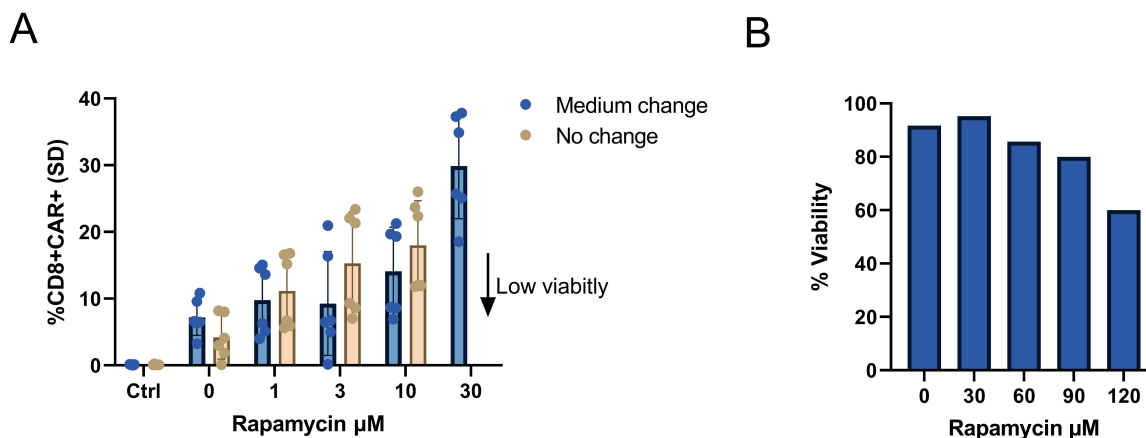
Figure 36: Rapamycin titration on PBMC and effect on transduction and viability.
(**A**) Pre-activated T cells inoculated with same dose of LV in presence of increasing concentration of rapamycin. Non-inoculated cells were used as control. Medium was either completely renewed after 1.5 hour of spinfection (blue bars) or not (golden bars) (N=6, donors=3). Transduction was determined after 3 days by flow cytometry. (**B**) Viability assessment

of increasing rapamycin concentrations from 30 to 120 µM by flow cytometry (N=1, donor=1, technical duplicates were pooled for one staining). *SD*: standard deviation.

2.3.4   Increased *in vivo* GFP transfer with CD8-LV through rapamycin

Having documented the high potency of utilizing rapamycin for enhancing gene transfer *in vitro*, its effect on *in vivo* gene delivery with CD8-LV was assessed. For that purpose, NSG mice were transplanted with pre-activated PBMC (10^7/mouse) one day prior LV administration (Figure 37A). The next day, two doses of rapamycin, or vehicle lacking the drug were intraperitoneally (i.p.) administered. One hour later CD8-LV particles were intravenously (i.v.) injected and mice were monitored for 7 days. GFP expression was assessed by flow cytometry in peripheral blood, spleen and bone marrow.

Intriguingly, the overall highest levels of GFP were observed in mice that had received the high rapamycin dose (8 mg/kg) (Figure 37B). This was equally well pronounced in blood, spleen, and bone marrow. Also, at the low dose, a slight increase of the average GFP value over the vehicle group was documented (Figure 37B). However, it was remarkable that for the high dose group the values obtained for the individual mice included in this group were much more consistent than in the vehicle or low dose groups (Figure 37B). The vector copy numbers (VNCs) present in splenic T lymphocytes and the MFIs of GFP expression further confirmed the *in vivo* transduction enhancement mediated by rapamycin (Figure 37C, D). Moreover, rapamycin did not perturb the *in vivo* specificity of CD8-LV for human CD8 cells, which reached to an average of 98.2% (±2.3%) in blood, 97% (±1.9%) in spleen and 97% (±1.7%) in bone marrow for rapamycin-treated mice (Figure 37E).
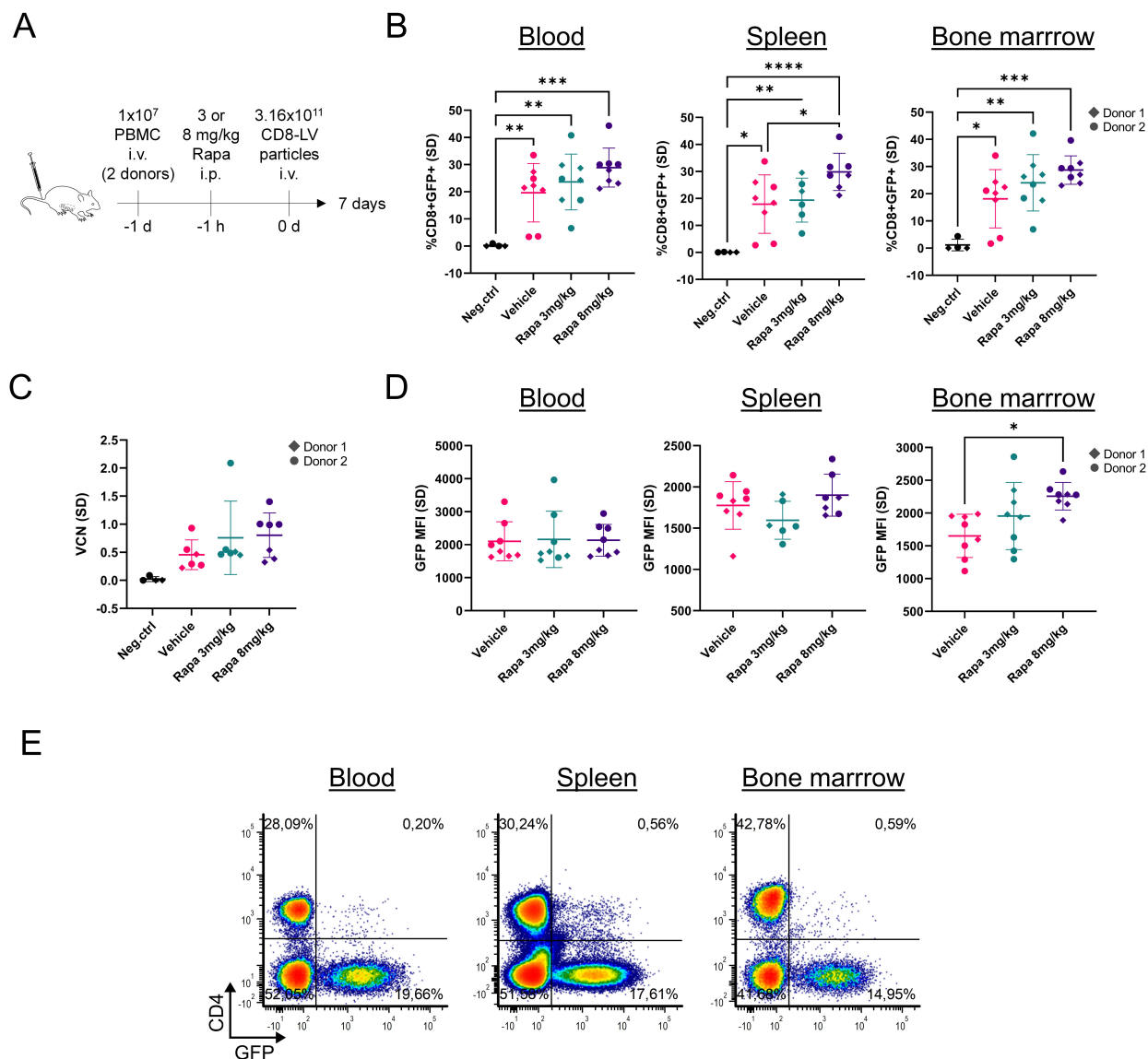
Figure 37: Enhancing *in vivo* GFP transfer with rapamycin.
(**A**) Experimental workflow of *in vivo* GFP transfer with CD8-LV into humanized NSG mice. Rapamycin was injected in concentrations of 3 or 8 mg/kg. Vehicle (2% DMSO, 30% PEG300, 5% Tween-80) was used as control. Study was repeated with two anonymous donors. (**B**) GFP expression in human CD8 T cells assessed by flow cytometry in blood, spleen and bone marrow samples. (**C**) Vector copy number (VCN) of GFP transfer gene integration in genomic DNA of human CD3 cells sorted from mouse spleens. (**D**) Mean fluorescence intensity (MFI) of GFP expression in *in vivo* transduced CD8 cells. (**E**) Flow cytometry plots of concatenated tissue specific samples from rapamycin treated mice for evaluating the *in vivo* selectivity of CD8-LV on human CD3 cells assessed as CD4 negative cells. *SD*: standard deviation. i.v. intravenous, i.p. intraperitoneal. *$p<0.05$, **$p<0.01$, ***$p<0.001$, ****$p<0.0001$.

In addition, there was no effect of rapamycin or vehicle on the reconstitution of human T cells in the mice. Particularly, the fractions of human CD8 T cells in blood, spleen and bone marrow were highly homogenous and did not significantly differ between the groups (Figure 38).
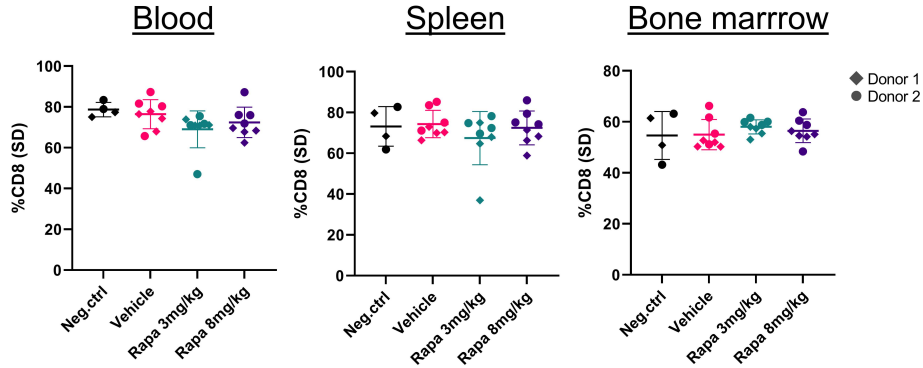
Figure 38: Frequency of target cells assessed in different tissues from the mouse study.
Frequency of target human CD8 T cells determined as CD4- cells in flow cytometry in blood, spleen and bone marrow. *SD*: standard deviation.

2.3.5 Rapamycin downmodulates various antiviral restriction factors in human T cells

To confirm the activity of rapamycin on downregulating the IFITMs in human T cells, PBMC from 3 donors were incubated with different rapamycin concentrations. The cellular levels of the three IFITMs were determined by Western blot. While incubation with IFNα further stimulated their expression, all applied doses of rapamycin led to a strong downmodulation of all three IFITMs within 1.5 hours (Figure 39A, B). This fold-change decrease was statistically significant for IFITM1, in all concentrations (Figure 39B). The decreased fold-change was also consistent in all three tested donors (Figure 39B).
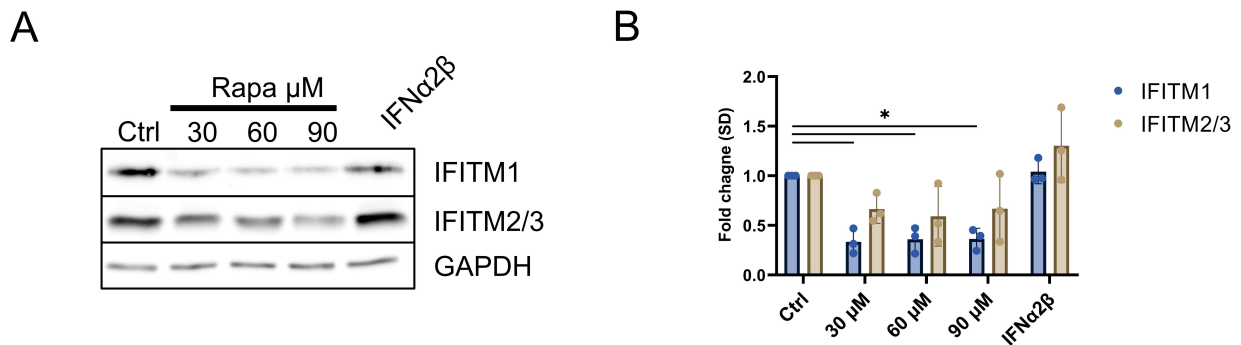
Figure 39: Western blot analysis of IFITMs upon rapamycin treatment.
(**A**) Western blot detecting IFITM1, IFITM2/3 and GAPDH in lysates of human T cells treated with increasing concentrations of rapamycin or 500 IU/mL IFNα2β for 1.5 hours. (**B**) Quantification of three western blots showing fold change differences of IFITMs normalized to GAPDH (donors=3). Statistical analysis was perfromed by two-way ANOVA test. *SD*: standard deviation. *$p < 0.05$.

To further explore the consequences of rapamycin treatment in T lymphocytes, liquid chromatography-mass spectrometry (LC-MS) proteome analysis was conducted on pre-activated PBMC from 6 donors, comparing untreated samples with rapamycin or DMSO (diluent) treated samples, respectively.

Intriguingly, not only the IFITM1 protein was downregulated upon rapamycin treatment, thus confirming the western blot data, but 16 other proteins featuring the IFN type I antiviral pathway were decreased, too (Figure 40A). These included LGALS3BP, IFI30, IRF2, TRIM38, TRIM32, IFIH1, IFI44, IRF7, IFI44L, IFIT3, IRF9, PARP10, IRF2BP2, MX1, IFIT1 and ISG15. In addition, proteins related with naïve (SELL) and quiescence (RIPOR2) cell state and T helper 2 (T_H2) phenotype (JUND) were downregulated upon rapamycin treatment, indicating either activation/mobilization or a selective pressure against naïve cells skewing the differentiation towards the T_H1 phenotype (Meixner et al., 2004). Also, some caspases were found to be downregulated (CASP3, CASP6, CASP9), while proliferation and DNA re-organization related proteins (TOP2A, TOP2B) were upregulated, showing a possible anti-apoptotic effect by rapamycin (Figure 40A). The downregulation of SOD2, GSR, GSTM1 and GSTM3 by rapamycin could indicate a possible susceptibility in oxidative stress (Figure 40A). However, at least in part this comes from DMSO used as diluent of rapamycin. While DMSO did not significantly influence the antiviral proteins, with the exception of IFI30, downregulation of SOD2 can be clearly accounted to its activity (Figure 40A). Overall, of the 882 proteins found to be dysregulated upon rapamycin treatment (711 down- and 171 up-regulated) 213 out of 429 identified upon DMSO treatment were in common with the rapamycin treated samples, although the majority of differences was less significant and less pronounced in DMSO treated samples (Figure 40B).

A

B
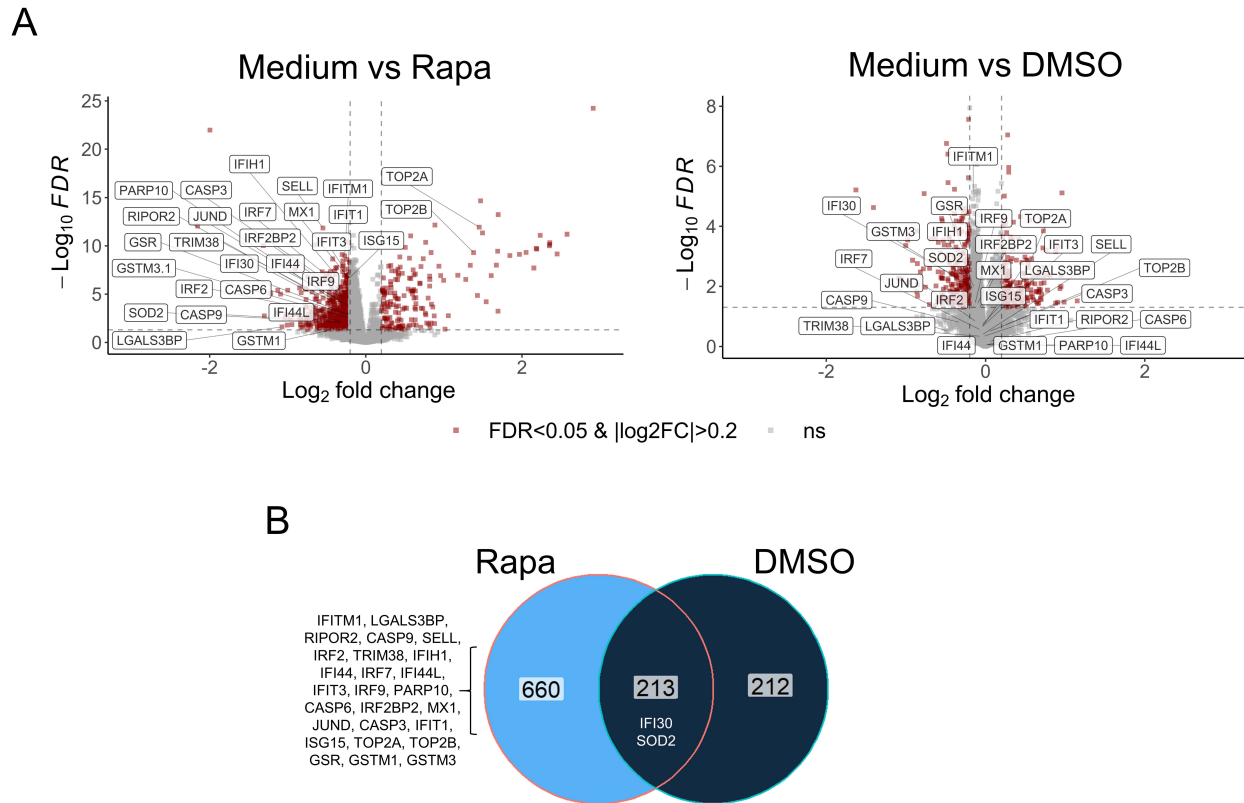
Figure 40: Proteomic alterations induced in human T cells by rapamycin. (**A**) Volcano plots of LC-MS proteome analysis of PBMC treated with 30 μM rapamycin versus untreated (donors=6, in technical triplicates) (left) and PBMC treated with 0.5% DMSO versus untreated (donors=6, technical replicates of each sample=3) (right). (**B**) Overlap of significantly up- and down-regulated proteins between rapamycin or DMSO treated samples ($|log_2FC| > 0.2$, FDR < 0.05). Differential protein expression data were provided by Dr. Ciara Tierney, Dr. Lisa Strasser and Dr. Jonathan Bones (NIBRT), who conducted the LC-MS run. Data were investigated and visualized at PEI.

2.3.6 *In vivo* CAR T cell generation with rapamycin shows faster tumor regression

To apply these findings to a therapeutic approach, it was next investigated if rapamycin improves CAR T cell generation with CD8-LV. First, the performance of CAR T cells generated in presence of rapamycin was compared with conventional CAR T cell *ex vivo*.

The presence of rapamycin did not result in any significant differences in proliferation rates of CAR T cells (Figure 41A). Also, their cytotoxicity against target NALM6 cells was indistinguishable (Figure 41B). Finally, the treatment did neither significantly impact on the exhaustion of CAR T cells nor on the memory phenotype mainly present in the majority of the analyzed donors (Figure 41C, D).
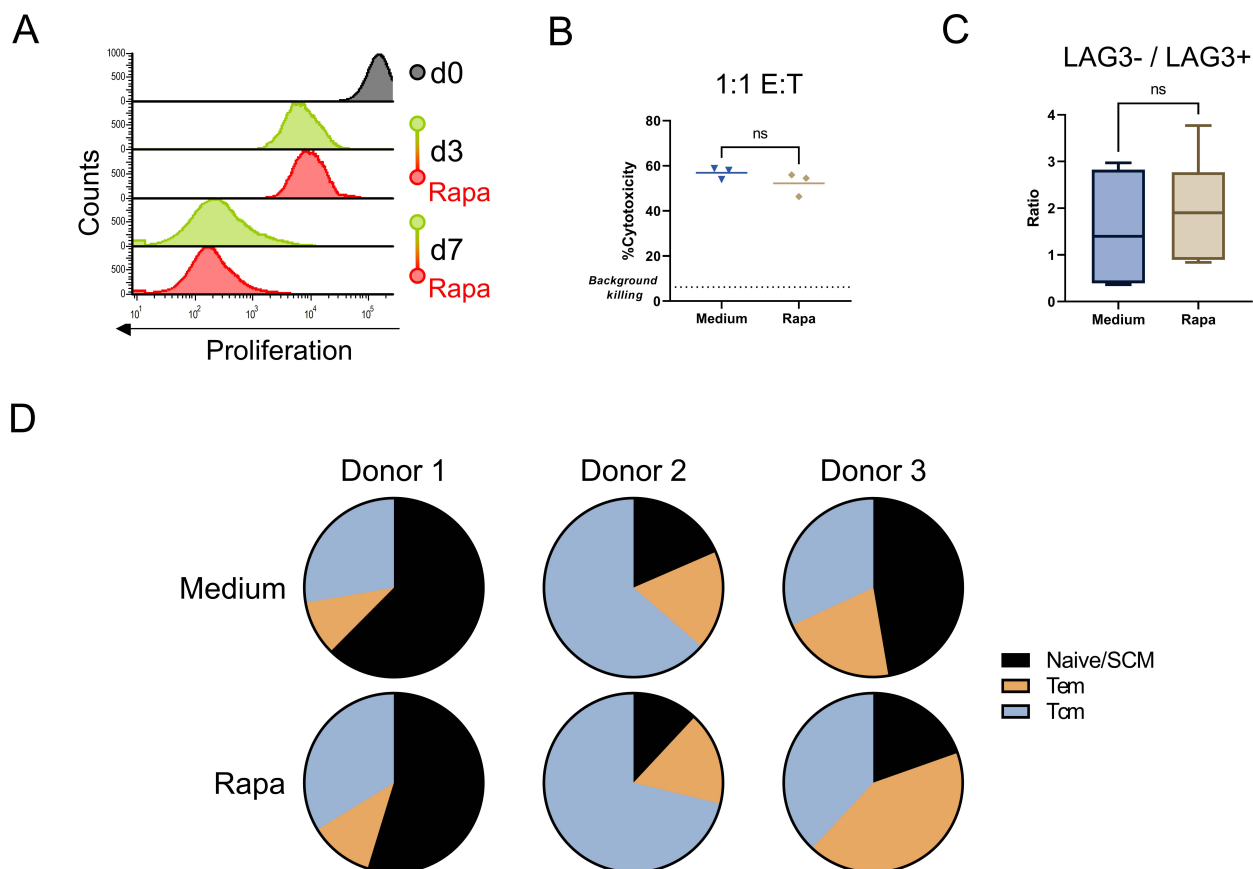
Figure 41: Effects of rapamycin on CAR expression, proliferation and CAR T cell phenotypes.
(**A**) Proliferation of CD8+CAR+ T cells generated by CD8-LV in presence or absence of rapamycin (donor=1). (**B**) Cytotoxicity assessment of CD8 CAR T cells generated with or without rapamycin co-cultured with NALM6 tumor cells in 1:1 effector to target ratio and assessed 4 hours later. Total T cell number was normalized with untransduced control T cells cultured with or without rapamycin. Dotted line indicates the background killing mediated by untransduced cells co-cultured with tumor cells. (**C**) Ratio of CD8+CAR+LAG3- to CD8+CAR+LAG3+ cells generated in presence or absence or rapamycin (n=11, donors=3). (**D**) Pie charts representing frequencies of memory phenotypes of CD8 CAR T cells of 3 donors generated in presence or absence of rapamycin (n=11, donors=3, SCM: stem cell memory). ns: non-significant.

Overall, these results showed that rapamycin did not significantly influence the performance of CAR T cells generated *ex vivo.*

For the *in vivo* setting (Figure 42A), mice were transplanted with NALM6-luc cells stably expressing firefly luciferase. After 4 days, mice were allocated to four different groups to achieve a similar distribution of tumor load (Figure 42B). Pre-activated human PBMC were injected and the following day we administered vehicle or rapamycin in two different doses followed by i.v. injection of CD8-LV transferring the CD19-CAR-28z gene.

55

A

5x10^5 NALM6-luc i.v. | 1x10^7 PBMC i.v. | 3 or 8 mg/kg Rapa i.p. | 9x10^{11} CD8-LV particles i.v.

-6 d   -1 d   -1 h   0 d   → 18 days

B

ANOVA: ns
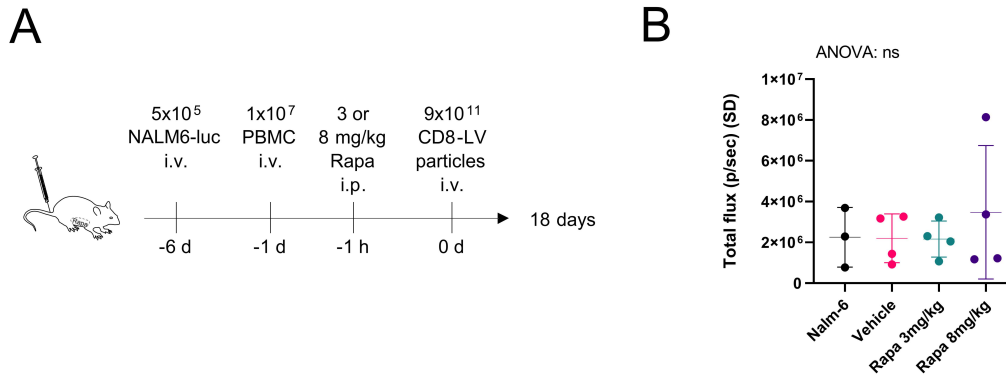
Figure 42: *In vivo* CAR T cell mouse model set-up and randomization.
(**A**) Experimental workflow. Rapamycin (rapa) was injected in concentrations of 3 or 8 mg/kg and vehicle (2% DMSO, 30% PEG300, 5% Tween-80) was used as control. (B) Randomization of mice into treating groups based on the tumor burden assessed by luminescence imaging of luciferase activity of engrafted NALM6-luc cells on day -2 prior CD8-LV injection. ANOVA test was performed in log-transformed data. i.v. intravenous, i.p. intraperitoneal. *SD*: standard deviation. ns: non-significant.

All vector-treated groups reached tumor control, becoming statistically significant latest by day 14 (Figure 43A, B). While most of the treated mice progressed until day 12 at rates comparable to the control and then declined and reached a plateau, the low dose rapamycin mice were much more rapid in tumor control reaching this status already by day 7. In this group, tumor loads remained at substantially lower levels with higher statistical significance ($p < 0.0001\text{-}0.05$) than the vehicle group ($p < 0.05$) (Figure 43A). At the endpoint of the experiment, 2 out of 4 mice had no detectable luciferase signals in the 3 mg/kg group, while this was the case for 1 out of 4 mice in the two other vector-treated groups (Figure 43B).

As expected for this type of tumor cells, the vast amount of NALM6 cells were present in bone marrow, making up around 40% of all cells on average (Figure 43C). Accordingly, only small amounts were detectable in spleen and blood of the untreated control animals, which due to their homing ability in bone marrow became less over time (Figure 43C). In all vector-treated animals tumor cell levels were substantially reduced or even undetectable as it was the case for most animals (Figure 43C). Especially the tumor cell elimination from bone marrow was clearly documented and was well in agreement with the data obtained by *in vivo* imaging (Figure 43B, C). Residual tumor cells were only detectable in a single animal of the vehicle and the high dose group, respectively (Figure 43C).

A

B

C
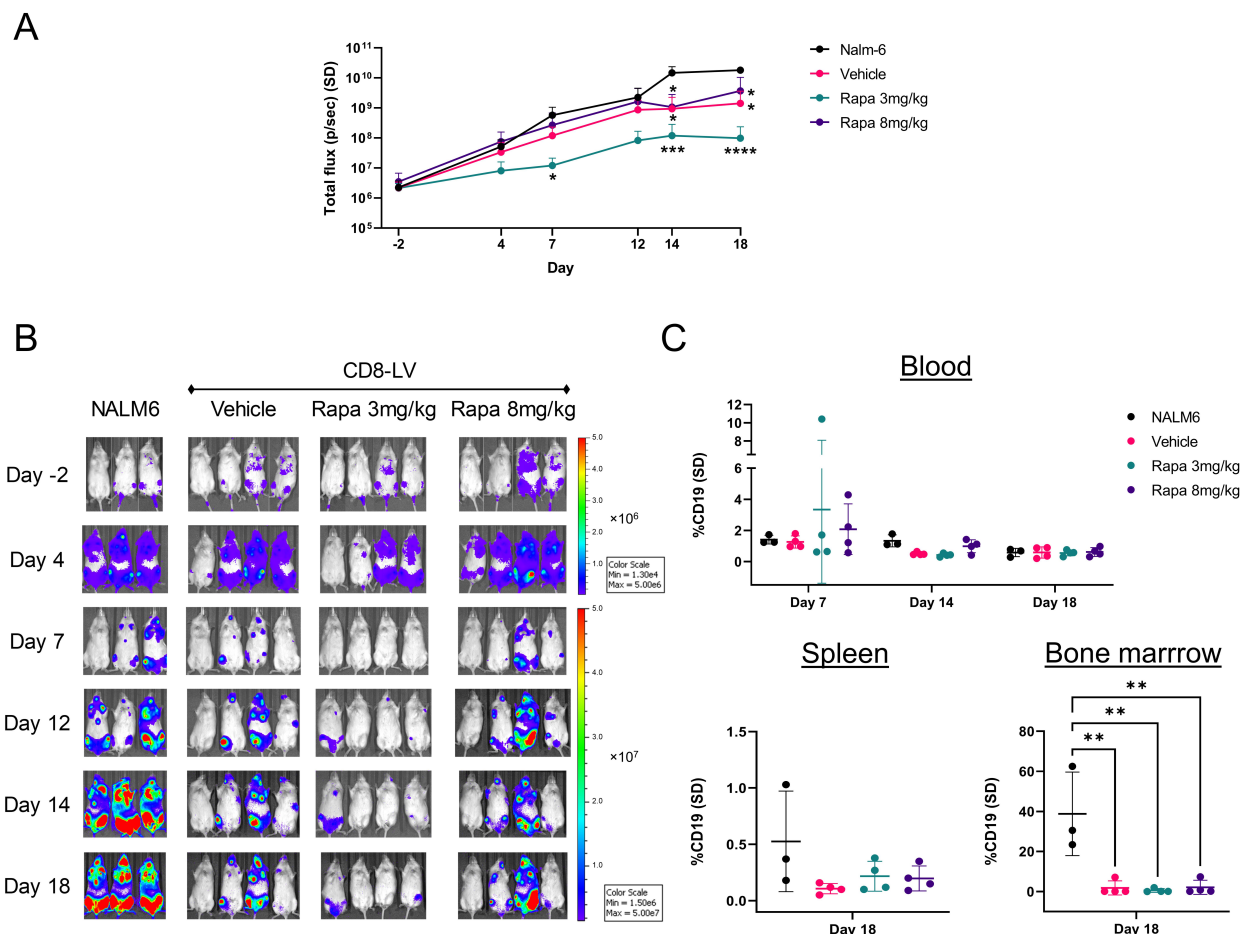
Figure 43: Monitoring tumor growth upon *in vivo* CD19-CAR generated T cells in mice pre-treated with rapamycin.
(**A**) Tumor burden assessed by luminescence in mice pre-treated with rapamycin in concentrations of 3 or 8 mg/kg or vehicle (2% DMSO, 30% PEG300, 5% Tween-80). Mice were monitored at the indicated days pre- and post CD8-LV and rapamycin injections. Two-way ANOVA with Tukey's multiple comparisons was performed on log-transformed data. (**B**) Luminescence imaging of ventral side of grouped mice on two different scales. (**C**) Frequencies of NALM6 (CD19+) cells in the indicated mouse tissues as detected by flow cytometry. i.v. intravenous, i.p. intraperitoneal. *SD*: standard deviation. *$p < 0.05$, **$p < 0.01$, ***$p < 0.001$, ****$p < 0.0001$.

Flow cytometry was performed to monitor the cellular compositions in blood during intermediate samplings and additionally in spleen and bone marrow on the day of final analysis. Rapamycin had no impact on the frequencies of human CD45 and CD8 cells (Figure 44A, B).

A

B
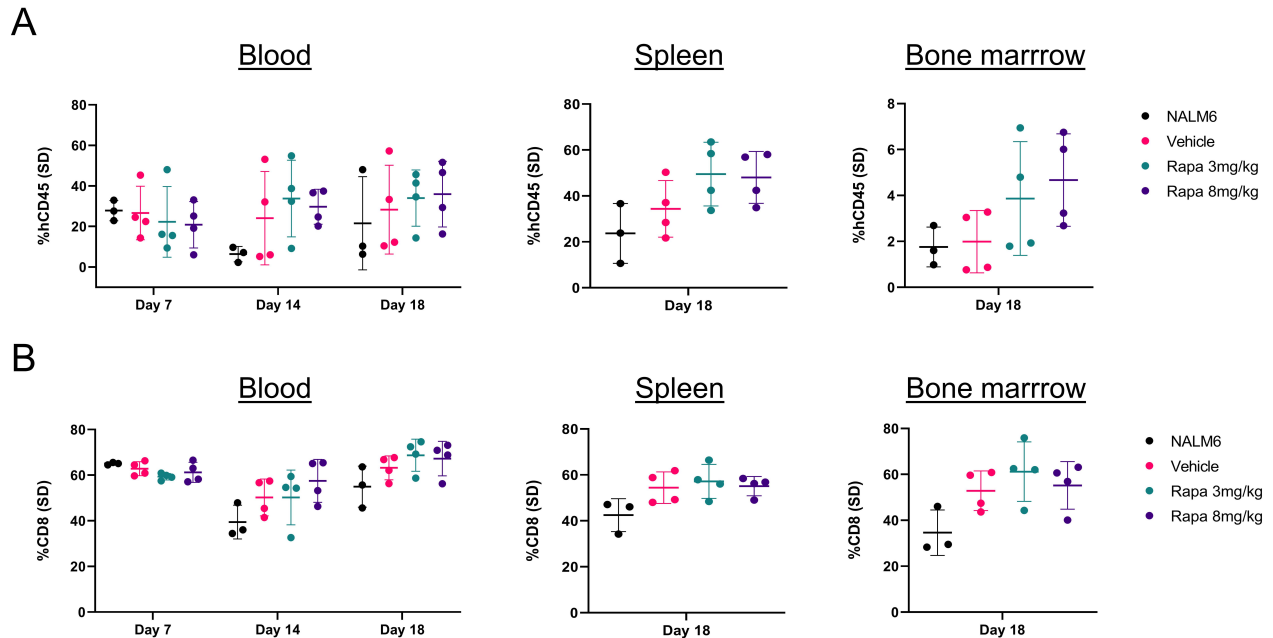
Figure 44: Humanization and frequency of target cells in tumor model mice.
(**A**) Humanization of mice defined as frequency of human CD45 cells detected by flow cytometry among experimental groups on day 7, 14 and 18 in blood and on day 18 in spleen and bone marrow after CD8-LV injection. (**B**) Frequency of human CD8 T cells in blood, spleen and bone marrow. *SD*: standard deviation.

On day 7 post vector injection CAR T cell levels in both rapamycin groups made up about 2% of CD8 cells, which was about 2-fold higher than in the vehicle group (Figure 45A), which nicely corresponded to the more rapid tumor cell clearance in the low dose group monitored by *in vivo* imaging. CAR T cell frequencies peaked on day 14 post-injection in all vector groups (Figure 45A). On day 18, CAR T cell levels had declined, thus correlating with tumor regression. In fact, it was the individuals with the highest remaining tumor loads that had detectable CAR T cells on that day, indicating a better expansion and persistence of CAR T cells in presence of tumor target cells (Figure 45A). Further proof for the successful *in vivo* generation of CAR T cells was provided by *ex vivo* co-culturing mouse splenocytes and bone marrow cells harvested from the vector-injected animals with irradiated tumor cells. CAR T cells quickly expanded in all the groups with frequencies nicely correlating to those detected directly in the harvested organs (Figure 45B). In addition, VCNs determined in human T lymphocytes on day 18 mirrored the unsynchronized decrease of CAR T cells between the LV groups, with the rapamycin treated mice having a faster decrease (Figure 45C).
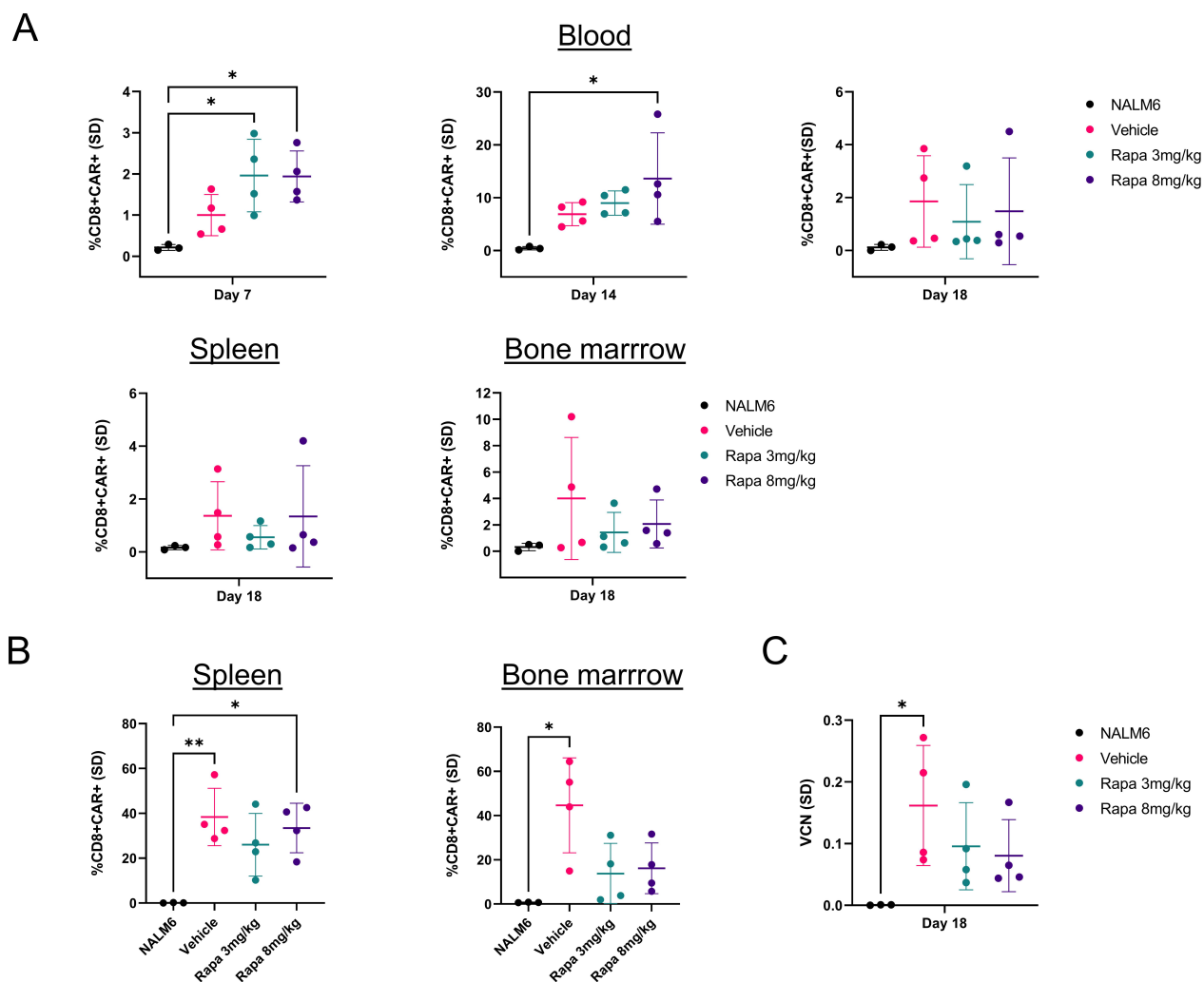
Figure 45: *In vivo* **CAR T cell generation in presence of rapamycin.** (**A**) CAR expression on human CD8 cells assessed by flow cytometry at the indicated days in blood and tissues of mice pre-treated with rapamycin with rapamycin in concentrations of 3 or 8 mg/kg or vehicle (2% DMSO, 30% PEG300, 5% Tween-80) prior CD19-CAR transferring CD8-LV injection. (**B**) Ex vivo CAR T cell expansion from spleen and bone marrow samples (day 18) by co-culturing with irradiated NALM6 cells. Flow cytometry analysis was performed after 7 days of co-culture, cells from each mouse were seeded in technical duplicates, which were averaged before plotting. (**C**) Vector copy number (VCN) of CAR transfer gene integration in genomic DNA of human CD3+ cells sorted from mouse spleens. *SD*: standard deviation. *p<0.05, **p<0.01.

Overall, rapamycin administration showed a potency to mediate CAR T cell generation with CD8-LV more rapidly *in vivo*, controlling tumor growth quicker. Last but not least, the single dose of rapamycin into mice did not result in any adverse effect.

3 DISCUSSION

3.1 ESTABLISHING SCRNA-SEQ ANALYSIS OF CAR T CELLS

3.1.1 Detecting CAR T cells via scRNA-seq

The local installation of the BD Rhapsody scRNA-seq pipeline at Paul-Ehrlich-Institut enabled the comprehensive characterization of CAR T cells generated by conventional or T cell receptor-targeted LVs. Both targeted and whole transcriptome approaches had their own impact on the investigation. The former rendered a more sensitive and higher resolution analysis in a relatively big sample size, but also ameliorated the set-up of the bioinformatic analysis workflow (Figure 46). The whole transcriptome analysis provided an unbiased and thorough investigation, revealing all genes and pathways related to successful T cell transduction.
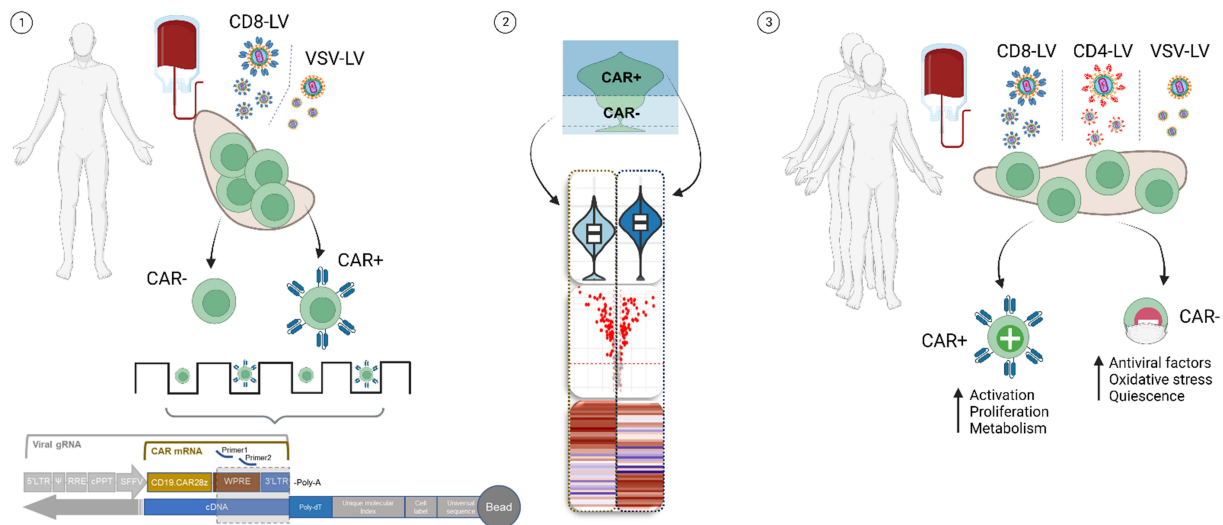
Figure 46: Overview of targeted and whole transcriptome scRNA-seq profiling of CAR T cells.
(1) For the establishment of single-cell transcriptomic analysis pipeline, T cells from a healthy donor, inoculated with CD8-LV or VSV-LV transferring CD19-CAR, were captured in single-cells with a nanowell-based system and processed for targeted gene analysis. Customized primers were implemented to detect *CAR* mRNA. (2) Setting-up a computational approach for identification of *CAR-* and *CAR+* cells and downstream *in silico* data analysis. (3) Whole transcriptome analysis performed with T cells from 3 donors inoculated with CD8-LV, CD4-LV or VSV-LV thoroughly investigating the molecular differences between *CAR-* and *CAR+* cells. Mutual gene expression signatures were identified across distinct LV types affecting the proper transduction of T cells. Adapted from Charitidis et al., 2021 and completed with BioRender.

As there is no gold standard for pre-processing scRNA-seq data, cloud-based platforms are continuously optimizing and standardizing these steps, in order to minimize user-based variabilities, which often lead to different outcomes (You et al., 2021). Such a platform is the Seven

60

Bridges (https://www.sevenbridges.com/), used during these studies. This platform offers various pre-processing pipelines, often fitted to the underlined methodology of scRNA-seq library preparation (i.e. BD Rhapsody), and generates the count matrices for the downstream analyses.

Commencing with the first targeted gene analysis (TGA), 6-day old CAR T cell generated with VSV-LV or CD8-LV, as well as control bystander cells, were investigated. The exact location of poly-A tail was identified to reside within the 3'-LTR region, which is in agreement with previous publications (Richardson et al., 1995; Guntaka, 1993). Customized primers specifically amplifying the 3'-end of the CAR transgene were validated to be compatible with the transgene construct and the predesigned panel of primers used in TGA. This enabled the detection of CAR expressing genes. In a similar manner, hybridization probes were used for sensitive and accurate detection of CAR expression in axicabtagene ciloleucel (axi-cel) infusion products, processed with the 10X Chromium pipeline (Deng et al., 2020). This method resulted in increased sequencing saturation of the CAR molecules, thus increased sensitivity of detecting the CAR T cells from whole transcriptome data (Deng et al., 2020).

For the identification of CD8 CAR T cells, a multimodal subsetting strategy was introduced due to the apparent trimodal distribution in the expression of *CD8A* and *CAR* genes (Figure 12). Investigating the intermediate population of either *CD8A* or *CAR* low-expressing cells, it became obvious that the transcriptomes of these cells were basically identical with the negative population (Figure 14). On the other hand, *CD8A^{high}* and *CAR^{high}* cells were accounted to be the actual CD8 and CAR T cells, respectively (Figure 16). Although the *CAR^{low}* cells were considered to be non-transduced, the *CD8A^{low}* expression can result from differential regulation of gene expression by its endogenous promoter (Erhard et al., 2019). This transient intrinsic mRNA fluctuation does not necessarily imply loss of the expressed protein (Erhard et al., 2019). Ideally, the identification of CAR T cells should be conducted through DNA sequencing in parallel with RNA, allowing the characterization of cells with integrated transgene into genomic DNA.

Utilizing a similar term of *CAR^{high} and CAR$^{neg/low}$* cells, Rodriguez-Marquez et al. (2022) sorted CAR T cells expressing highly the CAR molecule on their surface (CAR^{High}) or low (CAR^{Low}), based on the MFI range in flow cytometry. In contrary to these classifications, *CAR^{low}* cells (mRNA) from the TGA analysis conducted in this thesis do not represent the CAR^{Low} cells (protein), as the gene expression signature of *CAR^{low}* was closely linked to non-transduced cells (Figure 14). Eventually, their observation was an effect of increased vector copy integration, leading to higher CAR mRNA and protein expression.

Based on the computational subsetting strategy developed in this thesis, the frequencies of CAR T cells detected by scRNA-seq were highly consistent with the numbers detected by flow cytometry for both, CD8-LV and VSV-LV inoculated cells (Figure 15). X. Wang et al. (2021) did

also notice that the frequencies of CAR T cells detected by both methods were very similar. The use of CD8-LV successfully validated the subsetting approach, even by visual observation of *CAR^high* cells on UMAP plots. The *CAR^high* cells in CD8-LV were predominantly located in CD8 cluster, while in VSV-LV both, CD4 and CD8 *CAR^high* populations, are distinguishable (Figure 13). In contrary to TGA, the frequency of CAR+ cells in flow cytometry did not match with *CAR* mRNA expressing cells, in WTA (Table 3). That could be a result of delayed protein synthesis at early timepoints of an expressed gene (Cheng et al., 2016; Gedeon & Bokes, 2012). Similar observations were made in NK cells transduced with a LV to express GFP, where on day 7 the frequency and MFI reached to slightly higher levels than on day 3 (Bari et al., 2019). It is likely that in the present thesis, the day-6 samples in the TGA approach had reached to equilibrium of mRNA and protein expression, while the 3-day cultivated WTA samples had not. Nonetheless, transcriptomic differences were still detectable when comparing *CAR* mRNA positive with negative cells.

The transduction activity of a VSV-LV vector drops by half after 37 hours (Dautzenberg et al., 2020). At 72 hours, fewer but still intact LVs can potentially maintain viral gRNA in cell culture. Consequently, this would lead to confusion in distinguishing viral gRNA from integrated transgene's mRNA expression. To be detected, integral LV gRNA should be mostly located either in bound LVs on cell surface or in endocytosed unruptured capsids. The latter would prevent gRNA from degradation by endogenous RNases. To a lesser degree, freely floating unbound LVs, which were not removed during cell sorting and washes, could have contributed to some positive events. That would explain the cross-contamination noticed in untransduced samples when multiplexed in the same nanowell cartridge with LV-inoculated cells, where few *CAR^low* expressing cells were detected (Figure 21). However, further evaluations are needed to investigate this issue.

3.1.2 High selectivity of CD8-LV confirmed by scRNA-seq

An important finding of this thesis was the excellent specificity of a receptor-targeted vector assessed for the first time by scRNA-seq. Particularly, in CD8-LV inoculated T cells, 2.5% of total *CAR^high* cells were inquired as potential off-targets. Based on the expression of other marker genes and taking into account the mRNA fluctuations of *CD8A* by the intrinsic promoter (Erhard et al., 2019), these 59 possible off-target cells were attentively investigated. In fact, 9 of them were categorized as CD8 cells, based on *CD8B* expression, 32 were γδ T cells, 2 were NKT and 15 were *CD4* positive. Overall, 9 γδ T cells and 8 CD4 cells expressed none of the CD8 markers, accounting for 17 true off-target cells. Apart from double positive CD4/CD8 cells, transduction of some γδ T and NKT cells by CD8-LV is not surprising, as they can also express the target molecule, CD8α, on their surface (Gonzalez-Mancera et al., 2020; Kadivar et al., 2016; C. Wang

et al., 2015). Overall, the on-target specificity of CD8-LV, thus, outreached 99%. Similar investigation was not feasible in WTA, as the samples were magnetically sorted for the cell type of interest prior sequencing.

Up to date, there is no study extensively interrogating the biological identity of off-target cells in targeted gene therapy. This thesis demonstrated the significance of utilizing scRNA-seq technology in order to classify cells according to their transcriptomic profile. This allows overcoming drawbacks of flow cytometry analysis, such as impaired sensitivity of low surface protein expression, limited panel of examined markers, antigen masking and differential mRNA to protein translation.

3.1.3 Defining differentially expressed genes and computational approaches

Differentially expressed genes are usually defined to differ among the analyzed groups of cells at an absolute $\log_2$(fold-change) ($|\log_2FC|$) value of 0.25 (Lee et al., 2021; Pezoldt et al., 2021; Bai et al., 2021; X. Shi et al., 2021). In WTA study, the sequencing depth across the samples reached to an average of 29,000 reads/cell (Table 18), which was below the recommended 50,000 reads/cell (https://www.10xgenomics.com/). In general, shallower sequencing depths can potentially affect the detection of genes that do not vastly differ between the groups (low $\log_2$(fold-change)) (D. Li et al., 2021). Thus, by minimizing the $|\log_2FC|$ threshold to 0.2, the sensitivity of detecting biologically relevant differentially expressed genes, that otherwise would be excluded as false negative, increases. Common differentially expressed genes identified in TGA and WTA, where in the latter being within the $|\log_2FC|$ range of 0.2-0.25, validated this cutoff. Overall, the sequencing saturation[1] was above 80% for both TGA and WTA, exceeding 90% in the majority of the samples, meaning that the sequencing depths for both studies were adequate (https://www.10xgenomics.com/). Other scRNA-seq studies, performing even higher sequencing depth analyses (above 50,000 reads/cell), also utilized decreased $|\log_2FC|$ threshold of 0.2 to examine differences in same cell types across the assessed conditions (C. Guo et al., 2022; Sahu et al., 2021; Nam et al., 2019).

Manual revision of hundreds or even thousands differentially expressed genes is time consuming. Hence, a straightforward gene set enrichment analysis (GSEA) is often performed to identify the major pathways in which the up- or down-regulated genes are implicated (Liao et al., 2019). The principle relies on matching the differentially expressed genes with pre-existing gene sets from public repositories, such as Kyoto Encyclopedia of Genes and Genomes (KEGG) and Gene Ontology (GO) (Ashburner et al., 2000; Kanehisa & Goto, 2000). This approach provided

---

[1] Represents a measurement of mRNA molecules that have been sequenced more than once. A saturation of 90% means that the chances of a new read to correspond to a new molecule (UMI) is 10%.

some valuable information, depicted certain biological pathways to explore, and saved time in exploring the extensive list of differentially expressed genes.

The resolution and cell cluster separation was more pronounced in TGA compared to WTA, where in the former even smaller subclusters in the major immune cell populations were noticeable (Figure 11, Figure 24B). Similarly, in other scRNA-seq studies analyzing the whole transcriptome, CD4 and CD8 cells were indistinguishable in UMAP plots (Bai et al., 2021; Boroughs et al., 2020; Xhangolli et al., 2019).

To prevent heterogenous clustering of actually identical cell types due to different cell-cycle stages, a correction was applied in WTA prior downstream plotting. Cell-cycle stage was assigned to each cell and its impact was evaluated in principal component analysis (Figure 56). By regressing out the effect, cells in UMAP plots are not subjected to cluster based on different cell-cycle stages (Butler et al., 2018; A. T. Lun et al., 2016; Scialdone et al., 2015). Due to limited number of cell-cycle related genes in TGA, scoring and regression of cell-cycle stages was not possible.

In a similar manner, donor or technical variations are usually regressed by integrating different donors or technological approaches via canonical correlation analysis (CCA) (Stuart et al., 2019; Butler et al., 2018). According to this analysis, a shared gene structure is conserved between different data sets, thus by identifying the correlated gene modules representing a similar biological state (anchors), the variance can be reduced, letting biologically similar cells to cluster together (Stuart et al., 2019; Butler et al., 2018). Both cell-cycle and batch effect corrections affect only the plotting and clustering of cells rather than the differential gene expression analysis, which uses the normalized, but not scaled and regressed data. Thus, while there were no technical variations observed in both of the scRNA-seq approaches (Figure 9, Figure 57), donor to donor variation and cell-cycle effect were pronounced in WTA and subsequently corrected (Figure 57).

Apart from technical differences in the single-cell processing pipelines used in CAR T cell field (BD Rhapsody and 10X Chromium), certain data analysis approaches also varied. For instance, the default log-normalization method from *Seurat* package was applied in the majority of the studies (Rodriguez-Marquez et al., 2022; Bai et al., 2021; X. Wang et al., 2021; Boroughs et al., 2020; Deng et al., 2020; Sheih et al., 2020), similarly done in TGA study. For the WTA study in this thesis a deconvolution-based normalization from *scran* was selected as optimal method (4.2.6.13) (A. T. L. Lun et al., 2016). According to that, cells with comparable UMI counts are pooled together, the expression values are summed up, the genes are normalized against the average reference, and the pool-based factors are resolved to their cell-based counterparts (A. T. L. Lun et al., 2016). This method ensures that differences observed between cells are derived from biological perspective and not from technical bias.

Downstream of normalization, various statistical approaches of differential gene expression analysis have been utilized in CAR T cell scRNA-seq related publications, with the default Wilcoxon rank sum test from *Seurat* to be the most common (Rodriguez-Marquez et al., 2022; Bai et al., 2021; Boroughs et al., 2020; Deng et al., 2020)*.* In addition, t-test (X. Wang et al., 2021) or even a zero-inflated negative binomial approach, the model-based analysis of single-cell transcriptomics (MAST), were used for this purpose (Sheih et al., 2020). Overall, Wilcoxon non-parametric test has appointed to have the most robust performance in differential gene expression analysis of scRNA-seq data among other statistical tests (Mou et al., 2020; Soneson & Robinson, 2018). Thus, it was used for both TGA and WTA studies. Similarly, non-parametric Wilcox and Kruskal-Wallis tests were applied in violin plots for statistical comparisons of gene expression among certain groups.

P-value correction is carried out to prevent accumulating type I errors from the multiple comparisons, such as during differential gene expression analysis. The Bonferroni adjustment, used in TGA as a default setting in *Seurat,* has been criticized for its conservative and stringent approach (Perneger, 1998). The false discovery rate (FDR or q-value), proposed by Benjamini & Hochberg (1995), comprises an optimized adjustment to avoid overcorrection and increased likelihood of losing otherwise significant values (type II error). Hence, the analysis of WTA data was optimized to increase the sensitivity of detecting significant differentially expressed genes. In a similar manner, FDR-based p-value adjustment was also applied in other studies of CAR T cell transcriptomic analyses (Rodriguez-Marquez et al., 2022; X. Wang et al., 2021; Boroughs et al., 2020; Deng et al., 2020; Sheih et al., 2020).

3.2 DIFFERENTIALLY EXPRESSED GENES PROVIDE MOLECULAR BASIS FOR CAR T CELL HETEROGENEITY

3.2.1 Transcriptional differences induced by different LV types

Both TGA and WTA performed in this thesis deciphered differentially expressed genes across the compared cell subsets. The former approach aimed to point out the effects of VSV-LV and CD8-LV on CD8 cells. The limited panel of 400 immune-related genes allowed the manual screening and investigation of each differentially expressed gene. Hence, an initial overview of transcriptional alterations provided insights about T cell phenotypes, exhaustion and activation status among inoculated or non-inoculated, transduced or non-transduced cells, and pinpointed differences induced by the two LVs. The WTA, conducted with three donors and three LVs, namely

CD8-LV, CD4-LV and VSV-LV, confirmed the TGA findings, and aimed to unveil factors that perturb successful LV-mediated transduction, in both CD8 and CD4 T cells.

A first glance at differentially expressed genes found in TGA across subsets of control and LV-inoculated cells showed that the exposure of T cells to any type of LV caused alterations in gene expression profiles, disregarding the transduction status of the cells (Figure 17). Differences were also observed between *CAR^neg/low* and *CAR^high* cells, which provided some indications for transcriptional profiles prone for LV-mediated transduction. Similar observations were made in WTA, such as the distinct transcriptomic differences of every subset group of control, *CAR-* and *CAR+* from both VSV-LV and receptor-targeted vectors (Figure 25). Overall, vast induction of genes was observed in *CAR+* cells generated by VSV-LV compared to the rest of analyzed subsets of cells (Figure 25). When compared to the control cells, VSV-LV and CD4-LV induced more alterations than CD8-LV, which latter induced less apparent effects (Figure 26). In VSV-LV, both CD4 and CD8 cells were equally affected, thus the outcome was not related to a certain T cell type, but to the specific LV used (Figure 26).

3.2.2 Activation, exhaustion and T cell phenotype of CAR+ T cells

Transcriptional insights into converted CAR T cells indicated association with a more proliferative and activated profile, in both scRNA-seq studies (Figure 19, Figure 30, Figure 31). CAR tonic signaling can potentially induce these features, which has also been observed in other studies (Rodriguez-Marquez et al., 2022; Bai et al., 2021; X. Wang et al., 2021; Sheih et al., 2020; Long et al., 2015).

Furthermore, CD8+ CAR T cells expressed exhaustion and immune check point-related genes (*ENTPD1, LAG3, HAVCR2 – TIM3, LAT2, LIF, C10orf54 – VISTA*) (Figure 19). It is acknowledged that enrichment of exhausted T cells, specifically CD8 cells, in axi-cel infusion products correlates with partial response or progressive disease in patients with large B cell lymphomas (LBCL) (Deng et al., 2020). This can be avoided if the 4-1BB co-stimulatory domain is utilized instead of CD28 in the intracellular part of the CAR construct (Long et al., 2015). Another way would be to manipulate unstimulated or minimally activated T cells, omitting the activation-induced exhaustion by anti-CD3 and anti-CD28 (Balkhi et al., 2018). To further confront the exhaustion defects that CD8+ CAR T cells seem to possess, targeting CD4 T cells would potentially alleviate the challenges and improve the CAR T cell therapy. In Agarwal et al. (2020) targeted generation of CD4+ CAR T cells with the CD4-LV showed less exhaustion compared to CD8 cells and efficient tumor killing in mouse model. Indeed, two other independent mouse studies validated and confirmed the superiority of CD4+ CAR T cells in persistence, potent tumor killing and less exhaustion compared to CD8+ CAR T cells (D. Wang et al., 2018; Adusumilli et al., 2014). A

clinical verification of these studies came recently, where a follow-up in patients with leukemia remission showed that CD4+ CAR T cells had longer persistence, highlighting the superiority of CD4 cells over CD8 T cells (Melenhorst et al., 2022). Thus, clinical studies infusing CAR T cell products enriched in CD4 cells would provide new insights about the advantage of engineering CD4 cells instead of CD8.

Regarding T cell subtypes, Xhangolli et al. (2019) reported the co-existence of both T_H1 and T_H2 CAR T cells. In the current TGA study, T_H1 phenotype was more pronounced in *CAR^high* population (*IL12RB, IFNG, STAT4*), whereas no distinct T_H2 marker genes included in the panel were detected or substantially expressed (*GATA3, IL4R, IL4, IL5, IL13*) (Figure 19). Even though a study in a larger cohort would have provided more definite indications, the absence of T_H2 response in CAR T cell products has been associated with relapsed ALL patients (N=5) (Bai et al., 2022). Thus, a cytokine regiment capable of skewing T cells towards both T_H1 and T_H2 subsets may be beneficial.

3.2.3 Antiviral restriction factors inhibiting proper LV-mediated transduction

Thoroughly interrogating why certain T cells were not modified by LVs, distinct transcriptional profiles were identified compared to transduced cells. Non-transduced cells were shown to have elevated levels of genes associated with T cell quiescence and apoptosis (*PIK3IP1, CD37, BTG1, CASP5*) (Figure 19). Quiescent and non-activated T cells are known to not express the LDLR, target of VSV-G, preventing the entry of VSV-LV and subsequent transduction of them (Amirache et al., 2014). In theory, that would not perturb the ability of CD8-LV or CD4-LV to transduce unstimulated T cells due to constitutive expression of these molecules on the respective T cell types. Contrary to retroviral vectors, LVs have been demonstrated to be capable of integrating into cells that are not dividing (Naldini et al., 1996). Nevertheless, naïve T cells sustain limited gene expression and protein translation (Ricciardi et al., 2018; Araki et al., 2017), thus a proper activation following transgene integration would eventually be necessary.

An important finding of this thesis was that antiviral restriction factors were upregulated in *CAR*-cells, likely inhibiting LV-mediated gene transfer to these cells. Among them were *IFITM1, IFITM2* and *IFITM3*, known to prevent fusion of enveloped viruses to cellular membranes (Hornick et al., 2016; Lu et al., 2011), also *SAMHD1*, which inhibits reverse transcription (Goldstone et al., 2011), and other IFN-induced genes and factors (Figure 32). Among other antiviral factors found to be upregulated in CAR- cells, *SAMD9L* and *IFI44L* have been recently discovered. Their functionality is not yet fully understood (Y. Li et al., 2021; Meng et al., 2018). Also, *IFI6* has been shown to prevent IFN type I induced apoptosis in T cells, apart from its antiviral potency (Sajid et al., 2021; G.-H. Park et al., 2013). However, other known restriction factors of HIV-1, including the

hypermutation inducing *APOBEC3* genes, the *OAS* family of RNA sensors and the inhibitor of viral mRNA translation *EIF2AK2* (Colomer-Lluch et al., 2018; Schoggins, 2014; Peng et al., 2006), were not increased in *CAR-* cells.

In contrast to antiviral inhibitors, factors endorsing HIV entry were found to be expressed in CAR+ cells. In that manner, cyclophilin A (*PPIA*) and the karyopherin *KPNA2,* both important factors of HIV infectivity (Song et al., 2022; Braaten & Luban, 2001), were slightly elevated in *CAR+* cells. This result indicates the existence of T cells that are more prone to be transduced by LVs (Figure 32). Other HIV interacting and promoting factors, such as the nucleoporins *NUP358* and *NUP153*, which facilitate the translocation of the pre-integration complex into the nucleus (Di Nunzio et al., 2012), as well as the integrase interactor 1 (*INI1*), which enhances the integration of the transfer genome (Kalpana et al., 1994), were expressed in T cells, but did not significantly differ between transduced and non-transduced cells.

Intriguingly, other scRNA-seq studies (utilizing the Chromium 10X platform) did not describe differences between *CAR-* and *CAR+* cells from pre-infusion products (X. Wang et al., 2021; Deng et al., 2020). In one of this cases, both transduced and non-transduced cells were merged for downstream analysis, despite the fact that the median CAR expression in flow cytometry was less than 50% (Deng et al., 2020). The research presented in this thesis is thus the first dedicated analysis unveiling transcriptomic differences between CAR- and CAR+ cells. When CAR T cells are assessed, enrichment for CAR+ cells using cell sorting can prevent non-transduced cells from being present (Sheih et al., 2020).

3.3 ALLEVIATING INTRINSIC INHIBITORY MECHANISMS TO IMPROVE GENE DELIVERY

3.3.1 IFITMs and their role in viral restriction entry

Considering the increased gene expression of antiviral restriction factors in non-transduced cells, a strategy to manipulate them was implemented, aiming to improve the transduction efficiency of LVs. Thus, rapamycin, cyclosporin A and anti-IFNα were tested as possible ways to bypass cellular defending mechanisms. Despite the fact that rapamycin and cyclosporine A can improve the transduction of HSPC with VSV-LV by modulating two different cellular mechanisms (Ozog et al., 2019; G. Shi et al., 2018; Petrillo et al., 2015; C. X. Wang et al., 2014), they did not increase the efficiency of the VSV-G pseudotyped vector in transducing PBMC (Figure 33). Recent data have shown that rapamycin enhances the *in vitro* infectious yield of SARS-CoV-2 pseudoparticles up to 9-fold in A549 cells overexpressing the targeting molecule, angiotensin

converting enzyme-2 (ACE2) (G. Shi et al., 2022). For both, VSV-LV and SARS-CoV-2 pseudoparticles cases, the possible mechanism of rapamycin's action relies on downmodulating IFITM2 and IFITM3, rather than IFITM1. This thesis showed that rapamycin vastly enhanced T cell transduction by CD8 and CD4 receptor-targeted LVs (Figure 34), which was likely linked to reduction of IFITM1.

The diverse inhibitory effect of each IFITM against various enveloped viruses is a result of the different entry pathways. IFITM1, which resides mainly on the plasma membrane, is expected to restrict viruses utilizing a direct entry pathway (S. E. Smith et al., 2019; Weston et al., 2014). On the other hand, IFITM2 and IFITM3, found in clathrin-rich endosomal compartments, prevent the endosomal escape (Weston et al., 2014; Wee et al., 2012; Sun et al., 2005). Additionally, in some cases, IFITMs seem to function synergistically by preventing both early (IFITM1) and late (IFITM2, IFITM3) viral entry pathways (Narayana et al., 2015). Nevertheless, IFITMs do not inhibit all enveloped viruses. For instance, murine leukemia virus (MLV), Lassa (LASV), lymphocytic choriomeningitis (LCMV) and Machupo (MACV) arenaviruses seem not to be affected by any IFITM (Brass et al., 2009).

Other viruses have also been shown to be restricted by IFITM1, such as hepatitis C, Marburg and Ebola viruses, but so far there has been no study proving the enhancement of their infectivity by rapamycin (Narayana et al., 2015; Huang et al., 2011).

So far, various enveloped viruses have displayed inhibition by IFITMs, the most important of them are listed in Table 4, where the extent of inhibition by each IFITM is denoted.

Table 4: Viruses restricted by different IFITM proteins.

Virus	Restriction factor			References
	IFITM1	IFITM2	IFITM3	
IAV	++	+	++	Brass et al., 2009
DENV	+	+	++	Brass et al., 2009
WNV	+	+	++	Brass et al., 2009
HCV	++	+	+	Narayana et al., 2015; Wilkins et al., 2013
VSV	-	+	++	J. M. Weidner et al., 2010
HIV-1	+	++	++	Chutiwitoonchai et al., 2013; Lu et al., 2011
SARS-CoV-1	++	+	++	G. Shi et al., 2021; Huang et al., 2011
SARS-CoV-2	++	+	+	G. Shi et al., 2021
MARV	++	+	+	Huang et al., 2011
EBOV	++	+	+	Huang et al., 2011
RVFV	-	+	+	Mudhasani et al., 2013

IAV: influenza type A virus, DENV: dengue virus, WNV: West Nile virus, HCV: hepatitis C virus, VSV: vesicular stomatitis virus, HIV-1: human immunodeficiency type 1 virus, SARS-CoV-1/2: severe acute respiratory syndrome coronavirus 1 or 2, MARV: Marburg virus, EBOV: Ebola virus, RVFV: Rift Valley fever virus. ++ strong inhibition, + weak inhibition, - no inhibition.

In the majority of the mentioned studies though, the restriction though different IFITMs was cell line depended and usually assessed by overexpression of a particular IFITM. Thus, no direct evidence for the actual pathogen's virulence can be drawn. This also comes in agreement with the contradictory findings of SARS-CoV-1 and SARS-CoV-2 infections, where the endogenous expression of IFITM1 and, to a lesser extend IFITM2 and IFITM3, were eventually necessary for infecting *in vitro* primary human lung cells (Prelli Bozzo et al., 2021).

How IFITMs inhibit viral membrane fusion is not completely understood. It has been suggested that the transmembrane proteins induce an energetically unfavorable membrane curvature for the formation of the fusion pore (John et al., 2013). Other observations have provided evidence for the role of accumulated cholesterol in IFITM3-rich endosomes. Regarding these, cholesterol increases the bending rigidity of the membranes, while treatment with sterol-binding compounds or fatty acids that spontaneous alter the membrane curvature, render the membranes more fluidic promoting fusion (X. Guo et al., 2021; Lin et al., 2013; Amini-Bavil-Olyaee et al., 2013; K. Li et al., 2013). Post-transcriptional modification of cysteine residues with the covalent attachment of palmitic fatty acid (S-palmitoylation) as well as ubiquitination of conserved lysine residues were found to be important for IFITM3 stability, endosomal localization and antiviral restriction (Yount et al., 2010, 2012).

3.3.2 The use of rapamycin for improving LV-mediated gene transfer

The use of rapamycin in this thesis on human PBMC did not only affect IFITMs, but also downregulated other type I interferon-stimulated genes, which likely contributed to the transduction enhancement (Figure 40A). Importantly, this finding validates the biological significance of the identified differentially expressed antiviral genes in CAR- cells. Among IFITMs, only IFITM1 was found to be downregulated in LC-MS analysis (Figure 40), while IFITM2 and IFITM3 were not detected. By western blot analysis, all IFITMs were confirmed to be affected by rapamycin (Figure 39). The decrease of ISG-related proteins upon rapamycin treatment was in accordance with other LC-MS or gene expression analysis studies, but none of the IFITMs were detected (Figure 40A) (Mu et al., 2022; Lepelley et al., 2021; Namwanje et al., 2021; Schmitz et al., 2008; Kasukabe et al., 2005). In the concept of rapamycin preventing apoptosis via autophagy, the downregulation of caspase-3, -6 and -9 has also been previously noticed (Figure 40A) (Tsapras & Nezis, 2017; Ravikumar et al., 2006). Rapamycin has the ability to reverse CD62L downregulation (Stoycheva et al., 2015), although this was not shown in our investigation (Figure 40A). The rise in TOP2A and TOP2B topoisomerases contradicts claims that rapamycin inhibits the proliferation of T cells (Ferrer et al., 2011; Holden, 1999).

Increased vector integration may have contributed to the higher CAR MFI in rapamycin-treated T cells. (Figure 35). This was also observed in HSPC transduced with VSV-LV in presence of rapamycin (Petrillo et al., 2015). Rapamycin's inability to impact CAR expression suggests that cellular protein expression machinery was generally unaffected.

Summing up, the potential inhibitory pathways of LV-mediated transduction are shown in Figure 47, along with the antiviral restriction factors that rapamycin can influence, enhancing LV entry and cell transduction.
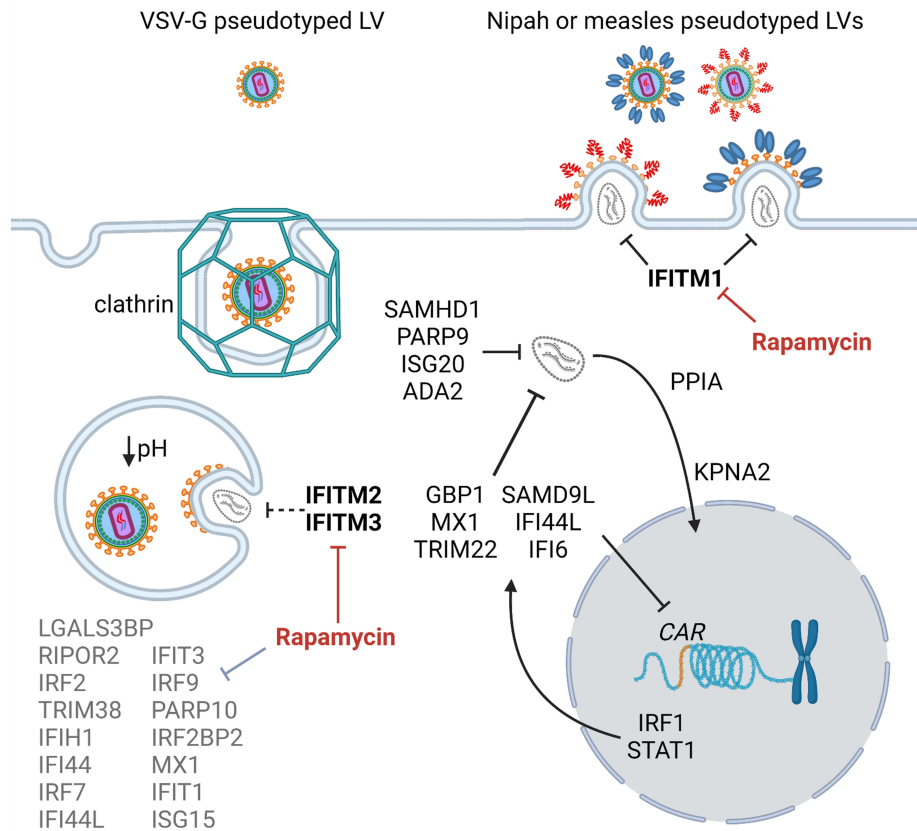
Figure 47: Rapamycin alleviates cellular restriction mechanisms for LV-mediated gene transfer.
Overview of antiviral restriction and promotion mechanisms in LV-mediated gene transfer and the downmodulation of them by rapamycin (edited Figure 4). Rapamycin downmodulates antiviral restriction factors (*in grey or black bold letters*), as found by LC-MS or western blot analysis. Further factors listed (*black* letters) were found to be upregulated in CAR- cells by scRNA-seq analysis. *Dashed line* indicates minimal effect as assessed in human PBMC.

Regarding the concentration of rapamycin used for *in vitro* applications, 30 µM have been shown to highly downregulate IFITM3 in HeLa cells, after 4 hour incubation (G. Shi et al., 2018). In HSPC studies, the applied concentrations varied from as low as 10 nM up to 40 µM and incubation times reached up to 24 hours (Petrillo et al., 2015; L. Li et al., 2014; C. X. Wang et al., 2014). However, IFITM expression is recovered back to normal levels after 6-8 hours of continuous incubation with rapamycin (G. Shi et al., 2018). Thus, it was anticipated that gene transfer would take place during the first few hours of LV inoculation. Eventually, 1.5 hours of spinoculation in presence of high concentration of rapamycin (30 µM) proved to be effective for LV-mediated gene transfer in PBMC.

Pre-treatment of humanized NSG mice with rapamycin resulted in an approximate 1.5-fold increased and more consistent *in vivo* gene transfer (Figure 37). Noticeably, the GFP transferring LVs had greater *in vivo* transduction efficiency than the ones transferring CD19-CAR (Figure 37, Figure 45A). The smaller size of GFP transgene compared to a CAR can explain the higher

efficiency of this vector (Sweeney & Vink, 2021). In spite of this, rapamycin accelerated the *in vivo* generation of CAR T cells and subsequently tumor killing (Figure 43, Figure 45A). As other parameters, such as CAR tonic signaling and interaction with tumor cells, contribute to CAR T cell proliferation, the evaluation of GFP transfer genuinely demonstrated the enhancement effect that rapamycin confers on CD8-LV.

The reason why there was no steep decline in tumor burden on day 18, like in Agarwal et al. (2019) study, may be the 5× times less tumor cells injected into those mice. Whether the higher dose of rapamycin influenced the activity of CAR T cells, is not completely known. From a pharmacodynamic perspective, as long as the drug is not bioavailable anymore, its effect is withdrawn. Thus, the approximate 6-hour half-life of rapamycin in periphery is not expected to affect the newly expanded CAR T cells (Comas et al., 2012). Besides, the tumor burden of the 8 mg/kg rapamycin group was controlled in a similar pace as in vehicle group (Figure 43A). Additionally, the higher tumor load of one mouse in the 8 mg/kg group during randomization contributed to the increased mean values of photon flux throughout the study (Figure 42B).

The extent of improved *in vitro* gene transfer in the presence of rapamycin was bigger than *in vivo* (7-fold versus 1.5-fold) (Figure 34, Figure 37). It is likely that this was due to a still suboptimal proof-of-concept *in vivo* study. For instance, the presence of Tween™ 80 in the drug's vehicle formulation and its systemic bioavailability could have impacted the efficiency of LVs and resulted in lower transduction rates than those observed in Agarwal et al. (2019). Apart from vehicle's composition, the *in vivo* dosage and route of drug's administration was not previously tested. For the latter, intraperitoneal injection was decided as a way to extend the drug's half-life and keep the optimal concentration bioavailable for a longer time. The lowest dose of 3 mg/kg per mouse was extrapolated from the *in vitro* 30 µM to *in vivo* concentration based on mouse body surface (Nair & Jacob, 2016). In addition, a higher dose of 8 mg/kg was decided, because of rapamycin's high absorption rate from the red blood cells (Yatscoff et al., 1993). Both of these dosages were tolerable for the mice and no adverse effects were observed.

In clinical prescriptions, the immunosuppressive and anticancer effect of rapamycin originate from daily or weekly administration of doses between 0.5 and 34 mg/m^2 or even higher (Guba et al., 2005; Zimmerman & Kahan, 1997). Extrapolating mouse to human doses, the 3 mg/kg corresponded to 8.9 mg/m^2 and the 8 mg/kg to 24 mg/m^2. Thus within the range that is currently in use for humans (Yatscoff et al., 1993).

Rapamycin is not the first described small molecule to act as a potent enhancer for LV-mediated gene transfer. Regarding other commercially available enhancers, vectofusin®-1 has been shown to increase the efficiency of both CD8-LV and CD4-LV, approaching to similar transduction levels to this thesis study (Jamali et al., 2019). Although its safety was assessed in

immunocompromised mice (Fenard et al., 2013), this amphipathic peptide has only been utilized in *ex vivo* gene transfer settings, and there is currently no proof of its tolerance in clinical application. Furthermore, using cationic polymers has been shown to improve *in vivo* gene delivery. Particularly, prior to i.v. injection, retroviral vectors mixed with transfectam® (Promega) improved the transduction of rat liver cells (Themis et al., 1998). Despite the fact that rats were able to tolerate this lipid molecule, cationic polymers are generally considered to be hazardous to organisms (Lv et al., 2006), and they may even influence the selectivity of receptor-targeted LVs.

Overall, the uncompromised *in vitro* performance of CAR T cells and the excellent tolerability of the drug in mice and humans, renders rapamycin potent and flexible transduction enhancer for LV-mediated gene transfer.

In conclusion, this doctoral project established a scRNA-seq pipeline for investigating the cellular diversity of CAR T cell products. Bioinformatic methodology was developed and optimized for purpose of each study, with a common aim of distinguishing CAR+ from CAR- cells. This allowed to detect transcriptional differences between transduced and non-transduced cells, but also between different LVs used during the studies. Eventually, antiviral restriction factors were identified to restrict gene transfer mediated by both conventional and receptor-targeted LVs. Downmodulation of IFITM1 as well as other antiviral factors by rapamycin showed a vast enhancement of transduction efficiency for CD8-LV and CD4-LV. In addition, rapamycin improved the *in vivo* gene transfer and CAR T cell generation, accelerating tumor clearance. Hence, incorporating cutting-edge single-cell transcriptomic technology into CAR T cell therapy can give insights and essential aspects for product optimization in both conventional and targeted gene therapy.

4 MATERIALS AND METHODS

4.1 MATERIALS

Materials used during this thesis and sources or vendors supplied them are listed below. Consumables and buffers utilized in cell cultures were either supplied sterile or autoclaved prior use.

4.1.1 Consumables

Name	Supplier
Amersham™ Hybond-ECL, nitrocellulose membrane	GE Healthcare
BD Micro-Fine™ Insulin syringes (29 gauge)	BD Biosciences
BD Microtainer® Blood Collection Tubes, Lithium Heparin	BD Biosciences
BD Rhapsody™ Cartridge Kit (set of 4)	BD Biosciences
Cell strainer, 70 µm	Corning
CellStar® conical centrifuge tubes, 15 mL and 50 mL	Greiner Bio-One
Centrifuge tubes, 225 mL	VWR
Cryovial, 2 mL	Greiner Bio-One
E-plates 16	Agilent
Gel casting tray and combs	PEI
Glassware	SCHOTT, VWR, SIMAX
Instrument disinfection tub, 5 L	Bode
LoBind, DNA tubes 1.5 mL	Eppendorf
LoBind, protein tubes 1.5 mL	Eppendorf
LS columns	Miltenyi Biotec
MACS multistand	Miltenyi Biotec
Micro-centrifuge tubes, 1.5 mL, 2 mL	Eppendorf
Mini-PROTEAN® Tetra Cell stand	Bio-Rad
Mr. Frosty™ Freezing container	Nalgene
OctoMACS™ Separator	Miltenyi Biotec
Pasteur pipet, glass, 14.6 cm	VWR
PCR 96-well TW-MT plates, white	Biozym
PCR tubes, 0.2 mL	Eppendorf
Petri dish, ⌀ 10 cm	Greiner Bio-One
Pipet tips, filtered (10 µL, 100 µL, 300 µL, 1000 µL)	Biozym
Pipette tips (no filtered)	Sarstedt
Pipettes Eppendorf Reference®	Eppendorf
Racks, stands, holders	Multiple
Rapid-Flow Bottle Top Filter 0.45 µm SFCE 500 mL	Thermo Fisher Scientific
Round bottom 14 mL tubes with caps	Greiner Bio-One
Serological pipets (5 ml, 10 ml, 25 ml)	Greiner Bio-One
Surgical equipment	Multiple
Syringe filters, Minisart, PTFE (0.45 µm, 0.2 µm)	Sartorius
Tissue culture flask (T25, T75, T125)	Greiner Bio-One
Tissue culture plates (6-, 24-, 96-well)	Thermo Fisher Scientific
Tubes 1.4 mL	Micronic
Water bath	GFL
Whatman filter paper	Whatman

4.1.2 Chemicals & reagents

Name	Supplier
4Cell® Nutri-T medium	Sartorius
Acridine Orange/Propidium Iodide Stain	Logos biosystem

Acrylamide bisacrylamide solution	Carl Roth
Agarose LE	Biozym
Ammonium persulfate (APS)	Carl Roth
Ampicillin	Roche
Agencourt® AMPure® XP magnetic beads	Beckman Coulter Life Sciences
Anode I buffer w/o alcohol	PEI
Anode II buffer w/o alcohol	PEI
BD Pharm Lyse™	BD Biosciences
Biguacid plus	Antiseptica
Bovine serum albumin (BSA)	Sigma-Aldrich
Bromophenol blue	Merck Millipore
Cathode buffer w/o alcohol	PEI
cOmplete™ protease inhibitor cocktail	Roche
Cyclosporin A	Hölzel Diagnostika
Dimethyl sulfoxide (DMSO), 99.9% p.a.	AppliChem GmbH
Dithiothreitol (DTT)	Sigma-Aldrich
D-luciferin	Perkin Elmer
DNA Away	Carl Roth
DNA ladder (2-log)	New England Biolabs
Dulbecco's Modified Eagle Medium (DMEM), high glucose	Sigma-Aldrich
Ethanol	Berkel AHK
Ethylenediaminetetraacetic acid (EDTA) 0.5 M pH 8	PEI
Ethylenediaminetetraacetic acid (EDTA) 2mM in PBS	PEI
Fetal bovine serum (FBS)	Sigma-Aldrich
Formaldehyde	Sigma-Aldrich
H_2O, cell culture	Sigma-Aldrich
H_2O, distilled (dH_2O)	PEI
H_2O, RNase-free	Qiagen
Isoflurane CP	CP-Pharma
Isopropanol	VWR
L-glutamine (200 mM)	Sigma-Aldrich
Luria-Bertani ampicillin agar plates	PEI
Luria-Bertani medium	PEI
MACSQuant® Buffers (Running, Wash, Storage)	Miltenyi Biotec
Midori Green Direct DNA loading dye	Nippon Genetics
N,N,N',N'-tetramethylenediamine (TEMED)	Carl Roth
N-2-hydroxyethylpiperazine-N'-2-ethanesulfonic acid (HEPES)	Sigma-Aldrich
NH_4Cl	Sigma-Aldrich
Nuclease-free H_2O	Applied Biosystems
PageRuler™ Plus Prestained Protein ladder	Thermo Fisher Scientific
Pancoll	PAN-Biotech
PBS w/o $Mg^{2+}Ca^{2+}$	Lonza, PEI
Penicillin-streptomycin	PEI
Pierce™ ECL Western blotting substrate	Thermo Fisher Scientific
Polyethylene glycol (PEG) 300	Sigma-Aldrich
Polyethyleneimine, branched, 25 kDa	Sigma-Aldrich
Purple DNA loading dye (6X)	New England Biolabs
Rapamycin	Hölzel Diagnostika
Roswell Park Memorial Institute (RPMI) 1640 medium	Sigma-Aldrich
Sodium azide (NaN_3) solution, 10% in cell-culture grade H_2O	PEI
Sodium dodecyl sulfate (SDS) 10% w/v	PEI

Sodium dodecyl sulfate (SDS) running buffer (10X)	PEI
Sucrose	Sigma-Aldrich
Terralin®	Schülke & Mayr
Terralin® Protect	Schülke & Mayr
Tris/HCl 1 M pH 6.8	PEI
Tris/HCl 1 M pH 8.8	PEI
Tris-acete-EDTA (TAE) buffer (20X)	PEI
Tris-buffered saline (TBS-T) buffer (10X)	PEI
Trypan blue	Sigma-Aldrich
Turbidimetric LAL reagents	Associates of Cape Cod Inc.
Tween™ 20	Sigma-Aldrich
Tween™ 80	Sigma-Aldrich
UltraComp eBeads™ Plus Compensation Beads	Thermo Fisher Scientific
Vectofusin-1	Miltenyi Biotec
β-mercaptoethanol (50 mM)	Thermo Fisher Scientific

4.1.3 Buffers & solutions

Name	Formulation
Anode I running buffer	300 mM Tris-HCl, 20% ethanol in dH_2O
Anode II running buffer	3 mM Tris-HCl, 20% ethanol in dH_2O
Blocking solution	2% BSA in PBS
Cathode running buffer	40 mM 6-aminohexanoic acid pH 9.4, 20% methanol in dH_2O
FACS fix solution	1% formaldehyde in PBS
FACS wash buffer	2% FBS, 0.1% NaN3 in PBS
PBS	137 mM NaCl, 2.7 mM KCl, 10 mM Na2HPO4, 1.8 mM KH2PO4 pH 7.1 in dH_2O
RIPA buffer (protease inhibitors)	50 mM Tris-HCl (pH 8.0), 150 mM NaCl, 1% NP-40, 0.5% sodium deoxycholate, 0.1% SDS, cOmplete™ 1 tablet per 10 mL
SDS loading solution (4X)	240 mM Tris-HCl (pH 6.8), 8% SDS, 40% glycerin, 0.2% bromophenol blue, 20% β-mercaptoethanol in dH_2O
SDS running buffer	25 mM Tris, 192 mM glycine, 1% SDS in dH_2O
Super Optimal broth with Catabolite repression (S.O.C.) medium	1% tryptone, 0.5% yeast extract, 1% NaCl, 2.5 mM KCl, 10 mM $MgCl_2$, 10 mM $MgSO_4$, 20 mM glucose in dH_2O
TAE buffer	40 mM Tris, 20 mM acetic acid, 1 mM EDTA in dH_2O
TBS-T	50 mM Tris(hydroxymethyl)-aminomethane, 150 mM NaCl, 25% HCl, 0.1% Tween™ 20 pH 7.4 in dH_2O
TE buffer	10 mM Tris-HCl, 1 mM EDTA in dH_2O
Transfection reagent	18 mM branched polyethyleneimine in dH_2O
Transfer buffer	48 mM Tris, 39 mM glycine, 20% methanol in dH_2O
Trypsin/EDTA	0.25% Trypsin, 1% EDTA in PBS

4.1.4 Cell culture media

Name	Formulation
Cryopreservation medium	10% DMSO, 90% FBS
DMEM complete	DMEM supplemented with 10% FBS, 2 mM L-glutamine
LB medium	1% tryptone, 0.5% yeast extract, 1% NaCl in dH2O, pH 7.2
RPMI complete	RPMI 1640 supplemented with 10% FBS, 2 mM L-glutamine
T cell medium (TCM)	RPMI complete supplemented with 25 mM HEPES, 0.4% penicillin-streptomycin

4.1.5 Mammalian & bacteria cell lines

Name	Description	Source	Culturing medium
A301	Human T lymphoblast cell line; CD4+	A. Pfeiffer, PEI	RPMI complete
E. coli Top10	Highly transformable laboratory strain of *Escherichia coli* (*E. coli*)	Life technologies	LB-Amp

HEK Lenti-X™ 293T	Human embryonic kidney cell line, transformed to express the SV40 large T antigen; cell clone selected for susceptibility towards transfection and efficient protein expression	Takara Bio Europe	DMEM complete
HEK-293T β2M$^{-/-}$ CD47^{high}	HEK-293T knocked-out for β2 microglobulin and overexpressing human CD47	(Milani et al., 2019)	DMEM complete
MOLT-4.8	Human T lymphoblast cell line; CD8+; clone 4.8	A. Pfeiffer, PEI	RPMI complete
NALM6	Human adult acute lymphoblastic leukemia cell line	ATCC, CRL-3273	RPMI complete
NALM6-luc-eBFP	Genetically modified NALM6 to express eBFP and firefly luciferase	L. Kapitza, PEI	RPMI complete
Raji	Human lymphoblast-like cell line derived from Burkitt's lymphoma	ATCC, CCL-86	RPMI complete

4.1.6 Recombinant proteins & kits

Name	Supplier
3' RACE System for Rapid Amplification of cDNA Ends	Thermo Fisher Scientific
Anti-FITC MicroBeads	Miltenyi Biotec
BD Rhapsody™ Cartridge Reagent Kit	BD Biosciences
BD Rhapsody™ cDNA Kit	BD Biosciences
BD Rhapsody™ Targeted Amplification Kit	BD Biosciences
BD Rhapsody™ WTA amplification	BD Biosciences
CD4+ T Cell Isolation Kit	Miltenyi Biotec
CD8+ T Cell Isolation Kit	Miltenyi Biotec
CellTrace™ Violet Cell Proliferation Kit	Thermo Fisher Scientific
Dead Cell Removal Kit	Miltenyi Biotec
DNase I	Invitrogen
DNeasy® Blood and Tissue Kit	Qiagen
Fixable Viability Dye, eFluor™ 780	Thermo Fisher Scientific
GeneJET® Gel Extraction Kit	Thermo Fisher Scientific
GeneJET® Plasmid Miniprep Kit	Thermo Fisher Scientific
Human IL-15, research grade	Miltenyi Biotec
Human IL-7, research grade or premium grade	Miltenyi Biotec
Human recombinant IFN-α2β protein	BioLegend
Klenow DNA polymerase I	New England Biolabs
LightCycler® 480 Probes Master, 2X	Roche
Nucleobond™ XtraMidi Kit	Macherey-Nagel
Pan T cell Isolation kit, human	Miltenyi Biotec
Q5 DNA polymerase	New England Biolabs
QIAmp viral RNA extraction kit	Qiagen
Restriction endonucleases	New England Biolabs
RNase-free DNase I	Qiagen
RNeasy mini kit	Qiagen
Standard T4 Ligase	Thermo Fisher Scientific
SuperScript III reverse transcriptase	Thermo Fisher Scientific
Trypsin (Melnick, 2.5% solution)	PEI
Vent DNA polymerase	New England Biolabs

4.1.7 Recombinant antibodies

Name	Clone	Application	Dilution	Supplier
Anti-c-myc [FITC]	SH1-26E7.1.3	Flow cytometry	1:200	Miltenyi Biotec
Anti-c-myc [PE]	9B11	Flow cytometry	1:200	Cell Signaling
Anti-fragilis	EPR5242	Western blot	1:1000	Abcam
Anti-GAPDH-HRP	14C10	Western blot	1:1000	Cell Signaling
Anti-human CD19 [PE-Vio770]	LT19	Flow cytometry	1:200	Miltenyi Biotec
Anti-human CD223 (LAG3) [PE]	3DS223H	Flow cytometry	1:20	Thermo Fisher Scientific

Anti-human CD279 (PD1) [PE-Vio770]	PD1.3.1.3	Flow cytometry	1:100	Miltenyi Biotec
Anti-human CD3 [BV605]	HIT3a	Flow cytometry	1:100	BD Biosciences
Anti-human CD3 [FITC or PerCP]	BW264/56	Flow cytometry	1:200	Miltenyi Biotec
Anti-human CD366 (TIM3) [APC]	REA635	Flow cytometry	1:33	Miltenyi Biotec
Anti-human CD4 [PerCP or APC or Viogreen]	VIT4	Flow cytometry	1:100 or 1:200	Miltenyi Biotec
Anti-human CD45 [BV510]	2D1	Flow cytometry	1:100	BioLegend
Anti-human CD45RA [Vioblue]	T6D11	Flow cytometry	1:100	Miltenyi Biotec
Anti-human CD45RO [APC]	UCHL1	Flow cytometry	1:100	Miltenyi Biotec
Anti-human CD62L [PE-Vio770]	145/15	Flow cytometry	1:100	Miltenyi Biotec
Anti-human CD8 [Vioblue or APC]	BW135/80	Flow cytometry	1:200	Miltenyi Biotec
Anti-human CD8 [Vioblue]	REA734	Flow cytometry	1:200	Miltenyi Biotec
Anti-human LAG3 [Alexa 647]	T47-530	Flow cytometry	1:20	BD Biosciences
Anti-human TIM3 [Viobright FITC]	F38-2E2	Flow cytometry	1:33	Miltenyi Biotec
Anti-IFITM1	EPR22620-12	Western blot	1:1000	Abcam
Anti-rabbit-HRP	Polyclonal	Western blot	1:2000	Agilent Dako
Fc receptor (FcR) blocking reagent, human	-	Flow cytometry	1:100	Miltenyi Biotec
FcR blocking reagent, murine	-	Flow cytometry	1:100	Miltenyi Biotec
Human Single-Cell Multiplexing Kit	-	BD Rhapsody™	1:10	BD Biosciences
Isotype controls	-	Flow cytometry		Miltenyi Biotec, BD Biosciences, BioLegend
Pure anti-human CD28	15E8	T cell activation	1:33	Miltenyi Biotec
Pure anti-human CD3	OKT3	T cell activation	1:100	Miltenyi Biotec
Pure anti-human IFN-α	LT27:295	Antiviral inhibition	0.5 µg/mL	Miltenyi Biotec

4.1.8 Plasmids

Nr.	Name	Description	Source
P1.01-01	pCMVΔR8.9	HIV-1 packaging plasmid	Naldini et al., 1996
P1.07-01	pMD2.G	Encodes the glycoprotein G of VSV	pMD2.G was a gift from Didier Trono RRID: Addgene_12259
P2.01-01	pSEW-GFP	HIV-1 transfer vector endcoding GFP	Demaison et al., 2004
P2.01-06	pSEW-mycCD19.CAR(28z)	HIV-1 transfer vector encoding the CD19-CAR	Oelsner et al., 2017
P2.01-12	pSEW qPCR Standard Albumin WPRE	HIV-1 transfer vector encoding WPRE and human albumin as qPCR standard	F. Thalheimer, PEI
P4.01-04	pHnse-DARPin.CD4.29.2	Encodes MV H Δ18 mutated fused to the CD4 specific DARPin 29.2 via (G4S)3 linker	Zhou et al., 2015
P4.04-01	pCG-Fnse-d30	Encodes MV FnseΔ30	Funke et al., 2008
P4.07-02	pCAGGS-NiV-Gd34mut4x-L3-scFvCD8Vh1	Encodes NiV-GcΔ34 fused to the antihuman CD8-specific scFv OKT8 humVh1	Bender et al., 2016
P4.09-01	pCAGGS-NiV-FcΔ22	Encodes NiV FcΔ22	Bender et al., 2016
P1.01-01	pCMVΔR8.9	HIV-1 packaging plasmid	Naldini et al., 1996
P1.07-01	pMD2.G	Encodes the glycoprotein G of VSV	pMD2.G was a gift from Didier Trono (RRID:Addgene_12259)
P2.01-01	pSEW-GFP	HIV-1 transfer vector endcoding GFP	Demaison et al., 2004
P2.01-06	pSEW-mycCD19.CAR(28z)	HIV-1 transfer vector encoding the CD19-CAR	Oelsner et al., 2017

4.1.9 Primers & probes

Nr.	Name	Sequence (5' → 3')
4002	ALB for (qPCR)	CAC ACT TTC TGA GAA GGA GAG AC
4003	ALB rev (qPCR)	GCT TGA ATT GAC AGT TCT TGC TAT
2371	AUAP (3' RACE)	GGC CAC GCG TCG ACT AGT AC
1083	CD8hinge for	TTT CTG CCC GCC AAG CCT AC
2359	N1_BD	CTG CTT TAA TGC CTT TGT ATC ATG CTA
2360	N2_BD	CCT CAA TCC AGC GGA CCT TCC TT
2457	N3_BD	CGA GAA GCA GGC TGA TTG GTT AAT
2458	N4_BD	GGA ATT AAT TCG AGC TCG GTA CC
4001	Probe-ALB	[6-FAM]-ACG TGA GGA GTA TTT CAT TAC TGC ATG TGT-[BHQ1]
5007	Probe-WPRE	[Cy5]-CGC CGC CTG CCT TGC CCG CT-[BHQ2]
4020S	WPRE for (qPCR)	CAC CAC CTG TCA GCT CCT TT
1067	WPRE rev	GGC ATT AAA GCA GCG TAT CC
4021S	WPRE rev (qPCR)	GGA CGA TGA TTT CCC CGA CA
	Human Immune Response Panel Hs	Pre-designed primers used in TGA scRNA-seq (BD Biosciences)
	Primer 1 (~N1_BD)	Customized from BD Biosciences
	Primer 2 (~N2_BD)	Customized from BD Biosciences
	Primer 3 (~N3_BD)	Customized from BD Biosciences
	Primer 4 (~N4_BD)	Customized from BD Biosciences

4.1.10 Electronic devices

Name	Supplier
BBD 6220 CO_2 Incubator	Thermo Fisher Scientific
BD Rhapsody™ Express	BD Biosciences
BD Rhapsody™ Scanner	BD Biosciences
Biometra WT12	Biometra
BrandTech™ accu-jet™	Brand
Centrifuge Multifuge™ X3	Thermo Fisher Scientific
CoolNat ice machine	Ziegra
Electronic Multipette pipettes	Eppendorf
Electronic scales	Sartorius
Freezer (-20°C, -80°C)	Liebherr, Thermo Fisher Scientific
Fridge	Liebherr
Gel documentation imager	Intas
Heraeus Biofuge Pico™, Fresco™	Thermo Fisher Scientific
Innova 4200 Incubator-Shaker	New Brunswick
IVIS® Imaging System	Perkin Elmer
LSRFortessa™	BD Biosciences
LUNA-FL™ automated fluorescence cell counter	Logos biosystems
MACSQuant® Analyzer 10	Miltenyi Biotec
MicroChemi	DNR Bio Imaging systems
Microscopes	Carl Zeiss, Echo
Microwave	Sharp
Mini-PROTEAN® Tetra vertical electrophoresis cell	Bio-Rad
Multichannel pipets	Thermo Fisher Scientific
NanoDrop™ 2000	Thermo Fisher Scientific
NanoSight™ NS300	Malvern Panalytical
Nitrogen tank Chronos, Apollo	Messer
PowerPac™ Basic Power Supply	Bio-Rad
Sonorex Digiplus DL	Bandelin
Thermocycler	Biozym, Bio-Rad
Thermomixer Comfort	Eppendorf
Trans-Blot® SD Semi-Dry Transfer Cell	Bio-Rad
Vaculab PL	MMM Group
Vacusafe™	Integra
Vortex Genie® 2	Scientific Industries
xCelligence® RTCA DP analyzer	Agilent
XGI-8 Gas Anesthesia system	Perkin Elmer

4.1.11 Software

Name	Version	Supplier
BD Rhapsody™ Scanner-Analysis	1.3.0.13	BD Biosciences
FACSDiva™	8.0	BD Biosciences
FastQC	0.11.9	Babraham Bioinformatics
FCS Express	6.06	De Novo Software
FlowJo™	10.7.1	FlowJo LLC
GraphPad Prism	9.2	GraphPad Software
Intas GelDoc	-	Intas
Integrative Genomics Viewer	2.15.1	Robinson et al., 2011
LightCycler® Software	1.5.1	Roche
Microsoft Office	2016	Microsoft
Microsoft Windows Operating System	10	Microsoft
NTA	3.3	Malvern Panalytical
Perseus	1.6.6	MaxQuant
PuTTY	0.76	Open source
R Programming Environment	4.2.1	Open source
RStudio	2022.11	Open source
SnapGene	5.3.2	Dotmatics
WinSCP	5.17.8	Open source
FiJi	2.9.2020	Open source
GelCaptureMC	2	DNR Bio Imaging systems

4.2 METHODS

All the experiments, both *in vitro* and *in vivo*, were carried out in designated biosafety level 2 facilities (S2) with the appropriate personal protective equipment (PPE). Genetic engineering work was conducted and reported according to the laboratory's project official approval from the Hessian State's authorities (Regierungspräsidium Darmstadt), and genetically modified organisms (GMOs) were produced, stored and handled accordingly.

Work with bacteria cells was carried out in a designated lab, where inoculations and culture handling were done in a laminar flow hood. Mammalian cell cultures were handled in sterile laminar flow hoods in a separate space from the bacteria lab. Pre-amplification workspace and DNA- or RNase-free hoods were used for the preparation of PCR master mixes, isolation of DNA or RNA, respectively (look below). Benches and equipment were regularly disinfected with alcohol (terralin® - Schülke & Mayr) or detergent (biguacid plus - Antiseptica).

4.2.1 Molecular biology

4.2.1.1 DNA restriction

Restriction endonuclease reactions of plasmid DNA, for editing new plasmid constructs or screening the transformed bacteria clones, were performed according to New England BioLabs (NEB) instructions in a total final volume of 20 µL. All restriction enzymes were purchased from NEB. Plasmid DNA was mixed with the components listed in Table 5. If necessary, a second restriction enzyme was added to the mixture. Reactions were incubated for 1 hour at 37℃ and

inactivated following electrophoresis of the DNA in an agarose gel (look at 4.2.1.4) or by heating at 65℃ for 20 min.

Table 5: DNA restriction digestion protocol.

Component	Quantity
Plasmid DNA	Up to 1 µg
Restriction Enzyme 1	0.5 µL / 5 Units
(Restriction Enzyme 2)	(0.5 µL / 5 Units)
Restriction buffer (10X)	2 µL
H_2O	Up to 20 µL

4.2.1.2   DNA recombination

Backbones and inserts with digested free overhangs were previously purified from agarose electrophoresis gel (4.2.1.4). To prevent re-ligation of the plasmid backbones without the insert, especially when digesting with one restriction enzyme, ends were blunt with the Klenow DNA polymerase I (NEB). After purifying the backbone from a gel, the following components listed in Table 6 were pipetted.

Table 6: Blunting digested plasmid DNA backbones protocol.

Component	Quantity
Backbone DNA	1-5 µg
dNTP mix (1 mM)	1.5 µL
Blunting buffer (10X)	1.5 µL
Klenow enzyme	1 µL / 5 Units
H_2O	Up to 30 µL

The reactions were incubated for 15 min at 20℃ and inactivated by adding 1 µL of 0.5 M EDTA and incubated at 75℃ for 20 min.

For ligating plasmid DNA backbones with new inserts previously cut with the same restriction enzymes, the standard T4 DNA ligase (NEB) was used. Vector (50 ng) was mixed with the insert in a molar ratio of 1:3, in a final reaction volume of 15 µL. The formula to calculate the required mass of the insert is:

$$Insert\ (ng) = \frac{Vector\ (ng) \times Insert\ (bp)}{Vector\ (bp) \times {^1/_3}}$$

An example of ligation reaction mix is presented in Table 7.

Table 7: DNA ligation reaction protocol.

Component	Quantity
T4 DNA ligase buffer (10X)	1.5 µL
Vector DNA (4 kb)	50 ng (0.02 pmol)
Insert DNA (1 kb)	37.5 ng (0.06 pmol)
T4 DNA ligase	0.75 µL / 300 Units
H_2O	Up to 15 µL

Ligation reactions were incubated at either 16℃ overnight or at room temperature for 2 hours, following by heat inactivation at 65℃ for 10 min. If bacteria transformation was directly proceeded, inactivation was not required (4.2.1.3).

4.2.1.3 Bacteria transformation

For bacteria transformation and plasmid cloning, chemically competent *Escherichia coli* Top10 bacteria were used. The bacteria, previously aliquoted in 100 µL volume and stored at -80℃, were thawed on ice and 10 µL of final ligation reaction was gently added (4.2.1.2). The tube was sequentially incubated for 20 min on ice, then 60 seconds at 42℃ and 3 min on ice. A volume of 900 µL of Luria-Bertani (LB)-S.O.C. (4.1.3) medium was added and the bacteria were incubated in a thermomixer for 1 hour at 37℃ and 600 rpm. Finally, 100 µL of the transformation were transferred on a LB-ampicillin agar plate (PEI) and placed it in the incubator at 37℃. The clones were observed and selected for screening the next day.

4.2.1.4 Bacteria culture

Bacteria cells transformed with plasmids bearing ampicillin resistance gene were cultured in LB medium supplemented with 100 µg/mL ampicillin (PEI). Accordingly, cloning of bacteria and plating was carried out in LB agar plates containing ampicillin (PEI) for the positive selection of recombined bacteria clones.

4.2.1.5 Plasmid isolation

For screening and identifying the bacteria clones with the correctly ligated plasmids, several clones were chosen and each inoculated 2 mL of LB-ampicillin medium. Cultures were incubated at 37℃ overnight while shaking at 180 rpm and plasmids were isolated via silica membrane with the GeneJET plasmid miniprep kit (Thermo Fisher Scientific), according to the manufacturer's instructions. Plasmids were then eluted in 30 µL of H_2O, restriction digestion reaction was conducted with the suitable enzymes, and agarose gel electrophoresis was performed to identify the clones transformed with the desirable newly ligated plasmid.

To produce and isolate larger amount of a particular plasmid for transfecting mammalian cells, 200 mL of LB-ampicillin medium was inoculated with the relative clone. After overnight incubation

at 37℃, shaking at 180 rpm, bacteria culture was pelleted down by centrifuging at 4,600 rpm for 15 min. Cell lysis and plasmid isolation was performed with the Nucleobond Xtra midi kit (Macherey-Nagel) according to the manufacturer's protocol. DNA pellet was reconstituted in 500 µL TE buffer, the concentration was determined by NanoDrop™ 2000 spectrophotometer, adjusted to 1 µg/µL and stored at -20℃ for further use.

To validate that no amplification errors were introduced to new inserts, plasmid DNA was sequenced as mentioned in 4.2.1.14.

4.2.1.6   *Agarose gel electrophoresis and DNA extraction*

Digested plasmid DNA or PCR products were analyzed by running into agarose gel electrophoresis. Agarose powder (Biozym) was dissolved in 1X TAE buffer (PEI) to cast 1% ($^{w}/_{v}$) gel. When the agarose was completely dissolved, the solution was cooled down and poured on a casting tray, while a comb was placed on top. Following solidification, comb was removed and gels were submerged into a chamber filled with 1X TAE buffer. A 2-log ladder spiked with 0.5 µL Midori green (Nippon Genetics) and samples mixed 5:1 with purple DNA loading dye (NEB) containing 25% $^{v}/_{v}$ Midori green were loaded into lanes. Gels were run at 120 V for 1 hour and separated bands were visualized on a gel doc UV trans-illuminator chamber with an adjacent camera.

Bands with the desirable size of digested vector or PCR amplicon were cut, DNA content was purified by the GeneJET gel extraction kit (Thermo Fisher Scientific) according to the manufacturer's instructions and eluted in 30 µL of H_2O. DNA concentration was quantified by NanoDrop.

4.2.1.7   *Polymerase chain reaction*

Polymerase chain reaction (PCR) was performed to amplify cDNA or DNA parts with primers that are listed above (0). Vent moderate-fidelity polymerase (NEB) was used for routine amplification analyses of shorter DNA regions, while high-fidelity Q5 polymerase (NEB) was used to minimize amplification errors introduced in longer DNA amplicons. The Table 8 shows the pipetting volumes for one reaction mix up to 50 µL prepared for each individual polymerase in a designated, template-free, pre-amplification workspace. Final concentration of primers for both master mixes were set at 500 nM, dNTPs at 0.2 mM and DMSO at 3% ($^{v}/_{v}$). GC enhancer buffer was used only for Q5 polymerase. Reaction volumes were often downsized to 15 µL.

Table 8: PCR reactions protocols.

Component	Vent	Q5
Template	1 pg – 10 ng	1 pg – 10 ng
Primer forward [10 µM]	2.5 µL	2.5 µL
Primer reverse [10 µM]	2.5 µL	2.5 µL
dNTPs [10 mM]	1 µL	1 µL
10X ThermoPol buffer / 5X Q5 Reaction Buffer	5 µL	10 µL
DMSO	1.5 µL	1.5 µL
GC enhancer buffer	-	0.5 µL
H_2O	Up to 50 µL	Up to 50 µL

PCRs were run for 25-30 cycles, with the thermocycler's settings indicated in Table 9. Optimal annealing temperatures were calculated for each pair of primers with the NEB's online tool.

Table 9: Thermocycler PCR settings.

Program	Vent		Q5		Cycles
	Temperature	Time	Temperature	Time	
Hot-start	95℃	3 min	98℃	30 sec	
Denaturation	95℃	30 sec	98℃	10 sec	
Annealing	55-65℃	30 sec	55-65℃	30 sec	x25-30
Extension	72℃	60 sec / 1 kb	72℃	30 sec / 1 kb	
Last extension	72℃	5 min	72℃	2 min	
Cooling	4℃	∞	4℃	∞	

After finishing the PCR, products were either run in agarose gel or stored at -20℃ for later use.

4.2.1.8 Genomic DNA isolation

For quantifying the vector copies integration in transduced cells derived from *in vitro* and *in vivo* experiments, genomic DNA was extracted from at least 2×10^5 cells with the DNeasy blood and tissue mini kit (Qiagen) according to the manufacturer's guidelines. DNA bound on columns was eluted in 100 µL of plasmid- and nuclease-free H_2O (Sigma-Aldrich).

4.2.1.9 Purification with DNase I

Samples from *in vitro* experiments were previously purified with DNase I (Invitrogen) to eliminate any residual plasmid. Plasmid purification was either performed on LV stocks before inoculations or on cell suspensions before DNA extraction, following deactivation with EDTA and/or washes to remove DNase I. A comprehensive protocol is shown in Table 10.

Table 10: Residual plasmid DNA digestion in LV stocks or cell suspension.

Component	LV	Cell suspension
Sample	10-15 µL	85 µL (in PBS)
10X buffer	2 µL	10 µL
DNase I [0.5 U/µL]	3 µL	3 µL
PBS	Up to 20 µL	Up to 100 µL
Incubate at 37℃ for 30 min		
EDTA [50mM]	2 µL	10 µL

4.2.1.10 Bulk RNA isolation and on column purification

For isolating CAR mRNA from transduced cells, total cellular RNA was extracted with the RNeasy mini kit (Qiagen), while LV gRNA was isolated with the QIAmp viral RNA extraction kit (Qiagen) out of 15-20 µL of concentrated stock, according to the manufacturer's protocols and under RNase-free consumables and environment. Isolates were eluted in 30 µL of RNase-free H_2O and purified with RNase-free DNase I (Qiagen) to eliminate any residual plasmids (Table 11).

Table 11: Residual plasmid DNA purification in RNA extracts.

Component	Quantity
RNA	20-30 µL
10X RDD buffer	10 µL
RNase-free DNase I [2.7 KU/µL]	2.5 µL
RNase-free H_2O	Up to 100 µL

Reaction was incubated for 10 min at room temperature, mixed with 350 µL of RLT buffer from the QIAmp RNeasy kit, spun into a QIAmp RNeasy silica column and washed sequentially with 500 µL of RPE and 80% Ethanol. Finally, purified RNA isolates were eluted with 30 µL of RNase-free H_2O.

RNA was aliquoted and stored at -80℃ or processed directly for reverse transcription and cDNA amplification analysis (4.2.1.12).

4.2.1.11 Quantitative PCR and vector copy number

The measurement of vector copy number (VNC) integration was carried out by TaqMan-based quantitative PCR (qPCR) on genomic DNA (4.2.1.8). LightCycler® 480 Probes Master (Roche), primers and TaqMan probes (Eurogentec) were mixed with the template as shown in Table 12. Reactions were normalized to a maximum of 100 ng of genomic DNA per input, whenever it was applicable. For the quantification of the transfer gene integration, primers and a probe recognizing the woodchuck hepatitis virus post-transcriptional regulatory element (WPRE) close to the 3'-end of the transgene cassette were used together in one reaction with oligo binders for human albumin

gene (*hALB*) as reference gene (0). Plasmid with known copies and concentration, bearing both the targets, was used for the standard curve (pSEW qPCR Standard Albumin WPRE). The qPCR was performed with LightCycler480®, in qPCR white plates (Biozym), in technical duplicates, and results were analyzed with its software (Roche). Finally, the VCN was calculated from the formula: $WPRE_{copies}/(hALB_{copies} \div 2)$. The amplification efficiency of each primer set ranged within 90-110%. For standardization purposes, protocol was optimized by Vanessa Riechert (former PEI) and qPCR runs were kindly performed by experienced technical staff (Manuela Gallet, PEI).

Table 12: qPCR protocol.

Component	Quantity
DNA	Up to 100 ng
LightCycler® Probes Master	1X
WPRE for	200 nM
WPRE rev	200 nM
WPRE probe (Cy5)	200 nM
ALB for	200 nM
ALB rev	200 nM
ALB probe (6-FAM)	200 nM
H_2O	Up to 25 µL

4.2.1.12 Reverse transcription

SuperScript III reverse transcriptase (Thermo Fisher Scientific) was used for the cDNA synthesis according to the manufacturer's instructions. A comprehensive protocol is shown in Table 13.

Table 13: Superscript III reverse transcription protocol.

Component	Quantity
RNA	1 ng – 5µg
Oligo(dT) [10 pmol]	1 µL
dNTP [2 mM]	1 µL
RNase-free H_2O	Up to 13 µL
Heat at 65℃ for 5 min and chill on ice	
5X first-strand buffer	4 µL
DTT [0.1 M]	1 µL
RNaseOUT [40 U/µL]	1 µL
SuperScript III	1 µL
Incubate at 50℃ for 30-60 min	
Inactivate at 70℃ for 15 min	

Removal of complementary RNA with RNase H treatment was optional. Synthesized product was aliquoted and stored at -20℃ or at -80℃ for longer preservation, and 1-5 µL was used for PCR reactions.

4.2.1.13 In silico poly-A site prediction and rapid amplification of cDNA end (3'RACE)

For the prediction of the poly-A signal site in CAR mRNA or viral gRNA, the online *in silico* tool DNAFSMiner was used (H. Liu et al., 2005).

For a more accurate detection of the exact starting point of the poly-A tail, the 3'RACE kit (Thermo Fisher Scientific) was utilized, which amplifies the 3'-end of the expressed genes. The principle of method relies on inserting an adaptor sequence by the end of the poly-A tail during reverse transcription, which then can be primed by an oligo in a PCR reaction, while using a forward gene specific primer. The method is displayed in summary in Figure 48. After running agarose gel electrophoresis and extracting the correct bands, the amplicons were sequenced and the poly-A starting site was determined (4.2.1.14). The same gene specific primer was provided to the sequencing company (GATC – Eurofins Genomics).
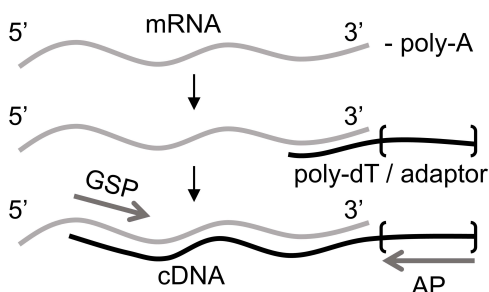
Figure 48: Principle of 3'RACE method for the amplification of gene's 3'-end region.
Adaptor sequence is introduced to the complement part of the mRNA's 3'-end during reverse transcription. An adaptor primer (AP) can be used paired with a gene specific primer (GSP) to amplify this region.

4.2.1.14 DNA sequencing

Sequencing of amplified PCR products or plasmid DNA was performed by GATC services (Eurofins Genomics). Templates mixed with one primer were prepared according to the guidelines. Results were aligned and evaluated in SnapGene software v5 (Dotmatics).

4.2.2 Cell biology & viral vectors

4.2.2.1 Counting, cryopreservation and thawing of cells

Cell suspensions were counted either on a Neubauer chamber stained with 0.2% trypan blue solution (Sigma-Aldrich) or with LUNA-FL™ automated fluorescence cell counter (Logos biosystems), while stained with acridine orange and propidium iodine staining solution (Logos biosystem). For the former, diluted cells with staining solution were counted in all of the 4 bigger squares and concentration was calculated with the formula: $Cells/mL = (Total\ cell\ number/4) \times dilution\ factor \times 10^4$. For the latter, 18 µL of cells were mixed with 2 µL of staining solution,

directly loaded in cell counting slides and measured with the device, specifying the approximate size of the counting cells and the dilution factor (DF=1.1).

For cryopreservation in the aerial phase of N_2, cells were re-suspended in freezing medium (90% $^v/_v$ FBS, 10% $^v/_v$ DMSO), in concentration that was determined based on the desired amount of cells needed to be preserved per vial, ranging from 2×10^6 to 1.5×10^7. From the cell suspension, 1 mL was transferred per cryovial (Greiner Bio-One), which then was placed to Mr. Frosty™ container (Thermo Fisher Scientific), immersed in absolute isopropanol (PEI) and stored overnight at -80℃. The next day, vials were transferred into the N_2 tank.

For thawing cryopreserved cells, cryovials were warmed up at 37℃ in a water bath and content was washed twice with warm medium, spun at 300×g, re-suspended and further cultivated.

4.2.2.2 Cell cultures

Adherent HEK Lenti-X™ 293T cells were cultured in complete DMEM medium (Biowest) (10% $^v/_v$ FBS, 2mM L-glutamine), while suspension MOLT4.8, A301, NALM6, NALM6-luc and Raji cell lines were cultivated in complete RPMI 1640 medium (Biowest) (10% $^v/_v$ FBS, 2mM L-glutamine). Cells were cultured in designated cell culture incubators at 37℃, 5% CO_2 and 90-95% of relative humidity. Detailed content of mediums is described in *Materials* (4.1.4). For *in vivo* studies, the modified HEK-293T β2M$^{-/-}$CD47^{high} cells were utilized during LV production.

For the detachment of adherent cells, cells were washed once with PBS and 0.25% $^w/_v$ trypsin with 2 mM EDTA (PEI) was added on top of them. After 1-2 min incubation at room temperature, flask was gently patted on the side to unstuck the cells, up to 10 mL complete DMEM was added to neutralize the trypsin and cells were re-suspended.

Cell lines were typically passaged in every 3-4 days. Confluent flask of adherent cells was split in 1:10, while suspension cell lines in 1:5.

4.2.2.3 Production, harvesting and concentration of lentiviral vectors

For production of 2nd generation LVs, HEK Lenti-X™ 293T or modified β2M knock-out CD47^{high} HEK-293T (Milani et al., 2019) cells were seeded in 2×10^7 cells per T175 flask. Cells were co-transfected with plasmids encoding proteins for the envelope (G or H and/or F) and packaging (gag, pol, rev, tat), and transcribing the viral gRNA containing the transfer gene cassette, expressing either a 2nd generation CD19-CAR or GFP. Plasmids used for transfection were either produced in-house and isolated with the midi prep kit mentioned above or purchased from PlasmidFactory GmbH & Co. KG (4.1.8). For conventional LV production, 200 ng/cm^2 of DNA was transfected into the cells bound to 0.8 $\mu L/cm^2$ of the cationic polymer polyethylenimine. DNA and polyethylenimine were mixed in a FBS-free medium and then transferred into flasks while

equilibrating the FBS in the culture at 10% $^v/_v$. For vesicular stomatitis virus (VSV)-LV, a plasmid transcribing the transfer gene (pSEW-mycCD19.CAR(28z)) was co-transfected together with a plasmid encoding the envelope's VSV-G glycoprotein (pMD2.G) and one for the packaging proteins (pCMV-dR8.91). For CD8 or CD4 receptor-targeted LVs, the same plasmids for the transfer gene or packaging proteins were used, but the envelopes were pseudotyped with either Nipah virus' truncated F protein (pCAGGS-NiV-Fd22), where the attachment was facilitated by the mutated G glycoprotein conjugated with a CD8A targeting scFv (pCAGGS-NiV-Gd34mut4x-L3-scFvCD8Vh1), or with Measles virus' truncated F protein (pCG-Fnse-d30) and mutated H glycoprotein conjugated with CD4 targeting DARPin (pHnse-DARPin.CD4.29.2), respectively. In addition, for the first mouse study, CD8-LV expressing GFP instead of CD19-CAR was generated.

More detailed DNA amounts and molar ratios for each LV are shown in Table 14.

Table 14: Transfection protocol for LV production.

		Transfer gene	G or H	F	Packaging
CD19-CAR VSV-LV	Plasmid #	P2.01-06	P1.07-01		P1.01-01
	ng/cm²	100	35	–	65
	Molar ratio	20	13		12
CD19-CAR CD8-LV	Plasmid #	P2.01-06	P4.07-02	P4.09-01	P1.01-01
	ng/cm²	86.69	5.13	25.64	82.54
	Molar ratio	20	2	10	17
GFP CD8-LV	Plasmid #	P2.01-01	P4.07-02	P4.09-01	P1.01-01
	ng/cm²	86.69	5.13	25.64	82.54
	Molar ratio	23	2	10	17
CD19-CAR CD4-LV	Plasmid #	P2.01-06	P4.01-04	P4.04-01	P1.01-01
	ng/cm²	86.69	7.69	23.08	82.54
	Molar ratio	20	3	9	17

After 6-18 hours of transfection, medium was exchanged and 48 hours post-transfection the supernatant was harvested, filtered through a 0.45 µm filter (Sartorius or Thermo Fisher Scientific), centrifuged at 4500×g, at 4℃ for 24 hours, on a 20% $^w/_v$ sucrose cushion (Sigma-Aldrich) (in PBS), and the LV pellet was re-suspended in 60 µL/flask PBS (Lonza) by gently shaking for 1 hour at 4℃, following pipetting at least 60 times, aliquoted in protein LoBind tubes (Eppendorf) and stored at -80℃ until further use.

For the *in vivo* mouse experiments, big batches of LVs were kindly produced by experienced technical staff (Gundula Braun).

4.2.2.4 Lentiviral vector titration and particle number

VSV-LV and CD8-LV stocks were titrated on MOLT4.8 cells, performing 1:5 serial dilutions of the highest 2.5 μL dose per 10^4 suspension cells, while CD4-LV stocks were titrated on A301 cells. Transduction efficiency was analyzed in flow cytometry and the titer, indicated as transduction units per mL (TU/mL), was measured on the linear range of the transduction – dilution curve. The number of transduction units per cell in a culture was referred as multiplicity of infection (MOI). Bystander cells that did not come across with a LV were mentioned as untransduced or control cells.

Particle size and concentration from LV stocks were measured by nanoparticle tracking analysis (NTA) based on Brownian motion with the NanoSight™ NS300 device (Malvern Panalytical). Stocks were diluted at least in 1:3000 with 0.2 μm filtered (Sartorius) PBS, loaded into the flow chamber and measured for 60 sec at 25℃ with a customized program in NTA3.3 software (Malvern Panalytical).

4.2.2.5 Isolation and culture of human peripheral blood mononuclear cells

For peripheral blood mononuclear cell (PBMC) isolation, blood from units collected at the German Red Cross donation (DRK-Blutspendedienst Baden-Württemberg-Hessen, Frankfurt) was mixed 1:1 with PBS and carefully overlaid on Pancoll (PAN-Biotech, Aidenbach, Germany) in a ratio of approximately 3:1. Buffy coat, resulted from the centrifugation at 700×g for 30 min at room temperature without decelerating break, was isolated, washed 2-3 times (300×g) with PBS, while also spun at 200×g for platelet removal, and, finally, cells were counted and cryopreserved in defined number (1.5×10^7 or 2×10^6, 1 mL per cryovial) (4.2.2.1).

4.2.2.6 Activation and transduction of human PBMC

For transduction of PBMC, pre-activation of T cells was required. For this purpose, PBMC were thawed and cultured for 3 days in well plates (1.5×10^7 cells in 6-well plate or 2×10^6 in 24-well plate), pre-coated overnight with anti-CD3 (1 μg/mL, clone OKT3) and blocked with 2% $^w/_v$ albumin (in PBS), in presence of soluble anti-CD28 (3 μg/mL, clone 15E8), IL-7 (25 IU/mL) and IL-15 (50 IU/mL) (all antibodies and cytokines from Miltenyi Biotec), in T cell medium (RPMI 1640, 10% $^v/_v$ FBS, 2 mM L-glutamine, 25 mM *N*-2-hydroxyethylpiperazine-*N'*-2-ethanesulfonic acid (HEPES), 0.4% $^v/_v$ penicillin-streptomycin) or in 4Cell® Nutri-T medium (Sartorius) with 0.4% penicillin-streptomycin (PEI).

The CAR gene transfer via LVs was performed in pre-activated PBMC, in presence of cytokines, while in absence of stimulating antibodies. Cells were seeded in 96-well plates in density of 8×10^4 cells per well and inoculated with different doses of concentrated or pre-diluted

LV, typically varying from 0.01 µL to 0.5 µL for VSV-LV and 0.5 µL to 4 µL for the CD8 or CD4 receptor-targeted LVs. Wells were topped up with medium up to 100 µL and cells were then spun (common terms: spinoculation or spinfection) in a pre-heated centrifuge at 850×g for 90 min. In order to increase transduction rates for *in vitro* experiments, vectofusin-1 (Miltenyi Biotec) was used as a transduction enhancer, particularly for receptor-targeted LVs, according to manufacturer's instructions. In this thesis, several compounds were tested as potential enhancers, such as rapamycin (working concentration: 30 µM and titrations), cyclosporine A (10 µM) and anti-IFNα (clone LT27:295, 1 µg/mL), which were added during spinoculation and either immediately removed (likewise vectofusin-1) by refreshing the medium or cell were further incubated in presence of them until the analysis. After spinoculation, cells were topped up with medium with or without the mentioned compounds, reaching 200 µL per well. Cells were cultivated the minimum for 3 days before the flow cytometry analysis and any further use.

4.2.2.7 Flow cytometry

Analysis of transgene expression and other phenotypic markers of T cells was primarily carried out by flow cytometry. Single cell suspension was acquired from cultured samples and $0.1\text{-}2 \times 10^5$ cells were processed for staining. Cells were re-suspended in 100 µL of cold washing/staining buffer (PBS, 2% $^v/_v$ FBS, 0.1% $^w/_v$ NaN₃) and incubated with the fixable viability dye eFluor™ 780 (Thermo Fisher Scientific) in 1:1000 dilution and the appropriated dilution of fluorescently labelled antibodies (listed in 4.1.7) for 30 min at 4℃. Cells were washed twice and fixated 1:1 with a cold fixation buffer (1% $^w/_v$ formaldehyde) to a final volume of 200 µL. Samples derived from mice were treated with murine and human FcR blockers (Miltenyi Biotec) for 20 min at 4℃ prior staining. Stained cells were run either in MACSQuant® Analyzer 10 (Miltenyi Biotec) or in BD LSRFortessa™ (BD Biosciences) and results were analyzed and visualized with FCS Express v6 (De Novo Software) or FlowJo™ v10 (FlowJo LCC), respectively.

4.2.2.8 Proliferation assay

To assess the proliferation of T cells, 3-day pre-activated PBMC were pre-labeled with the CellTrace™ violet proliferation kit (Thermo Fisher Scientific) according to the manufacturer's guidelines, before proceeding with the LV inoculation. Proliferation of the cells was assessed by flow cytometry as reduction of the violet intracellular stain. CAR T cells generated by different LVs were either stimulated with target Raji cells or simply kept in culture for a short period of time, while assessed in between those days.

4.2.2.9   Tumor and CAR T cell co-culture assay

To evaluate CAR T cell cytotoxic potency against tumor cells, transduced cells expressing the CD19-CAR were co-cultured with CD19 expressing tumor cell line, Raji or NALM6, which were optionally pre-labeled with cell trace violet (as mentioned in 4.2.2.8), 10 Gy irradiated or not, in different ratios. As effector to target cell (E:T) ratio of 1:1 was referred to a cell density of 10^4 cells for both, seeded in 96-well plate. For typical co-culture experiments, total T cell number of different conditions was normalized with untransduced cells. Background killing was evaluated by co-culturing untransduced with tumor cells. All the cultures were performed in plain TCM or Nutri-T medium, without supplementing any cytokine.

4.2.2.10 Real-time cytotoxicity assessment

Real-time cytotoxicity assessment was carried out with the xCelligence® RTCA DP analyzer (Agilent), which monitors the proliferation of tethered cells on microelectrode-coated plates by electron flow impedance (converted into a readout called cell index). To tether target suspension cells, E-plates 16 (Agilent) were pre-coated overnight at 4℃ with 10 ng/µL anti-CD40 (Miltenyi Biotec) in PBS. Wells were then washed twice with PBS and 50 µL of complete RPMI or TCM was added to the wells. Plates were equilibrated for 30 min at 37℃ and background noise was measured. Next, 100 µL of 10^4 wild-type Raji cells were seeded per well and incubated for 30 min at room temperature before placing the plates on the device, while immediate warming could push the cells to the well's perimeter by convection. Attachment and proliferation of target cells were then monitored for 24 hours and 3-day generated CAR T cells were seeded on top in declining E:T ratios. Appropriate controls were prepared and unused well were covered by the same TCM medium without cytokines. The cytotoxicity was measured as drop in cell index every 15 min for 24 hours, as tethered tumor cells were detached upon killing.

4.2.3   Protein biochemistry

4.2.3.1   SDS-PAGE

Sodium dodecyl sulfate–polyacrylamide gel electrophoresis (SDS-PAGE) was carried out to separate proteins and peptides from cellular lysates based on their molecular masses (Daltons - Da). For this purpose, cell pellets were washed at least twice with PBS to remove FBS and re-suspended in RIPA buffer with protease inhibitors (4.1.3) in concentration of 8×10^3 cells/µL. Cell were lysed by incubating for 10 min on ice. Lysates were centrifuged at 16000×g, at 4℃, for 15 min, supernatants were mixed 3:1 with 4X SDS loading buffer (4.1.3) and baked at 95℃ for 10 min. Gels were placed into Mini-PROTEAN® Tetra vertical electrophoresis cell (Bio-Rad) with 1X SDS running buffer (4.1.3) and pre-run at 100V for 5 min before loading the samples. Lysate from

approximately 2×10^5 cells was loaded per lane into SDS-PAGE gels of 6% stacking gel (top layer) and 12% resolving gel (bottom layer), casted with the Mini-PROTEAN® Tetra Cell stand (Bio-Rad). PageRuler™ plus pre-stained protein ladder (Thermo Fisher Scientific) was loaded in the first lane. The Table 15 shows the recipe of the SDS-PAGE gel.

Table 15: SDS-PAGE gel casting ingredients.

Component	Quantity	
	6% stacking gel	12% resolving gel
30% $^w/_v$ Acrylamide	1.8 mL	9 mL
dH$_2$O	6 mL	2 mL
1M Tris-HCl (pH 8.8)	—	6.8 mL
1M Tris-HCl (pH 6.8)	1.1 mL	—
10% $^w/_v$ SDS	90 µL	180 µL
20% $^w/_v$ APS	45 µL	90 µL
TEMED	9 µL	18 µL

After loading the samples, gels were run at 80V until the bands passed the stacking gel, then voltage was increased at 120V for approximately 1 hour.

4.2.3.2 Western blot

Dedicated protocol and kind assistance were provided by Samuel Arthur Theuerkauf (PEI). For detection and relative quantification of proteins from crude cellular extracts, proteins from SDS-PAGE were semi-dry blotted to nitrocellulose membrane. In detail, resolving gels from SDS-PAGE runs were removed, soaked for 5 min into cathode buffer (4.1.3) and placed on top of a wet nitrocellulose membrane (with cathode buffer), between 12 wet Whatman papers, 6 on top with cathode buffer, first 4 at the bottom with anode buffer I and last 2 with anode buffer II (4.1.3) (Figure 49). Proteins were transferred with a stable current set at 0.14 mA for 1 hour.
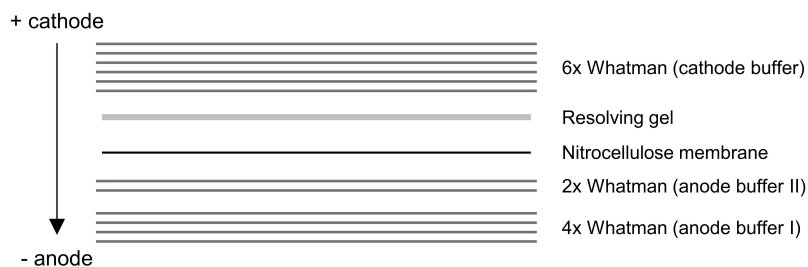
Figure 49: Sandwich assembly of semi-dry protein transfer to nitrocellulose membrane.

Blotted nitrocellulose membranes were horizontally cut, separating the protein of interest (IFITM1 or IFITM2/3: 15kDa) from the reference protein (GAPDH: 47kDa), blocked with 10% $^v/_v$ horse serum in TBS-T buffer (4.1.3) at room temperature for 1 hour. Membranes were incubated overnight at 4℃ with primary antibodies, diluted 1:1000 to TBS-T buffer (4.1.3) with 5% $^v/_v$ horse

serum. Detection of IFITM1 was done with Anti-IFITM1 (Abcam, clone EPR22620-12), IFITM2 and/or 3 with anti-fragilis (Abcam, clone EPR5242) and GAPDH with anti-GAPDH conjugated with horseradish peroxidase (HRP) (Abcam). After washing the excess of primary antibody with TBS-T buffer, secondary anti-rabbit-HRP (Agilent Dako) antibody diluted 1:2000 in TBS-T (5% $^v/_v$ horse serum) was incubated on the membrane at room temperature for 4 hours. Membranes were finally washed, chemiluminescence reaction was performed by Pierce™ ECL Western blotting substrate (Thermo Fisher Scientific), visualization was done by MicroChemi device with the GelCaptureMC v2 software (DNR Bio Imaging systems) and quantification of protein expression was performed by densitometry with FiJi v2 (former ImageJ). Area and density of the bands were calculated and percentages were estimated. Fold change difference of a protein expression upon treatment with rapamycin or 500 IU/mL IFNα was calculated by the formula: $Fold\ change = \frac{\%\ treated_{IFITM} \times \%\ ctrl_{GAPDH}}{\%\ treated_{GAPDH} \times \%\ ctrl_{IFITM}}$.

4.2.3.3 Liquid chromatography – mass spectrometry (LC-MS)

In order to identify which other proteins are up- or down-regulated upon rapamycin treatment, LC-MS was performed in samples derived from 6 donors. After activation of PBMC, approximately 1.5×10^7 cells were divided into three equal parts, spun down and re-suspended in TCM with cytokines or medium supplemented either with 30 µM rapamycin (Hölzel Diagnostika) or with the vehicle 0.5% $^v/_v$ DMSO. Cells were incubated for 90 min at 37℃, washed 3 times with cold PBS, re-suspended in 200 µL RIPA buffer with protease inhibitors, sonicated for 5 min at 100% power in a cold ultrasonic bath sonicator (Sonorex DL, Bandelin) and centrifuged at 16000×g. Supernatant was collected in LoBind protein tubes and delivered to the National Institute for Bioprocessing Research and Training (NIBRT) in Dublin, Ireland. Protein trypsinization and LC-MS runs were performed by skilled scientific and technical group. Differential protein expression with FDR calculated by Benjamini-Hochberg procedure was performed with the Perseus software (v1.6.6, MaxQuant). As significantly up- or down-modulated proteins were accounted the ones with changes of $|log_2FC| > 0.2$ and FDR < 0.05. Results were plotted in volcano plots constructed by the *ggplot2* package in R (v4.2.1).

4.2.4 Experimental mouse studies

Animal experiments were carried out according to the German animal protection law and European Union guidelines for humane animal handling. Four- to five- week old female NSG (NOD.Cg.Prkdc^scid^IL2rg^tmWjl^/SzJ) were purchased from the Jackson Laboratory (local distributor: Charles River Germany GmbH) and housed in groups of 2-4 in individually ventilated cages, where food pellet and water were offered *ad libitum.* After 7-day acclimatization period, weight, posture

and health status were monitored at least twice per week. Animals were handled under laminar flow hoods in a designated animal facility. The design of the animal studies was a collaborative effort with Naphang Ho, Angela Braun and Frederic Thalheimer (all from PEI). Protocols were provided or adjusted from Naphang Ho (PEI), Angela Braun (PEI), Dr. Shiwani Agarwal and Dr. Laura Kapitza (both former PEI).

4.2.4.1 Humanization of mice

In order to humanize the immune system of the mice with human T cells, donor's PBMC were thawed and pre-activated in Nutri-T medium as previously mentioned (4.2.2.6). Cells were then washed with PBS, counted and re-suspended in warm PBS in concentration of 10^8 cells/mL. Thus, upon intravenous (i.v.) injection of 100 µL in the tail vein of the mice, every mouse had been transplanted with 10^7 human PBMC, one day prior injection of the drug and the LV. All injections were performed with 0.5 mL insulin syringes with fixed 29-gauge needle (BD Biosciences).

4.2.4.2 Drug formula

For evaluating whether rapamycin could be used as an *in vivo* enhancer of gene transfer via CD8-LV, two concentrations of 0.75 and 2 mg/mL rapamycin were formulated according to the recipe suggested by Selleck Chemicals. Calculations were made in order a 25 g mouse injected with 100 µL of the drug formula would receive a dose of either 3 mg/kg or 8 mg/kg, respectively, for the low and high concentration. Based on that, 100 mg/mL stock concentration of rapamycin prepared in DMSO (AppliChem GmbH) was diluted in 30% $^W/_v$ PEG300 (Sigma-Aldrich), 5% $^v/_v$ Tween™ 80 (Sigma-Aldrich) and cell culture grade H_2O (Sigma-Aldrich), bringing the DMSO content to 2% $^v/_v$. Vehicle lacking the drug was also prepared to be used as control. Both rapamycin drug concentrations and vehicle were tested for endotoxins with kinetic turbidimetric plate assay (Associates of Cape Cod Inc.) with experienced technical staff (Björn Becker, PEI), detecting less than 0.1 EU/mL. The drug formula or the vehicle was administered via intraperitoneal (i.p.) route 1 hour prior LV injection.

4.2.4.3 LV injection

CD8-LVs transferring GFP or CD19-CAR were thawed on ice until the administration of the drug into mice (4.2.4.2) and warmed up by holding them in hands shortly before the injection. Mice were restrained and the LVs were injected at 200 µL of dose per mouse through the tail vein (i.v.). Due to the experimental repetition of the GFP transfer, vectors were normalized on particle number per dose. The Table 16 shows the particle number dose and transduction units that each mouse received during the studies.

Table 16: Particles and transduction units (TUs) of each CD8-LV administered per mouse.

Vector	Particles	TUs
GFP CD8-LV (1st)	3.16×10^{11}	0.79×10^{7}
GFP CD8-LV (2nd)	3.16×10^{11}	1.49×10^{7}
CD19-CAR CD8-LV	1.83×10^{11}	4.69×10^{5}

4.2.4.4 Tumor engraftment and in vivo cell imaging

For the tumor model study of *in vivo* generation of CD19-CAR T cells, 5×10^{6} NALM6-luc-eBFP cells, stably expressing firefly luciferase and enhanced blue fluorescent protein (eBFP), were i.v. injected into the tail vein of the mice, 6 days prior LV injection. Cells were washed and re-suspended in warm PBS, calculating each mouse to receive 100 µL of cell suspension. Tumor burden was assessed maximum 2x times per week via bioluminescence *in vivo* imaging, where 150 mg/kg D-luciferin (in PBS – Perkin Elmer) were injected intraperitoneally. After 10 min, mice were placed in IVIS® imaging system (Perkin Elmer) under anesthesia with 2-3% $^{v}/_{v}$ isoflurane CP (CP-Pharma) in medical air (21% $^{v}/_{v}$ O$_2$). Images were captured from mice positioned on their ventral or dorsal sides, with the exposure set at 1 sec or at 30 sec, electron bin at 4 or 8, and visualization done with bin 4 in two scales of photon radiance, $1.3\times10^{4}-5\times10^{6}$ p/sec/cm^2/sr for early time points or $1.5\times10^{6}-5\times10^{7}$ p/sec/cm^2/sr for later time points. Two days before LV injection, mice were imaged and randomized to equilibrate tumor flux along the groups.

4.2.4.5 Blood sampling and erythrocyte lysis

Peripheral blood was collected from anesthetized mice via retro-orbital sinus bleeding with sterile Pasteur glass pipettes (VWR). For intermediate bleeding during the tumor model study, weekly collection of 30-60 µL of blood was performed after LV injection, while for terminal bleeding, maximum blood volume was withdrawn right before euthanization via cervical dislocation. Blood was directly transferred and inverted 2x times into heparin coated BD Microtainer® tubes (BD Biosciences), washed once with PBS, and erythrocytes were lysed with 1X BD Pharm Lyse™ buffer (diluted in H$_2$O) for 15 min at room temperature. Nucleated cells were washed twice with PBS and FcRs were blocked followed by stain with antibodies for flow cytometry analysis (4.2.2.7). Cells were counted from samples of final bleeding, but usually the majority of the samples used for flow cytometry analysis (~2×10^{5} cells).

4.2.4.6 Splenocyte harvesting and DNA isolation

Mouse necropsies were performed to isolate spleens and hind leg bones. Thus, spleens were excised, immersed into cold RPMI 1640 medium without any supplements, and mashed through a 70 µm cell strainer (Corning) with the thumb rest of a 5 mL Omnifix® syringe's plunger (B.

Braun). Single cell suspension was washed once with PBS and erythrocytes were lysed as mentioned in 4.2.4.5. Finally, cells were counted and 2×10^5 cells were processed for flow cytometry analysis, while 2×10^6 splenocytes were enriched for human T cells with magnetic-activated cell sorting (MACS) by positive selection via staining with human anti-CD3-FITC antibody (Miltenyi Biotec) and isolating with anti-FITC MicroBeads (Miltenyi Biotec). Cell separation was performed with MS columns (Miltenyi Biotec) and 1 µL of the anti-CD3 was enough for the positive selection. Excess cells were cryopreserved or used in co-cultures as described in 4.2.4.8.

4.2.4.7 Bone marrow cell harvesting

Hind legs were removed from mouse cadavers and placed into plain RPMI 1640 medium. Bones (hip, femur and tibia) were separated, skeletal muscles were removed with scalpel and forceps, and both the ends were cut open. Bones from one leg were placed in one sterile bottom-pierced 0.5 mL tube inside another 1.5 mL tube containing 50 µL plain RPMI 1640. Bones were centrifuged at 4600×g for 3 min, cells were re-suspended, passed through a 70 µm cell strainer, washed once with PBS and erythrocytes were lysed as mentioned in 4.2.4.5. Cells were counted, stained for flow cytometry (2×10^5 cells per sample) and excess cells were cryopreserved or used in co-cultures (4.2.4.8).

4.2.4.8 Ex vivo CAR T cell expansion assay

For *ex vivo* CAR T cell expansion from mouse splenocytes and bone marrow cells, 10^5 cells were co-seeded in duplicates with the same number of irradiated NALM6-luc-eBFP cells in Nutri-T medium supplemented with cytokines (IL-7, IL15) and antibiotics. Medium was refreshed after 3 days and cells were stained for CAR expression analysis in flow cytometry after 6 days of co-culturing.

4.2.5 Statistical analysis

For typical *in vitro* and *in vivo* studies, mean values with standard deviation (SD) of numeric results derived from flow cytometry or other analyses were visualized on graphs with GraphPad Prism 9 (GraphPad Software Inc.). Statistical differences between multiple groups were tested with one-way ANOVA with Tukey's multiple comparisons. Paired samples were shown as fold change difference, when applicable, and paired t test was performed. Logarithmic non-normally distributed raw photon flux (photons/sec) data were log-transformed prior statistical analyses, while raw data were still plotted on the graphs. Two-way ANOVA with Tukey's multiple comparisons was performed on tumor flux log-transformed results between different groups of mice on each particular day. Statistical results were displayed in abbreviations such as ns= non-

significant, *p<0.05, **p<0.01, ***p<0.001 and ****p<0.0001. For scRNA-seq data, statistical analysis methods are described in 4.2.6.17. Statistical analysis methods and results were validated by Dr. Colin Clarke (NIBRT), Dr. Liam Childs (PEI), Dr. Christel Kamp (PEI) and Kay-Martin Hanschmann (PEI).

4.2.6 Single-cell RNA sequencing

For scRNA-seq studies, LV stocks were purified with DNase I as mentioned in 4.2.1.9 prior inoculation of PBMC. Transduction enhancer vectofusin-1 was used for the CD8-LV and CD4-LV during the WTA study. The single-cell capturing and RNA processing was performed with the nanowell technology of BD Rhapsody™ single cell analysis system and the respective kits (BD Biosciences). The BD Rhapsody™ technology prepares transcriptome libraries from single-cells for conducting 3'-end sequencing, meaning that the 3'-end part of a transcribed gene is sequenced and aligned to the reference genome. Next generation sequencing (NGS) was kindly carried out from experienced technical and scientific staff at Paul-Ehrlich-Institut (Dr. Csaba Miskey) (NextSeq™ 550, Illumina) or at Max-Planck-Institute for Heart- and Lung Research (Dr. Stefan Güther) (NextSeq™ 2000, Illumina) and technical assistance as well as customized primers for targeted gene analysis were provided according to the customer service by Dr. Vadir Lopez-Salmeron, Edyta Kowalczyk, Dr. Siobhan Cashman (all BD Biosciences) and Michael Rieger and WeiJia Yu (Goethe University Hospital Frankfurt).

4.2.6.1 Single-cell preparation, RNA capturing and cDNA synthesis

Few days after LV inoculation, PBMC were re-suspended, the expression of CAR transgene was analyzed by flow cytometry, and the viability and cell concentration were measured in LUNA-FL™ cell counter. For whole transcriptome analysis, live cells were magnetically sorted with the dead cell removal kit (Miltenyi Biotec) followed by negative magnetic selection of target cells (CD3 or CD4 or CD8 cells) with the LS columns, according to the manufacturer's instructions. For targeted gene analysis, unsorted cells from the whole samples were used. For VCN assay, genomic DNA from 2×10^5 cells per sample was isolated (4.2.1.8).

Single-cells (approximately 1.6×10^5) were re-suspended in 200 µL cold sample buffer provided by the kit (BD Biosciences) and stained with the viability dyes Calcein AM (final concentration 10 nM, Thermo Fisher Scientific) and DRAQ7™ (final concentration 1.5 nM, BD Biosciences) at 37℃ for 5 min, as described in manufacturer's guideline. Cells were counted with BD Rhapsody™ scanner and a new dilution of 4.6×10^4 cells/mL or 5.7×10^4 cells/mL was prepared to seed 20,000 or 25,000 cells per nanowell cartridge, respectively. Doublet rates were estimated for each respective concentration to be at 4.8% or 6%. Cells were then immediately

seeded and RNA from single-cells was captured by poly-dT coated magnetic beads and cDNA was synthesized. Finally, based on the number of retrieved beads with 1+ viable cells measured by the BD Rhapsody scanner, cDNA-bound beads were down-sampled according to the desired number of cells to be processed for sequencing.

To combine more than one sample in one cartridge, multiplexing antibodies were utilized (described in 4.2.6.2).

4.2.6.2 *Multiplexing cell samples*

In order to pool more samples in one nanowell cartridge and still be possible to distinguish them during the analysis, human BD® single-cell multiplexing kit with oligo-tagged antibodies was utilized. Reduction of the suggested amount of antibodies to 20% was enough to distinguish the samples post-sequencing. Particularly, 4 µL of an antibody tag was mixed with 1.6×10^5 cells, re-suspended in 40 µL of stain buffer (FBS) (BD Biosciences). Cells were incubated for 20 min at room temperature, washed 3 times with the stain buffer by centrifuging at 400×g for 5 min and cell pellets were finally pooled together in 200 µL cold sample buffer and proceeded for viability stain and capturing as described above. Sample tag libraries were prepared separately from the transcriptome libraries, following a similar protocol to that of a TGA, and pooled before sequencing depending on the desired total reads were aimed (4.2.6.8).

4.2.6.3 *Targeted gene amplification*

Targeted gene amplification (TGA) analysis was carried out on 6-day expanded CAR T cell products and control untransduced PBMC, investigating a panel of 399 immune related genes (human Immune Response Panel, BD Biosciences). Customized primers (BD Biosciences) detecting the CAR mRNA expression in transduced cells were also included during amplification steps and library preparation, according to the manufacturer's guidelines. After the cDNA synthesis, three PCR amplifications were performed, with the final one multiplexing the different libraries with distinct i7 adapters included in the kit (4.2.6.7). Between the amplifications, amplicons were purified with Agencourt® AMPure® XP magnetic beads (Beckman Coulter Life Sciences), and quality control of final libraries was performed with Fragment Analyzer (4.2.6.6).

4.2.6.4 *Whole transcriptome analysis library preparation*

For analyzing the whole transcribed mRNA content from the single-cells, whole transcriptome analysis (WTA) was performed according to the manufacturer's instructions (BD Biosciences). In brief, random priming and extension of cDNA libraries was conducted, followed by two PCR amplifications. After the first PCR, DNA concentration of specific product size (150-600 bp) was

measured by Fragment Analyzer (4.2.6.6), which was also utilized for assessing the quality and the size of the final sequencing libraries.

4.2.6.5 Qubit: high-sensitivity DNA quantification

DNA quantification of sequencing libraries was done with Qubit® 2.0 fluorometer (Thermo Fisher Scientific), using the high-sensitivity dsDNA kit (Thermo Fisher Scientific).

4.2.6.6 Fragment analyzer assessment

Quality control (QC) of sequencing libraries was carried out with the high-sensitivity NGS kit with Fragment Analyzer™ (Agilent). Generated data were analyzed with ProSize v2 software (Advanced Analytical Technologies). Representative results passed the QC from TGA, WTA and oligo-tag (multiplexing) libraries are shown in Figure 50A-D.
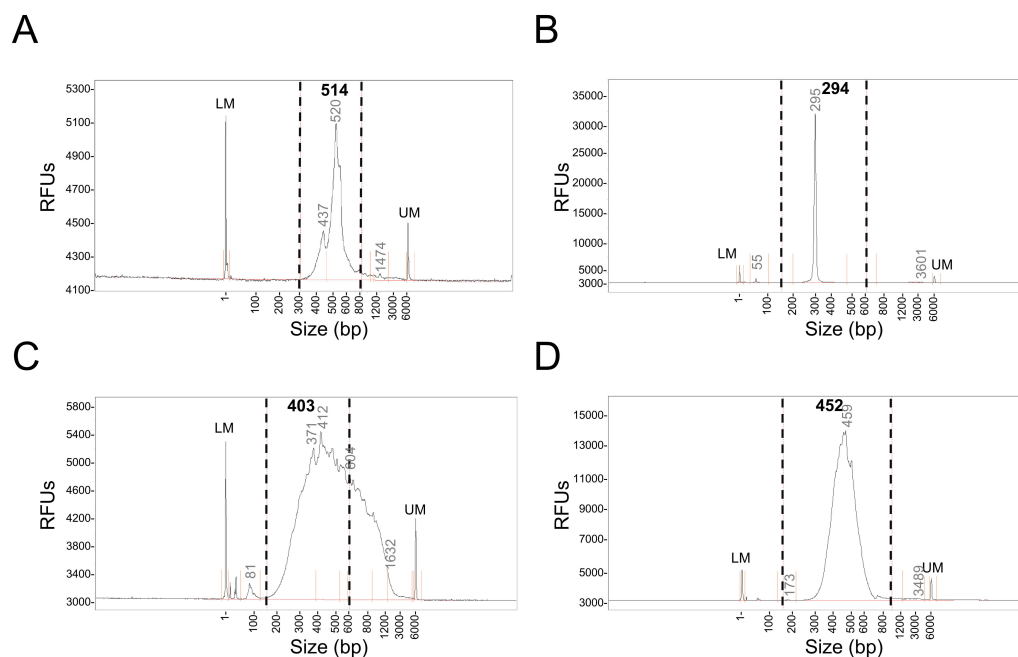
Figure 50: Representative QC plots from Fragment Analyzer.
(**A**) TGA library. (**B**) Sample oligo-tag multiplexing library. (**C**) DNA concentration measurement of random priming and extension PCR amplicons at 150-600 bp. (**D**) Final WTA library. *LM: lower marker, UP:* upper marker*, dashed lines:* major fragment's limits*, grey numbers:* size of peaks (bp)*, black numbers:* mean size of indicated area by the dashed lines (bp).

4.2.6.7 Multiplexing libraries

Although one nanowell cartridge resulted in one sequencing library, it was possible to multiplex different libraries derived from multiple cartridges and pool them in one sequencing run. Thus, different i7 Illumina adapters (referred in the kit as library reverse primers 1-4) were used during index PCR amplification with the same i5 adapter (library forward primer) for all. Hence, it was possible to generate up to 4 sequencing libraries, mix them for the final sequencing run and demultiplex them after finishing due to the distinct barcodes.

4.2.6.8   Next generation sequencing

Transcriptomic libraries generated from single-cells were sequenced with Illumina's next generation sequencing technology (NextSeq™ 550 or NextSeq™ 2000) by pre-mentioned experienced scientific staff (Dr. Csaba Miskey, PEI; Dr. Stefan Günther, Max-Planck-Institute for Heart- and Lung Research). For NextSeq™ 550, 1.5-2 pM of DNA library were spiked with 20% of PhiX and loaded into the Illumina flow cell and paired-end sequencing was performed with the 150 cycles kit (2×75 cycles, maximized to 2×80 cycles). For NextSeq™ 2000, 1 nM of library spiked with 20% PhiX (Illumina) was inserted and sequencing was performed with the 100 cycles kit (2×50 cycles, maximized to 2×75 cycles). Barcode sequences located in the i7 adapters of the multiplexed libraries were specified in the device's software, which automatically demultiplexed them at the end of the run. The information that each read contains is shown in Figure 51. The sequences from read 1 are bound to the magnetic beads, where each individual bead carries one particular cell label (CL) to indicate the single cell, and a random unique molecular index (UMI), which distinguishes the number of different mRNA molecules derived from the same expressed gene. The read 2 contains the 3'-end sequence of an mRNA transcribing gene. Eventually, reads are paired based on the coordinates of the fluorescent PCR reaction that is performed in the flow cell of the sequencer.
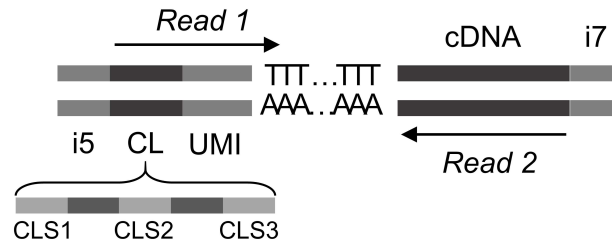
Figure 51: Structure of reads in paired-end sequencing.
Read 1 contains the cell label (CL), which comprises of 3 cell label sequences (CLS) interrupted by a common sequence in between, and Unique Molecular Index (UMI). Read 2 contains the gene information.

4.2.6.9   Quality control of sequencing reads

To assess base call errors that can results during NGS, a quick per base quality control of the raw sequencing reads was carried out by the FastQC tool (Babraham Bioinformatics). The quality was translated into Phred quality score by the software and representative results are shown in Figure 52. The respective base call accuracies of a Phred score are shown in Table 17.
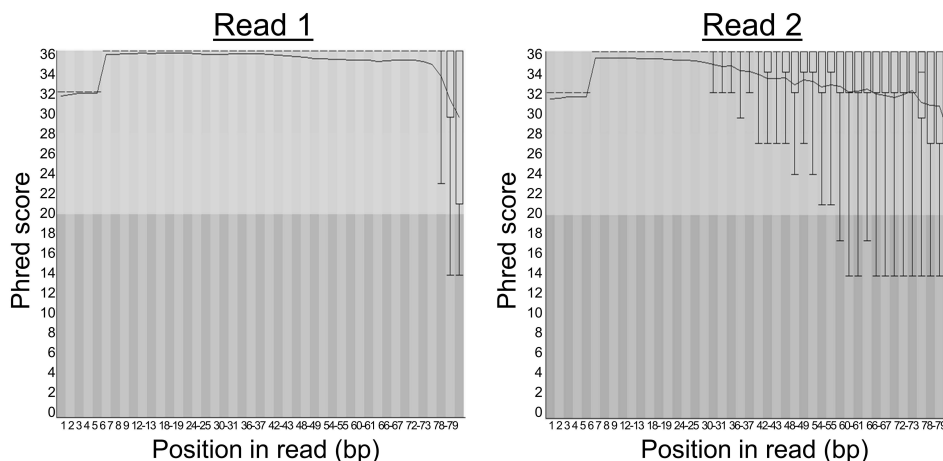
Figure 52: Representative base call accuracy score plots of read 1 and 2.
Bars of Phred score per base pair position showing the accuracy of a base call by the Illumina sequencer. Line on the graphs indicates the mean value of the Phred score for the bases in a particular position.

Table 17: Translation of Phred score to base call accuracy.

Phred score	Base call accuracy
10	90%
20	99%
30	99.9%
40	99.99%

4.2.6.10 Read alignment with Seven Bridges

Raw sequencing reads were aligned to the reference genome with the Seven Bridges bioinformatics pipeline (Seven Bridges) for BD Rhapsody libraries. Either a local installation running in a physical server or a cloud version was used for the filtering and alignment of the reads. The read 2 containing the gene sequence was mapped with Bowtie2 method, reads were merged and molecules differing due to single base substitution errors occurred during PCR amplification were identified and collapsed into fewer with the recursive substitution error correction (RSEC) algorithm. The access to the local server was done through the open-source terminal emulator PuTTY and file transfer through the open-source SSH file transfer protocol WinSCP. The latest YML templates and the CWL file versions were provided by BD Biosciences. Targeted gene amplicons in a simple fasta format or STAR index of human genome coding sequences from genome reference consortium human build 38 (GRCh38 version 29) together with a GTF annotation file were used for the alignment of TGA or WTA reads, respectively. For any extra sequences, such as CAR gene, another fasta file was supplemented to the pipeline containing the name and the 5'→3' DNA sequence of the whole transgene until the poly-A starting

site. Sequencing saturation was above 80% for all the libraries, mean number of reads per cell for TGA was 4,500 (reads/cell) and for WTA 29,200 (reads/cell). The Table 18 shows some of the basic output metrics from Seven Bridges pipeline from all the sequencing experiments. Eventually, the alignment of two paired reads generates a count matrix with a unique cell identification number on the rows and the gene name on the columns, while the number in the matrix indicates the molecules of the particular gene per cell.

Table 18: Seven Bridges generated sequencing metrics from all the experiments.

Assay	Sample	Cell #	Seq. saturation	Reads/cell	Molecules/cell
TGA	Untransduced	2711	80.0 %	4264	1706
TGA	VSV-LV	9023	84.0 %	4597	1237
TGA	CD8-LV	9793	82.8 %	4618	1429
WTA 1	Untransduced	1042	96.7 %	26045	4722
WTA 1	VSV-LV	1887	95.2 %	31587	7028
WTA 1	CD8-LV	1387	89.4 %	29933	10200
WTA 1	CD4-LV	1274	91.5 %	30081	9247
WTA 2	All combined	10320	91.9 %	28497	8280
Tags (WTA 2)	All combined	10320	—	223.41	—

4.2.6.11 Bioinformatics analysis

Count matrices generated by Seven Bridges alignment and pre-processing pipeline were analyzed in R programming environment (R 4.2.1) with its integrated development environment of RStudio (v2022.11), using the *Seurat* tool package and the packages and tools mentioned in 6.1 (Hao et al., 2021).

4.2.6.12 Filtering of low-quality cells

Putative single-cells were filtered for low quality of cells based on the distribution of UMIs per cell and genes per cell (in TGA and WTA), but also for mitochondrial mRNA and ribosomal-related mRNA content (only in WTA). Although the filtering was done manually in TGA (Figure 53A), the outliers in WTA were detected and removed with the quickPerCellQC function from *scuttle* package (Figure 53B). Typically, putative cells containing high or low number of genes and UMIs as well as high mitochondrial and ribosomal mRNA content were considered to be potential duplet cells or apoptotic-necrotic cells and subsequently were removed with one or the other of the pre-mentioned methods.
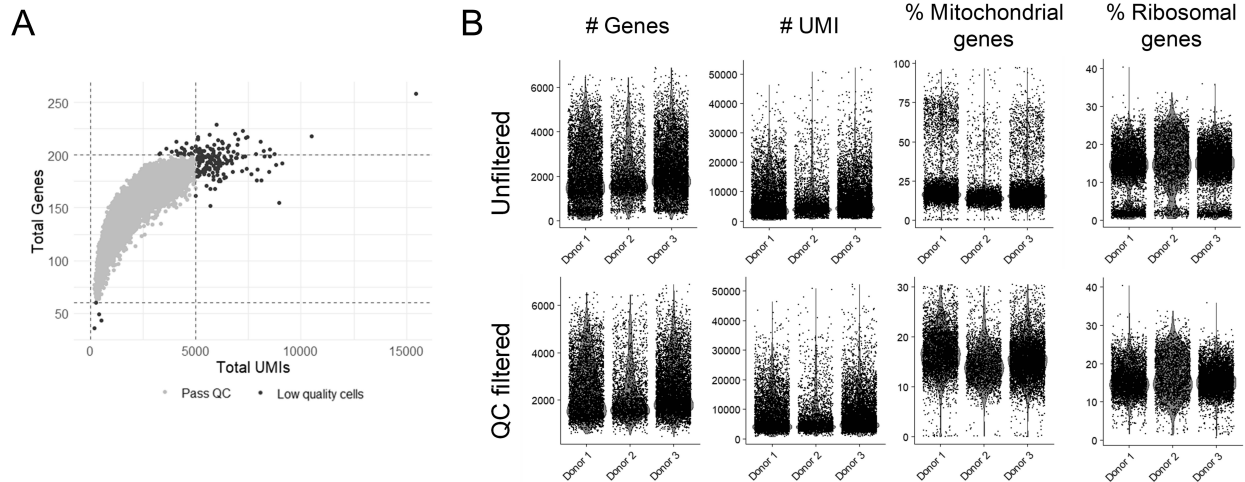
Figure 53: QC filtering of low-quality single-cells.
(**A**) Manual filtering of TGA scRNA-seq data. (**B**) Computational-based filtering of WTA scRNA-seq data with *scuttle*. Top row shows the pre-processed cells, while bottom row the post-processed QC filtered cells.

4.2.6.13 Normalization

After removing the low quality of cells, gene expressions per cell were normalized and log-transformed. More specifically, the gene expression per cell was normalized to the total expression, scaled by 10,000 and log-transformed with the natural logarithm. In order to avoid undefined numbers due to an unexpressed gene (0 counts), the function (NormalizeData from *Seurat*) adds 1 before log-transforming, often mentioned as log1p(normalized UMIs of gene A), instead of ln(normalized UMIs of gene A + 1). The formula that the normalization is based on is:

$$\text{Normalized gene expression} = \ln(\frac{\text{UMI counts of gene A}_{\text{Cell 1}}}{\text{Total UMI counts of all genes}_{\text{Cell 1}}} \times 10{,}000 + 1)$$

The default *Seurat* normalization was performed in TGA scRNA-seq data, while in WTA the deconvolution-based normalization, a very similar to Seurat, approach of the *scran* package was selected (A. T. L. Lun et al., 2016).

4.2.6.14 Principal component analysis and cell-cycle regression

Highly variable features were identified and selected via *Seurat* FindVariableFeatures ("vst" method). For TGA, all the 400 genes were chosen as highly variable, while in WTA the default settings of selecting 2000 variable genes were applied (Figure 54).
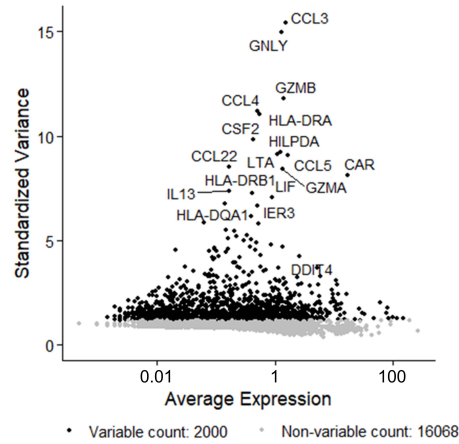
Figure 54: Representative plot of selecting highly variable features in WTA.

Prior uniform manifold approximation and projection (UMAP) plotting, principal component analysis of cellular and transcriptional variations was performed by *Seurat* RunPCA function generating 50 principal components. The most significant principal components with the highest standard deviations were chosen empirically, as shown in Elbow plot in Figure 55, up to the point where the plot flattens.
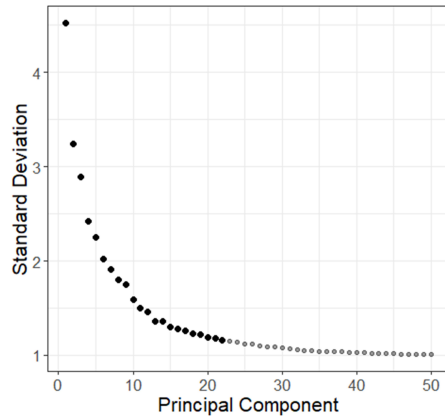
Figure 55: Elbow plot of principal components.
Black dots indicate the first 22 highly significant principal components until the plot flattens.

In WTA, cell-cycle phases were scored with *Seurat* function CellCycleScoring and cell-cycle effects were regressed via ScaleData, along with mitochondrial mRNA content, UMIs and gene number. Thus, the effects driven by these factors that affect the principal component analysis (PCA) and subsequently the UMAP plotting were smoothened. Due to gene limitations in TGA, only effects from UMIs and gene number were regressed. The Figure 56A shows the effect of cell-cycle genes on the first 2 principal components, while after regression the intra-sample variations due to the cell-cycle phase was corrected (Figure 56B).

106
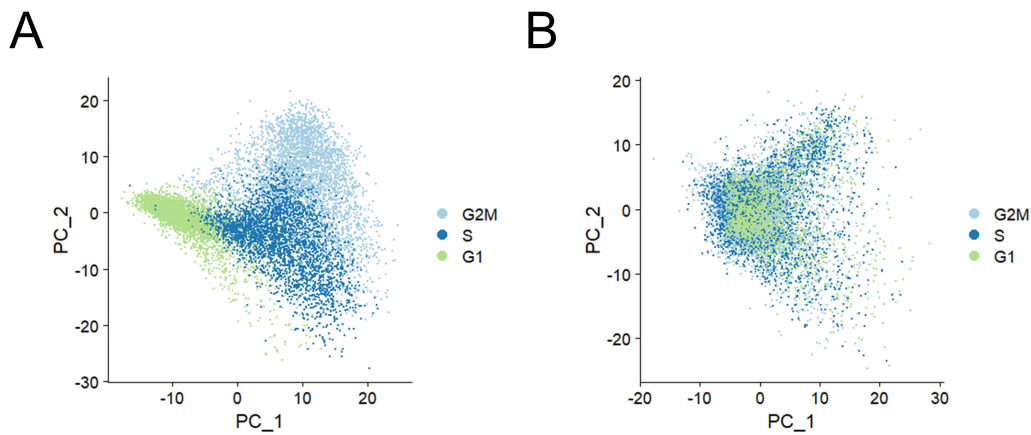
Figure 56: Principal component analysis and cell-cycle effect.
(**A**) Pronounced cell-cycle effect in the first 2 principal components. (**B**) Cell-cycle corrected principal component analysis. *G2M, S, G1: cell-cycle phases.*

4.2.6.15 Uniform Manifold Approximation and Projection and clustering

By selecting the top significant principal components, unsupervised clustering analysis and dimensionality reduction by uniform manifold approximation and projection (UMAP) plotting were conducted. The latter reduces the principal components into 2 dimensions (2D) providing a topological analysis of biologically similar or unassociated cells. Hence, neighbor cells tend to have a closer biological relevance than distant clusters. Cell types were assigned to clusters identified by unsupervised clustering analysis and shown in UMAP plots. Clusters comprising the same immune cell types, such as CD4, CD8, γδ, NKT and B cells were usually merged together to make a more simplified representation.

4.2.6.16 Batch effect assessment and correction

Likewise the cell-cycle, batch effect derived from inter-sample variations, such as libraries from different cartridges or different donors, was assessed and corrected whenever it was necessary. Although technical variation was observed in none of the cases (Figure 57), donor to donor variation resulted in separation of cell clusters, while portraying the same biological features. Thus, batch effect correction was performed by identifying "anchors" (mutual nearest neighbors - MNN) on aligned data with canonical correlation analysis (CCA) and integrating samples from different donors based on these "anchors", without disturbing the cluster formation due to biological variation of cells (over-correction) as far as possible (Figure 57).
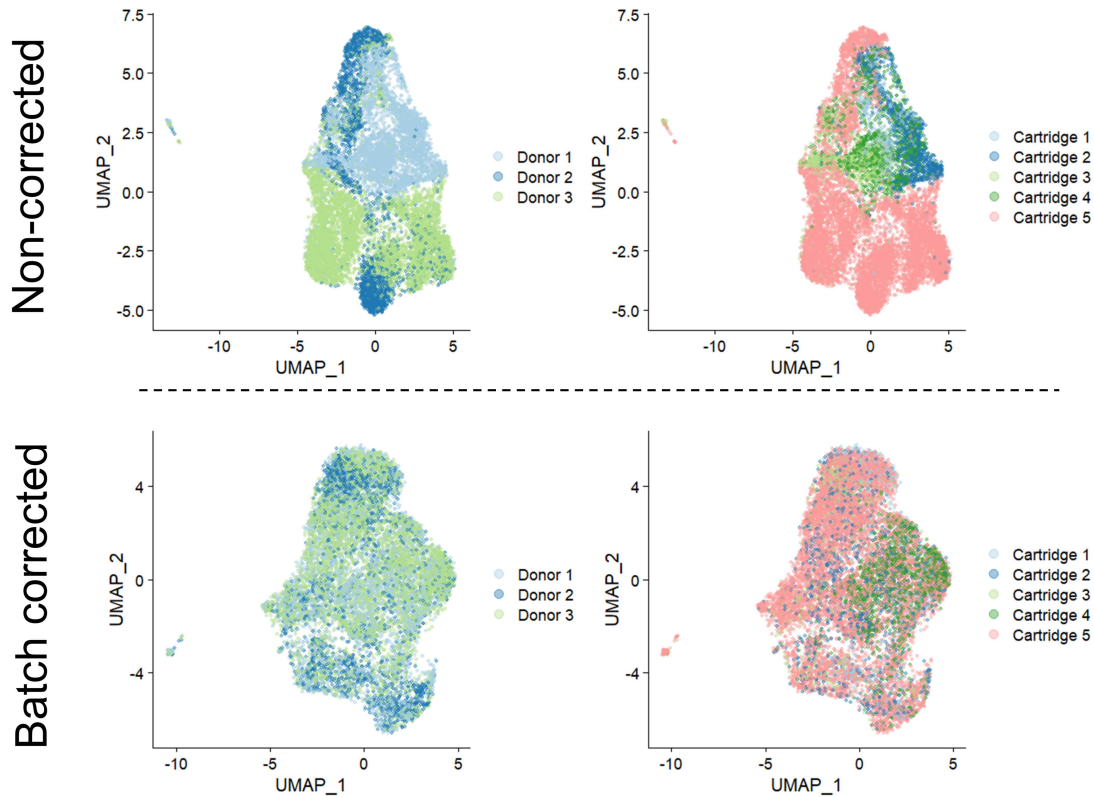
Figure 57: Batch effect correction and integration.
Batch effect due to donor variations was observed in WTA data, while there were no substantial technical variations derived from the use of different nanowell cartridges.

4.2.6.17 Subsetting CAR T cells via multimodal gene analysis

For subsetting CD8, CD4, CAR+ and CAR- T cells, multimodal analysis (*multimode* package) was conducted in *CD8A* and *CAR* genes due to their trimodal expression (negative, low and high expressing cells). The computational method identifies the modes (peaks) and antimodes (pits), which latter were used as thresholds for subsetting cell populations.

4.2.6.18 Differential gene expression and statistical analyses

Differential gene expression analysis was conducted with Wilcoxon rank sum test, set as default statistical test in *Seurat*. P-values of multiple comparisons were adjusted with either Bonferroni correction (in TGA) or with the less conservative Benjamini-Hochberg procedure (in WTA). Differentially expressed (DE) genes identified across all the subsets (groups of cells/populations) by the function FindAllMarkers were plotted in heat map plots displaying a comprehensive difference in gene expression. On the other hand, FindMarkers function done between two subsets provided more specific insights of DE genes between the analyzed groups and differences were shown on volcano plots (*EnhancedVolcano*). As DE genes were considered genes that were significantly (adjusted p-value < 0.05 or FDR < 0.05) up- or down-regulated with an absolute $\log_2$(fold change) value above 0.2 (in WTA) or 0.25 (in TGA) ($|\log_2FC| > 0.2$ or 0.25),

meaning dysregulation of genes of the order of 15% or 20%, respectively. The reason why lower $\log_2$FC threshold was set in WTA and FDR was calculated was to increase sensitivity of gene detection in a sensible way by including biologically relevant genes. Same thresholds and p-value adjustment method were used also in LC-MS analysis (4.2.3.3). For a quick representation of overlaps between DE genes identified in different comparisons, Venn plots (*ggVennDiagram*) were constructed. Finally, genes of interest were displayed on violin plots (*ggplot2*), where Kruskal-Wallis test with Wilcoxon multiple comparison and Bonferroni adjustment (in TGA) or Benjamini-Hochberg procedure (in WTA) were performed and statistical significance was displayed on the graphs as ns= non-significant, *p<0.05, **p<0.01, ***p<0.001 and ****p<0.0001.

4.2.6.19 Gene set enrichment analysis

Gene set enrichment analysis (GSEA) was performed to briefly investigate which biological pathways were related with the DE genes identified during the differential gene expression analysis. For that reason, GSEA was carried out with the independent enrichment analysis online tool from Appyters collection (Clarke et al., 2021) with gene lists of either significantly up- or down-regulated DE genes from TGA (adjusted p-value<0.05, $\log_2$FC>0.25 or $\log_2$FC<-0.25), correcting the analysis for the background genes from the immune response panel. Likewise, a gene lists together with the $\log_2$FC values from the analyses done in WTA ($|\log_2$FC$|$>0.2, FDR<0.05) were provided to the *WebGestaltR* tool for performing the GSEA (Liao et al., 2019). In these ways, gene lists were analyzed for their overlap relations with gene sets from the Gene Ontology (GO) Biological Process or Kyoto Encyclopedia of Genes and Genomes (KEGG) pathways (Ashburner et al., 2000; Kanehisa & Goto, 2000). Finally, top 10 significant categories were plotted.

5 BIBLIOGRAPHY

Adusumilli, P. S., Cherkassky, L., Villena-Vargas, J., Colovos, C., Servais, E., Plotkin, J., Jones, D. R., & Sadelain, M. (2014). Regional delivery of mesothelin-targeted CAR T cell therapy generates potent and long-lasting CD4-dependent tumor immunity. *Science Translational Medicine*, *6*(261). https://doi.org/10.1126/SCITRANSLMED.3010162

Agarwal, S., Hanauer, J. D. S., Frank, A. M., Riechert, V., Thalheimer, F. B., & Buchholz, C. J. (2020). In Vivo Generation of CAR T Cells Selectively in Human CD4+ Lymphocytes. *Molecular Therapy*, *28*(8). https://doi.org/10.1016/J.YMTHE.2020.05.005

Agarwal, S., Weidner, T., Thalheimer, F. B., & Buchholz, C. J. (2019). *In vivo generated human CAR T cells eradicate tumor cells. 8*(12). https://doi.org/10.1080/2162402X.2019.1671761

Aguilar, H. C., & Iorio, R. M. (2012). *Henipavirus Membrane Fusion and Viral Entry*. 79–94. https://doi.org/10.1007/82_2012_200/FIGURES/1

Al-Mutairi, M. S., Cadalbert, L. C., Adrienne McGachy, H., Shweash, M., Schroeder, J., Kurnik, M., Sloss, C. M., Bryant, C. E., Alexander, J., & Plevin, R. (2010). MAP kinase phosphatase-2 plays a critical role in response to infection by Leishmania mexicana. *PLoS Pathogens*, *6*(11). https://doi.org/10.1371/journal.ppat.1001192

Alberts, B., Johnson, A., Lewis, J., Raff, M., Roberts, K., & Walter, P. (2002). *T Cells and MHC Proteins*. https://www.ncbi.nlm.nih.gov/books/NBK26926/

Aldovini, A., & Young, R. A. (1990). Mutations of RNA and protein sequences involved in human immunodeficiency virus type 1 packaging result in production of noninfectious virus. *Journal of Virology*, *64*(5), 1920–1926. https://doi.org/10.1128/JVI.64.5.1920-1926.1990

Amini-Bavil-Olyaee, S., Choi, Y. J., Lee, J. H., Shi, M., Huang, I. C., Farzan, M., & Jung, J. U. (2013). The Antiviral Effector IFITM3 Disrupts Intracellular Cholesterol Homeostasis to Block Viral Entry. *Cell Host & Microbe*, *13*(4), 452. https://doi.org/10.1016/J.CHOM.2013.03.006

Amirache, F., Lévy, C., Costa, C., Mangeot, P. E., Torbett, B. E., Wang, C. X., Nègre, D., Cosset, F. L., & Verhoeyen, E. (2014). Mystery solved: VSV-G-LVs do not allow efficient gene transfer into unstimulated T cells, B cells, and HSCs because they lack the LDL receptor. *Blood*, *123*(9), 1422–1424. https://pubmed.ncbi.nlm.nih.gov/24578496/

Ammann, J. U., Cooke, A., & Trowsdale, J. (2013). Butyrophilin Btn2a2 inhibits T cell receptor activation, PI3K/Akt pathway signaling, and induces Foxp3 expression in T lymphocytes. *Journal of Immunology (Baltimore, Md. : 1950)*, *190*(10), 5030. https://doi.org/10.4049/JIMMUNOL.1203325

Anderson, S. L., Carton, J. M., Lou, J., Xing, L., & Rubin, B. Y. (1999). Interferon-Induced Guanylate Binding Protein-1 (GBP-1) Mediates an Antiviral Effect against Vesicular Stomatitis Virus and Encephalomyocarditis Virus. *Virology*, *256*(1), 8–14. https://doi.org/10.1006/VIRO.1999.9614

Araki, K., Morita, M., Bederman, A. G., Konieczny, B. T., Kissick, H. T., Sonenberg, N., & Ahmed, R. (2017). Translation is actively regulated during effector CD8+ T cell differentiation. *Nature Immunology*, *18*(9), 1046. https://doi.org/10.1038/NI.3795

Ashburner, M., Ball, C. A., Blake, J. A., Botstein, D., Butler, H., Cherry, J. M., Davis, A. P., Dolinski, K., Dwight, S. S., Eppig, J. T., Harris, M. A., Hill, D. P., Issel-Tarver, L., Kasarskis, A., Lewis, S., Matese, J. C., Richardson, J. E., Ringwald, M., Rubin, G. M., & Sherlock, G. (2000). Gene ontology: tool for the unification of biology. The Gene Ontology Consortium. *Nature Genetics*, *25*(1), 25–29. https://doi.org/10.1038/75556

Backliwal, G., Hildinger, M., Hasija, V., & Wurm, F. M. (2008). High-density transfection with HEK-293 cells allows doubling of transient titers and removes need for a priori DNA complex formation with PEI. *Biotechnology and*

Bioengineering, *99*(3), 721–727. https://doi.org/10.1002/BIT.21596

Bai, Z., Lundh, S., Kim, D., Woodhouse, S., Barrett, D. M., Myers, R. M., Grupp, S. A., Maus, M. V, June, C. H., Camara, P. G., Melenhorst, J. J., & Fan, R. (2021). Single-cell multiomics dissection of basal and antigen-specific activation states of CD19-targeted CAR T cells. *Journal for ImmunoTherapy of Cancer*, *9*(5), e002328. https://doi.org/10.1136/JITC-2020-002328

Bai, Z., Woodhouse, S., Zhao, Z., Arya, R., Govek, K., Kim, D., Lundh, S., Baysoy, A., Sun, H., Deng, Y., Xiao, Y., Barrett, D. M., Myers, R. M., Grupp, S. A., June, C. H., Fan, R., Camara, P. G., & Melenhorst, J. J. (2022). Single-cell antigen-specific landscape of CAR T infusion product identifies determinants of CD19-positive relapse in patients with ALL. *Science Advances*, *8*(23). https://doi.org/10.1126/SCIADV.ABJ2820/SUPPL_FILE/SCIADV.ABJ2820_TABLE_S2.ZIP

Baldauf, H. M., Pan, X., Erikson, E., Schmidt, S., Daddacha, W., Burggraf, M., Schenkova, K., Ambiel, I., Wabnitz, G., Gramberg, T., Panitz, S., Flory, E., Landau, N. R., Sertel, S., Rutsch, F., Lasitschka, F., Kim, B., König, R., Fackler, O. T., & Keppler, O. T. (2012). SAMHD1 restricts HIV-1 infection in resting CD4(+) T cells. *Nature Medicine*, *18*(11), 1682–1687. https://doi.org/10.1038/NM.2964

Balkhi, M. Y., Wittmann, G., Xiong, F., & Junghans, R. P. (2018). YY1 Upregulates Checkpoint Receptors and Downregulates Type I Cytokines in Exhausted, Chronically Stimulated Human T Cells. *IScience*, *2*, 105. https://doi.org/10.1016/J.ISCI.2018.03.009

Bari, R., Granzin, M., Tsang, K. S., Roy, A., Krueger, W., Orentas, R., Pfeifer, R., Moeker, N., Verhoeyen, E., Dropulic, B., & Leung, W. (2019). A distinct subset of highly proliferative and lentiviral vector (LV)-transducible NK cells define a readily engineered subset for adoptive cellular therapy. *Frontiers in Immunology*, *10*(AUG), 2001. https://doi.org/10.3389/FIMMU.2019.02001/BIBTEX

Barré-Sinoussi, F., Chermann, J. C., Rey, F., Nugeyre, M. T., Chamaret, S., Gruest, J., Dauguet, C., Axler-Blin, C., Vézinet-Brun, F., Rouzioux, C., Rozenbaum, W., & Montagnier, L. (1983). Isolation of a T-lymphotropic retrovirus from a patient at risk for acquired immune deficiency syndrome (AIDS). *Science (New York, N.Y.)*, *220*(4599), 868–871. https://doi.org/10.1126/SCIENCE.6189183

Bender, R. R., Muth, A., Schneider, I. C., Friedel, T., Hartmann, J., Plückthun, A., Maisner, A., & Buchholz, C. J. (2016). Receptor-Targeted Nipah Virus Glycoproteins Improve Cell-Type Selective Gene Delivery and Reveal a Preference for Membrane-Proximal Cell Attachment. *PLoS Pathogens*, *12*(6), e1005641. https://doi.org/10.1371/JOURNAL.PPAT.1005641

Benjamini, Y., & Hochberg, Y. (1995). Controlling the False Discovery Rate: A Practical and Powerful Approach to Multiple Testing. *Journal of the Royal Statistical Society: Series B (Methodological)*, *57*(1), 289–300. https://doi.org/10.1111/J.2517-6161.1995.TB02031.X

Boroughs, A. C., Larson, R. C., Marjanovic, N. D., Gosik, K., Castano, A. P., Porter, C. B. M., Lorrey, S. J., Ashenberg, O., Jerby, L., Hofree, M., Smith-Rosario, G., Morris, R., Gould, J., Riley, L. S., Berger, T. R., Riesenfeld, S. J., Rozenblatt-Rosen, O., Choi, B. D., Regev, A., & Maus, M. V. (2020). A Distinct Transcriptional Program in Human CAR T Cells Bearing the 4-1BB Signaling Domain Revealed by scRNA-Seq. *Molecular Therapy*, *28*(12), 2577–2592. https://doi.org/10.1016/j.ymthe.2020.07.023

Bourdon, J. C., Renzing, J., Robertson, P. L., Fernandes, K. N., & Lane, D. P. (2002). Scotin, a novel p53-inducible proapoptotic protein located in the ER and the nuclear membrane. *The Journal of Cell Biology*, *158*(2), 235–246. https://doi.org/10.1083/JCB.200203006

Braaten, D., & Luban, J. (2001). Cyclophilin A regulates HIV-1 infectivity, as demonstrated by gene targeting in human T cells. *The EMBO Journal*, *20*(6), 1300. https://doi.org/10.1093/EMBOJ/20.6.1300

Brass, A. L., Huang, I. C., Benita, Y., John, S. P., Krishnan, M. N., Feeley, E. M., Ryan, B. J., Weyer, J. L., van der

Weyden, L., Fikrig, E., Adams, D. J., Xavier, R. J., Farzan, M., & Elledge, S. J. (2009). The IFITM proteins mediate cellular resistance to influenza A H1N1 virus, West Nile virus, and dengue virus. *Cell*, *139*(7), 1243–1254. https://doi.org/10.1016/J.CELL.2009.12.017

Brudno, J. N., Somerville, R. P. T., Shi, V., Rose, J. J., Halverson, D. C., Fowler, D. H., Gea-Banacloche, J. C., Pavletic, S. Z., Hickstein, D. D., Lu, T. L., Feldman, S. A., Iwamoto, A. T., Kurlander, R., Maric, I., Goy, A., Hansen, B. G., Wilder, J. S., Blacklock-Schuver, B., Hakim, F. T., … Kochenderfer, J. N. (2016). Allogeneic T cells that express an anti-CD19 chimeric antigen receptor induce remissions of B-cell malignancies that progress after allogeneic hematopoietic stem-cell transplantation without causing graft-versus-host disease. *Journal of Clinical Oncology*, *34*(10), 1112–1121. https://doi.org/10.1200/JCO.2015.64.5929

Buenrostro, J. D., Wu, B., Chang, H. Y., & Greenleaf, W. J. (2015). ATAC-seq: A Method for Assaying Chromatin Accessibility Genome-Wide. *Current Protocols in Molecular Biology*, *109*, 21.29.1-21.29.9. https://doi.org/10.1002/0471142727.MB2129S109

Butler, A., Hoffman, P., Smibert, P., Papalexi, E., & Satija, R. (2018). Integrating single-cell transcriptomic data across different conditions, technologies, and species. *Nature Biotechnology 2018 36:5*, *36*(5), 411–420. https://doi.org/10.1038/NBT.4096

Charitidis, F. T., Adabi, E., Thalheimer, F. B., Clarke, C., & Buchholz, C. J. (2021). Monitoring CAR T cell generation with a CD8-targeted lentiviral vector by single-cell transcriptomics. *Molecular Therapy - Methods & Clinical Development*, *23*, 359–369. https://doi.org/10.1016/j.omtm.2021.09.019

Chen, G., Ning, B., & Shi, T. (2019). Single-Cell RNA-Seq Technologies and Related Computational Data Analysis. *Frontiers in Genetics*, *10*(APR). https://doi.org/10.3389/FGENE.2019.00317

Chen, K., Wang, S., Qi, D., Ma, P., Fang, Y., Jiang, N., Wu, E., & Li, N. (2022). Clinical Investigations of CAR-T Cell Therapy for Solid Tumors. *Frontiers in Immunology*, *13*, 3767. https://doi.org/10.3389/FIMMU.2022.896685/BIBTEX

Cheng, Z., Teo, G., Krueger, S., Rock, T. M., Koh, H. W., Choi, H., & Vogel, C. (2016). Differential dynamics of the mammalian mRNA and protein expression response to misfolding stress. *Molecular Systems Biology*, *12*(1), 855. https://doi.org/10.15252/MSB.20156423

Chmielewski, M., & Abken, H. (2015). TRUCKs: the fourth generation of CARs. *Https://Doi-Org.Ep.Fjernadgang.Kb.Dk/10.1517/14712598.2015.1046430*, *15*(8), 1145–1154. https://doi.org/10.1517/14712598.2015.1046430

Chutiwitoonchai, N., Hiyoshi, M., Hiyoshi-Yoshidomi, Y., Hashimoto, M., Tokunaga, K., & Suzu, S. (2013). Characteristics of IFITM, the newly identified IFN-inducible anti-HIV-1 family proteins. *Microbes and Infection*, *15*(4), 280–290. https://doi.org/10.1016/J.MICINF.2012.12.003

Clarke, D. J. B., Jeon, M., Stein, D. J., Moiseyev, N., Kropiwnicki, E., Dai, C., Xie, Z., Wojciechowicz, M. L., Litz, S., Hom, J., Evangelista, J. E., Goldman, L., Zhang, S., Yoon, C., Ahamed, T., Bhuiyan, S., Cheng, M., Karam, J., Jagodnik, K. M., … Ma'ayan, A. (2021). Appyters: Turning Jupyter Notebooks into data-driven web apps. *Patterns*, *2*(3), 100213. https://doi.org/10.1016/J.PATTER.2021.100213

Coiras, M., Bermejo, M., Descours, B., Mateos, E., García-Pérez, J., López-Huertas, M. R., Lederman, M. M., Benkirane, M., & Alcamí, J. (2016). IL-7 Induces SAMHD1 Phosphorylation in CD4+ T Lymphocytes, Improving Early Steps of HIV-1 Life Cycle. *Cell Reports*, *14*(9), 2100. https://doi.org/10.1016/J.CELREP.2016.02.022

Collins, F. S., & Fink, L. (1995). The Human Genome Project. *Alcohol Health and Research World*, *19*(3), 190–195. https://doi.org/10.5005/jp/books/10279_22

Colomer-Lluch, M., Ruiz, A., Moris, A., & Prado, J. G. (2018). Restriction Factors: From Intrinsic Viral Restriction to Shaping Cellular Immunity Against HIV-1. *Frontiers in Immunology*, *9*, 2876.

https://doi.org/10.3389/FIMMU.2018.02876

Comas, M., Toshkov, I., Kuropatwinski, K. K., Chernova, O. B., Polinsky, A., Blagosklonny, M. V., Gudkov, A. V., & Antoch, M. P. (2012). New nanoformulation of rapamycin Rapatar extends lifespan in homozygous p53-/- mice by delaying carcinogenesis. *Aging*, *4*(10), 715–722. https://doi.org/10.18632/AGING.100496

Cooper, M. D., & Alder, M. N. (2006). The evolution of adaptive immune systems. *Cell*, *124*(4), 815–822. https://doi.org/10.1016/j.cell.2006.02.001

Dai, H., Zhang, W., Li, X., Han, Q., Guo, Y., Zhang, Y., Wang, Y., Wang, C., Shi, F., Zhang, Y., Chen, M., Feng, K., Wang, Q., Zhu, H., Fu, X., Li, S., & Han, W. (2015). Tolerance and efficacy of autologous or donor-derived T cells expressing CD19 chimeric antigen receptors in adult B-ALL with extramedullary leukemia. *Oncoimmunology*, *4*(11). https://doi.org/10.1080/2162402X.2015.1027469

Dautzenberg, I. J. C., Rabelink, M. J. W. E., & Hoeben, R. C. (2020). The stability of envelope-pseudotyped lentiviral vectors. *Gene Therapy 2020 28:1*, *28*(1), 89–104. https://doi.org/10.1038/s41434-020-00193-y

Defrances, M. C., Debelius, D. R., Cheng, J., & Kane, L. P. (2012). Inhibition of T-Cell Activation by PIK3IP1. *European Journal of Immunology*, *42*(10), 2754. https://doi.org/10.1002/EJI.201141653

Demaison, C., Parsley, K., Brouns, G., Scherr, M., Battmer, K., Kinnon, C., Grez, M., & Thrasher, A. J. (2004). High-Level Transduction and Gene Expression in Hematopoietic Repopulating Cells Using a Human Imunodeficiency Virus Type 1-Based Lentiviral Vector Containing an Internal Spleen Focus Forming Virus Promoter. *Https://Home.Liebertpub.Com/Hum*, *13*(7), 803–813. https://doi.org/10.1089/10430340252898984

Deng, Q., Han, G., Puebla-Osorio, N., Ma, M. C. J., Strati, P., Chasen, B., Dai, E., Dang, M., Jain, N., Yang, H., Wang, Y., Zhang, S., Wang, R., Chen, R., Showell, J., Ghosh, S., Patchva, S., Zhang, Q., Sun, R., … Green, M. R. (2020). Characteristics of anti-CD19 CAR T cell infusion products associated with efficacy and toxicity in patients with large B cell lymphomas. *Nature Medicine*, *26*(12), 1878–1887. https://doi.org/10.1038/s41591-020-1061-7

Depil, S., Duchateau, P., Grupp, S. A., Mufti, G., & Poirot, L. (2020). 'Off-the-shelf' allogeneic CAR T cells: development and challenges. *Nature Reviews Drug Discovery 2020 19:3*, *19*(3), 185–199. https://doi.org/10.1038/S41573-019-0051-2

Di Nunzio, F., Danckaert, A., Fricke, T., Perez, P., Fernandez, J., Perret, E., Roux, P., Shorte, S., Charneau, P., Diaz-Griffero, F., & Arhel, N. J. (2012). Human nucleoporins promote HIV-1 docking at the nuclear pore, nuclear import and integration. *PloS One*, *7*(9). https://doi.org/10.1371/JOURNAL.PONE.0046037

Dull, T., Zufferey, R., Kelly, M., Mandel, R. J., Nguyen, M., Trono, D., & Naldini, L. (1998). A Third-Generation Lentivirus Vector with a Conditional Packaging System. *Journal of Virology*, *72*(11), 8463–8471. https://doi.org/10.1128/jvi.72.11.8463-8471.1998

Duvergé, A., & Negroni, M. (2020). Pseudotyping Lentiviral Vectors: When the Clothes Make the Virus. *Viruses 2020, Vol. 12, Page 1311*, *12*(11), 1311. https://doi.org/10.3390/V12111311

Ellis, G. I., Sheppard, N. C., & Riley, J. L. (2021). Genetic engineering of T cells for immunotherapy. *Nature Reviews. Genetics*, *22*(7), 427. https://doi.org/10.1038/S41576-021-00329-9

Erhard, F., Baptista, M. A. P., Krammer, T., Hennig, T., Lange, M., Arampatzi, P., Jürges, C. S., Theis, F. J., Saliba, A.-E., & Dölken, L. (2019). scSLAM-seq reveals core features of transcription dynamics in single cells. *Nature 2019 571:7765*, *571*(7765), 419–423. https://doi.org/10.1038/s41586-019-1369-y

Fenard, D., Ingrao, D., Seye, A., Buisset, J., Genries, S., Martin, S., Kichler, A., & Galy, A. (2013). Vectofusin-1, a new viral entry enhancer, strongly promotes lentiviral transduction of human hematopoietic stem cells. *Molecular Therapy. Nucleic Acids*, *2*(5), e90. https://doi.org/10.1038/MTNA.2013.17

Ferrer, I. R., Araki, K., & Ford, M. L. (2011). Paradoxical Aspects of Rapamycin Immunobiology in Transplantation. *American Journal of Transplantation*, *11*(4), 654–659. https://doi.org/10.1111/J.1600-6143.2011.03473.X

Finkelshtein, D., Werman, A., Novick, D., Barak, S., & Rubinstein, M. (2013). LDL receptor and its family members serve as the cellular receptors for vesicular stomatitis virus. *Proceedings of the National Academy of Sciences of the United States of America*, *110*(18), 7306–7311. www.pnas.org/cgi/doi/10.1073/pnas.1214441110

Finn, J. D., Smith, A. R., Patel, M. C., Shaw, L., Youniss, M. R., van Heteren, J., Dirstine, T., Ciullo, C., Lescarbeau, R., Seitzer, J., Shah, R. R., Shah, A., Ling, D., Growe, J., Pink, M., Rohde, E., Wood, K. M., Salomon, W. E., Harrington, W. F., … Morrissey, D. V. (2018). A Single Administration of CRISPR/Cas9 Lipid Nanoparticles Achieves Robust and Persistent In Vivo Genome Editing. *Cell Reports*, *22*(9), 2227–2235. http://www.cell.com/article/S2211124718301827/fulltext

Florkiewicz, R. Z., & Rose, J. K. (1984). A cell line expressing vesicular stomatitis virus glycoprotein fuses at low pH. *Science (New York, N.Y.)*, *225*(4663), 721–723. https://doi.org/10.1126/SCIENCE.6087454

Frank, A. M., Braun, A. H., Scheib, L., Agarwal, S., Schneider, I. C., Fusil, F., Perian, S., Sahin, U., Thalheimer, F. B., Verhoeyen, E., & Buchholz, C. J. (2020). Combining T-cell-specific activation and in vivo gene delivery through CD3-targeted lentiviral vectors. *Blood Advances*, *4*(22), 5702–5715. https://doi.org/10.1182/BLOODADVANCES.2020002229

Frank, A. M., & Buchholz, C. J. (2019). Surface-Engineered Lentiviral Vectors for Selective Gene Transfer into Subtypes of Lymphocytes. *Molecular Therapy - Methods & Clinical Development*, *12*, 19–31. https://doi.org/10.1016/J.OMTM.2018.10.006

Friedmann, T. (1992). A brief history of gene therapy. *Nature Genetics 1992 2:2*, *2*(2), 93–98. https://doi.org/10.1038/NG1092-93

Froehlich, J., Versapuech, M., Megrelis, L., Largeteau, Q., Meunier, S., Tanchot, C., Bismuth, G., Delon, J., & Mangeney, M. (2016). FAM65B controls the proliferation of transformed and primary T cells. *Oncotarget*, *7*(39), 63215. https://doi.org/10.18632/ONCOTARGET.11438

Funke, S., Maisner, A., Mühlebach, M. D., Koehl, U., Grez, M., Cattaneo, R., Cichutek, K., & Buchholz, C. J. (2008). Targeted cell entry of lentiviral vectors. *Molecular Therapy*, *16*(8), 1427–1436. https://doi.org/10.1038/MT.2008.128/ATTACHMENT/D83CDB0F-7E83-4373-AF6E-D7075CFD1B95/MMC5.DOC

Gao, C., Zhang, M., & Chen, L. (2020). The Comparison of Two Single-cell Sequencing Platforms: BD Rhapsody and 10x Genomics Chromium. *Current Genomics*, *21*(8). https://doi.org/10.2174/1389202921999200625220812

Garrido-Cardenas, J. A., Garcia-Maroto, F., Alvarez-Bermejo, J. A., & Manzano-Agugliaro, F. (2017). DNA Sequencing Sensors: An Overview. *Sensors 2017, Vol. 17, Page 588*, *17*(3), 588. https://doi.org/10.3390/S17030588

Gattinoni, L., Lugli, E., Ji, Y., Pos, Z., Paulos, C. M., Quigley, M. F., Almeida, J. R., Gostick, E., Yu, Z., Carpenito, C., Wang, E., Douek, D. C., Price, D. A., June, C. H., Marincola, F. M., Roederer, M., & Restifo, N. P. (2011). A human memory T cell subset with stem cell-like properties. *Nature Medicine*, *17*(10), 1290–1297. https://doi.org/10.1038/NM.2446

Gedeon, T., & Bokes, P. (2012). Delayed Protein Synthesis Reduces the Correlation between mRNA and Protein Fluctuations. *Biophysical Journal*, *103*(3), 377–385. https://doi.org/10.1016/J.BPJ.2012.06.025

Goldstone, D. C., Ennis-Adeniran, V., Hedden, J. J., Groom, H. C. T., Rice, G. I., Christodoulou, E., Walker, P. A., Kelly, G., Haire, L. F., Yap, M. W., De Carvalho, L. P. S., Stoye, J. P., Crow, Y. J., Taylor, I. A., & Webb, M. (2011). HIV-1 restriction factor SAMHD1 is a deoxynucleoside triphosphate triphosphohydrolase. *Nature*, *480*(7377), 379–382. https://doi.org/10.1038/NATURE10623

Golubovskaya, V., & Wu, L. (2016). Different Subsets of T Cells, Memory, Effector Functions, and CAR-T Immunotherapy. *Cancers*, *8*(3). https://doi.org/10.3390/CANCERS8030036

Gonzalez-Mancera, M. S., Bolaños, N. I., Salamanca, M., Orjuela, G. A., Rodriguez, A. N., & Gonzalez, J. M. (2020).

Percentages of CD4+CD8+ Double-positive T Lymphocytes in the Peripheral Blood of Adults from a Blood Bank in Bogotá, Colombia. *Turkish Journal of Haematology : Official Journal of Turkish Society of Haematology*, *37*(1), 36–41. https://doi.org/10.4274/TJH.GALENOS.2019.2019.0256

Gross, G., Gorochov, G., Waks, T., & Eshhar, Z. (1989). Generation of effector T cells expressing chimeric T cell receptor with antibody type-specificity. *Transplantation Proceedings*, *21*(1 Pt 1), 127–130. https://pubmed.ncbi.nlm.nih.gov/2784887/

Guba, M., Koehl, G. E., Neppl, E., Doenecke, A., Steinbauer, M., Schlitt, H. J., Jauch, K. W., & Geissler, E. K. (2005). Dosing of rapamycin is critical to achieve an optimal antiangiogenic effect against cancer. *Transplant International : Official Journal of the European Society for Organ Transplantation*, *18*(1), 89–94. https://doi.org/10.1111/J.1432-2277.2004.00026.X

Guntaka, R. V. (1993). Transcription termination and polyadenylation in retroviruses. *Microbiological Reviews*, *57*(3), 511. https://doi.org/10.1128/MR.57.3.511-521.1993

Guo, C., Liu, Q., Zong, D., Zhang, W., Zuo, Z., Yu, Q., Sha, Q., Zhu, L., Gao, X., Fang, J., Tao, J., Wu, Q., Li, X., & Qu, K. (2022). Single-cell transcriptome profiling and chromatin accessibility reveal an exhausted regulatory CD4+ T cell subset in systemic lupus erythematosus. *Cell Reports*, *41*(6), 111606. https://doi.org/10.1016/J.CELREP.2022.111606

Guo, X., Steinkühler, J., Marin, M., Li, X., Lu, W., Dimova, R., & Melikyan, G. B. (2021). Interferon-induced transmembrane protein 3 blocks fusion of diverse enveloped viruses by altering mechanical properties of cell membranes. *ACS Nano*, *15*(5), 8155–8170. https://doi.org/10.1021/ACSNANO.0C10567/SUPPL_FILE/NN0C10567_SI_002.AVI

Haddock, A. N., Labuzan, S. A., Haynes, A. E., Hayes, C. S., Kakareka, K. M., & Waddell, D. S. (2019). Dual-specificity phosphatase 4 is upregulated during skeletal muscle atrophy and modulates extracellular signal-regulated kinase activity. *American Journal of Physiology - Cell Physiology*, *316*(4), C567–C581. https://doi.org/10.1152/ajpcell.00234.2018

Hall, N. (2007). Advanced sequencing technologies and their wider impact in microbiology. *Journal of Experimental Biology*, *210*(9), 1518–1525. https://doi.org/10.1242/JEB.001370

Haller, O., & Kochs, G. (2011). Human MxA protein: an interferon-induced dynamin-like GTPase with broad antiviral activity. *Journal of Interferon & Cytokine Research : The Official Journal of the International Society for Interferon and Cytokine Research*, *31*(1), 79–87. https://doi.org/10.1089/JIR.2010.0076

Hao, Y., Hao, S., Andersen-Nissen, E., Mauck, W. M., Zheng, S., Butler, A., Lee, M. J., Wilk, A. J., Darby, C., Zager, M., Hoffman, P., Stoeckius, M., Papalexi, E., Mimitou, E. P., Jain, J., Srivastava, A., Stuart, T., Fleming, L. M., Yeung, B., … Satija, R. (2021). Integrated analysis of multimodal single-cell data. *Cell*, *184*(13), 3573-3587.e29. https://doi.org/10.1016/J.CELL.2021.04.048

Hartmann, J., Schüßler-Lenz, M., Bondanza, A., & Buchholz, C. J. (2017). Clinical development of CAR T cells—challenges and opportunities in translating innovative treatment concepts. *EMBO Molecular Medicine*, *9*(9), 1183. https://doi.org/10.15252/EMMM.201607485

Hatziioannou, T., Perez-Caballero, D., Yang, A., Cowan, S., & Bieniasz, P. D. (2004). Retrovirus resistance factors Ref1 and Lv1 are species-specific variants of TRIM5α. *Proceedings of the National Academy of Sciences of the United States of America*, *101*(29), 10774–10779. https://doi.org/10.1073/PNAS.0402361101/ASSET/D1251957-6420-4B38-9E44-A8F6E1FB0C30/ASSETS/GRAPHIC/ZPQ0290454300004.JPEG

Hayes, J. D., Dinkova-Kostova, A. T., & Tew, K. D. (2020). Oxidative Stress in Cancer. *Cancer Cell*, *38*(2), 167. https://doi.org/10.1016/J.CCELL.2020.06.001

Henson, S. M., & Akbar, A. N. (2009). KLRG1—more than a marker for T cell senescence. *AGE 2009 31:4*, *31*(4), 285–

291. https://doi.org/10.1007/S11357-009-9100-9

Hofmann, H., Logue, E. C., Bloch, N., Daddacha, W., Polsky, S. B., Schultz, M. L., Kim, B., & Landau, N. R. (2012). The Vpx Lentiviral Accessory Protein Targets SAMHD1 for Degradation in the Nucleus. *Journal of Virology*, *86*(23), 12552. https://doi.org/10.1128/JVI.01657-12

Holden, J. A. (1999). DNA Topoisomerase II-alpha as a marker of cell proliferation in endocrine and other neoplasms. *Endocrine Pathology 1999 10:2*, *10*(2), 97–102. https://doi.org/10.1007/BF02739821

Hornick, A. L., Li, N., Oakland, M., McCray, P. B., Jr., & Sinn, P. L. (2016). Human, Pig, and Mouse Interferon-Induced Transmembrane Proteins Partially Restrict Pseudotyped Lentiviral Vectors. *Human Gene Therapy*, *27*(5), 354. https://doi.org/10.1089/HUM.2015.156

Huang, I. C., Bailey, C. C., Weyer, J. L., Radoshitzky, S. R., Becker, M. M., Chiang, J. J., Brass, A. L., Ahmed, A. A., Chi, X., Dong, L., Longobardi, L. E., Boltz, D., Kuhn, J. H., Elledge, S. J., Bavari, S., Denison, M. R., Choe, H., & Farzan, M. (2011). Distinct Patterns of IFITM-Mediated Restriction of Filoviruses, SARS Coronavirus, and Influenza A Virus. *PLoS Pathogens*, *7*(1), 1001258. https://doi.org/10.1371/JOURNAL.PPAT.1001258

Jackson, R. S., Cho, Y. J., Stein, S., & Liang, P. (2007). CYFIP2, a direct p53 target, is leptomycin-B sensitive. *Cell Cycle (Georgetown, Tex.)*, *6*(1), 95–103. https://doi.org/10.4161/CC.6.1.3665

Jacobson, A., Yang, D., Vella, M., & Chiu, I. M. (2021). The intestinal neuro-immune axis: crosstalk between neurons, immune cells, and microbes. *Mucosal Immunology 2021 14:3*, *14*(3), 555–565. https://doi.org/10.1038/s41385-020-00368-1

Jamali, A., Kapitza, L., Schaser, T., Johnston, I. C. D., Buchholz, C. J., & Hartmann, J. (2019). *Highly Efficient and Selective CAR-Gene Transfer Using CD4- and CD8-Targeted Lentiviral Vectors*. *13*, 371–379. https://pubmed.ncbi.nlm.nih.gov/30997367/

Jardine, L., Barge, D., Ames-Draycott, A., Pagan, S., Cookson, S., Spickett, G., Haniffa, M., Collin, M., & Bigley, V. (2013). Rapid detection of dendritic cell and monocyte disorders using CD4 as a lineage marker of the human peripheral blood antigen-presenting cell compartment. *Frontiers in Immunology*, *4*(DEC). https://doi.org/10.3389/FIMMU.2013.00495

Jefferies, C. A. (2019). Regulating IRFs in IFN driven disease. *Frontiers in Immunology*, *10*(MAR), 325. https://doi.org/10.3389/FIMMU.2019.00325/BIBTEX

John, S. P., Chin, C. R., Perreira, J. M., Feeley, E. M., Aker, A. M., Savidis, G., Smith, S. E., Elia, A. E. H., Everitt, A. R., Vora, M., Pertel, T., Elledge, S. J., Kellam, P., & Brass, A. L. (2013). The CD225 domain of IFITM3 is required for both IFITM protein association and inhibition of influenza A virus and dengue virus replication. *Journal of Virology*, *87*(14), 7837–7852. https://doi.org/10.1128/JVI.00481-13

Johnson, N. M., Alvarado, A. F., Moffatt, T. N., Edavettal, J. M., Swaminathan, T. A., & Braun, S. E. (2021). HIV-based lentiviral vectors: origin and sequence differences. *Molecular Therapy - Methods and Clinical Development*, *21*, 451–465. https://doi.org/10.1016/J.OMTM.2021.03.018/ATTACHMENT/ED808908-2A31-45B5-B11F-35531C62CFF5/MMC1.PDF

Kadivar, M., Petersson, J., Svensson, L., & Marsal, J. (2016). CD8αβ+ γδ T Cells: A Novel T Cell Subset with a Potential Role in Inflammatory Bowel Disease. *Journal of Immunology (Baltimore, Md. : 1950)*, *197*(12), 4584–4592. https://doi.org/10.4049/JIMMUNOL.1601146

Kalpana, G. V., Marmon, S., Wang, W., Crabtree, G. R., & Goff, S. P. (1994). Binding and Stimulation of HIV-1 Integrase by a Human Homolog of Yeast Transcription Factor SNF5. *Science*, *266*(5193), 2002–2006. https://doi.org/10.1126/SCIENCE.7801128

Kanehisa, M., & Goto, S. (2000). KEGG: kyoto encyclopedia of genes and genomes. *Nucleic Acids Research*, *28*(1), 27–30. https://doi.org/10.1093/NAR/28.1.27

Kasukabe, T., Okabe-Kado, J., Kato, N., Sassa, T., & Honma, Y. (2005). Effects of combined treatment with rapamycin and cotylenin A, a novel differentiation-inducing agent, on human breast carcinoma MCF-7 cells and xenografts. *Breast Cancer Research*, *7*(6), R1097. https://doi.org/10.1186/BCR1344

Khodadadi, I., Abdi, M., Ahmadi, A., Wahedi, M. S., Menbari, S., Lahoorpour, F., & Rahbari, R. (2011). Analysis of serum adenosine deaminase (ADA) and ADA1 and ADA2 isoenzyme activities in HIV positive and HIV–HBV co-infected patients. *Clinical Biochemistry*, *44*(12), 980–983. https://doi.org/10.1016/J.CLINBIOCHEM.2011.05.020

Kim, H. J., Lee, K., & O'Rear, J. J. (1994). A short sequence upstream of the 5' major splice site is important for encapsidation of HIV-1 genomic RNA. *Virology*, *198*(1), 336–340. https://doi.org/10.1006/VIRO.1994.1037

Kim, K., Dauphin, A., Komurlu, S., McCauley, S. M., Yurkovetskiy, L., Carbone, C., Diehl, W. E., Strambio-De-Castillia, C., Campbell, E. M., & Luban, J. (2019). Cyclophilin A protects HIV-1 from restriction by human TRIM5α. *Nature Microbiology*, *4*(12), 2044–2051. https://doi.org/10.1038/S41564-019-0592-5

Lee, R. D., Munro, S. A., Knutson, T. P., LaRue, R. S., Heltemes-Harris, L. M., & Farrar, M. A. (2021). Single-cell analysis identifies dynamic gene expression networks that govern B cell development and transformation. *Nature Communications*, *12*(1). https://doi.org/10.1038/S41467-021-27232-5

Lepelley, A., Mina, E. Della, van Nieuwenhove, E., Waumans, L., Fraitag, S., Rice, G. I., Dhir, A., Frémond, M. L., Rodero, M. P., Seabra, L., Carter, E., Bodemer, C., Buhas, D., Callewaert, B., de Lonlay, P., de Somer, L., Dyment, D. A., Faes, F., Grove, L., … Crow, Y. J. (2021). Enhanced cGAS-STING–dependent interferon signaling associated with mutations in ATAD3A. *The Journal of Experimental Medicine*, *218*(10), 18. https://doi.org/10.1084/JEM.20201560

Lever, A., Gottlinger, H., Haseltine, W., & Sodroski, J. (1989). Identification of a sequence required for efficient packaging of human immunodeficiency virus type 1 RNA into virions. *Journal of Virology*, *63*(9), 4085. https://doi.org/10.1128/JVI.63.9.4085-4087.1989

Li, D., Gong, B., Xu, J., Ning, B., & Tong, W. (2021). Impact of Sequencing Depth and Library Preparation on Toxicological Interpretation of RNA-Seq Data in a "three-Sample" Scenario. *Chemical Research in Toxicology*, *34*(2), 529–540. https://doi.org/10.1021/ACS.CHEMRESTOX.0C00368/SUPPL_FILE/TX0C00368_SI_001.ZIP

Li, K., Markosyan, R. M., Zheng, Y. M., Golfetto, O., Bungart, B., Li, M., Ding, S., He, Y., Liang, C., Lee, J. C., Gratton, E., Cohen, F. S., & Liu, S. L. (2013). IFITM Proteins Restrict Viral Membrane Hemifusion. *PLoS Pathogens*, *9*(1), 1003124. /pmc/articles/PMC3554583/

Li, L., Torres-Coronado, M., Gu, A., Rao, A., Gardner, A. M., Epps, E. W., Gonzalez, N., Tran, C.-A., Wu, X., Wang, J.-H., Digiusto, D. L., & Onica Torres-Coronado, M. ´. (2014). Enhanced Genetic Modification of Adult Growth Factor Mobilized Peripheral Blood Hematopoietic Stem and Progenitor Cells With Rapamycin. *Stem Cells Translational Medicine*, *3*(10), 1199–1208. https://doi.org/10.5966/SCTM.2014-0010

Li, Y., Zhang, J., Wang, C., Qiao, W., Li, Y., & Tan, J. (2021). IFI44L expression is regulated by IRF-1 and HIV-1. *FEBS Open Bio*, *11*(1), 105–113. https://doi.org/10.1002/2211-5463.13030

Liao, Y., Wang, J., Jaehnig, E. J., Shi, Z., & Zhang, B. (2019). WebGestalt 2019: gene set analysis toolkit with revamped UIs and APIs. *Nucleic Acids Research*, *47*(W1), W199–W205. https://doi.org/10.1093/NAR/GKZ401

Lin, T. Y., Chin, C. R., Everitt, A. R., Clare, S., Perreira, J. M., Savidis, G., Aker, A. M., John, S. P., Sarlah, D., Carreira, E. M., Elledge, S. J., Kellam, P., & Brass, A. L. (2013). Amphotericin B increases influenza A virus infection by preventing IFITM3-mediated restriction. *Cell Reports*, *5*(4), 895–908. https://doi.org/10.1016/J.CELREP.2013.10.033

Liu, C., Perilla, J. R., Ning, J., Lu, M., Hou, G., Ramalho, R., Himes, B. A., Zhao, G., Bedwell, G. J., Byeon, I. J., Ahn, J., Gronenborn, A. M., Prevelige, P. E., Rousso, I., Aiken, C., Polenova, T., Schulten, K., & Zhang, P. (2016). Cyclophilin A stabilizes the HIV-1 capsid through a novel non-canonical binding site. *Nature Communications*

2016 7:1, *7*(1), 1–10. https://doi.org/10.1038/ncomms10714

Liu, H., Han, H., Li, J., & Wong, L. (2005). DNAFSMiner: a web-based software toolbox to recognize two types of functional sites in DNA sequences. *Bioinformatics*, *21*(5), 671–673. https://doi.org/10.1093/BIOINFORMATICS/BTH437

Lokugamage, M. P., Sago, C. D., & Dahlman, J. E. (2018). Testing thousands of nanoparticles in vivo using DNA barcodes. *Current Opinion in Biomedical Engineering*, *7*, 1–8. https://doi.org/10.1016/J.COBME.2018.08.001

Long, A. H., Haso, W. M., Shern, J. F., Wanhainen, K. M., Murgai, M., Ingaramo, M., Smith, J. P., Walker, A. J., Kohler, M. E., Venkateshwara, V. R., Kaplan, R. N., Patterson, G. H., Fry, T. J., Orentas, R. J., & Mackall, C. L. (2015). 4-1BB costimulation ameliorates T cell exhaustion induced by tonic signaling of chimeric antigen receptors. *Nature Medicine*, *21*(6), 581–590. https://doi.org/10.1038/nm.3838

Louis, C. U., Savoldo, B., Dotti, G., Pule, M., Yvon, E., Myers, G. D., Rossig, C., Russell, H. V., Diouf, O., Liu, E., Liu, H., Wu, M. F., Gee, A. P., Mei, Z., Rooney, C. M., Heslop, H. E., & Brenner, M. K. (2011). Antitumor activity and long-term fate of chimeric antigen receptor–positive T cells in patients with neuroblastoma. *Blood*, *118*(23), 6050. https://doi.org/10.1182/BLOOD-2011-05-354449

Lu, J., Pan, Q., Rong, L., Liu, S.-L., & Liang, C. (2011). The IFITM Proteins Inhibit HIV-1 Infection. *Journal of Virology*, *85*(5), 2126–2137. https://journals.asm.org/doi/10.1128/JVI.01531-10

Luban, J., & Goff, S. P. (1994). Mutational analysis of cis-acting packaging signals in human immunodeficiency virus type 1 RNA. *Journal of Virology*, *68*(6), 3784–3793. https://doi.org/10.1128/JVI.68.6.3784-3793.1994

Lun, A. T. L., Bach, K., & Marioni, J. C. (2016). Pooling across cells to normalize single-cell RNA sequencing data with many zero counts. *Genome Biology*, *17*(1), 1–14. https://doi.org/10.1186/S13059-016-0947-7/TABLES/2

Lun, A. T., McCarthy, D. J., Marioni, J. C., Ji, H., duVerle, D., Rausell, A., & Descartes, P. (2016). A step-by-step workflow for low-level analysis of single-cell RNA-seq data with Bioconductor. *F1000Research*, *5*, 2122. https://doi.org/10.12688/f1000research.9501.2

Lusso, P., Di Marzo Veronese, F., Ensoli, B., Franchini, G., Jemma, C., DeRocco, S. E., Kalyanaraman, V. S., & Gallo, R. C. (1990). Expanded HIV-1 cellular tropism by phenotypic mixing with murine endogenous retroviruses. *Science (New York, N.Y.)*, *247*(4944), 848–852. https://doi.org/10.1126/SCIENCE.2305256

Lv, H., Zhang, S., Wang, B., Cui, S., & Yan, J. (2006). Toxicity of cationic lipids and cationic polymers in gene delivery. *Journal of Controlled Release*, *114*(1), 100–109. https://doi.org/10.1016/J.JCONREL.2006.04.014

Ma, S., Li, X., Wang, X., Cheng, L., Li, Z., Zhang, C., Ye, Z., & Qian, Q. (2019). Current Progress in CAR-T Cell Therapy for Solid Tumors. *International Journal of Biological Sciences*, *15*(12), 2548. https://doi.org/10.7150/IJBS.34213

Maeder, M. L., Stefanidakis, M., Wilson, C. J., Baral, R., Barrera, L. A., Bounoutas, G. S., Bumcrot, D., Chao, H., Ciulla, D. M., DaSilva, J. A., Dass, A., Dhanapal, V., Fennell, T. J., Friedland, A. E., Giannoukos, G., Gloskowski, S. W., Glucksmann, A., Gotta, G. M., Jayaram, H., … Jiang, H. (2019). Development of a gene-editing approach to restore vision loss in Leber congenital amaurosis type 10. *Nature Medicine 2019 25:2*, *25*(2), 229–233. https://doi.org/10.1038/s41591-018-0327-9

Maher, J., Brentjens, R. J., Gunset, G., Rivière, I., & Sadelain, M. (2002). Human T-lymphocyte cytotoxicity and proliferation directed by a single chimeric TCRζ/CD28 receptor. *Nature Biotechnology*, *20*(1), 70–75. https://doi.org/10.1038/nbt0102-70

Mair, F., Erickson, J. R., Voillet, V., Simoni, Y., Bi, T., Tyznik, A. J., Martin, J., Gottardo, R., Newell, E. W., & Prlic, M. (2020). A Targeted Multi-omic Analysis Approach Measures Protein Expression and Low-Abundance Transcripts on the Single-Cell Level. *Cell Reports*, *31*(1), 107499. https://doi.org/10.1016/J.CELREP.2020.03.063

Manganaro, L., Hong, P., Hernandez, M. M., Argyle, D., Mulder, L. C. F., Potla, U., Diaz-Griffero, F., Lee, B., Fernandez-Sesma, A., & Simon, V. (2018). IL-15 regulates susceptibility of CD4+ T cells to HIV infection. *Proceedings of the*

National Academy of Sciences of the United States of America, *115*(41), E9659–E9667. https://doi.org/10.1073/PNAS.1806695115/-/DCSUPPLEMENTAL

Mann, R., Mulligan, R. C., & Baltimore, D. (1983). Construction of a retrovirus packaging mutant and its use to produce helper-free defective retrovirus. *Cell*, *33*(1), 153–159. https://doi.org/10.1016/0092-8674(83)90344-6

Mao, J., Luo, H., & Wu, J. (2008). Drak2 overexpression results in increased beta-cell apoptosis after free fatty acid stimulation. *Journal of Cellular Biochemistry*, *105*(4), 1073–1080. https://doi.org/10.1002/JCB.21910

Marcucci, K. T., Jadlowsky, J. K., Hwang, W. T., Suhoski-Davis, M., Gonzalez, V. E., Kulikovskaya, I., Gupta, M., Lacey, S. F., Plesa, G., Chew, A., Melenhorst, J. J., Levine, B. L., & June, C. H. (2018). Retroviral and Lentiviral Safety Analysis of Gene-Modified T Cell Products and Infused HIV and Oncology Patients. *Molecular Therapy*, *26*(1), 269. https://doi.org/10.1016/J.YMTHE.2017.10.012

Marofi, F., Motavalli, R., Safonov, V. A., Thangavelu, L., Yumashev, A. V., Alexander, M., Shomali, N., Chartrand, M. S., Pathak, Y., Jarahian, M., Izadi, S., Hassanzadeh, A., Shirafkan, N., Tahmasebi, S., & Khiavi, F. M. (2021). CAR T cells in solid tumors: challenges and opportunities. *Stem Cell Research & Therapy 2021 12:1*, *12*(1), 1–16. https://doi.org/10.1186/S13287-020-02128-1

Maude, S. L., Laetsch, T. W., Buechner, J., Rives, S., Boyer, M., Bittencourt, H., Bader, P., Verneris, M. R., Stefanski, H. E., Myers, G. D., Qayed, M., De Moerloose, B., Hiramatsu, H., Schlis, K., Davis, K. L., Martin, P. L., Nemecek, E. R., Yanik, G. A., Peters, C., … Grupp, S. A. (2018). Tisagenlecleucel in Children and Young Adults with B-Cell Lymphoblastic Leukemia. *New England Journal of Medicine*, *378*(5), 439–448. https://doi.org/10.1056/nejmoa1709866

Mehta, P. H., Fiorenza, S., Koldej, R. M., Jaworowski, A., Ritchie, D. S., & Quinn, K. M. (2021). T Cell Fitness and Autologous CAR T Cell Therapy in Haematologic Malignancy. *Frontiers in Immunology*, *12*, 4971. https://doi.org/10.3389/FIMMU.2021.780442/BIBTEX

Mehta, R. S., & Rezvani, K. (2018). Chimeric Antigen Receptor Expressing Natural Killer Cells for the Immunotherapy of Cancer. *Frontiers in Immunology*, *9*(FEB). https://doi.org/10.3389/FIMMU.2018.00283

Meixner, A., Karreth, F., Kenner, L., & Wagner, E. F. (2004). JunD regulates lymphocyte proliferation and T helper cell cytokine expression. *The EMBO Journal*, *23*(6), 1325. https://doi.org/10.1038/SJ.EMBOJ.7600133

Melenhorst, J. J., Chen, G. M., Wang, M., Porter, D. L., Chen, C., Collins, M. K. A., Gao, P., Bandyopadhyay, S., Sun, H., Zhao, Z., Lundh, S., Pruteanu-Malinici, I., Nobles, C. L., Maji, S., Frey, N. V., Gill, S. I., Tian, L., Kulikovskaya, I., Gupta, M., … June, C. H. (2022). Decade-long leukaemia remissions with persistence of CD4+ CAR T cells. *Nature 2022 602:7897*, *602*(7897), 503–509. https://doi.org/10.1038/s41586-021-04390-6

Meng, X., Zhang, F., Yan, B., Si, C., Honda, H., Nagamachi, A., Sun, L. Z., & Xiang, Y. (2018). A paralogous pair of mammalian host restriction factors form a critical host barrier against poxvirus infection. *PLOS Pathogens*, *14*(2), e1006884. https://doi.org/10.1371/JOURNAL.PPAT.1006884

Michels, A., Ho, N., & Buchholz, C. J. (2022). Precision medicine: In vivo CAR therapy as a showcase for receptor-targeted vector platforms. *Molecular Therapy*, *30*(7), 2401–2415. https://doi.org/10.1016/J.YMTHE.2022.05.018

Milani, M., Annoni, A., Moalli, F., Liu, T., Cesana, D., Calabria, A., Bartolaccini, S., Biffi, M., Russo, F., Visigalli, I., Raimondi, A., Patarroyo-White, S., Drager, D., Cristofori, P., Ayuso, E., Montini, E., Peters, R., Iannacone, M., Cantore, A., & Naldini, L. (2019). Phagocytosis-shielded lentiviral vectors improve liver gene therapy in nonhuman primates. *Science Translational Medicine*, *11*(493). https://doi.org/10.1126/SCITRANSLMED.AAV7325

Miller, D. G., Adam, M. A., & Miller, A. D. (1990). Gene transfer by retrovirus vectors occurs only in cells that are actively replicating at the time of infection. *Molecular and Cellular Biology*, *10*(8), 4239–4242. https://doi.org/10.1128/MCB.10.8.4239-4242.1990

Mittrücker, H. W., Visekruna, A., & Huber, M. (2014). Heterogeneity in the differentiation and function of CD8+ T cells.

Archivum Immunologiae et Therapiae Experimentalis, *62*(6), 449–458. https://doi.org/10.1007/S00005-014-0293-Y

Mock, U., Nickolay, L., Philip, B., Cheung, G. W. K., Zhan, H., Johnston, I. C. D., Kaiser, A. D., Peggs, K., Pule, M., Thrasher, A. J., & Qasim, W. (2016). Automated manufacturing of chimeric antigen receptor T cells for adoptive immunotherapy using CliniMACS Prodigy. *Cytotherapy*, *18*(8), 1002–1011. https://doi.org/10.1016/J.JCYT.2016.05.009

Morozova, O., Hirst, M., & Marra, M. A. (2009). Applications of New Sequencing Technologies for Transcriptome Analysis. *Https://Doi.Org/10.1146/Annurev-Genom-082908-145957*, *10*, 135–151. https://doi.org/10.1146/ANNUREV-GENOM-082908-145957

Mou, T., Deng, W., Gu, F., Pawitan, Y., & Vu, T. N. (2020). Reproducibility of Methods to Detect Differentially Expressed Genes from Single-Cell RNA Sequencing. *Frontiers in Genetics*, *10*, 1331. https://doi.org/10.3389/FGENE.2019.01331/BIBTEX

Mousset, C. M., Hobo, W., Woestenenk, R., Preijers, F., Dolstra, H., & van der Waart, A. B. (2019). Comprehensive Phenotyping of T Cells Using Flow Cytometry. *Cytometry Part A*, *95*(6), 647–654. https://doi.org/10.1002/CYTO.A.23724

Mu, W., Rezek, V., Martin, H., Carrillo, M. A., Tomer, S., Hamid, P., Lizarraga, M. A., Tibbe, T. D., Yang, O. O., Jamieson, B. D., Kitchen, S. G., & Zhen, A. (2022). Autophagy inducer rapamycin treatment reduces IFN-I–mediated Inflammation and improves anti–HIV-1 T cell response in vivo. *JCI Insight*, *7*(22). https://doi.org/10.1172/JCI.INSIGHT.159136

Mudhasani, R., Tran, J. P., Retterer, C., Radoshitzky, S. R., Kota, K. P., Altamura, L. A., Smith, J. M., Packard, B. Z., Kuhn, J. H., Costantino, J., Garrison, A. R., Schmaljohn, C. S., Huang, I.-C., Farzan, M., & Bavari, S. (2013). IFITM-2 and IFITM-3 but Not IFITM-1 Restrict Rift Valley Fever Virus. *Journal of Virology*, *87*(15), 8451. https://doi.org/10.1128/JVI.03382-12

Münch, R. C., Mühlebach, M. D., Schaser, T., Kneissl, S., Jost, C., Plückthun, A., Cichutek, K., & Buchholz, C. J. (2011). DARPins: An Efficient Targeting Domain for Lentiviral Vectors. *Molecular Therapy*, *19*(4), 686. https://doi.org/10.1038/MT.2010.298

Nair, A. B., & Jacob, S. (2016). A simple practice guide for dose conversion between animals and human. *Journal of Basic and Clinical Pharmacy*, *7*(2), 27. https://doi.org/10.4103/0976-0105.177703

Naldini, L., Blömer, U., Gallay, P., Ory, D., Mulligan, R., Gage, F. H., Verma, I. M., & Trono, D. (1996). In vivo gene delivery and stable transduction of nondividing cells by a lentiviral vector. *Science (New York, N.Y.)*, *272*(5259), 263–267. https://doi.org/10.1126/SCIENCE.272.5259.263

Nam, A. S., Kim, K. T., Chaligne, R., Izzo, F., Ang, C., Taylor, J., Myers, R. M., Abu-Zeinah, G., Brand, R., Omans, N. D., Alonso, A., Sheridan, C., Mariani, M., Dai, X., Harrington, E., Pastore, A., Cubillos-Ruiz, J. R., Tam, W., Hoffman, R., … Landau, D. A. (2019). Genotyping of Transcriptomes links somatic mutations and cell identity. *Nature*, *571*(7765), 355. https://doi.org/10.1038/S41586-019-1367-0

Namwanje, M., Bisunke, B., Rousselle, T. V., Lamanilao, G. G., Sunder, V. S., Patterson, E. C., Kuscu, C., Kuscu, C., Maluf, D., Kiran, M., Mas, V., Eason, J. D., & Bajwa, A. (2021). Rapamycin alternatively modifies mitochondrial dynamics in dendritic cells to reduce kidney ischemic reperfusion injury. *International Journal of Molecular Sciences*, *22*(10). https://doi.org/10.3390/IJMS22105386/S1

Narayana, S. K., Helbig, K. J., McCartney, E. M., Eyre, N. S., Bull, R. A., Eltahla, A., Lloyd, A. R., & Beard, M. R. (2015). The Interferon-induced Transmembrane Proteins, IFITM1, IFITM2, and IFITM3 Inhibit Hepatitis C Virus Entry. *Journal of Biological Chemistry*, *290*(43), 25946–25959. https://doi.org/10.1074/JBC.M115.657346

Navaratnarajah, C. K., Leonard, V. H. J., & Cattaneo, R. (2009). Measles virus glycoprotein complex assembly, receptor

attachment, and cell entry. *Current Topics in Microbiology and Immunology*, *329*, 59–76. https://doi.org/10.1007/978-3-540-70523-9_4

Nishiyama, A., Matsui, M., Iwata, S., Hirota, K., Masutani, H., Nakamura, H., Takagi, Y., Sono, H., Gon, Y., & Yodoi, J. (1999). Identification of thioredoxin-binding protein-2/vitamin D(3) up-regulated protein 1 as a negative regulator of thioredoxin function and expression. *The Journal of Biological Chemistry*, *274*(31), 21645–21650. https://doi.org/10.1074/JBC.274.31.21645

Oelsner, S., Friede, M. E., Zhang, C., Wagner, J., Badura, S., Bader, P., Ullrich, E., Ottmann, O. G., Klingemann, H., Tonn, T., & Wels, W. S. (2017). Continuously expanding CAR NK-92 cells display selective cytotoxicity against B-cell leukemia and lymphoma. *Cytotherapy*, *19*(2), 235–249. https://doi.org/10.1016/j.jcyt.2016.10.009

Ozog, S., Timberlake, N. D., Hermann, K., Garijo, O., Haworth, K. G., Shi, G., Glinkerman, C. M., Schefter, L. E., D'Souza, S., Simpson, E., Sghia-Hughes, G., Carillo, R. R., Boger, D. L., Kiem, H.-P., Slukvin, I., Ryu, B. Y., Sorrentino, B. P., Adair, J. E., Snyder, S. A., … Torbett, B. E. (2019). Resveratrol trimer enhances gene delivery to hematopoietic stem cells by reducing antiviral restriction at endosomes. *Blood*, *134*(16), 1298–1311. https://doi.org/10.1182/BLOOD.2019000040

Panda, D., Gjinaj, E., Bachu, M., Squire, E., Novatt, H., Ozato, K., & Rabin, R. L. (2019). IRF1 maintains optimal constitutive expression of antiviral genes and regulates the early antiviral response. *Frontiers in Immunology*, *10*(MAY), 1019. https://doi.org/10.3389/FIMMU.2019.01019/BIBTEX

Park, G.-H., Kim, K.-Y., Cho, S. W., Cheong, J. Y., Yu, G. I., Shin, D. H., & Kwack, K. B. (2013). Association between Interferon-Inducible Protein 6 (IFI6) Polymorphisms and Hepatitis B Virus Clearance. *Genomics & Informatics*, *11*(1), 15. https://doi.org/10.5808/GI.2013.11.1.15

Park, P. J. (2009). ChIP–seq: advantages and challenges of a maturing technology. *Nature Reviews Genetics 2009 10:10*, *10*(10), 669–680. https://doi.org/10.1038/nrg2641

Peng, G., Ke, J. L., Jin, W., Greenwell-Wild, T., & Wahl, S. M. (2006). Induction of APOBEC3 family proteins, a defensive maneuver underlying interferon-induced anti-HIV-1 activity. *Journal of Experimental Medicine*, *203*(1), 41–46. https://doi.org/10.1084/jem.20051512

Pereira, L. A., Bentley, K., Peeters, A., Churchill, M. J., & Deacon, N. J. (2000). A compilation of cellular transcription factor interactions with the HIV-1 LTR promoter. *Nucleic Acids Research*, *28*(3), 663–668. https://doi.org/10.1093/NAR/28.3.663

Perneger, T. V. (1998). What's wrong with Bonferroni adjustments. *BMJ : British Medical Journal*, *316*(7139), 1236. https://doi.org/10.1136/BMJ.316.7139.1236

Petersen, B. S., Fredrich, B., Hoeppner, M. P., Ellinghaus, D., & Franke, A. (2017). Opportunities and challenges of whole-genome and -exome sequencing. *BMC Genetics 2017 18:1*, *18*(1), 1–13. https://doi.org/10.1186/S12863-017-0479-5

Petrillo, C., Cesana, D., Piras, F., Bartolaccini, S., Naldini, L., Montini, E., & Kajaste-Rudnitski, A. (2015). Cyclosporin a and rapamycin relieve distinct lentiviral restriction blocks in hematopoietic stem and progenitor cells. *Molecular Therapy : The Journal of the American Society of Gene Therapy*, *23*(2), 352–362. https://doi.org/10.1038/MT.2014.193

Pezoldt, J., Wiechers, C., Erhard, F., Rand, U., Bulat, T., Beckstette, M., Brendolan, A., Huehn, J., Kalinke, U., Mueller, M., Strobl, B., Deplancke, B., Čičin-Šain, L., & Sitnik, K. M. (2021). Single-cell transcriptional profiling of splenic fibroblasts reveals subset-specific innate immune signatures in homeostasis and during viral infection. *Communications Biology*, *4*(1). https://doi.org/10.1038/S42003-021-02882-9

Pfaender, S., Mar, K. B., Michailidis, E., Kratzel, A., Boys, I. N., V'kovski, P., Fan, W., Kelly, J. N., Hirt, D., Ebert, N., Stalder, H., Kleine-Weber, H., Hoffmann, M., Hoffmann, H. H., Saeed, M., Dijkman, R., Steinmann, E., Wight-

Carter, M., McDougal, M. B., … Thiel, V. (2020). LY6E impairs coronavirus fusion and confers immune control of viral disease. *Nature Microbiology 2020 5:11*, *5*(11), 1330–1339. https://doi.org/10.1038/s41564-020-0769-y

Pfeiffer, A., Thalheimer, F. B., Hartmann, S., Frank, A. M., Bender, R. R., Danisch, S., Costa, C., Wels, W. S., Modlich, U., Stripecke, R., Verhoeyen, E., & Buchholz, C. J. (2018). In vivo generation of human CD 19- CAR T cells results in B-cell depletion and signs of cytokine release syndrome . *EMBO Molecular Medicine*, *10*(11), e9158. https://doi.org/10.15252/emmm.201809158

Poirot, L., Philip, B., Schiffer-Mannioui, C., Le Clerre, D., Chion-Sotinel, I., Derniame, S., Potrel, P., Bas, C., Lemaire, L., Galetto, R., Lebuhotel, C., Eyquem, J., Cheung, G. W.-K., Duclert, A., Gouble, A., Arnould, S., Peggs, K., Pule, M., Scharenberg, A. M., & Smith, J. (2015). Multiplex Genome-Edited T-cell Manufacturing Platform for "Off-the-Shelf" Adoptive T-cell Immunotherapies. *Cancer Research*, *75*(18), 3853–3864. https://doi.org/10.1158/0008-5472.CAN-14-3321

Pokhilko, A., Handel, A. E., Curion, F., Volpato, V., Whiteley, E. S., Bøstrand, S., Newey, S. E., Akerman, C. J., Webber, C., Clark, M. B., Bowden, R., & Zameel Cader, M. (2021). Targeted single-cell RNA sequencing of transcription factors enhances the identification of cell types and trajectories. *Genome Research*, *31*(6), 1069–1081. https://doi.org/10.1101/GR.273961.120/-/DC1

Prakadan, S. M., Shalek, A. K., & Weitz, D. A. (2017). Scaling by shrinking: empowering single-cell 'omics' with microfluidic devices. *Nature Reviews. Genetics*, *18*(6), 345. https://doi.org/10.1038/NRG.2017.15

Prelli Bozzo, C., Nchioua, R., Volcic, M., Koepke, L., Krüger, J., Schütz, D., Heller, S., Stürzel, C. M., Kmiec, D., Conzelmann, C., Müller, J., Zech, F., Braun, E., Groß, R., Wettstein, L., Weil, T., Weiß, J., Diofano, F., Rodríguez Alfonso, A. A., … Kirchhoff, F. (2021). IFITM proteins promote SARS-CoV-2 infection and are targets for virus inhibition in vitro. *Nature Communications 2021 12:1*, *12*(1), 1–13. https://doi.org/10.1038/s41467-021-24817-y

Rajabzadeh, A., Hamidieh, A. A., & Rahbarizadeh, F. (2021). Spinoculation and retronectin highly enhance the gene transduction efficiency of Mucin-1-specific chimeric antigen receptor (CAR) in human primary T cells. *BMC Molecular and Cell Biology*, *22*(1), 1–9. https://doi.org/10.1186/S12860-021-00397-Z/FIGURES/4

Raphael, I., Nalawade, S., Eagar, T. N., & Forsthuber, T. G. (2015). T cell subsets and their signature cytokines in autoimmune and inflammatory diseases. *Cytokine*, *74*(1), 5. https://doi.org/10.1016/J.CYTO.2014.09.011

Ravikumar, B., Vacher, C., Berger, Z., Davies, J. E., Luo, S., Oroz, L. G., Scaravilli, F., Easton, D. F., Duden, R., & O'kane, C. J. (2006). Rapamycin pre-treatment protects against apoptosis. *Human Molecular Genetics*, *15*(7), 1209–1216. https://doi.org/10.1093/HMG/DDL036

Ricciardi, S., Manfrini, N., Alfieri, R., Calamita, P., Crosti, M. C., Gallo, S., Müller, R., Pagani, M., Abrignani, S., & Biffo, S. (2018). The translational machinery of human CD4+ T cells is poised for activation and controls the switch from quiescence to metabolic remodelling. *Cell Metabolism*, *28*(6), 895. https://doi.org/10.1016/J.CMET.2018.08.009

Richardson, J. H., Kaye, J. F., Child, L. A., & Lever, A. M. L. (1995). Helper virus-free transfer of human immunodeficiency virus type 1 vectors. *Journal of General Virology*, *76*(3), 691–696. https://doi.org/10.1099/0022-1317-76-3-691/CITE/REFWORKS

Riedel, H., Kondor-Koch, C., & Garoff, H. (1984). Cell surface expression of fusogenic vesicular stomatitis virus G protein from cloned cDNA. *The EMBO Journal*, *3*(7), 1477. https://doi.org/10.1002/J.1460-2075.1984.TB01999.X

Robinson, J. T., Thorvaldsdóttir, H., Winckler, W., Guttman, M., Lander, E. S., Getz, G., & Mesirov, J. P. (2011). Integrative genomics viewer. *Nature Biotechnology*, *29*(1), 24–26. https://doi.org/10.1038/NBT.1754

Rodriguez-Marquez, P., Calleja-Cervantes, M. E., Serrano, G., Oliver-Caldes, A., Palacios-Berraquero, M. L., Martin-Mallo, A., Calviño, C., Español-Rego, M., Ceballos, C., Lozano, T., Martin-Uriz, P. S., Vilas-Zornoza, A., Rodriguez-Diaz, S., Martinez-Turrillas, R., Jauregui, P., Alignani, D., Viguria, M. C., Redondo, M., Pascal, M., … Prosper, F. (2022). CAR density influences antitumoral efficacy of BCMA CAR T cells and correlates with clinical

outcome. *Science Advances*, *8*(39), 514. https://doi.org/10.1126/SCIADV.ABO0514/SUPPL_FILE/SCIADV.ABO0514_TABLES_S1_TO_S8.ZIP

Safarzadeh Kozani, P., Safarzadeh Kozani, P., Ahmadi Najafabadi, M., Yousefi, F., Mirarefin, S. M. J., & Rahbarizadeh, F. (2022). Recent Advances in Solid Tumor CAR-T Cell Therapy: Driving Tumor Cells From Hero to Zero? *Frontiers in Immunology*, *13*. https://doi.org/10.3389/FIMMU.2022.795164

Sahu, B., Pihlajamaa, P., Zhang, K., Palin, K., Ahonen, S., Cervera, A., Ristimäki, A., Aaltonen, L. A., Hautaniemi, S., & Taipale, J. (2021). Human cell transformation by combined lineage conversion and oncogene expression. *Oncogene 2021 40:36*, *40*(36), 5533–5547. https://doi.org/10.1038/s41388-021-01940-0

Sajid, M., Ullah, H., Yan, K., He, M., Feng, J., Shereen, M. A., Hao, R., Li, Q., Guo, D., Chen, Y., & Zhou, L. (2021). The Functional and Antiviral Activity of Interferon Alpha-Inducible IFI6 Against Hepatitis B Virus Replication and Gene Expression. *Frontiers in Immunology*, *12*. https://doi.org/10.3389/FIMMU.2021.634937

Sanger, F., Air, G. M., Barrell, B. G., Brown, N. L., Coulson, A. R., Fiddes, J. C., Hutchison, C. A., Slocombe, P. M., & Smith, M. (1977). Nucleotide sequence of bacteriophage φX174 DNA. *Nature 1977 265:5596*, *265*(5596), 687–695. https://doi.org/10.1038/265687a0

Schaller, T., Ocwieja, K. E., Rasaiyaah, J., Price, A. J., Brady, T. L., Roth, S. L., Hué, S., Fletcher, A. J., Lee, K. E., KewalRamani, V. N., Noursadeghi, M., Jenner, R. G., James, L. C., Bushman, F. D., & Towers, G. J. (2011). HIV-1 Capsid-Cyclophilin Interactions Determine Nuclear Import Pathway, Integration Targeting and Replication Efficiency. *PLoS Pathogens*, *7*(12), 1002439. https://doi.org/10.1371/JOURNAL.PPAT.1002439

Schietinger, A., & Greenberg, P. D. (2014). Tolerance and exhaustion: defining mechanisms of T cell dysfunction. *Trends in Immunology*, *35*(2), 51–60. https://doi.org/10.1016/J.IT.2013.10.001

Schluns, K. S., Kieper, W. C., Jameson, S. C., & Lefrançois, L. (2000). *Interleukin-7 mediates the homeostasis of naïve and memory CD8 T cells in vivo. 1*(5), 426–432. https://doi.org/10.1038/80868

Schmitz, F., Heit, A., Dreher, S., Eisenächer, K., Mages, J., Haas, T., Krug, A., Janssen, K. P., Kirschning, C. J., & Wagner, H. (2008). Mammalian target of rapamycin (mTOR) orchestrates the defense program of innate immune cells. *European Journal of Immunology*, *38*(11), 2981–2992. https://doi.org/10.1002/EJI.200838761

Schoggins, J. W. (2014). Interferon-stimulated genes: roles in viral pathogenesis. *Current Opinion in Virology*, *6*(1), 40. https://doi.org/10.1016/J.COVIRO.2014.03.006

Schuster, S. J., Svoboda, J., Chong, E. A., Nasta, S. D., Mato, A. R., Anak, Ö., Brogdon, J. L., Pruteanu-Malinici, I., Bhoj, V., Landsburg, D., Wasik, M., Levine, B. L., Lacey, S. F., Melenhorst, J. J., Porter, D. L., & June, C. H. (2017). Chimeric Antigen Receptor T Cells in Refractory B-Cell Lymphomas. *New England Journal of Medicine*, *377*(26), 2545–2554. https://doi.org/10.1056/nejmoa1708566

Scialdone, A., Natarajan, K. N., Saraiva, L. R., Proserpio, V., Teichmann, S. A., Stegle, O., Marioni, J. C., & Buettner, F. (2015). Computational assignment of cell-cycle stage from single-cell transcriptome data. *Methods (San Diego, Calif.)*, *85*, 54–61. https://doi.org/10.1016/J.YMETH.2015.06.021

Sheih, A., Voillet, V., Hanafi, L. A., DeBerg, H. A., Yajima, M., Hawkins, R., Gersuk, V., Riddell, S. R., Maloney, D. G., Wohlfahrt, M. E., Pande, D., Enstrom, M. R., Kiem, H. P., Adair, J. E., Gottardo, R., Linsley, P. S., & Turtle, C. J. (2020). Clonal kinetics and single-cell transcriptional profiling of CAR-T cells in patients undergoing CD19 CAR-T immunotherapy. *Nature Communications*, *11*(1), 1–13. https://doi.org/10.1038/s41467-019-13880-1

Shi, G., Chiramel, A. I., Li, T., Lai, K. K., Kenney, A. D., Zani, A., Eddy, A. C., Majdoul, S., Zhang, L., Dempsey, T., Beare, P. A., Kar, S., Yewdell, J. W., Best, S. M., Yount, J. S., & Compton, A. A. (2022). Rapalogs downmodulate intrinsic immunity and promote cell entry of SARS-CoV-2. *The Journal of Clinical Investigation*. https://doi.org/10.1172/JCI160766

Shi, G., Kenney, A. D., Kudryashova, E., Zani, A., Zhang, L., Lai, K. K., Hall-Stoodley, L., Robinson, R. T., Kudryashov,

---

D. S., Compton, A. A., & Yount, J. S. (2021). Opposing activities of IFITM proteins in SARS-CoV-2 infection. *The EMBO Journal*, *40*(3). https://doi.org/10.15252/EMBJ.2020106501

Shi, G., Ozog, S., Torbett, B. E., & Compton, A. A. (2018). MTOR inhibitors lower an intrinsic barrier to virus infection mediated by IFITM3. *Proceedings of the National Academy of Sciences of the United States of America*, *115*(43), E10069–E10078. https://doi.org/10.1073/PNAS.1811892115/SUPPL_FILE/PNAS.1811892115.SAPP.PDF

Shi, X., Zhang, L., Li, Y., Xue, J., Liang, F., Ni, H. W., Wang, X., Cai, Z., Shen, L. H., Huang, T., & He, B. (2021). Integrative Analysis of Bulk and Single-Cell RNA Sequencing Data Reveals Cell Types Involved in Heart Failure. *Frontiers in Bioengineering and Biotechnology*, *9*. https://doi.org/10.3389/FBIOE.2021.779225

Shimabukuro-Vornhagen, A., Gödel, P., Subklewe, M., Stemmler, H. J., Schlößer, H. A., Schlaak, M., Kochanek, M., Böll, B., & von Bergwelt-Baildon, M. S. (2018). Cytokine release syndrome. *Journal for Immunotherapy of Cancer*, *6*(1). https://doi.org/10.1186/S40425-018-0343-9

Sholder, G., Lanz, T. A., Moccia, R., Quan, J., Aparicio-Prat, E., Stanton, R., & Xi, H. S. (2020). 3'Pool-seq: An optimized cost-efficient and scalable method of whole-transcriptome gene expression profiling. *BMC Genomics*, *21*(1), 1–11. https://doi.org/10.1186/S12864-020-6478-3/TABLES/2

Shum, E. Y., Walczak, E. M., Chang, C., & Christina Fan, H. (2019). Quantitation of mRNA Transcripts and Proteins Using the BD Rhapsody™ Single-Cell Analysis System. *Advances in Experimental Medicine and Biology*, *1129*, 63–79. https://doi.org/10.1007/978-981-13-6037-4_5

Smith, L. M., Sanders, J. Z., Kaiser, R. J., Hughes, P., Dodd, C., Connell, C. R., Heiner, C., Kent, S. B. H., & Hood, L. E. (1986). Fluorescence detection in automated DNA sequence analysis. *Nature*, *321*(6071), 674–679. https://doi.org/10.1038/321674A0

Smith, S. E., Busse, D. C., Binter, S., Weston, S., Soria, C. D., Laksono, B. M., Clare, S., Nieuwkoop, S. Van, Hoogen, B. G. Van den, Clement, M., Marsden, M., Humphreys, I. R., Marsh, M., Swart, R. L. de, Wash, R. S., Tregoning, J. S., & Kellam, P. (2019). Interferon-Induced Transmembrane Protein 1 Restricts Replication of Viruses That Enter Cells via the Plasma Membrane. *Journal of Virology*, *93*(6). https://doi.org/10.1128/JVI.02003-18

Soneson, C., & Robinson, M. D. (2018). Bias, robustness and scalability in single-cell differential expression analysis. *Nature Methods 2018 15:4*, *15*(4), 255–261. https://doi.org/10.1038/nmeth.4612

Song, Y., Zhang, H., Wang, Y., Guo, J., Tang, S., Wang, L., Peng, K., & Dong, C. sheng. (2022). Importin KPNA2 confers HIV-1 pre-integration complex nuclear import by interacting with the capsid protein. *Antiviral Research*, *200*. https://doi.org/10.1016/J.ANTIVIRAL.2022.105289

Stoycheva, D., Deiser, K., Stärck, L., Nishanth, G., Schlüter, D., Uckert, W., & Schüler, T. (2015). IFN-γ Regulates CD8 + Memory T Cell Differentiation and Survival in Response to Weak, but Not Strong, TCR Signals . *The Journal of Immunology*, *194*(2), 553–559. https://doi.org/10.4049/JIMMUNOL.1402058

Stuart, T., Butler, A., Hoffman, P., Hafemeister, C., Papalexi, E., Mauck, W. M., Hao, Y., Stoeckius, M., Smibert, P., & Satija, R. (2019). Comprehensive Integration of Single-Cell Data. *Cell*, *177*(7), 1888-1902.e21. https://doi.org/10.1016/j.cell.2019.05.031

Sun, X., Yau, V. K., Briggs, B. J., & Whittaker, G. R. (2005). Role of clathrin-mediated endocytosis during vesicular stomatitis virus entry into host cells. *Virology*, *338*(1), 53–60. https://doi.org/10.1016/J.VIROL.2005.05.006

Sweeney, N. P., & Vink, C. A. (2021). The impact of lentiviral vector genome size and producer cell genomic to gag-pol mRNA ratios on packaging efficiency and titre. *Molecular Therapy - Methods and Clinical Development*, *21*, 574–584. https://doi.org/10.1016/j.omtm.2021.04.007

Tada, T., Norton, T. D., Leibowitz, R., & Landau, N. R. (2022). Directly injected lentiviral vector-based T cell vaccine protects mice against acute and chronic viral infection. *JCI Insight*, *7*(18). https://doi.org/10.1172/JCI.INSIGHT.161598

Tetsuka, T., Uranishi, H., Imai, H., Ono, T., Sonta, S. I., Takahashi, N., Asamitsu, K., & Okamoto, T. (2000). Inhibition of nuclear factor-kappaB-mediated transcription by association with the amino-terminal enhancer of split, a Groucho-related protein lacking WD40 repeats. *The Journal of Biological Chemistry*, *275*(6), 4383–4390. https://doi.org/10.1074/JBC.275.6.4383

Themis, M., Forbes, S. J., Chan, L., Cooper, R. G., Etheridge, C. J., Miller, A. D., Hodgson, H. J. F., & Coutelle, C. (1998). Enhanced in vitro and in vivo gene delivery using cationic agent complexed retrovirus vectors. *Gene Therapy 1998 5:9*, *5*(9), 1180–1186. https://doi.org/10.1038/SJ.GT.3300715

Towers, G. J., Hatziioannou, T., Cowan, S., Goff, S. P., Luban, J., & Bieniasz, P. D. (2003). Cyclophilin A modulates the sensitivity of HIV-1 to host restriction factors. *Nature Medicine 2003 9:9*, *9*(9), 1138–1143. https://doi.org/10.1038/NM910

Tsapras, P., & Nezis, I. P. (2017). Caspase involvement in autophagy. *Cell Death and Differentiation*, *24*(8), 1369. https://doi.org/10.1038/CDD.2017.43

Tsoucas, D., & Yuan, G. C. (2017). Recent Progress in Single-Cell Cancer Genomics. *Current Opinion in Genetics & Development*, *42*, 22. https://doi.org/10.1016/J.GDE.2017.01.002

Turrini, F., Marelli, S., Kajaste-Rudnitski, A., Lusic, M., Lint, C., Das, A. T., Harwig, A., Berkhout, B., & Vicenzi, E. (2015). HIV-1 transcriptional silencing caused by TRIM22 inhibition of Sp1 binding to the viral promoter. *Retrovirology*, *12*(1), 1–8. https://doi.org/10.1186/S12977-015-0230-0/FIGURES/4

Turtle, C. J., Hanafi, L. A., Berger, C., Gooley, T. A., Cherian, S., Hudecek, M., Sommermeyer, D., Melville, K., Pender, B., Budiarto, T. M., Robinson, E., Steevens, N. N., Chaney, C., Soma, L., Chen, X., Yeung, C., Wood, B., Li, D., Cao, J., … Maloney, D. G. (2016). CD19 CAR–T cells of defined CD4+:CD8+ composition in adult B cell ALL patients. *The Journal of Clinical Investigation*, *126*(6), 2123. https://doi.org/10.1172/JCI85309

Tvedt, T. H. A., Vo, A. K., Bruserud, Ø., & Reikvam, H. (2021). Cytokine Release Syndrome in the Immunotherapy of Hematological Malignancies: The Biology behind and Possible Clinical Consequences. *Journal of Clinical Medicine*, *10*(21). https://doi.org/10.3390/JCM10215190

Uche, U. U., Piccirillo, A. R., Kataoka, S., Grebinoski, S. J., D'Cruz, L. M., & Kane, L. P. (2018). PIK3IP1/TrIP restricts activation of T cells through inhibition of PI3K/Akt. *Journal of Experimental Medicine*, *215*(12), 3165–3179. https://doi.org/10.1084/jem.20172018

Valsamakis, A., Zeichner, S., Carswell, S., & Alwine, J. C. (1991). The human immunodeficiency virus type 1 polyadenylylation signal: a 3' long terminal repeat element upstream of the AAUAAA necessary for efficient polyadenylylation. *Proceedings of the National Academy of Sciences of the United States of America*, *88*(6), 2108–2112. https://doi.org/10.1073/PNAS.88.6.2108

van Spriel, A. B., Puls, K. L., Sofi, M., Pouniotis, D., Hochrein, H., Orinska, Z., Knobeloch, K.-P., Plebanski, M., & Wright, M. D. (2004). A Regulatory Role for CD37 in T Cell Proliferation. *The Journal of Immunology*, *172*(5), 2953–2961. https://doi.org/10.4049/jimmunol.172.5.2953

Verhelst, J., Parthoens, E., Schepens, B., Fiers, W., & Saelens, X. (2012). Interferon-Inducible Protein Mx1 Inhibits Influenza Virus by Interfering with Functional Viral Ribonucleoprotein Complex Assembly. *Journal of Virology*, *86*(24), 13445–13455. https://doi.org/10.1128/JVI.01682-12/ASSET/FEE6F6B3-A09A-4ABA-AA17-8F4D628B937D/ASSETS/GRAPHIC/ZJV9990969470008.JPEG

Wang, C., Liu, X., Li, Z., Chai, Y., Jiang, Y., Wang, Q., Ji, Y., Zhu, Z., Wan, Y., Yuan, Z., Chang, Z., & Zhang, M. (2015). CD8+NKT-like cells regulate the immune response by killing antigen-bearing DCs. *Scientific Reports 2015 5:1*, *5*(1), 1–13. https://doi.org/10.1038/srep14124

Wang, C. X., Sather, B. D., Wang, X., Adair, J., Khan, I., Singh, S., Lang, S., Adams, A., Curinga, G., Kiem, H. P., Miao, C. H., Rawlings, D. J., & Torbett, B. E. (2014). Rapamycin relieves lentiviral vector transduction resistance in

human and mouse hematopoietic stem cells. *Blood*, *124*(6). https://doi.org/10.1182/BLOOD-2013-12-546218

Wang, D., Aguilar, B., Starr, R., Alizadeh, D., Brito, A., Sarkissian, A., Ostberg, J. R., Forman, S. J., & Brown, C. E. (2018). Glioblastoma-targeted CD4+ CAR T cells mediate superior antitumor activity. *JCI Insight*, *3*(10). https://doi.org/10.1172/JCI.INSIGHT.99048

Wang, S., & El-Deiry, W. S. (2003). TRAIL and apoptosis induction by TNF-family death receptors. *Oncogene 2003 22:53*, *22*(53), 8628–8633. https://doi.org/10.1038/sj.onc.1207232

Wang, X., Peticone, C., Kotsopoulou, E., Göttgens, B., & Calero-Nieto, F. J. (2021). Single-cell transcriptome analysis of CAR T-cell products reveals subpopulations, stimulation, and exhaustion signatures. *OncoImmunology*, *10*(1). https://doi.org/10.1080/2162402X.2020.1866287

Wee, Y. S., Roundy, K. M., Weis, J. J., & Weis, J. H. (2012). Interferon-inducible transmembrane proteins of the innate immune response act as membrane organizers by influencing clathrin and v-ATPase localization and function. *Innate Immunity*, *18*(6), 834–845. https://doi.org/10.1177/1753425912443392

Weidner, J. M., Jiang, D., Pan, X.-B., Chang, J., Block, T. M., & Guo, J.-T. (2010). Interferon-Induced Cell Membrane Proteins, IFITM3 and Tetherin, Inhibit Vesicular Stomatitis Virus Infection via Distinct Mechanisms. *Journal of Virology*, *84*(24). https://doi.org/10.1128/JVI.01328-10

Weston, S., Czieso, S., White, I. J., Smith, S. E., Kellam, P., & Marsh, M. (2014). A Membrane Topology Model for Human Interferon Inducible Transmembrane Protein 1. *PLOS ONE*, *9*(8), e104341. https://doi.org/10.1371/JOURNAL.PONE.0104341

Wherry, E. J. (2011). T cell exhaustion. *Nature Immunology*, *12*(6), 492–499. https://doi.org/10.1038/NI.2035

Wilkening, S., Pelechano, V., Järvelin, A. I., Tekkedil, M. M., Anders, S., Benes, V., & Steinmetz, L. M. (2013). An efficient method for genome-wide polyadenylation site mapping and RNA quantification. *Nucleic Acids Research*, *41*(5), e65–e65. https://doi.org/10.1093/NAR/GKS1249

Wilkins, C., Woodward, J., Lau, D. T. Y., Barnes, A., Joyce, M., McFarlane, N., McKeating, J. A., Tyrrell, D. L., & Gale, M. (2013). IFITM1 is a tight junction protein that inhibits hepatitis C virus entry. *Hepatology*, *57*(2), 461–469. https://doi.org/10.1002/HEP.26066

Wu, N., Nguyen, X. N., Wang, L., Appourchaux, R., Zhang, C., Panthu, B., Gruffat, H., Journo, C., Alais, S., Qin, J., Zhang, N., Tartour, K., Catez, F., Mahieux, R., Ohlmann, T., Liu, M., Du, B., & Cimarelli, A. (2019). The interferon stimulated gene 20 protein (ISG20) is an innate defense antiviral factor that discriminates self versus non-self translation. *PLoS Pathogens*, *15*(10). https://doi.org/10.1371/JOURNAL.PPAT.1008093

Xhangolli, I., Dura, B., Lee, G. H., Kim, D., Xiao, Y., & Fan, R. (2019). Single-cell Analysis of CAR-T Cell Activation Reveals A Mixed TH1/TH2 Response Independent of Differentiation. *Genomics, Proteomics & Bioinformatics*, *17*(2), 129. https://doi.org/10.1016/J.GPB.2019.03.002

Xin, T., Cheng, L., Zhou, C., Zhao, Y., Hu, Z., & Wu, X. (2022). In-Vivo Induced CAR-T Cell for the Potential Breakthrough to Overcome the Barriers of Current CAR-T Cell Therapy. *Frontiers in Oncology*, *12*, 42. https://doi.org/10.3389/FONC.2022.809754/BIBTEX

Xing, J., Zhang, A., Du, Y., Fang, M., Minze, L. J., Liu, Y. J., Li, X. C., & Zhang, Z. (2021). Identification of poly(ADP-ribose) polymerase 9 (PARP9) as a noncanonical sensor for RNA virus in dendritic cells. *Nature Communications 2021 12:1*, *12*(1), 1–17. https://doi.org/10.1038/s41467-021-23003-4

Xu, Y., Zhang, M., Ramos, C. A., Durett, A., Liu, E., Dakhova, O., Liu, H., Creighton, C. J., Gee, A. P., Heslop, H. E., Rooney, C. M., Savoldo, B., & Dotti, G. (2014). Closely related T-memory stem cells correlate with in vivo expansion of CAR.CD19-T cells and are preserved by IL-7 and IL-15. *Blood*, *123*(24), 3750. https://doi.org/10.1182/BLOOD-2014-01-552174

Yatscoff, R., LeGatt, D., Keenan, R., & Chackowsky, P. (1993). Blood distribution of rapamycin. *Transplantation*, *56*(5),

1202–1206. https://doi.org/10.1097/00007890-199311000-00029

You, Y., Tian, L., Su, S., Dong, X., Jabbari, J. S., Hickey, P. F., & Ritchie, M. E. (2021). Benchmarking UMI-based single-cell RNA-seq preprocessing workflows. *Genome Biology*, *22*(1), 1–32. https://doi.org/10.1186/S13059-021-02552-3/FIGURES/7

Yount, J. S., Karssemeijer, R. A., & Hang, H. C. (2012). S-palmitoylation and ubiquitination differentially regulate interferon-induced transmembrane protein 3 (IFITM3)-mediated resistance to influenza virus. *The Journal of Biological Chemistry*, *287*(23), 19631–19641. https://doi.org/10.1074/JBC.M112.362095

Yount, J. S., Moltedo, B., Yang, Y. Y., Charron, G., Moran, T. M., López, C. B., & Hang, H. C. (2010). Palmitoylome profiling reveals S-palmitoylation-dependent antiviral activity of IFITM3. *Nature Chemical Biology*, *6*(8), 610–614. https://doi.org/10.1038/NCHEMBIO.405

Zhang, H., Ye, Z. L., Yuan, Z. G., Luo, Z. Q., Jin, H. J., & Qian, Q. J. (2016). New Strategies for the Treatment of Solid Tumors with CAR-T Cells. *International Journal of Biological Sciences*, *12*(6), 718. https://doi.org/10.7150/IJBS.14405

Zhang, T., Cao, L., Xie, J., Shi, N., Zhang, Z., Luo, Z., Yue, D., Zhang, Z., Wang, L., Han, W., Xu, Z., Chen, H., & Zhang, Y. (2015). Efficiency of CD19 chimeric antigen receptor-modified T cells for treatment of B cell malignancies in phase I clinical trials: a meta-analysis. *Oncotarget*, *6*(32), 33961. https://doi.org/10.18632/ONCOTARGET.5582

Zhao, J., Hyman, L., & Moore, C. (1999). Formation of mRNA 3' ends in eukaryotes: mechanism, regulation, and interrelationships with other steps in mRNA synthesis. *Microbiology and Molecular Biology Reviews : MMBR*, *63*(2), 405–445. https://doi.org/10.1128/MMBR.63.2.405-445.1999

Zhao, X., Li, J., Winkler, C. A., An, P., & Guo, J. T. (2019). IFITM genes, variants, and their roles in the control and pathogenesis of viral infections. In *Frontiers in Microbiology* (Vol. 10, Issue JAN, p. 3228). Frontiers Media S.A. https://doi.org/10.3389/fmicb.2018.03228

Zheng, G. X. Y., Terry, J. M., Belgrader, P., Ryvkin, P., Bent, Z. W., Wilson, R., Ziraldo, S. B., Wheeler, T. D., McDermott, G. P., Zhu, J., Gregory, M. T., Shuga, J., Montesclaros, L., Underwood, J. G., Masquelier, D. A., Nishimura, S. Y., Schnall-Levin, M., Wyatt, P. W., Hindson, C. M., … Bielas, J. H. (2017). Massively parallel digital transcriptional profiling of single cells. *Nature Communications 2017 8:1*, *8*(1), 1–12. https://doi.org/10.1038/ncomms14049

Zhivotovsky, B., Samali, A., Gahm, A., & Orrenius, S. (1999). Caspases: their intracellular localization and translocation during apoptosis. *Cell Death and Differentiation*, *6*(7), 644–651. https://doi.org/10.1038/SJ.CDD.4400536

Zhou, Q., Uhlig, K. M., Muth, A., Kimpel, J., Lévy, C., Münch, R. C., Seifried, J., Pfeiffer, A., Trkola, A., Coulibaly, C., von Laer, D., Wels, W. S., Hartwig, U. F., Verhoeyen, E., & Buchholz, C. J. (2015). Exclusive Transduction of Human CD4+ T Cells upon Systemic Delivery of CD4-Targeted Lentiviral Vectors. *Journal of Immunology (Baltimore, Md. : 1950)*, *195*(5), 2493–2501. https://doi.org/10.4049/JIMMUNOL.1500956

Ziegler, H., Welker, C., Sterk, M., Haarer, J., Rammensee, H. G., Handgretinger, R., & Schilbach, K. (2014). Human Peripheral CD4(+) Vδ1(+) γδT Cells Can Develop into αβT Cells. *Frontiers in Immunology*, *5*(DEC). https://doi.org/10.3389/FIMMU.2014.00645

Zimmerman, J. J., & Kahan, B. D. (1997). Pharmacokinetics of Sirolimus in Stable Renal Transplant Patients after Multiple Oral Dose Administration. *The Journal of Clinical Pharmacology*, *37*(5), 405–415. https://doi.org/10.1002/J.1552-4604.1997.TB04318.X

Zufferey, R., Donello, J. E., Trono, D., & Hope, T. J. (1999). Woodchuck Hepatitis Virus Posttranscriptional Regulatory Element Enhances Expression of Transgenes Delivered by Retroviral Vectors. *Journal of Virology*, *73*(4), 2886–2892. https://doi.org/10.1128/jvi.73.4.2886-2892.1999

6 APPENDIX

6.1 SESSION INFO OF R ENVIRONMENT

The up-to-date versions of packages used in this thesis are presented below as generated by the function sessionInfo.

```
R version 4.2.1 Patched (2022-08-05 r82694 ucrt)
Platform: x86_64-w64-mingw32/x64 (64-bit)
Running under: Windows 10 x64 (build 22000)

Matrix products: default

locale:
[1]        LC_COLLATE=English_United        States.utf8        LC_CTYPE=English_United        States.utf8
LC_MONETARY=English_United States.utf8
[4] LC_NUMERIC=C            LC_TIME=English_United States.utf8

attached base packages:
[1] stats4  stats   graphics grDevices utils   datasets methods  base

other attached packages:
 [1] extrafont_0.18     EnsDb.Hsapiens.v86_2.99.0 ensembldb_2.20.1     AnnotationFilter_1.20.0
 [5] GenomicFeatures_1.48.1  WebGestaltR_0.4.4     org.Hs.eg.db_3.15.0     AnnotationDbi_1.58.0
 [9] ChIPpeakAnno_3.30.0    randomcoloR_1.1.0.1    Azimuth_0.4.5       shinyBS_0.61.1
[13] EnhancedVolcano_1.14.0  multimode_1.5       ggVennDiagram_1.2.0    rstatix_0.7.0
[17] RColorBrewer_1.1-3    forcats_0.5.1      stringr_1.4.0       purrr_0.3.4
[21] readr_2.1.2       tibble_3.1.7       tidyverse_1.3.1     DESeq2_1.36.0
[25] MAST_1.22.0       dittoSeq_1.8.0      escape_1.6.0       scran_1.24.0
[29] scater_1.24.0      scuttle_1.6.2      scRNAseq_2.10.0     SingleCellExperiment_1.18.0
[33] SummarizedExperiment_1.26.1 GenomicRanges_1.48.0  GenomeInfoDb_1.32.2    IRanges_2.30.0
[37] S4Vectors_0.34.0    MatrixGenerics_1.8.0  matrixStats_0.62.0   ggrepel_0.9.1
[41] ggpubr_0.4.0      umap_0.2.8.0      openxlsx_4.2.5      xlsx_0.6.5
[45] rJava_1.0-6       sctransform_0.3.3    pbmcref.SeuratData_1.0.0 pbmc3k.SeuratData_3.1.4
[49] SeuratData_0.2.2    sp_1.4-7        SeuratObject_4.1.0    Seurat_4.1.1
[53] dplyr_1.0.9       metap_1.8        multtest_2.52.0     Biobase_2.56.0
[57] BiocGenerics_0.42.0  tidyr_1.2.0       Nebulosa_1.6.0      patchwork_1.1.1
[61] ggplot2_3.3.6

loaded via a namespace (and not attached):
 [1] pbapply_1.5-0       lattice_0.20-45     GSVA_1.44.0         haven_2.5.0
 [5] vctrs_0.4.1        V8_4.2.0        mgcv_1.8-40        blob_1.2.3
 [9] survival_3.3-1      RBGL_1.72.0        spatstat.data_2.2-0    later_1.3.0
[13] DBI_1.1.2        rappdirs_0.3.3     uwot_0.1.11        dqrng_0.3.0
[17] SeuratDisk_0.0.0.9020  zlibbioc_1.42.0     rgeos_0.5-9        htmlwidgets_1.5.4
[21] mvtnorm_1.1-3      future_1.25.0      hdf5r_1.3.5        leiden_0.4.2
[25] parallel_4.2.1      irlba_2.3.5       Rcpp_1.0.8.3       KernSmooth_2.23-20
[29] DT_0.23         promises_1.2.0.1    DelayedArray_0.22.0    limma_3.52.1
[33] graph_1.74.0       apcluster_1.4.9     RSpectra_0.16-1      fs_1.5.2
[37] presto_1.0.0       mnormt_2.0.2      digest_0.6.29       png_0.1-7
[41] bluster_1.6.0      cowplot_1.1.1      pkgconfig_2.0.3      spatstat.random_2.2-0
[45] DelayedMatrixStats_1.18.0 ggbeeswarm_0.6.0    iterators_1.0.14     reticulate_1.25
[49] beeswarm_0.4.0     xfun_0.31        zoo_1.8-10        tidyselect_1.1.2
[53] reshape2_1.4.4     ica_1.0-2        viridisLite_0.4.0    rtracklayer_1.56.0
[57] rlang_1.0.2       RVenn_1.1.0       glue_1.6.2        modelr_0.1.8
[61] lambda.r_1.2.4     ggsignif_0.6.3     labeling_0.4.2      mutoss_0.1-12
[65] httpuv_1.6.5      Rttf2pt1_1.3.10     BiocNeighbors_1.14.0   TH.data_1.1-1
[69] annotate_1.74.0     jsonlite_1.8.0     XVector_0.36.0      tmvnsim_1.0-2
[73] systemfonts_1.0.4    bit_4.0.4        mime_0.12        gridExtra_2.3
```

[77] Rsamtools_2.12.0   stringi_1.7.6   spatstat.sparse_2.1-1   scattermore_0.8
[81] rbibutils_2.2.8   bitops_1.0-7   cli_3.3.0   Rdpack_2.3
[85] rhdf5filters_1.8.0   RSQLite_2.2.14   pheatmap_1.0.12   data.table_1.14.2
[89] rstudioapi_0.13   GenomicAlignments_1.32.0 nlme_3.1-158   locfit_1.5-9.5
[93] ks_1.13.5   listenv_0.8.0   miniUI_0.1.1.1   dbplyr_2.1.1
[97] readxl_1.4.0   lifecycle_1.0.1   ExperimentHub_2.4.0   munsell_0.5.0
[101] cellranger_1.1.0   codetools_0.2-18   InteractionSet_1.24.0   vipor_0.4.5
[105] lmtest_0.9-40   msigdbr_7.5.1   xlsxjars_0.6.1   xtable_1.8-4
[109] ROCR_1.0-11   diptest_0.76-0   googlesheets4_1.0.0   formatR_1.12
[113] BiocManager_1.30.18   abind_1.4-5   farver_2.1.0   parallelly_1.31.1
[117] AnnotationHub_3.4.0   RANN_2.6.1   askpass_1.1   BiocIO_1.6.0
[121] RcppAnnoy_0.0.19   goftest_1.2-3   futile.options_1.0.1   cluster_2.1.3
[125] extrafontdb_1.0   future.apply_1.9.0   Matrix_1.4-1   ellipsis_0.3.2
[129] prettyunits_1.1.1   lubridate_1.8.0   ggridges_0.5.3   googledrive_2.0.0
[133] shinydashboard_0.7.2   reprex_2.0.1   mclust_5.4.10   VennDiagram_1.7.3
[137] igraph_1.3.1   shinyjs_2.1.0   TFisher_0.2.0   gargle_1.2.0
[141] spatstat.utils_2.3-1   htmltools_0.5.2   BiocFileCache_2.4.0   yaml_2.3.5
[145] utf8_1.2.2   plotly_4.10.0   interactiveDisplayBase_1.34.0 XML_3.99-0.9
[149] withr_2.5.0   fitdistrplus_1.1-8   BiocParallel_1.30.2   bit64_4.0.5
[153] rngtools_1.5.2   doRNG_1.8.2   foreach_1.5.2   rootSolve_1.8.2.3
[157] multcomp_1.4-19   ProtGenerics_1.28.0   Biostrings_2.64.0   spatstat.core_2.4-4
[161] progressr_0.10.0   rsvd_1.0.5   ScaledMatrix_1.4.0   memoise_2.0.1
[165] evaluate_0.15   geneplotter_1.74.0   tzdb_0.3.0   curl_4.3.2
[169] qqconf_1.2.3   fansi_1.0.3   GSEABase_1.58.0   tensor_1.5
[173] edgeR_3.38.1   regioneR_1.28.0   cachem_1.0.6   deldir_1.0-6
[177] babelgene_22.3   metapod_1.4.0   rjson_0.2.21   tools_4.2.1
[181] sandwich_3.0-1   magrittr_2.0.3   RCurl_1.98-1.6   car_3.0-13
[185] xml2_1.3.3   httr_1.4.3   assertthat_0.2.1   rmarkdown_2.14
[189] globals_0.15.0   R6_2.5.1   Rhdf5lib_1.18.2   progress_1.2.2
[193] genefilter_1.78.0   KEGGREST_1.36.0   statmod_1.4.36   beachmat_2.12.0
[197] BiocVersion_3.15.2   HDF5Array_1.24.0   BiocSingular_1.12.0   rhdf5_2.40.0
[201] splines_4.2.1   carData_3.0-5   colorspace_2.0-3   generics_0.1.2
[205] pracma_2.3.8   pillar_1.7.0   sn_2.0.2   GenomeInfoDbData_1.2.8
[209] plyr_1.8.7   gtable_0.3.0   futile.logger_1.4.3   rvest_1.0.2
[213] zip_2.2.0   restfulr_0.0.13   knitr_1.39   biomaRt_2.52.0
[217] fastmap_1.1.0   doParallel_1.0.17   broom_0.8.0   UCell_2.0.0
[221] openssl_2.0.2   BSgenome_1.64.0   scales_1.2.0   filelock_1.0.2
[225] backports_1.4.1   plotrix_3.8-2   hms_1.1.1   Rtsne_0.16
[229] shiny_1.7.1   polyclip_1.10-0   grid_4.2.1   numDeriv_2016.8-1.1
[233] mathjaxr_1.6-0   lazyeval_0.2.2   whisker_0.4   crayon_1.5.1
[237] MASS_7.3-58.1   sparseMatrixStats_1.8.0 svglite_2.1.0   viridis_0.6.2
[241] rpart_4.1.16   compiler_4.2.1   spatstat.geom_2.4-0

7 ABBREVIATIONS

® ....original
6-FAM 6-carboxyfluorescein
ACE2.. angiotensin converting enzyme-2
ACTB...actin beta
ADA2... Adenosine Deaminase 2
AES .... amino enhancer of split
AIDS...acquired immunodeficiency syndrome
ALB ....albumin
ALL...acute lymphoblastic leukemia
AML...acute myeloid leukemia
ANOVA ....analysis of variance
anti ....antibody
AP .... adaptor primer
APC ....antigen presenting cell
APC ....allophycocyanin
APO ....apolipoprotein
APOBEC3 ....apolipoprotein B messenger ribonucleic acid editing enzyme catalytic subunit 3
APS ....ammonium persulfate
ATAC-seq... transposase-accessible chromatin sequencing
AUAP .... abridged universal amplification primer
BD ....Becton Dickinson
BGHpA... bovine growth hormone polyadenylation signal
BLAST...basic local alignment search tool
bp .... base pair
BSA .... bovine serum albumin
BTG1.. B cell translocation gene 1
BTLA .... B- and T-lymphocyte attenuator
BTN3A2..butyrophilin subfamily 3 member A2
BV ....brilliant violet
CAR .... chimeric antigen receptor
CASP ....caspase
CCA ....canonical correlation analysis
CD.. cluster of differentiation
cDNA .... complementary deoxyribonucleic acid
CHCHD2 ....coiled-coil-helix-coiled-coil-helix domain containing 2
ChIP-seq ....chromatin immunoprecipitation sequencing
CL .... cell label
CMV ....human cytomegalovirus
cPPT/CTS ....central polypurine tract/central termination sequence
CRISPR.. clustered regularly interspaced short palindromic repeats
CRS ....cytokine release syndrome
CsA ....cyclosporin A
CSF2.. colony stimulating factor 2
CTLA-4 .... cytotoxic T-lymphocyte–associated antigen 4
CTSD .... cathepsin D
Cy5..cyanine 5
CYFIP2..cytoplasmic fragile X messenger ribonucleoprotein 1 interacting protein 2
CypA .... cyclophilin A
Da, kDa ....Dalton, kilodalton
DARPin .... designed ankyrin repeat protein
DE ....differentially expressed
DENV ....dengue virus
dH2O..distilled water
DMEM ....Dulbecco's Modified Eagle Medium
DMSO ....dimethyl sulfoxide
DNA .... deoxyribonucleic acid
dNTP..deoxynucleotide triphosphate
dsDNA ....double-stranded deoxyribonucleic acid
DTT ....dithiothreitol
DUSP4 ....dual specificity phosphatase 4
E. coli .... *Escherichia coli*
E:T .... effector to target ratio
eBFP ....enhanced blue fluorescent protein
EBOV .... Ebola virus

EDTA..Ethylenediaminetetraacetic acid
EIF2AK2..eukaryotic translation initiation factor 2 alpha kinase 2
ENTPD1 .... ectonucleoside triphosphate diphosphohydrolase 1
F..fusion protein
FACS..fluorescence-activated cell sorting
FBS ....Fetal bovine serum
FC .... fold-change
FCGR3A .... Fc gamma receptor IIIa
FcR .... Fc receptor
FDR.. false discovery rate
FITC .... Fluorescein isothiocyanate
FoxP3..forkhead-box-protein P3
G ....glycoprotein
GAPDH ....glyceraldehyde 3-phosphate dehydrogenase
GBP .... guanylate binding protein
GFP.. Green fluorescent protein
GmbH...Gesellschaft mit beschränkter Haftung
GM-CSF ....granulocyte-macrophage colony-stimulating factor
GNLY ....granulysin
GO .... Gene Ontology
GO-BP...Gene Ontology - Biological Process
gRNA... genomic ribonucleic acid
GSEA .... gene set enrichment analysis
GSP .... gene specific primer
GSR .... glutathione-disulfide reductase
GST.. glutathione S-transferase
GvHD .... graft-versus-host disease
GZM .... granzyme
H ....hemagglutinin
HAVCR2..hepatitis A virus cellular receptor 2
HCV ....hepatitis C virus
HEK293...human embryonic kidney 293 cells
HeLa .... Henrietta Lacks cells
HEPES ....N-2-hydroxyethylpiperazine-N'-2-ethanesulfonic acid
HIV .... human immunodeficiency virus
HLA ....human leukocyte antigen
HRP .... horseradish peroxidase
HSPC .... human hematopoietic stem and progenitor cell
i.p. ....intraperitoneal
i.v. ....intravenous
IAV .... influenza type A virus
ICANS ....immune effector cell-associated neurotoxicity syndrome
ICOS .... inducible T cell costimulator
ID ....identity
IFI...interferon induced
IFIT.. interferon induced protein with tetratricopeptide repeats
IFITM...interferon-induced transmembrane protein
IFN ....Interferon
IgG .... immunoglobulin gamma
IL...interleukin
IL12RB2 ....interleukin 12 receptor subunit beta 2
IL2RA ....interleukin 2 receptor subunit alpha
Inc. .... incorporated
INI1 ....integrase interactor 1
IRF ....interferon related factors
ISG...interferon-stimulated gene
ITGAX .... integrin subunit alpha X
IU .... international units
JUND...JUN D proto-oncogene
KEGG.. Kyoto encyclopedia of genes and genomes
kg, g, mg, µg ....kilogram, gram, milligram, microgram
KLRF1...killer cell lectin like receptor F1
KPNA2 ....karyopherin subunit alpha 2
KU .... Kunitz unit
L, mL, µL, nL ....liter, milliliter, microliter, nanoliter
LAG3 .... lymphocyte activating 3
LASV...Lassa virus

LAT2..linker for activation of T cells, transmembrane adaptor 2
LB..Luria-Bertani
LC-MS.. liquid chromatography-mass spectrometry
LDLR...low-density lipoprotein receptor
LIF...leukemia inhibitory factor
LIPA ....lysosomal enzyme lipase A
LTR ....long terminal repeat
luc ....luciferase
LV... lentiviral vector
LY6E ....lymphocyte antigen 6 family member E
m, cm, μm ....meter, centimeter, micrometer
mA...milliampere
MACS .... magnetic-activated cell sorting
MARV.. Marburg virus
MFI...mean fluorescence intensity
MHC...major histocompatibility complex
MLV.. murine leukemia virus
mM, μM, nM ....millimolar, micromolar, nanomolar
MOI .... multiplicity of infection
mRNA..messenger ribonucleic acid
mTOR .... mammalian target of rapamycin
mTORC1 ....mammalian target of rapamycin complex 1
MV.. measles virus
MX...myxoma resistance protein
NEB... New England Biolabs
NGS .... next-generation sequencing
NIBRT .... National Institute for Bioprocessing Research and Training
NiV .... Nipah virus
NK..natural killer
NKT... natural killer T cell
NOD .... non-obese diabetic
NPC .... nuclear pore complex
NSG ....non-obese diabetic severe combined immunodeficiency gamma
NTA ....nanoparticle tracking analysis
NUP ....nucleoporin
OAS .... 2'-5'-oligoadenylate synthetase 1
pA, poly-A... polyadenylation
PAMP...pathogen-associated molecular pattern
PARP ....poly (adenosine diphosphate ribose) polymerase
PBMC... Peripheral Blood Mononuclear Cell
PBS..phosphate-buffered saline
PCA.. principal component analysis
PCR ....polymerase chain reaction
PD-1 ....programmed cell death protein 1
PE ....phycoerythrin
PEG300.. polyethylene glycol 300
PEI .... Paul-Ehrlich-Institut
PerCP ....peridinin chlorophyll protein
PIC...pre-integration complex
PIK3IP1 ....phosphoinositide-3-kinase interacting protein 1
PPIA... peptidylprolyl Isomerase A
PRDX ....peroxiredoxin
PRF1 ....perforin
QC... quality control
qPCR...quantitative polymerase chain reaction
RACE ....rapid amplification of complementary deoxyribonucleic acid ends
Rapa...rapamycin
RIPA .... radioimmunoprecipitation assay
RIPOR2...Ras homologous protein family interacting cell polarization regulator 2
RISC..ribonucleic acid-induced silencing complex
RNA ....ribonucleic acid
RPMI .... Roswell Park Memorial Institute
RSEC ....recursive substitution error correction
RVFV..Rift Valley fever virus
S.O.C. ....super optimal broth with catabolite repression
SAMD9L... sterile alpha motif domain containing 9 like

SAMHD1 ....
.................sterile alpha-motif and histidine-aspartate domain containing deoxynucleoside triphosphate triphosphohydrolase 1
SARS-CoV .... severe acute respiratory syndrome coronavirus
scFv ....single-chain variable fragment
SCID..severe combined immunodeficiency
scRNA-seq ....single-cell RNA sequencing
SDS ....sodium dodecyl sulfate
SDS-PAGE... sodium dodecyl sulfate-polyacrylamide gel electrophoresis
SELL ....selectin L
seq ....sequencing
SFFV..spleen focus-forming virus
shRNA... short hairpin ribonucleic acid
SIN ....self-inactivating
SIV .... simian immunodeficiency virus
SOD .... superoxide dismutase
ssRNA .... single-stranded ribonucleic acid
STAT...signal transducer and activator of transcription
STK17B.. serine/threonine kinase 17b
SV40pA..the simian virus 4 polyadenylation signal
TAE ....Tris-acete-EDTA
TBS ....Tris-buffered saline
TBS-T...Tris-buffered saline with Tween 20
Tc .... T cytotoxic
TCF7 ....transcription factor 7
TCM ....T cell medium
TCR...T cell receptor
TEMED.. N,N,N',N'-tetramethylenediamine
TGA.. targeted gene analysis
TGF ....transforming growth factor
TH .... T helper
TIM3 .... T cell immunoglobulin mucin 3
TMBIM6 ....transmembrane BCL2 associated X inhibitor motif containing 6
TMD ....transmembrane domain
TNF ....tumor necrosis factor
TNFSF10.. tumor necrosis factor superfamily member 10
TOP2...topoisomerase II
TRAC ....T cell receptor alpha constant
TRAIL .... tumor necrosis factor related apoptosis-inducing ligand
TRDC .... T cell receptor delta constant
TRIM .... tripartite motif containing
t-SNE...t-stochastic neighbor embedding
TU ....transduction unit
TXNIP...thioredoxin interacting protein
™ .... trademark
UMAP... uniform manifold approximation and projection
UMI ....unique molecular index
v ....version
V...volts
VCN ....vector copy number
VSV ....vesicular stomatitis virus
w/o ....without
WNV.. West Nile virus
WPRE ....woodchuck hepatitis virus posttranscriptional regulatory element
WTA ....whole transcriptome analysis

8 LIST OF FIGURES AND TABLES

8.1 FIGURES

8.2   TABLES

9 CURRICULUM VITAE

Personal information

Name: Filippos Theofilos Charitidis
Date of birth: 15.07.1992
Place of birth: Kavala, Greece

Education

Since June 2019   PhD studies in Genetic Immunotherapy at the Technical University of Darmstadt, in Germany.

                         PhD thesis was conducted in the research group of Prof. Dr. Christian Buchholz, in Paul-Ehrlich-Institut, in Germany.

                         Title: Deploying single-cell transcriptomics for assessing CAR T cell generation: alleviating antiviral restriction factors enhances gene transfer.

Sep 2016 – Nov 2018   Master of Science in Immunology and Inflammation at the University of Copenhagen, in Denmark.

                         Master thesis was carried out under supervision of Dr. Janne Koch in LEO Pharma A/S.

                         Title: Development of an air pouch mouse model of induced psoriasis-like inflammation.

Sep 2010 – Aug 2016   Bachelor of Science in Biology at the Aristotle University of Thessaloniki, in Greece.

                         Bachelor thesis was conducted under co-supervision of Prof. Dr. Maria Touraki and Dr. Angeliki Xagorari, in "George Papanikolaou" General Hospital of Thessaloniki.

                         Title: Study on the effect of cryopreservation of umbilical cord blood transplants on the cellular antioxidant profile – possible part of CD34+ microparticles.

Sep 2007 – Aug 2010   High school diploma (Apolytirion) obtained from the 1st General High School of Veria, Greece.

Research experience

Sep 2015 – May 2016   Erasmus+ internship in the group of Prof. Dr. Marita Cohn at the Lund University, in Sweden.

Mar 2014 – May 2014   Trainee student under supervision of Dr. Georgios Geromichalos in "Theagenio" Anticancer Hospital, in Greece.

10 LIST OF PUBLICATIONS AND DISSEMINATION

Part of this thesis has been published.

10.1 ORIGINAL RESEARCH ARTICLES

Charitidis, F. T., Adabi, E., Thalheimer, F. B., Clarke, C., & Buchholz, C. J. (2021). Monitoring CAR T cell generation with a CD8-targeted lentiviral vector by single-cell transcriptomics. Molecular Therapy - Methods & Clinical Development, 23, 359–369. https://doi.org/10.1016/j.omtm.2021.09.019. Erratum: Monitoring CAR T cell generation with a CD8-targeted lentiviral vector by single-cell transcriptomics. Molecular Therapy. Methods & Clinical Development, 24, 207–209. https://doi.org/10.1016/J.OMTM.2022.01.010

10.2 ORAL PRESENTATIONS

25th American Society of Gene and Cell Therapy 2022, Washington D.C., USA
Enhanced CAR T Cell Generation by CD8-LV Through Alleviating Antiviral Mechanisms with mTOR Inhibitors
Filippos T. Charitidis, Naphang Ho, Angela Braun, Frederic B. Thalheimer, Christian J. Buchholz

TU Darmstadt BioScience Symposium 2022, Darmstadt
Enhanced CAR T Cell Generation by CD8-LV Through Alleviating Antiviral Mechanisms with mTOR Inhibitors
Filippos T. Charitidis, Naphang Ho, Elham Adabi, Angela Braun, Frederic B. Thalheimer, Christian J. Buchholz

10.3 CONFERENCE POSTER PRESENTATIONS

3rd International Conference on Lymphocyte Engineering 2022, Munich, Germany
Monitoring early transcriptional profiles of CAR T cell products generated with conventional or CD8-targeted lentiviral vectors
Filippos T. Charitidis, Elham Adabi, Frederic B. Thalheimer, Csaba Miskey, Liam Childs, Colin Clarke, Christian J. Buchholz

24th American Society of Gene and Cell Therapy 2021, USA (virtual)

Analyzing the Effectiveness of CD8-Receptor Targeted Transduction for CAR T Cell Therapy Using Single Cell Transcriptomics

Filippos T. Charitidis, Elham Adabi, Frederic B. Thalheimer, Csaba Miskey, Colin Clarke, Christian J. Buchholz

2nd Rhein-Main Cancer Retreat 2021, Frankfurt, Germany (virtual)

Characterization of CAR T cells by single-cell expression profiling

Filippos T. Charitidis, Elham Adabi, Laura Kapitza, Frederic Thalheimer, Christian J. Buchholz

29th European Society of Gene and Cell Therapy 2022, Dublin, UK

Tracking CAR gene delivery with conventional and T cell-targeted lentiviral vectors by single-cell multiomics

E Adabi, **FT Charitidis**, FB Thalheimer, A Braun, C Clarke, CJ Buchholz

11 AWARDS

- 3rd place in Junior Scientist Awards 2022 (Langener Nachwuchwissenschaftpreis) for the publication Charitidis et al., 2021*.
- American Society of Gene and Cell Therapy 2022 Meritorious Abstract Travel Award

12 EHRENWÖRTLICHE ERKLÄRUNG – DECLARATION OF HONOR

Ich erkläre hiermit, dass ich die vorliegende Arbeit entsprechend den Regeln guter wissenschaftlicher Praxis selbstständig und ohne unzulässige Hilfe Dritter angefertigt habe.

Sämtliche aus fremden Quellen direkt oder indirekt übernommenen Gedanken sowie sämtliche von Anderen direkt oder indirekt übernommenen Daten, Techniken und Materialien sind als solche kenntlich gemacht. Die Arbeit wurde bisher bei keiner anderen Hochschule zu Prüfungszwecken eingereicht. Die eingereichte elektronische Version stimmt mit der schriftlichen Version überein.

Ort und Datum: Unterschrift: